Synthesis and Evaluation of Novel Ligands for Quantum Dot Stabilisation and Polymerisation Studies

Siobhan Sophia Cummins

Doctor of Philosophy

Aston University

January 2006

Thesis Summary

Synthesis and Evaluation of Novel Ligands for Quantum Dot Stabilisation and Polymerisation Studies

Siobhan Sophia Cummins

Doctor of Philosophy

Aston University

January 2006

This thesis describes the design and synthesis of a variety of functionalised phosphine oxides and sulfides, based on the structure of trioctylphosphine oxide, synthesised for the purpose of surface modification of quantum dots. The ability of the ligands to modify the surface chemistry via displacement of the original hexadecylamine capping layer of quantum dots was evaluated. Finally the surface modified quantum dots were investigated for enhancement in their inherent properties and improved compatibility with the various applications for which they were initially designed.

Upon the commencement of research involving quantum dots it became apparent that more information on their behaviour and interaction with the environment was required. The limits of the inherent stability of hexadecylamine capped quantum dots were investigated by exposure to a number of different environments. The effect upon the stability of the quantum dots was monitored by changes in the photoluminescence ability of their cores. Subtle differences between different batches of quantum dots were observed and the necessity to account for these in future applications noted. Lastly the displacement of the original hexadecylamine coating with the "designer" functionalised ligands was evaluated to produce a set of conditions that would result in the best possible surface modification. A general procedure was elucidated however it was discovered that each displacement still required slight adjustment by consideration of the other factors such as the difference in ligand structure and the individuality of the various batches of quantum dots.

This thesis also describes a procedure for the addition of a protective layer to the surface of quantum dots by cross-linking the functionalised ligands bound to the surface *via* an acyclic diene metathesis polymerisation. A detailed description of the problems encountered in the analysis of these materials combined with the use of novel techniques such as diffusion ordered spectroscopy is provided as a means to overcome the limitations encountered. Finally a demonstration of the superior stability, upon exposure to a range of aggressive environments of these protected materials compared with those before cross-linking provided physical proof of the cross-linking process and the advantages of the cross-linking modification.

Finally this thesis includes the presentation of initial work into the production of luminescent nanocrystal encoded resin beads for the specific use in solid phase combinatorial chemistry. Demonstration of the successful covalent incorporation of quantum dots into the polymeric matrices of non-functionalised and functionalised resin beads is described. Finally by preliminary work to address and overcome the possible limitations that may be encountered in the production and general employment of these materials in combinatorial techniques is given.

Key Words: Nanoparticle, Surface coating, Polymerisation, Phosphine Oxide.

For my Mother who only ever asked me to do my best,

but who always knew that was enough.

Acknowledgement

I would like to thank Dr. Andrew Sutherland for all his help, guidance and support throughout the time we worked together.

I am also grateful to Mrs Karen Farrow and Mr Peter Ashton for their assistance in performing low and high resolution mass spectrometry. I am thankful to Dr Mike Perry for his help and guidance in the field of NMR spectroscopy and also for his numerous suggestions of techniques designed to make my life easier.

I would also like to thank Pr. Morris and Gareth Smith for their invaluable input and expertises in the area of diffusion ordered ^{1}H NMR Spectroscopy. I also extend my gratitude to the Department of Chemistry at the University of Manchester for their generous donation of NMR machine time.

Thank you to my friends and members of the Sutherland group, Steve Ryley, Peter Chisnall, Mark M^{c}Carin and Katy Parker who elevated the time I spent working in the lab from good to fantastic, and who also on many occasions said exactly the right thing to keep me together.

Lastly I want to thank my Mother, Alan, Tam and Reggie for always having confidence in my ability to do Chemistry.

Contents

Abbreviations

ADMET	Acyclic diene metathesis polymerisation
AIBN	Azobis-*iso*-butyronitrile
$AlCl_3$	Aluminium trichloride
ATRP	Atom transfer radical polymerisation
BN	Boxed nanocrystals
CM	Cross metathesis
CMS	Chloromethylstyrene
DBU	1,8-Diazabicyclo[5.4.0]undec-7-ene
DCM	Dichloromethane
DMF	Dimethylformamide
DMSDPO	Dimethylstyryl(decane)phosphine oxide
DMSOPO	Dimethylstyryl(octane)phosphine oxide
DMSPA	Dimethylstyrylphospinous acid
DMSPSA	Dimethylstyrylphosphosulfinous acid
DNA	Deoxyribose nucleic acid
DODPO	Dioctyl(decanol)phosphine oxide
DOMSPO	Dioctyl(methylstyrene)phosphine oxide
DOOPO	Dioctyl(octene)phosphine oxide
DOPA	Dioctylphospinous acid
DODPO	Dioctyl(silyl-protected-decanol)phosphine
DOSY	Diffusion ordered spectroscopty

DOUPO	Dioctyl(undecene)phosphine oxide
DUDPO	Diundecene(decanol)phosphine oxide
DUPA	Diundecenephospinous acid
DUPDPO	Diundecene(silyl-protected-decanol)phosphine oxide
DUPSA	Diundecenephosphosulfinous acid
DVB	Divinylbenzene
EDCTP	Ethyldichlorothiophosphate
HBr	Hydrogen Bromide
HDA	Hexadecylamine
HRMS	High resolution mass spectroscopy
IBX	Iodobenzoic acid
IR	Infra red
$KMnO_4$	Potassium permanganate
KOH	Potassium hydroxide
LED	Light emitting diode
$LiAlH_4$	Lithium aluminium hydride
LR	Lawessons Reagnet
LRMS	Low resolution mass spectroscopy
MeOH	Methanol
MMD	Miniature memory device
NaH	Sodium hydride
n-BuLi	*n*-Butyl lithium
NMR	Nuclear magnetic resonance

PL	Photoluminescence
PS-DVB	Polystrene-divinylbenzene
PS-TR	Polymer supported thionating reagent
PVA	Polyvinylalcohol
RCM	Ring closing metathesis
ROM	Ring opening metathesis
ROMP	Ring opening metathesis polymerisation
SPOC	Solid phase organic chemistry
TBAF	*tert*-butyl-amoniumfluoride
TEM	Transition electron microscope
TFA	Trifluroacetic acid
THF	Tetrahydrofuran
TLC	Thin layer chromatography
TMSPO	Trimethylstyrenephosphine oxide
TOP	Trioctylphosphine
TOPO	Trioctylphosphine oxide
TOPS	Trioctylphosphine sulfide
TPhPO	Triphenylphosphine oxide
TPhPS	Triphenylphosphine sulfide
TPN	TUPO polymer coated NanoDots
TUPO	Triundecenephosphine oxide
UV	Ultra violet
Vinyl MgBr	Vinyl magnesium bromide

Structures and Acronyms of Synthesised Ligands

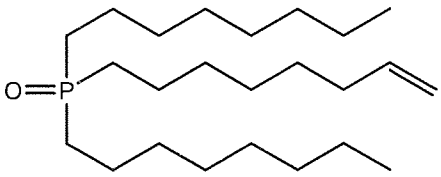

DOOPO **6**

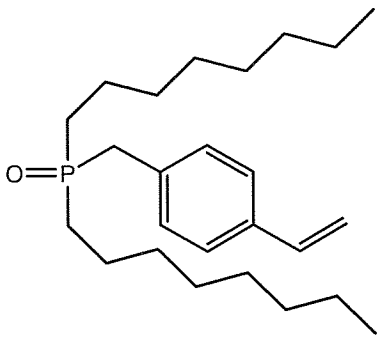

DOMSPO **7**

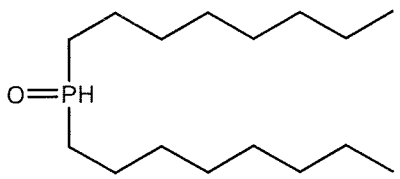

DOPA **14**

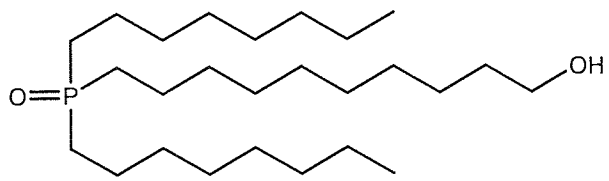

DODPO **16**

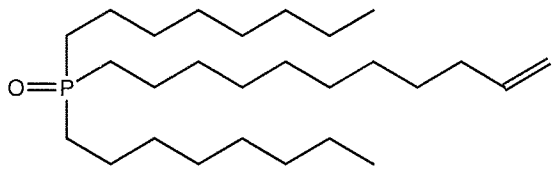

DOUPO **19**

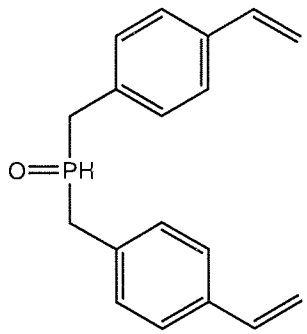

DMSPSA **20**

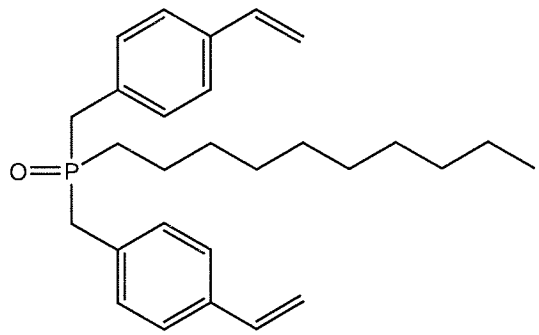

DMSDPO **21**

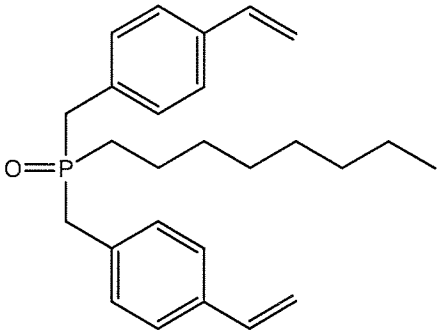

DMSOPO **22**

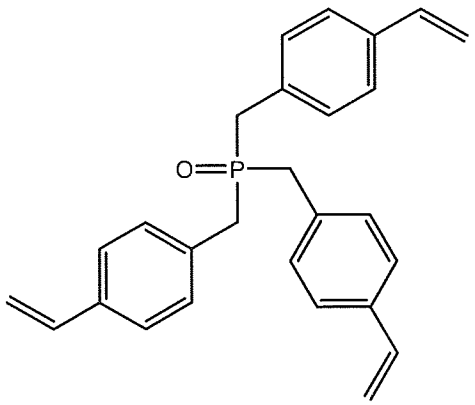

TMSPO **23**

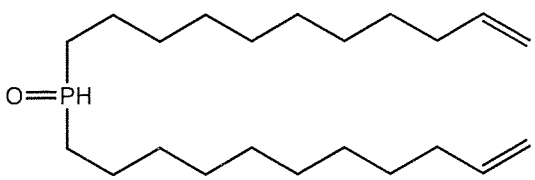

DUPA **24**

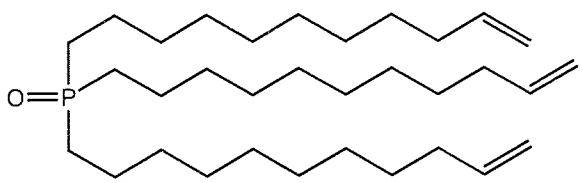

TUPO **25**

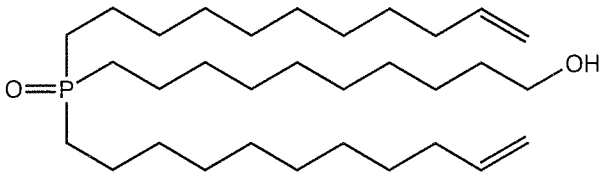

DUDPO **27**

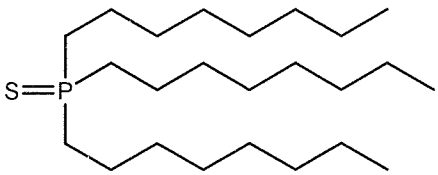

TOPS **28**

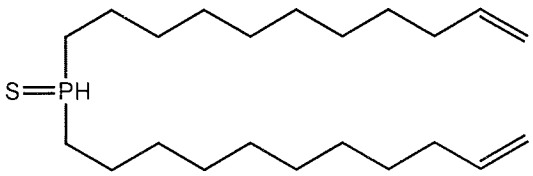

DUPSA **33**

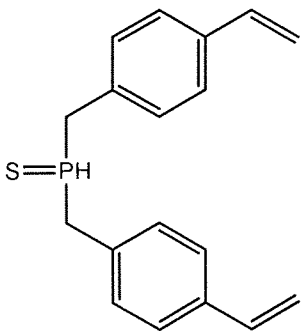

DMSPSA **34**

Figures, Schemes and Tables

CHAPTER 1

INTRODUCTION

1.1 Quantum Dots

Quantum dots are nanoparticles or nanocrystals of semiconducting material(s).[1,2] Generally they are relatively spherical discrete clusters of atoms (a few hundred to a few thousand)[3] typically between 1-12 nm in diameter,[4] however synthesis of quantum dots with sizes ranging from 1-20nm is possible.[5] Quantum dots have attracted the attention of chemists, physicists, biologists and electronic engineers.[2] The interest, both theoretically and commercially, in quantum dots is due to their unique properties that differ significantly from the bulk materials from which they are derived.

The differences in these properties can be attributed to three main factors:[1, 6]

1. The large surface to volume ratio of the atoms comprising the quantum dot.
2. The confinement of charge carriers in a 'quantum mechanical box'.
3. The nature of the surface.

The electronic, optical and catalytic properties of a bulk semiconductor are determined by the band gap and the material type. The same properties in a quantum dot however, are determined by the nanocrystal size and the material type.[1] When discussing the behaviour of bulk semiconductors the size of the material is not an important factor since the material may be viewed as an extended solid. The behaviour exhibited by the bulk semiconductor is a direct consequence of the electronic structure produced by the internal geometry of the crystal lattice.[7]

The electronic structure of bulk semiconductors can be described as continuous bands that are delocalised over the whole structure.[3] These bands result from the overlap of atomic orbitals of neighbouring metal atoms, and comprise of a valence band and a conduction band. The valence band consists of bonding orbitals that each contain a pair

of valence electrons, conversely the conduction band is composed of empty anti-bonding orbitals. In both bands the concentration of molecular orbitals is greater towards the centre and begins to thin out towards the edges.[8] The valence and conduction bands are separated by an energy difference known as the band gap **Figure 1**.[8]

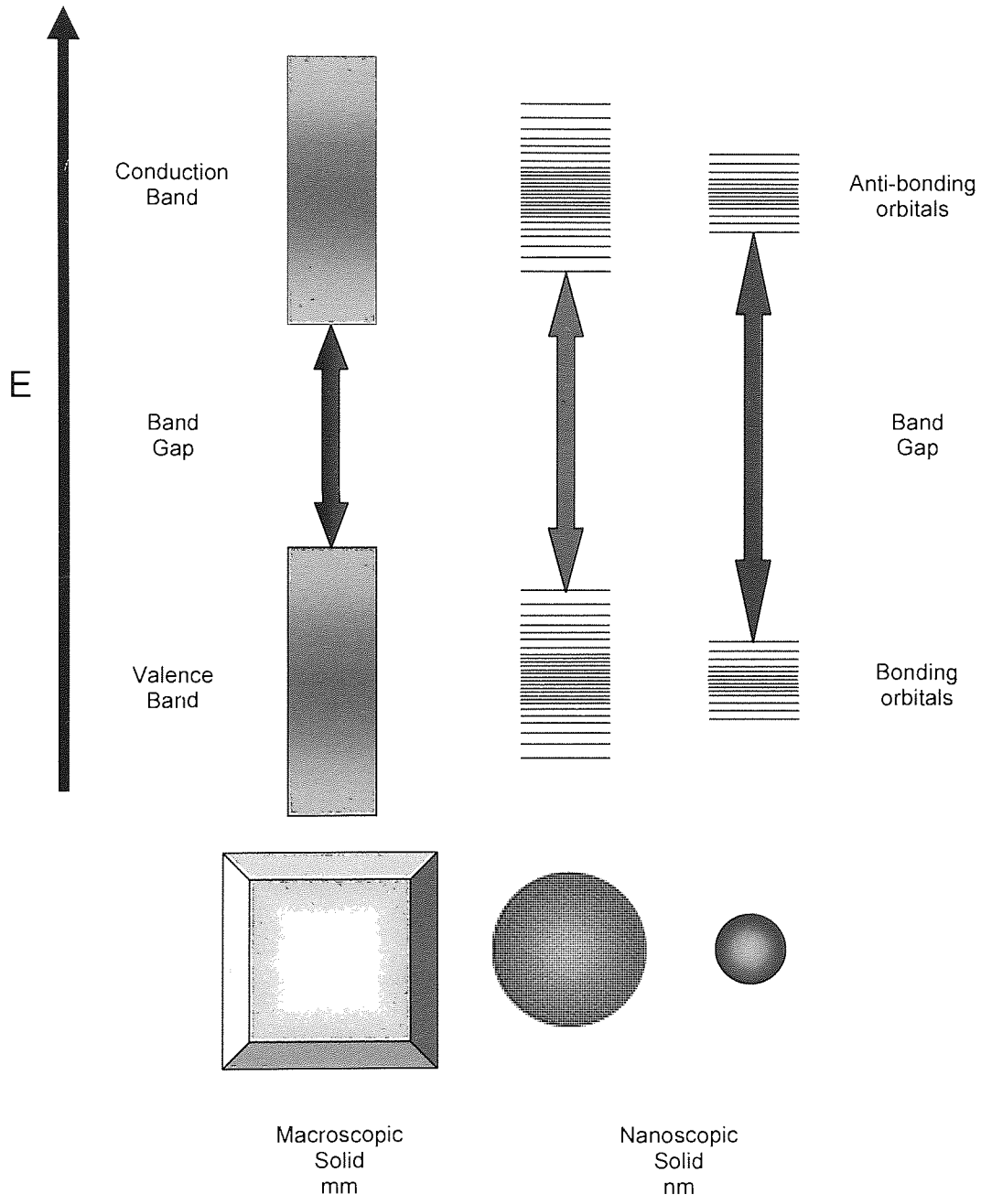

Figure 1: A schematic representation of the electronic structure of bulk semiconductors and that of quantum dots

Bulk semiconductors are defined as possessing a completely full valence band and an empty conduction band separated by a band gap of between 0.5-3.0 eV. Since the band gap is of a reasonable size it is possible for an electron from the valence band to be excited by a quantum of light into the conduction band.[6] The electron and the positive hole formed by its departure are termed charge carriers and are free to move independently of each other resulting in electrical conductivity.[1,4] Since the charge carriers experience columbic forces and the laws of quantum mechanics require the carriers be one Bohr radius apart[3], the electron will move to a position outside that of the excitation radius (5-10nm)[2] of the positive hole.[6]

When discussing the electronic nature of semiconductors with overall diameters of just a few nanometres (i.e. nanocrystal size) their electronic structure must be described more like that of a molecule than that of an extended solid.[4, 9] Quantum dots are unique clusters that preserve their parent bulk crystal structure, but are unable to retain its electronic structure due to this being a consequence of the extended crystal lattice.[10, 11, 12] Therefore the model describing electronic structure of quantum dots needs to be modified in order to take into account the smaller number of atoms each cluster contains and the implications of this.

In order to modify the electronic structure of extended solids to account for the behaviour and properties exhibited by quantum dots, the macroscopic semiconductor needs to be shrunk to the nanoscopic size of a quantum dot[12]. This can be visualised by atoms being removed from the surface of the bulk semiconductor so that ultimately all the dimensions of the crystal are reduced to a few nanometres. As each atom is removed its orbital contribution to both the valence and conduction band is removed. Referring to

Figure 1 it can be seen that continuing to remove atoms and their orbital contributions will eventually lead to the breakdown of the continuous bands and the revelation of individual orbitals.[8] Ultimately this results in the bands beginning to split into discrete bonding and anti-bonding orbitals with quantised energy levels.[6, 8, 12]

Another major consequence arising from the small size of quantum dots is that of confinement of charge carriers.[1, 5, 12] As in bulk semiconductors when energy is absorbed an electron can be promoted leaving behind a positive hole. In extended solids the electron moved outside the Bohr or excitation radius of the positive hole.[3, 6] However in quantum dots the excitation radius of the material is usually larger than the entire dot and leads to confinement of the exciton.[2, 6] This situation breaks the laws of quantum mechanics and as a result the charge carriers assume a higher state of kinetics.[3, 6] It requires a greater amount of energy to confine the exciton and this is accomplished by an increase in the band gap.[1, 3, 6, 12, 13, 14] It follows that as quantum dots decrease in size the energy required for confinement of the charger carriers increases, subsequently the band gaps of these materials increases to compensate. This is demonstrated by a shift in emission to the blue (higher energies) as the sizes of a nanocrystals decreases **Figure 2**.[3, 10, 15]

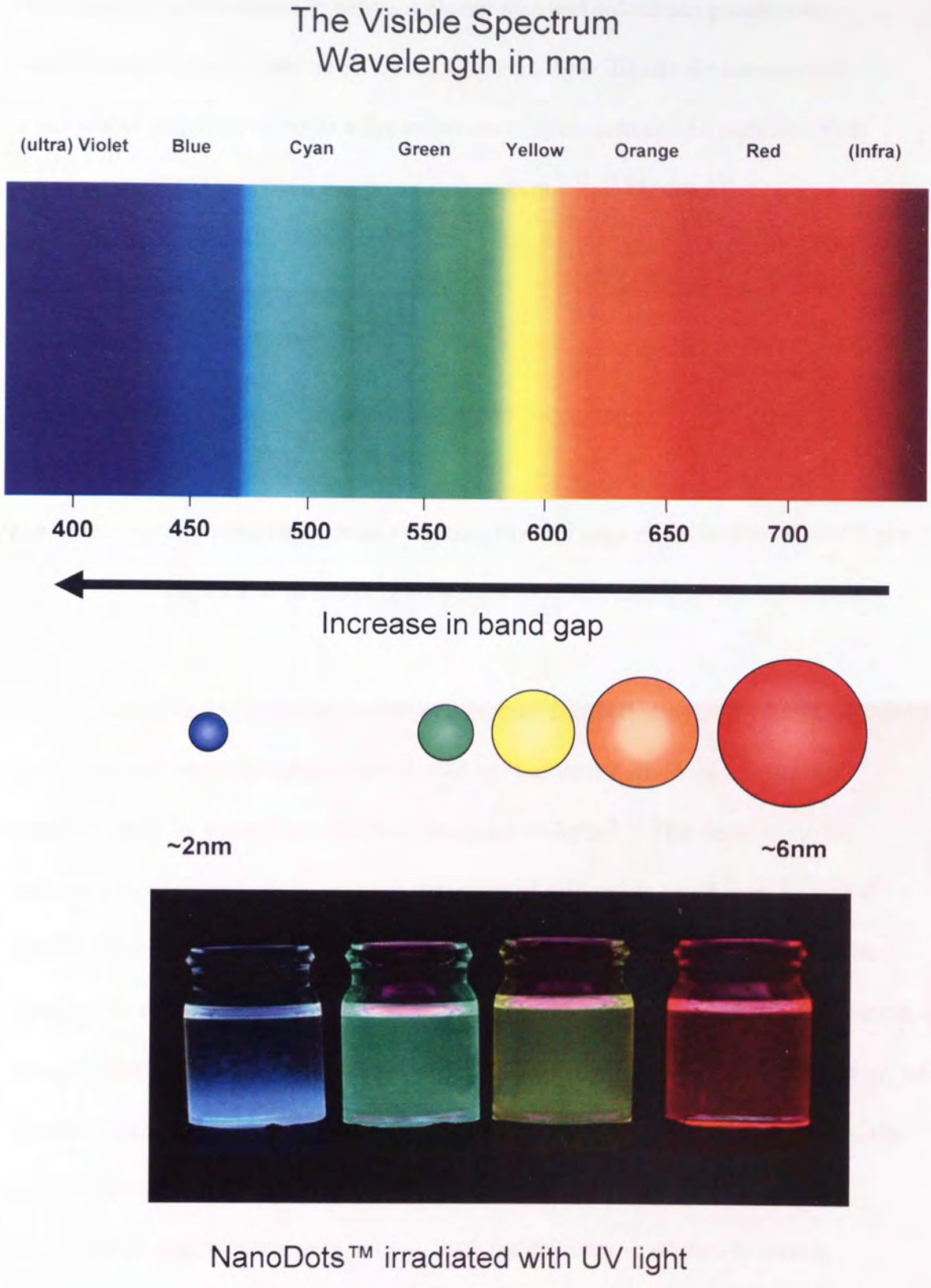

Figure 2: **A schematic demonstration of the relationship between the colour of emitted light and the size of quantum dots**

This simple linear relationship between cluster size and colour can produce size tuneable emissions over the entire visible spectrum. Specifically for nanocrystals composed of cadmium selenide a full spectrum of emissions can be obtained from particles ranging in size from two to six nanometers.[2, 13, 16] **Figure 3**[15]

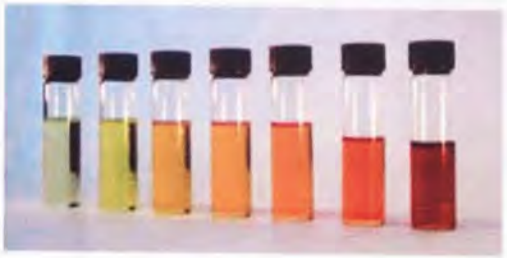

Figure 3: **A photograph demonstrating that a range of CdSe NanoDots™ are capable of producing emissions over the entire visible spectrum**

Another unique and exploitable feature of quantum dots is that a range of different sized (multicoloured) nanocrystals can be induced to emit their individual frequencies simultaneously by excitation with a single source of light.[3, 16] This feature can be explained by examining the electronic structures of differently sized dots. **Figure 4**[8] depicts the electronic structure of two different sized dots of the same material. The quantisation of the bands has not been included in an effort to simplify the explanation. When both the green and blue dots are exposed to UV light of sufficient high energy, an electron is promoted from the upper level of the valence band to the upper level of the conduction band, this is represented in **Figure 4** by the grey arrows. The energy required to accomplish this promotion in both the different sized dots is almost identical. This explains why excitation by a single source of light is possible even though the band gaps of the two differ significantly.[8] The promoted electron then tumbles down the quantised energy levels present in the conduction band.[8, 17] Energy is

released as heat (red chevron in **Figure 4**) at each stage until the electron occupies the lowest possible energy level in the conduction band.

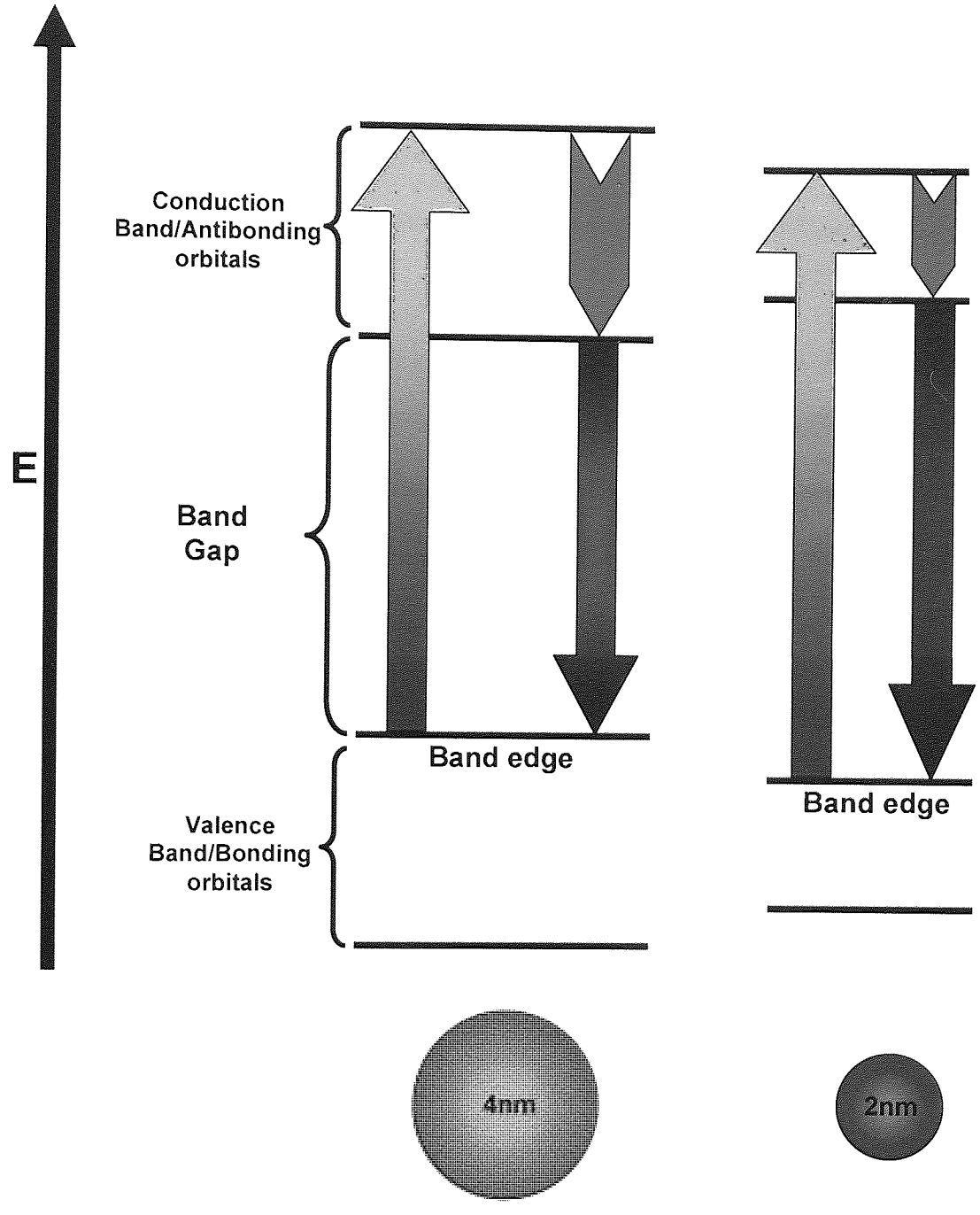

Figure 4: **An energy diagram comparing the different energies encountered in two sizes of quantum dots**

The electron then falls back to the valence band through the band gap now emitting its excess energy as visible light rather than heat.[8] The green dot has a smaller band gap than the blue dot and therefore the wavelength of light released is larger than that released by the blue dot. The size of the wavelength produced corresponds to different colours in the visible spectrum **Figure 2**. A wavelength of 550nm will be visible as a green emission whereas a shorter wavelength of 475nm will produce a blue emission.

The basic structure of a quantum dot is a crystalline core composed of a semiconducting material surrounded by a capping agent that serves as a surface pacifier. Examples of both organic **Figure 5** and a mixture of inorganic and organic surface passivation **Figure 6** and **Figure 7** have been reported. Examples of purely organic ligand passivated quantum dots include nanocrystaline core materials of CdS[18, 19, 20, 21], ZnS[22], CdSe[23, 24], ZnSe[25], InS[26] and InSe.[25] More complex core-shell particles coated with an outer organic layer for example CdSe/ZnS[27, 28, 29, 30] and CdSe/CdS[31] are also produced routinely. Finally examples of even more complex multi-shell materials are beginning to appear in the literature, for example CdS/HgS/CdS.[32, 33]

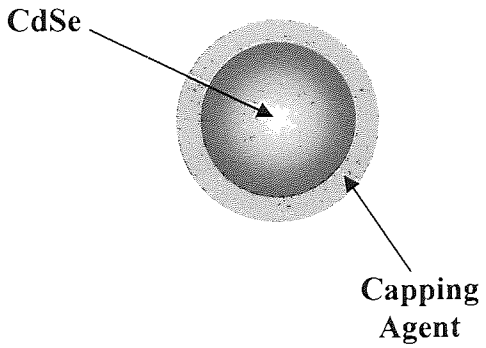

Figure 5: **A schematic representation of a quantum dot with solely organic surface passivation**

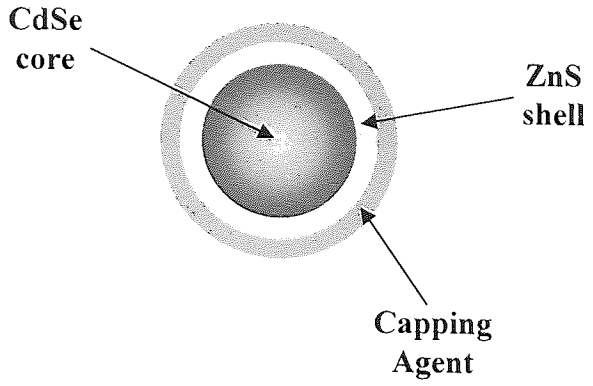

Figure 6: **A schematic representation of a core-shell quantum dot**

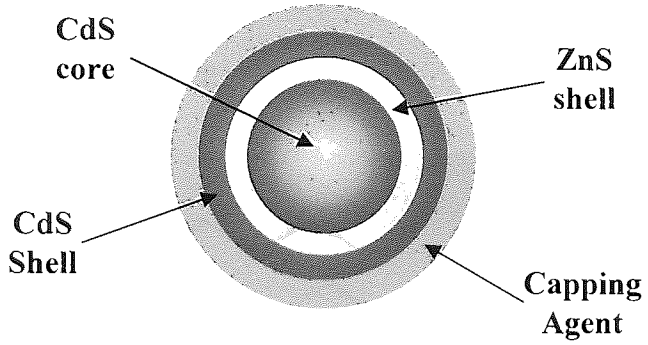

Figure 7: **A schematic representation of a multi-shell quantum dot**

Organic capping groups are normally present during the synthesis of nanocrystals and serve as stabilising agents where they have two main functions:[5,12, 34]

1. To mediate the growth of the nanocrystal
2. To passivate the surface of the nanocrystal, preventing aggregation of the nanoparticles thus allowing purification and long term storage.

Organic capping groups are typically composed of electron rich donating groups such as phosphine oxides, phosphines, amines or thiols.[12] The nature of the interaction between

the capping ligand and nanocrystal surface is thought to be analogous to that of ligand binding in traditional coordination chemistry.[5] The capping agents are believed to behave as Lewis bases and coordinate to the Lewis acid-like electron poor metal sites of the semiconductor.[12] Examination of the surface of CdSe capped with trioctylphosphine oxide (TOPO) **1** revealed that only the electron poor Cd sites are coordinated, the basic Se^{2-} sites remain unbound.[35, 36] The coordination of the capping agent passivates the exposed orbitals at the surface of the nanocrystal, preventing aggregation and aids in solubility.[12]

Quantum dots are often produced with a surface capping layer of trioctylphosphine oxide **1** trioctylphosphine (TOP) **2**, or a long chain amine such as hexadecylamine (HDA) **3 Figure 8**.

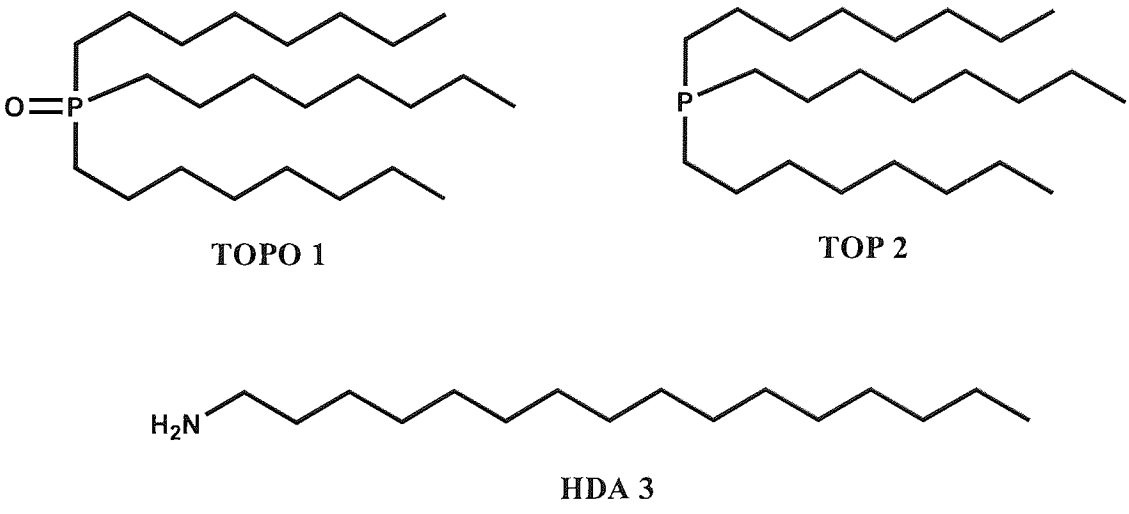

Figure 8: Structures of TOPO, TOP and HDA

These capping agents are not ideal for all potential applications of the nanocrystals.[4] Fortunately modification of the surface of the nanocrystal can be accomplished with

ligand exchange.[37, 38, 39] Due to the weak nature of the coordination bonds, most capping agents can be exchanged by a simple displacement procedure using an excess of a desired agent.[12] Synthetic techniques allow for the preparation of a wide range of capping agents tailored to the specific application of the nanocrystal.[5, 12] Examples of a wide variety of surface modified nanocrystal suitable for many different applications have been reported.

Nanocrystals can be dispersed in water via surface derivatisation with a number of capping agents. Displacement with various thiols,[40, 41, 42, 43, 44, 45] for example 1,2-dimercapto-ethane-1,2-diol **4 Figure 9** or mercaptopropionic acid **5 Figure 10**, gives rise to hydrophilic, nanocrystals that are relatively biocompatible and can be utilised as fluorescent tags.

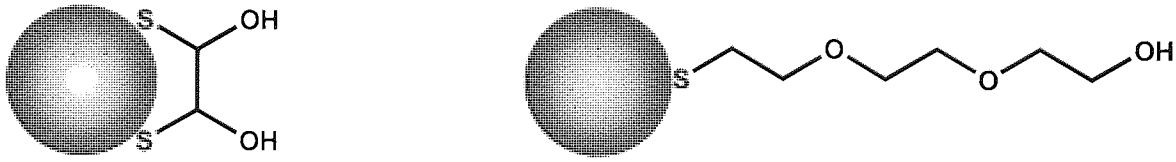

Figure 9: **A schematic representation of the surface derivatisation of quantum dots with ligands that possess thiol-based anchoring groups**

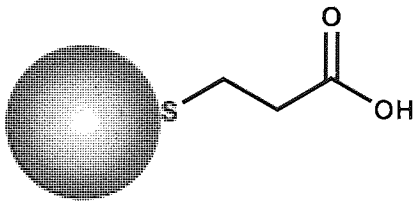

Figure 10: **A schematic representation of the surface derivatisation of a quantum dot with mercaptopropionic acid**

Conversely displacement with dioctyl(octene)phosphine oxide[37] (DOOPO) **6 Figure 11**, dioctyl(methylstyrene)phosphine oxide[37, 38] (DOMSPO) **7 Figure 12** and allyl terminated dendrimers[46] leads to organic compatible, readily polymerisable nanocrystals. Examples of amphiphilic nanocrystals have also been reported. Displacement of TOPO **1** with pegylated pyridines **Figure 13** afforded nanocrystals that produced optically clear solutions in both aqueous and organic media.[47] The surface modification of nanocrystals with various organic capping agents is often desirable as it leads to better compatibility of the nanocrystal in its chosen application.

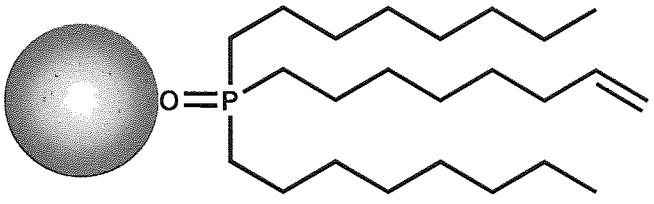

Figure 11: **A schematic representation of the surface derivatisation of a quantum dot with DOOPO**

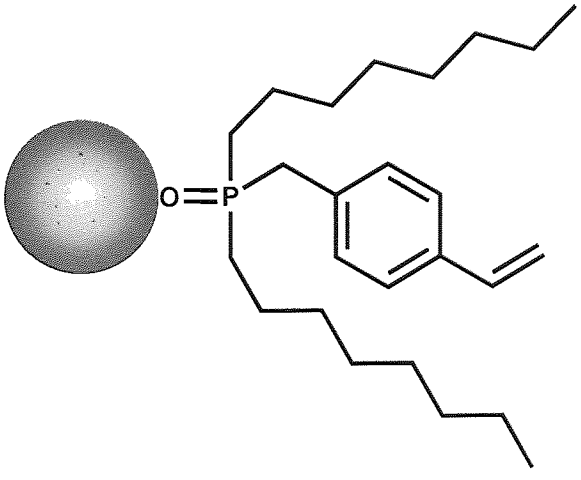

Figure 12: **A schematic representation of the surface derivatisation of a quantum dot with DOMSPO**

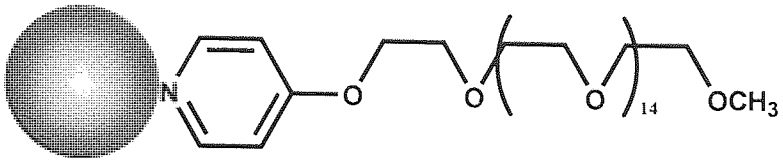

Figure 13: A schematic representation of the surface derivatisation of a quantum dot with a pegylated pyridine

Nanocrystals passivated with an inorganic material, prior to the coating with an organic capping agent are generally considered to be more robust than the previously discussed organic capped nanocrystals. This is because the orbitals on the surface of the core can be completely passified. This differs from the situation found with organic capping agents, where only the cationic or anionic sites are passified with a chosen ligand.[27, 35, 36] Both types of nanocrystal, core and core-shell are important. However, it has been shown that the addition of a second layer of a semiconductor with a larger band gap than that of the core material can improve the photoluminescence and stability of the dot.[5,10, 48] Core/shell nanocrystals show greater stability compared to core nanocrystals when incorporated in electroluminescent devices such as light emitting diodes (LED's).[10, 49] The additional stability conferred by the inorganic shell can also be advantageous if the encapsulation of the quantum dot into the chosen application requires the use of harsh conditions.[10]

Nanocrystal cores have been passified with a number of different inorganic materials **Figure 6 & 7**. Inorganic passivation is possible due to the highly reactive surface of the core, resulting from the incomplete coordination of the orbitals present.[27] The precursor for the inorganic shell is added slowly to a mixture of the cores and stabilising agent. If the shell precursor is added slowly enough heterogeneous nucleation on the surface of the cores occur. The rate of addition of the shell precursor must never exceed the rate of

deposition as this can result in homogeneous nucleation producing a second core.[5] The size of the core and the thickness of the shell deposited can be varied giving control over the band edge luminescence and the quantum yields produced.[27]

In the last twenty five years there has been intense interest in the field of "preparation" and "synthesis" of nanocrystals.[12, 50] Many synthetic routes to the preparation of high quality nanocrystals have been reported, the most important of these fall into three main areas:[1, 50]

1. Colloidal routes
2. Preparation in size controlled environments
3. Synthesis from the decomposition of organic metal precursors

To be considered an 'ideal' synthetic route the method needs to produce pure isolated clusters that are monodisperse with regards to size, shape, internal structure and surface chemistry.[7]

Nanocrystals were first synthesised by arrested precipitation from dilute aqueous solutions.[1, 51] LaMer and Dinegar[52] discovered that controlling the initial concentrations of sodium thiosulfate and hydrochloric acid during decomposition produced nearly monodisperse colloids. It was proposed that this control in particle size resulted in a very short period of consecutive nucleation, followed by steady uniform deposition on the surface of the seeds (nuclei).[1, 53] Subsequent work that built upon this observation has lead to the situation where nucleation and growth can be carefully controlled by the utilisation of a process know as Ostwald ripening.[1, 5] Small less stable crystals dissolve due to their high surface energy and recrystallise onto the surface of larger more stable nanocrystals. Over time this results in an increase in the size of the individual

nanocrystals and a decrease in the number of nanocrystals produced.[5] The success of this process is dependent on the low solubility of the nanocrystal produced and can be controlled by the variation in the choice of solvent, dilution[52], pH[52], temperature[9, 54] and passivating agent.[18]

Colloid methods are, on the whole, an effective route for the production of nanocrystals with reproducible sizes. However, a disadvantage of colloidal routes is that some important semiconductors cannot be synthesised in high enough quality. In addition air sensitivity and poor crystallinity can result from the annealing of amorphous colloid particles in some materials.[1]

Synthesis in a size controlled environment refers to synthesis in confined matrices. The matrices can be assumed to be nanometre sized reaction vessels used to restrict the growth of the nanocrystal.[1] Various types of matrices have been employed to aid in the production of nanocrystals. Zeolites,[55, 56, 57, 58] molecular sieves,[59] micelles,[60, 61] porous glass[62] and polymers.[61, 63] have all been used as structured reaction media.

Growing particles in the cavities of zeolites limits the particle size of the nanocrystal produced to the size of the cavity chosen. Zeolite Y and mordenite have been used to produce CdS,[55] PbS,[55] GaP[56] and Cu[57] nanocrystals below 13 Å in diameter. The use of zeolite A in its sodium and potassium forms demonstrates a limited control over the size of the CdTe nanocrystal formed. Sodium in place of potassium is thought to narrow the effective pore diameter of the zeolite and in turn inhibit the growth of the nanocrystals produced.[58]

Herron and Wang synthesised CdS and PbS nanocrystals encapsulated in zeolites in 1987. They argued the attractiveness of their method over the more traditional colloid routes of the time as follows:[55]

1. The zeolite provides a solid solvent for the nanocrystals. Due to its highly porous nature and cation exchange properties the zeolite facilitates low temperature cluster synthesis.
2. The inherent internal framework of the zeolites allows the formation of smaller and more uniform nanocrystals.
3. The zeolite prevents aggregation of the nanocrystals and thus protects the unique properties of the cluster.
4. Zeolites allow the possibility of investigation of a superlattice formed by clusters inhabiting all internal cavities.

The precise control over size is useful, however the disadvantages of this method lie in the lack of suitable zeolites for the production of significantly larger quantum dots and the difficulty in recovering the nanocrystals formed in this manner.[7]

Synthesis of nanocrystals encapsulated within molecular sieves is similar to that in zeolites, the sieve provides a template for size restricted growth. However molecular sieves are available in a range of pore sizes, MCM-41 has been developed with uniform pore openings ranging from 2-10 nm situated in a regular hexagonal array. Iwamoto *et al* describe a method of synthesising of Fe_2O_3 nanocrystals in the pores of MCM-41.[59]

The growth of nanocrystals inside various polymer matrices has also been reported in the literature. A particularly elegant method developed by Cole-Hamilton *et al* describes

the functionalisation of polybutadiene with group 12 metal alkyls.[64] These metal alkyl/polymer adducts remain soluble in toluene and exposure to H_2Se or H_2S gas results in the formation of coloured precipitates. The polymer/semiconductor adducts can then be isolated by simple filtration and the incorporated particle size can be controlled by the choice of solvent and the reaction temperature.[63]

Inverse micelle solutions are also capable of providing a suitable medium for the synthesis of nanocrystals.[7] Organic micelles and vesicles are usually composed of surfactants or polymers, where each unit contains hydrophobic and hydrophilic region. The interaction between these regions and the solvent media produces an organisation of the individual units into micelles.[61] It is possible to grow nanocrystals inside certain micelles. Fendler *et al* discovered that CdSe nanocrystals encapsulated in micelles are incredibly stable against flocculation.[65] The surfactant molecules passivate the surface discouraging agglomeration. Brus *et al* reported the same phenomenon in a similar system using CdSe, they also discovered that the surface ligands were labile. Subsequent addition of inorganic sources of Cd^{2+} and Se^{2-} was found to displace the stabilising agent allowing for further growth of the nanocrystal.[7] Surface passivation of the nanocrystal can also be accomplished in this manner. The addition of Ph-Se^{2-} results in the production of effectively covalently bound organic passivating layer.[60]

Organometallic based routes to high quality monodisperse nanocrystals have been widely researched and as a result contribute a substantial number of publications to the area of literature dealing with the production of nanocrystals. In 1993 Bawendi *et al* reported that supersaturation followed by immediate nucleation of nanocrystals can be achieved by the rapid injection of a mixture of organometallic precursors into a hot,

vigorously stirred coordinating solvent.[5, 66] TOP/TOPO capped CdSe nanocrystals were synthesised by heating a vigorously stirred flask containing TOPO to 300°C. Immediate, rapid injection of a mixture of dimethylcadmium and trioctylphosphine selenide dispersed in TOP produced nucleation that was accompanied by a drop in temperature to 108°C. Further nucleation is prevented by the sudden temperature drop and the depletion of organometallic reagents through the initial nucleation process. Slow growth and annealing of the crystallites is achieved by gentle heating of the reaction mixture to 230-260°C for several hours. The growth can be controlled by the careful control of temperature making it possible to produce surface capped highly crystalline particles in a range of sizes.[66]

The organometallic precursors can be varied depending on the required composition of the nanocrystal. Other metal alkyls such as diethylcadmium, diethylzinc and dibenzylmercury can be mixed with chalcogenides such as *bis*trimethylsilyl or tertiary alkyl phosphine sulphides, tellurides and selurides. Mixing different metal alkyls and chalcogenides before injection produces a variety of nanocrystals with different compositions. [5, 66]

A similar approach can be used to synthesise core/shell nanocrystals. Peng *et al* reported a method where mixtures of dimethylcadmium and tributylphosphine selluride were injected into hot TOPO, to form TOPO capped CdSe cores. The cores were then refluxed overnight in pyridine to remove the TOPO capping agent before the growth of the shell by drop-wise addition of a mixture of dimethylcadmium and bistrimethylsilyl sulphide at 100°C.[27] Dabbousi et al prepare CdSe/ZnS in a similar way, however the zinc and sulfur precursors were added directly to the TOPO capped cores.[10]

Quantum dots prepared by organometallic based methods are generally of a high quality. Unfortunately however major disadvantages stem from the safety aspect of injecting hazardous compounds at high temperatures well above the flash point of TOPO **1** and the relatively dilute reaction conditions that prevent effective reaction scale up. These disadvantages have been overcome in work published by the O'Brien group who explored the use of a single-molecular precursor in which the metal-chalcogen bond exists from the outset. The first single-molecular precursors investigated were air sensitive,[1, 67, 68] however this research resulted in the first route to ZnSe nanoclusters that were isolated and well defined.[25] As work in this area advanced these early methods were rapidly superseded by the discovery of air stable precursors that could be used in a 'one pot' synthesis of certain quantum dots. CdSe, CdS, ZnSe and ZnS have all been prepared directly by thermolysis of the air stable corresponding precursors in TOPO **1** at 200°C.[1, 22] CdSe nanocrystals are synthesised using air stable precursor simply by injecting a solution of *bis*[methyl(n-hexyl)diselenocarbamato]-cadmium in TOP **2** into TOPO **1** at 200°C and stirring at this temperature for 40 minutes. This is followed by precipitation in anhydrous methanol and re-dispersion in toluene before isolation of the nanocrystals under reduced pressure.[22]

Core/shell structures such as CdSe/CdS have also been prepared via this 'one pot' method. The cores (e.g. CdSe) are formed as previously described, but prior to precipitation the corresponding shell precursor (e.g. of *bis*[methyl(n-hexyl)disulphocarbamato]-cadmium) is injected and the mixture heated for a further 30 minutes at 200°C. Precipitation in methanol followed by re-dispersion and isolation from toluene produces highly monodisperse core/shell samples.[29]

The literature dealing with the production of nanoparticles is vast and rapidly and continuously growing. The choice of the optimum route for the preparation of nanocrystals is highly complex and the material type, the quality and the intended application of the nanocrystals needs to be considered before a particular synthetic strategy is employed. Quantum dots have the potential for being invaluable in many areas of science and industry. Their unique and novel properties are essential for nanoparticle based devices such as tuneable lasers,[69] LED,[8, 49] photovoltaic cells[12] and biological probes[70]. However, perhaps the most important application for quantum dots is their use as optical tags in combinatorial based encoding techniques. Resent research by Nie et al has begun to explore this area by embedding different sized dots into polymeric microbeads for the purpose of encoding a combinatorial produced library.[71]

1.2 Combinatorial Chemistry

Combinatorial chemistry is an area concerned with the rapid synthesis of large collections of diverse molecules.[72] This is accomplished by employing a range of techniques designed to synthesise many molecules simultaneously using a large variety of different reagents.[73] The application of combinatorial chemistry appeared particularly attractive to the pharmaceutical industry as it was suggested that it could provide the philosopher's stone for the drug discovery process. The principle problem with traditional drug discovery was that it could not satisfy the demand for lead compounds created by automated high throughput screening methods.[74] Therefore the purpose of combinatorial chemistry is:[73]

1. To create, as rapidly as possible, a library of compounds for screening.
2. Once a lead compound is identified, to use combinatorial techniques to improve the synthesis, selectivity, potency etc.

Combinatorial chemistry can be performed in solution or on a solid support. Both methods have advantages and disadvantages, these are summarised briefly in **Table 1**.[73]

Advantages On Solid Phase	Disadvantages On Solid Phase
1. Simple purification of the product via washing and filtration 2. Reagents can be used in excess without purification difficulties 3. Automation of synthesis possible 4. Split and mix synthesis possible 5. Solid phase resins commercially available	1. Solid phase chemistry is not as well developed as standard solution chemistry 2. Additional synthetic steps required for linkage and cleavage to and from the resin 3. Limited types of supports and linkers retard chemistry 4. Monitoring of reactions not as simple compared with solution phase chemistry 5. Solid supports/supported reagents are expensive or time consuming to prepare
Advantages In Solution	**Disadvantages In Solution**
1. All traditional organic reactions can be utilised with no modification 2. No additional steps for attachment and cleavage to a support 3. Large amounts of product can be produced 4. Progress of reaction can be followed using traditional monitoring techniques	1. Automation of reactions can be problematic 2. Purification of product can be time consuming 3. The use of excess reactants adds further time and complication to the purification of the product 4. No split and mix synthesis

Table 1: **Advantages and disadvantages of combinatorial chemistry on solid support and in solution**

The choice of whether to employ solid or solution phase technique will ultimately depend heavily on the particular requirements and conditions of the target reaction scheme. However, future success in this field would benefit from the amalgamation of solid and solution phase techniques in an effort to overcome their individual drawbacks. An elegant example of this in practice is the development polymer supported reagents. This hybrid synthesis technique overcomes inherent purification problems common in solution phase, while performing reactions in solution enables the vast synthetic flexibility that can be impaired by synthesis solely on solid support.[75]

1.2.1 Solid Phase

A solid support can be defined as an insoluble polymeric material that is in possession of functionalisation to facilitate the tethering of molecules (either reactants or products) for the purpose of separation from the reaction mixture.[72] Merrifield first established the technique of solid phase synthesis reporting the stepwise assembly of a peptide chain anchored to an insoluble chlorometylstyrene (CMS)-functionalised polystyrene-divinylbenzene (PS-DVB) resin.[74] The solid phase support of choice in the vast majority of combinatorial reactions consists of a spherical insoluble functionalised PS-DVB resin.[76] Monodispersity in regards to size, spherical shape and uniformity of cross-linking is vital for mechanical robustness and ease of handling in many applications.[77]

PS-DVB based resins are normally prepared by a radically initiated suspension copolymerisation reaction. [77] A common functionalised resin can be produced from a copolymerisation reaction involving a mixture of styrene **8**, divinylbenzene (DVB) **9**

(cross-linking agent) and chlorometylstyrene (CMS) **10** (functionality) monomers. Polymerisation is accomplished by the addition of a radical initiator such as azobis-*iso*-butyronitrile (AIBN) **11**.[78] The monomer mixture containing the initiator is added to a large volume of an aqueous solution that contains one or more stabilising agent(s), the mixture is then stirred.[79] Commonly employed stabilising agents, such as polyvinyl alcohol (PVA) **12**, are present in low concentrations as surface active agents to assist with the separation and maintenance of the aqueous suspended monomer droplets formed by the dispersion resulting from stirring of the two phases.[78] The reaction temperature of the system is then increased to facilitate the thermolytic fission of AIBN into free radical initiating species.[79]

These initiating radicals are now capable of starting the polymerisation process via reaction with the monomer molecules producing initiator monomer adducts.[79] These adducts begin the growth and cross-linking of many polymer molecules via free radical chain propagation. In the initial stages regions of discrete microgelation occurs, but as the polymerisation proceeds the growing regions begin to merge and cross-linking occurs producing a complex polymeric network throughout the droplet.[77] The polymerisation process can take up to 12 hours and results in spherical insoluble (in cases where a cross-linking agent is employed) polymer beads. These beads can then be collected by filtration and washed with a range of solvents Finally extraction with hot solvent such as dichloromethane (DCM) in a soxhlet will remove any trace amounts of un-reacted initiator, monomer, short chain oligomers and other impurities.[79] The beads are then dried under vacuum and sized via passage through a series of sieves with decreasing pore sizes.

1.2.2 Resin Morphology[77]

The majority of commonly used polymer beads can be categorised as either gel-type or macroreticular. Gel-type beads result from the polymerisation of styrene and DVB. The DVB acts as a cross-linking agent, the greater the percentage concentration of DVB the more highly cross-linked the resin becomes. In theory the percentage of DVB can be varied from 0-100%, the closer to 100% it becomes the more compact and glassy the bead. Most common and commercially available resins contain a range of 0-20% DVB, depending on their particular application. Gel-type resins utilised in combinatorial chemistry usually contain between 0.5-2% DVB. This percentage results from a compromise between mechanical strength and the ability of the resin to swell. Lightly cross-linked PS-DVB resins can be made to swell by the addition of a suitable solvent. The ability of a gel-type resin to swell is of great importance as it results in the accessibility of the internal polymer matrix to solvent and reagents, allowing the desired chemical reactions to occur since 98% of the reactive sites are inside. Therefore the level of cross-linking must be low enough to permit sufficient swelling, but not too low as to severely compromise the mechanical strength of the individual bead.

Macroreticular resins differ from gel-type resins in the fact that they contain a well defined internal pore structure. These pores result from the addition of a porogen (appropriate organic solvent such as toluene) to the co-monomer mixture prior to polymerisation. The presence of this porogen produces beads with a non-uniform internal matrix consisting of areas of highly cross-linked polymer indispersed with empty cavities or pores. A consequence of this heterogeneous internal morphology is that swelling of the resin to facilitate chemical reactions is not required. The resin can

be used in both thermodynamically compatible and non-compatible solvents. Since the pore structure remains permanently accessible these resins can be produced with a greater level of cross-linking and are generally considered to be more robust. Control of the pore size is possible by careful selection of the porogen and variation of the level of cross-linking.

1.2.3 Functionalisation of Polymer Supports

When Merrifield first began to develop solid supported synthesis the resin used was functionalised after the polymerisation reaction by subjecting the beads to a chloromethylation reaction.[74] Today, however, CMS is added to the monomer mix prior to polymerisation.[80] Merrifield's resin is widely used but in order for solid phase combinatorial chemistry to expand, resins with different linkers suitable for a diverse range of reactions needed to be produced. Resins often named according to the nature of the linker present and there are a growing number of varieties available.

In 1973 Wang[81] modified Merrifield's resin by substituting the chlorine with 4-hydroxybenzylalcohol. This linker enables cleavage from the resin to be achieved under milder conditions than for Merrifield's resin, 50% TFA can be used rather than hydrogen fluoride. In 1987 Merrifield's resin was modified by Rink[82] who exchanged the chlorine for a trialkoxy-diphenylmethyl-ester. Compounds can be cleaved from this resin by treatment with 95% TFA and, as a result, this resin is slightly more acid tolerant than Wang's Resin. Another important resin was developed in 1988 by Mergler who produced the super acid sensitive Sasrin linker that is cleaved by treatment with 1%

TFA. Many other linkers are available that are compatible with many combinations of reactions. A highly desirable property of future linkers would be cleavage reagents that are easily separated from the newly cleaved compounds.[76]

1.2.4 Split and Mix Synthesis

Reactions on solid supports have many advantages, perhaps one of the most significant is the utilisation of "split and mix" synthesis. Split and mix or recombine synthesis is useful as it facilitates the rapid and synthetically economic production of a large number of different compounds that are then available for screening **Figure 14**.[73]

Split and mix synthesis is accomplished by dividing a batch of resin beads into, for example, three portions reacting each of these portions with a different reagent (A, B and C). The beads are then recombined and the batch split again into three portions. Each of these new portions is then again reacted with a second set of three different reagents (D, E and F) and so on. This splitting and recombining is continued until the desired reaction sequence has been completed. This methodology results in a large number of structurally defined compounds and is even more powerful when tagging is employed. Tagging or encoding enables active compounds present in a library to be identified quickly and simply after screening either "on" or "off" bead.

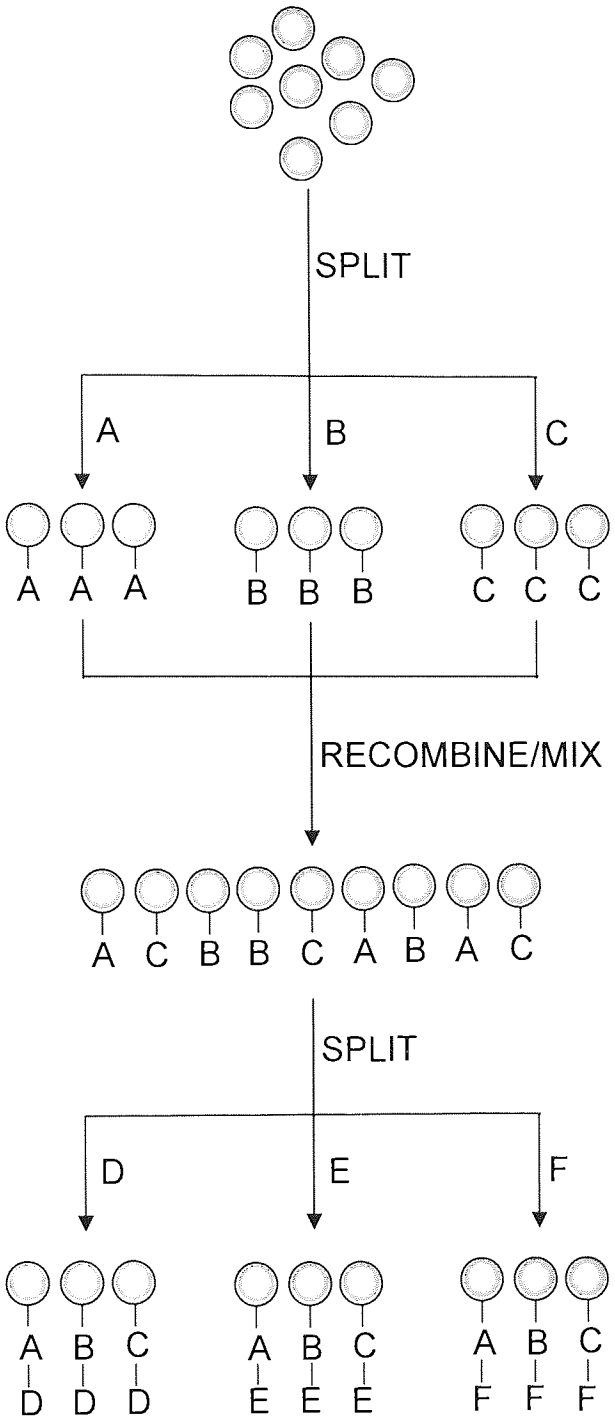

Figure 14: Split and Mix diagram

1.2.5 Encoding Methods

Many different encoding methods exist. Not only do they allow rapid identification of compounds in a library but they also allow for the possibility of automation. The technique of that is encoding chosen will depend upon the reaction conditions required to synthesis the desired library. It is important to remember that if a tag is used the tag itself or the method by which it is added should not adversely affect the reactions to construct the library molecules or indeed the library molecules themselves. The tag will reside on the reaction platform or on the compound itself so careful consideration is required when choosing the best tagging system. Some of the more popular encoding strategies are described under the following headings.[83]

Positional encoding

This type of encoding involves the synthesis of library compounds in discrete reactors. The sequence of synthetic reactions is thus linked intrinsically to the location of the reactor. Spatially addressing is usually accomplished using a 2-dimensional well plate array. This type of encoding was first described by Geysen *et al* where a polypeptide library was synthesised on a 2-dimensional rack of plastic pins.[84]

Electronic encoding

This type of tagging utilises various electronic devices as a means of identification. These devices are attached either to the outside or embedded into micro reactors. Radiofrequency encoded chemistry has been used to produce a 400-membered solid supported taxol library. The solid phase resin used to synthesis the target molecules were encapsulated inside a porous microreactor that contained a radio frequency

transponder. Each stage of the reaction was radiofrequency encoded to allow deconvolution at the end of the process.[85] Another method involves the use of a miniature memory device (MMD) to encode semi-porous micro-reactors[86] that contain a variety of synthesised library members. The MMD enables the identification of a particular reactor at the end of each chemical synthesis step. The sorting of these reactors can be automated by employing "Synthesis Manager" software resulting in automated multi-step syntheses. However, a major disadvantage with electronic tagging devices is with their size that in general is in upward of several millimetres, this in turn results in large reaction volumes being required for library synthesis.

Chemical encoding

This type of encoding involves the attachment of a unique selection of readily analysable molecular tags to each bead that designates the particular set of reaction conditions to which that specific bead has been exposed. This method requires a post assay chemical separation or analysis step to decipher the code.

Certain library molecules are made by syntheses that can be described as self coding. This is where the product is for example a peptide, whose structure can be deconvoluted using standard analytical techniques in the case of a peptide by an automated Edman degradation process. However not all targets that utilise combinatorial chemistry are composed of naturally occurring amino acids that give reproducible results upon Edman sequencing. In order to encode a variety of target molecules a reaction separate from the intended synthesis is required to incorporate a tag. One of the first methods of tagging used the co-synthesis of a peptide chain as the chemical tag. Zuckermann *et al*[87] produced and encoded a peptide library of non natural amino acids by the parallel and

alternating synthesis of two peptide chains. They synthesised a target chain and a coding chain. The target chain was composed of base labile protected none-natural amino acids and the coding chain of acid labile protected naturally occurring amino acids. A bifunctional orthogonally protected linker attached both target and coding chain to the polymer support. **Figure 15** shows a schematic representation of this.

The first step is a synthetic step, a target monomer is added under basic conditions, the acid labile side of the linker is left unmodified. The next step adds the coding monomer under acidic conditions, conversely the target chain is left untouched. The resin portions are then mixed and split and the synthesis followed by tagging processes continued until the synthesis of the target chain is accomplished. Deconvolution is achieved via cleavage of both chains giving a 1:1 solution phase of target and coding adducts, subsequent Edman degradation based sequencing of the coding chain results in the structure of the target chain.

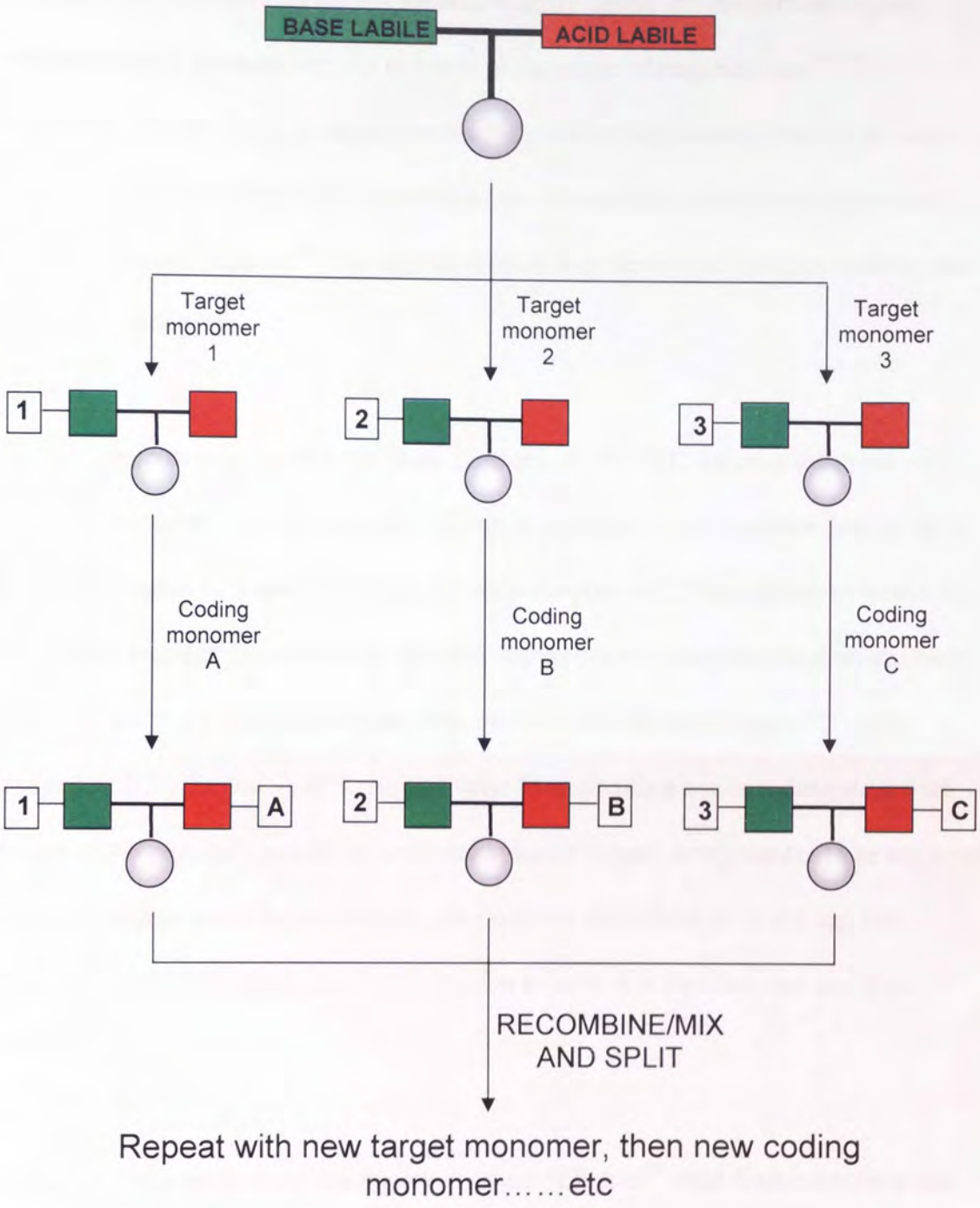

Figure 15: Schematic representation of tagging via the co-synthesis of a peptide chain as the chemical tag

Unfortunately, biopolymers are not suitable tagging agents for use in most organic syntheses simply because they are not inert to the range of reagents used.[88] To circumvent this limitation in tagging technology Still *et al* pioneered the use of inert chemical tags in a binary code that could record the synthetic history of a compound attached to a solid support.[89] The tagging method they developed is represented by the scheme in **Figure 16**.

The solid support resin is split into three portions. A, B and C are coupled to the resin. The portions of resin are then encoded. T_1 tag is attached to the beads bearing A, T_2 to the beads coupled to B and T_1 & T_2 to the resin coupled to C. The batches of beads are then pooled together and randomly split into three portions ready for the next synthetic step. D, E and F are coupled to each of the portions and the solid support is again encoded with T_3, T_4 and T_3 & T_4 respectively. Two coupling and encoding steps with the use of 4 tags results in a library of 9 individually tagged components. Thus any bead picked at random could be successfully decoded via identification of the tag. For example a bead with tags T_1 and T_3 is decoded to have A at position one and D at position two.

In the first demonstration of this tagging method Still *et al*[89] used diazoketones as the molecular tags. The tags were attached to the polymeric backbone of the solid support by a carbene insertion reaction. After assay, detection and deconvolution of the tags was achieved by cleaving the coding tags from the beads, silylating them and analysing them by capillary gas chromatography. Inspection of the resultant chromatograph revealed which tags were present and which were not.[88]

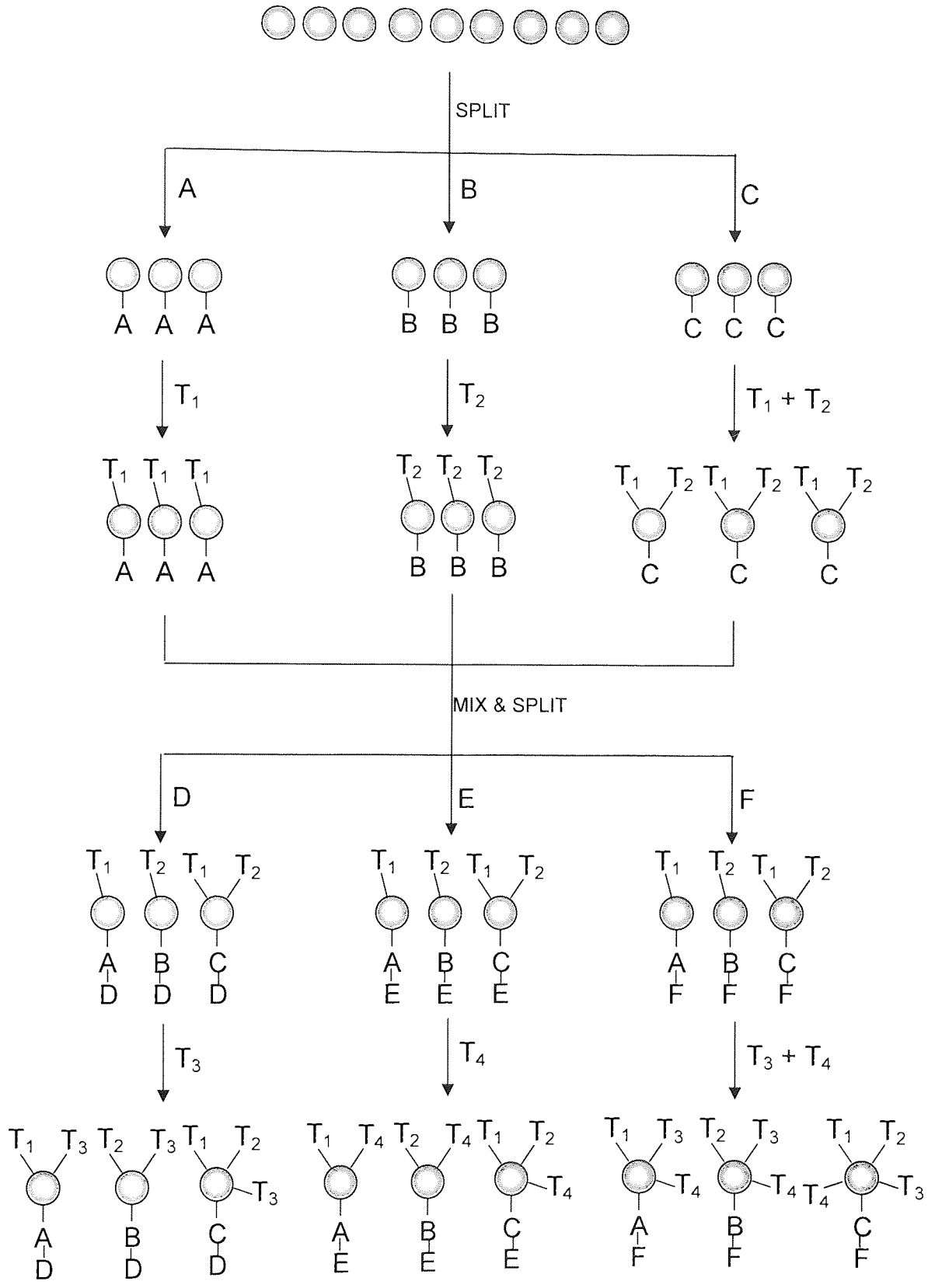

Figure 16: **A schematic representation of the use of inert chemical tags to produce a binary coding system**

Spectrometric encoding

Spectrometric encoding can best be described as including any method where target structure determination is achieved by placing the solid support directly into a spectrometer, therefore eliminating the need for extra steps such as addition or cleavage of the tag.[83] One example of such an approach utilises mass spectrometry that can be used to decode a library if every member of the library has a different mass. Since this will not always be the case isotopically varied chemical tags can be used to encode the reaction history of each member of a library.

Optical encoding

Optical encoding of combinatorial libraries is a new, interesting and challenging area. Lead compound identification could be accelerated if an encoding system based on simply measuring the absorption or fluorescence emission of a bead would enable deconvolution. In order for this methodology to be successful the spectrophotometrically active agent must not be destroyed by the conditions of the chemical synthesis and the optical properties the agent exhibits must not be obscured by the bead or by the compound attached to it.[83] Optical encoding also offers the possibility of extremely rapid sorting and deconvolution of the encoded beads by the employment of fluorescence assisted cell sorting (FACS) equipment.

Bradley *et al*[90] illustrated the use of coloured and fluorescent beads to encode the synthesis of solid supported peptides. The beads used in this study were dyed covalently prior to the synthesis and subsequently inspected under a microscope to identify individual beads on the basis of their photoemissive properties. This is an example of a

non-destructive tagging method that has the added advantage of being very sensitive to detection.

Various other studies similar to the one described above using organic dyes, coloured colloids[91] and in some cases lanthanide complexes, have been reported. Many of the ideas/applications discussed in these papers are excellent but all suffer from the potential limitation of the unfavourable absorption and emission properties exhibited by the fluorophores.

Nie *et al*[71] resolved the problems associated with unsuitable fluorophores by the utilisation of the unique properties exhibited by quantum dots. They describe a method for encoding solid supports optically by embedding different sized quantum dots into polymeric beads in highly controlled ratios. Quantum dots are ideal fluorophores for this purpose because as described earlier their emission wavelength can be tuned readily, and different sized dots can be excited simultaneously by a single wavelength of light.

Nie *et al* incorporated quantum dots into microbeads to optically encode biomolecules. They explained the principles of multiplexed coding, describing how the use of different colours combined with varying intensity levels can produce a large number of individual codes. For example, three colours (Red, Yellow and Blue) at three intensity levels (0, 1 and 2) gives 26 detectable unique codes **Figure 17**.

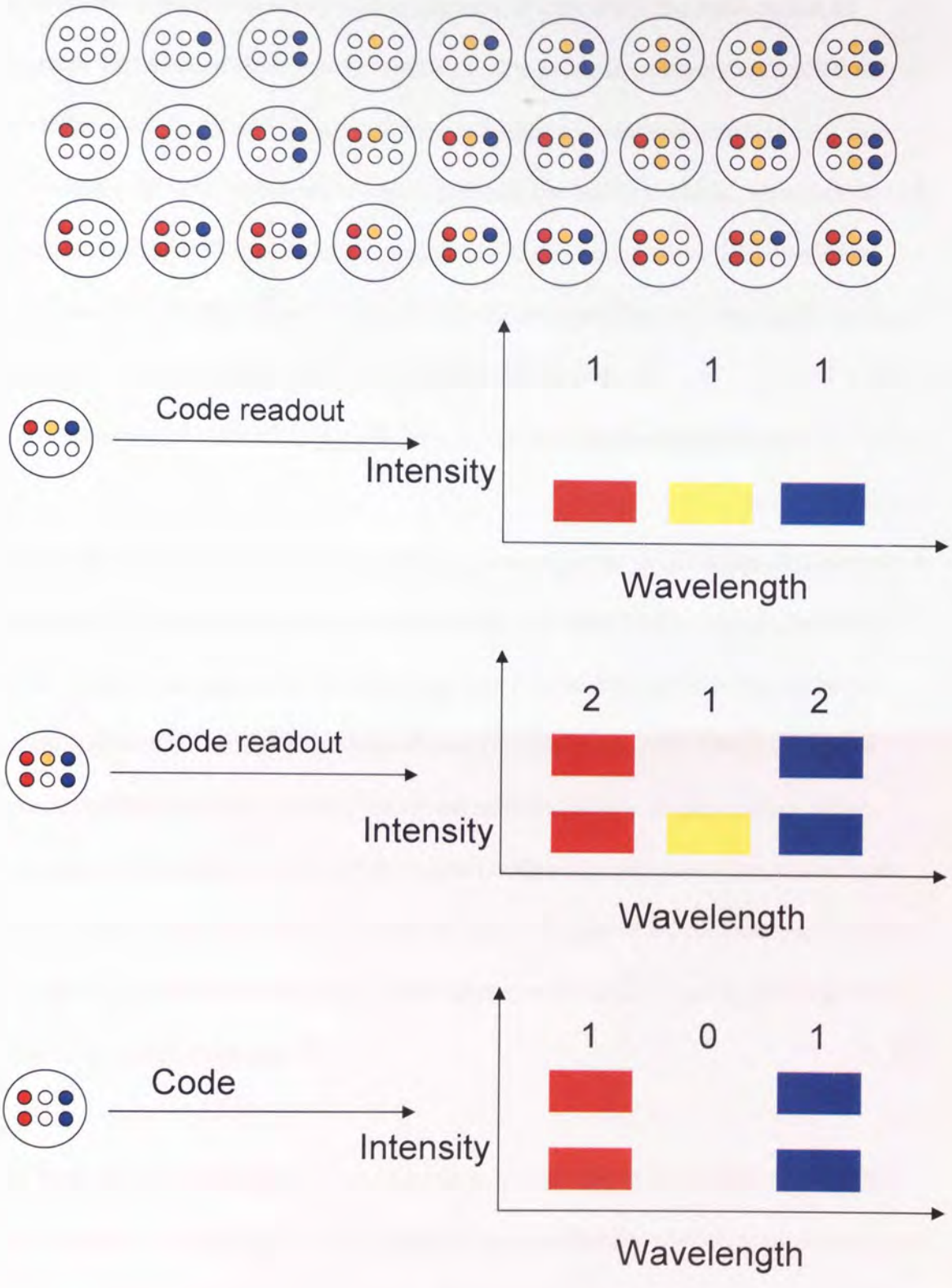

Figure 17: **A schematic representation of the multiplex encoding employed by Nie *et al***

27 codes are possible but when all 3 colours are at intensity 0 the bead cannot be detected. The quantum dots are embedded into the beads in precisely controlled ratios by swelling the beads in different solvents and adding the largest quantum dots first followed by the next largest and so on. The beads are highly uniform, reproducible and yield bead identification accuracies as high as 99.99% under favourable conditions. Since these beads were designed specifically for the encoding of biomolecules it was sufficient to seal the pores via surface polymerisation of 3-mercaptopropyltrimethoxysilane, resulting in aqueous/biochemical tolerance.[71]

Whilst this encapsulation method is ideal for biocompatible applications it is unlikely to be capable of withstanding the rigors associated with solid phase organic chemistry (SPOC) due to an unfortunate disadvantage that results directly from the method of encapsulation and sealing. The encapsulation procedure generates beads where the nanocrystals are incorporated in a non-covalent manner towards the surface of the microbeads. The surface pores are then sealed with a silyl polymer. Consequently the only protection afforded to the nanocrystals from the aggressive reagents and conditions encountered in SPOC is derived from the resistance of the pore sealing polymer to the organic reaction conditions. [37]

The first step towards a quantum dot optically encoded SPOC compatible resin was made recently by O'Brien *et al* who reported the covalent incorporation of nanocrystals into the polymer matrices of resin beads. The surface of the nanocrystal was modified with a ligand that contained a polymerisable unit and the modified nanocrystals dispersed in the monomer phase prior to polymerisation and formation of the beads.[37] Analysis of the beads revealed uniform and irreversible incorporation of the

nanocrystals into the beads.[37, 92] These resin beads still require the addition of functionalisation and evaluation of their ability to tolerate the wide range of commonly encountered reagents. However, additional protection of the dots before they are added to the suspension polymerisation is possible if this is required.

The stability of nanocrystals is related to the ligand coating that they posses. It is the coating that protects the surface from aggressive agents and prevents aggregation of the particles with each other. It has been suggested that there are two main types of stability issues relating to nanocrystal/ligand complexes. Type 1 addresses the dissociation of the ligand from the inorganic core, when this occurs it is likely to lead to loss of the nanocrystals unique properties and precipitation of the nanocrystal from solution. Type 2 results from the attack of the inorganic core by aggressive agents. The degree of protection offered to the core depends vastly on the type of ligand present.[46] Therefore in order to increase the stability of nanocrystals in their chosen application both these issues need to be attended to.

Various methods of nanoparticle have been reported, however the vast majority attempt to stabilise the nanoparticle core by the deposition of a shell layer or coating on the nanocrystal that acts as a physical barrier to the penetration of aggressive agents. This type of approach deals with type 2 instability, issues relating to type 1 and to a certain extent type 2 also, can be tackled by global cross-linking or polymerisation of the coating agent.[39]

In the majority of cases the coating is added after the initial synthesis of the nanocrystal. However an interesting method known as monomer self-assembly, uses the formation of

the polymer coat as a template to restrict the growth of the nanocrystal. This method produces poly(methyl methacrylate) thin coated PbS nanocrystals that are instantaneously stable, resistant to aggregation and ideal for applications in the field of LED's.[93]

More commonly though the coating is added to the pre-synthesised nanocrystal. The addition of the coating after nanoparticle synthesis is a more generic coating strategy as it allows for a greater diversity in the core material chosen and subsequently a better tailoring of the composite to its chosen application. For example Au/SiO_2,[94] CdS/SiO_2[94] and $CdSe/ZnS/SiO_2$[95] composites have all been prepared using a similar procedure. The deposition of a silica shell onto the surface of nanocrystals has been shown to improve the photostability and luminescence compared with nanocrystals of the same type with no shell.[94]

Core-shell CdSe/ZnS silica coated nanocrystals have been prepared via the polymerisation of surface bound (3-sulfonylpropyl)trimethoxysilane (MPS). The polymerisation can be controlled to an extent producing water compatible particles with a final diameter ranging from 30nm to 1μm. The tuneable diameter of the final particles make them ideal for use in photonic crystal applications.[95]

Living radical polymerisation or atom transfer radical polymerisation (ATRP) has also been utilised to produce polymer coated nanoparticles.[96] Dense uniform polymer shells can be grown directly from the surface of the particle creating a barrier to the environment. Displacement of the surface ligand with an initiating species turns each individual particle into a macro-initiator **Figure 18**.

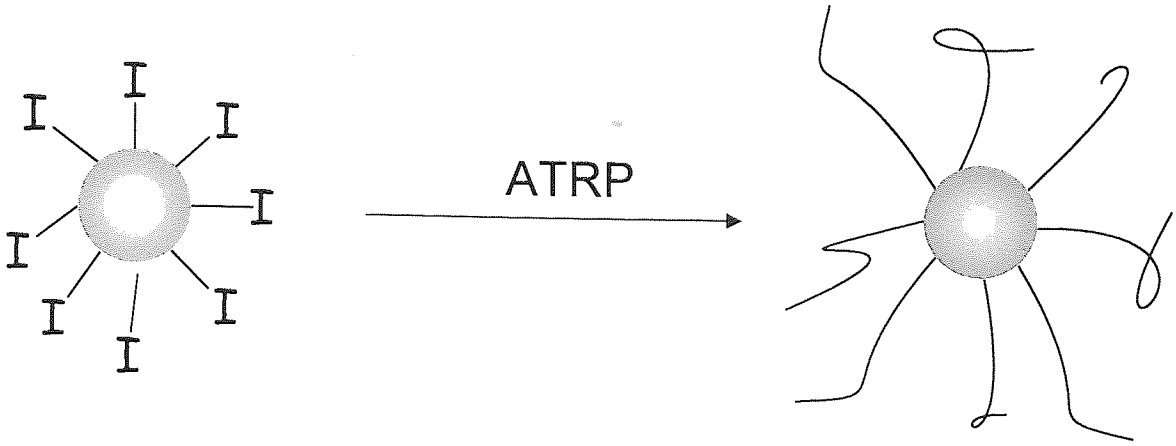

Figure 18: **A schematic of living radical polymerisation on the surface of a nanoparticle**

Various different monomers can be added to the surface tailoring the polymer layer for specific applications. The thickness of the shell will increase until the stock monomer is depleted resulting a degree of control over the final particle size. Gold nanoparticles have been coated in this manner with polybutylacrylate[97] and polymethylmethacrylate[98] for potential applications in nanoelectronics, optics and DNA diagnostics.

Dendron ligands have also proved to be an important and useful way of stabilising pre-synthesised nanocrystals. Organic dendron ligands used for this purpose possess a focal binding functionality at one end and hyperbranched organic functionality at the other **Figure 19**. This inherent cone shape renders them ideal for filling the spherical ligand layer on the surface of the nanocrystal. It is thus possible for the dendrons to close pack at the surface forming a sterically crowded barrier to the surface of the nanocrystal.[99] The flexible branches become inter- and intra-molecularly tangled, resulting in a more impenetrable barrier, slowing diffusion of aggressive agents. Photochemical and chemical stability of dendron derivatised nanocrystals increases with the generation of dendron used.

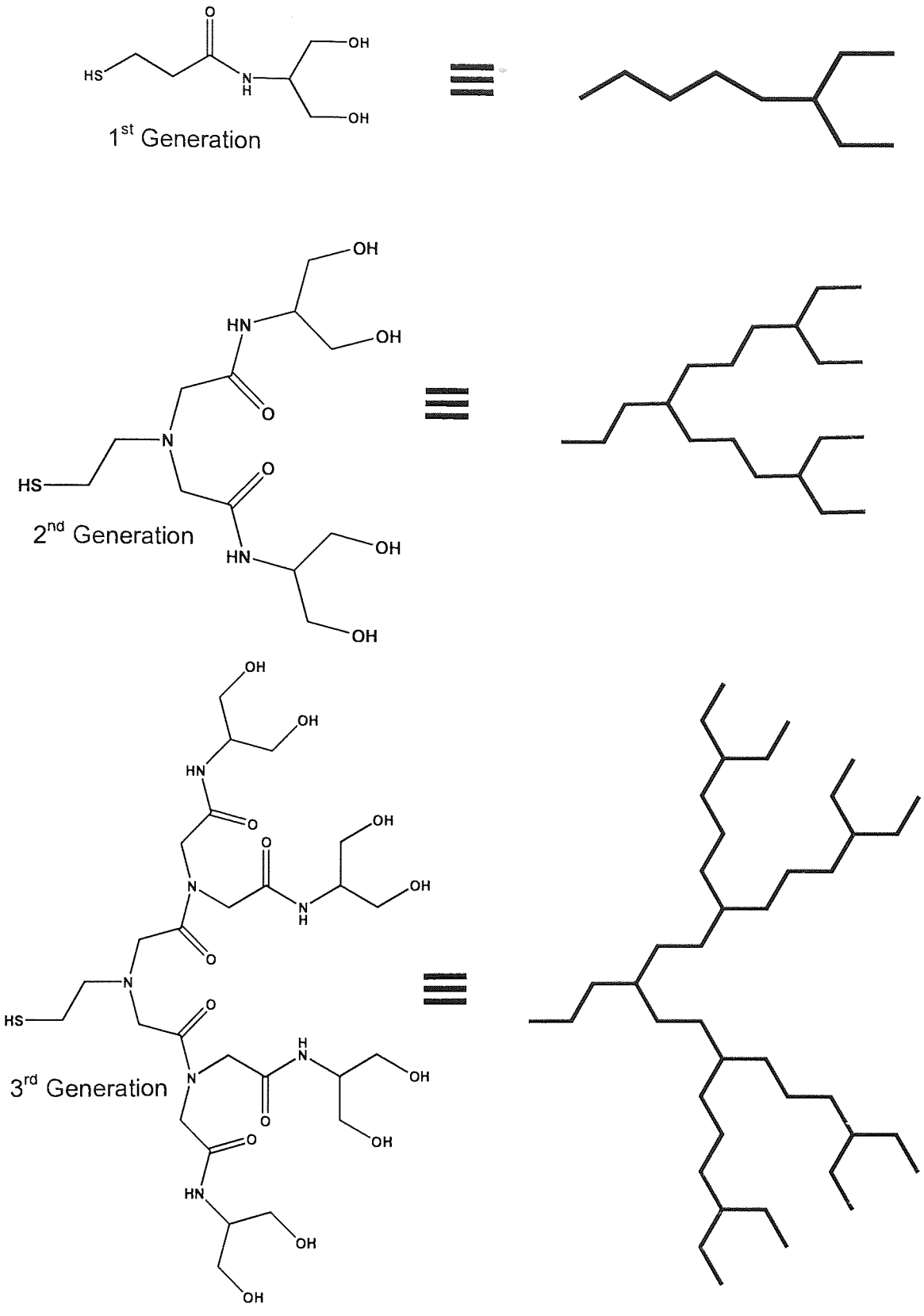

Figure 19: **Examples of 1st, 2nd and 3rd generation dendron cone ligands and their corresponding schematic representations**

Figure 20 demonstrates schematically the difficulty encountered with diffusion of aggressive agents through a ligand layer with increasing branching. However it should be noted that a thick ligand shell is not always desired as this increase in size may detrimentally affect the nanocrystal for its chosen application.[39]

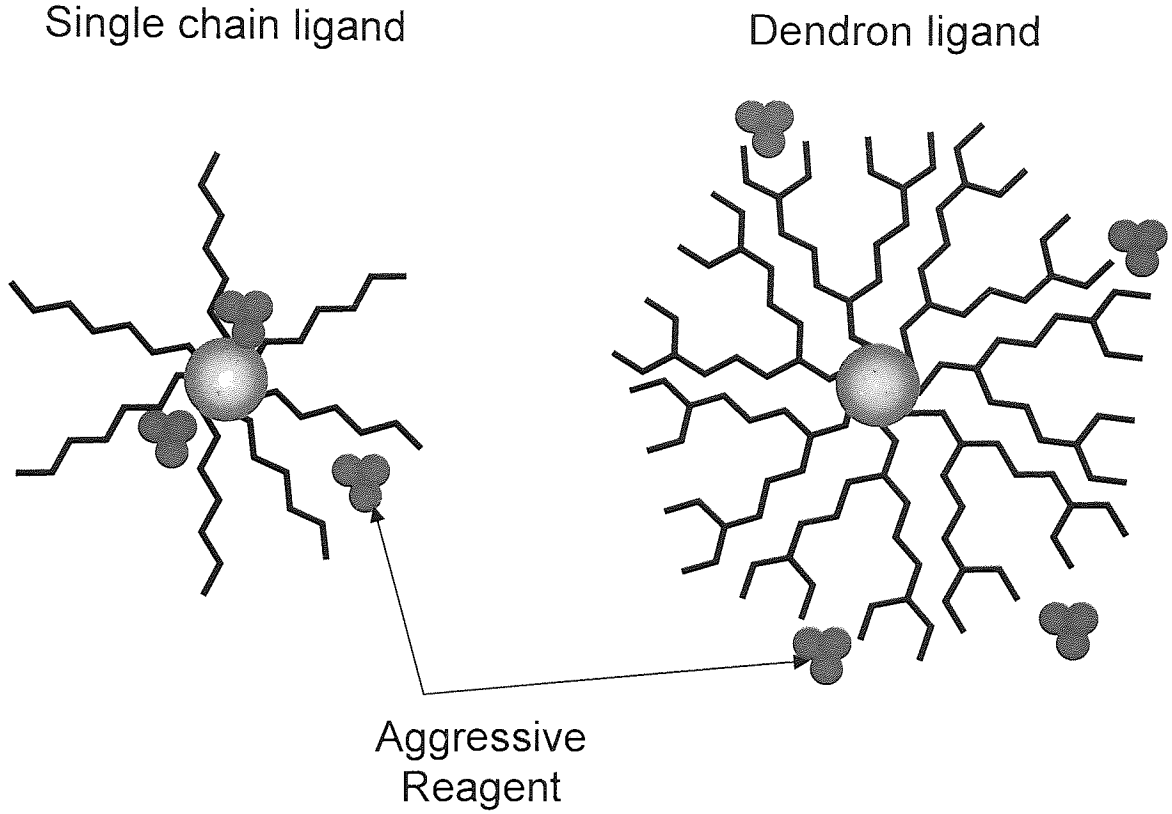

Figure 20: A schematic representation demonstrating the possible steric effects encountered by a molecule attempting to diffuse through different ligand layers

The substantial improvement in the stability of nanocrystals derivatised with branched ligands instead of single chains can be further increased by extensive global cross-linking of these surface ligands. Global cross-linking of a monolayer of dendrons leads to the encapsulation of the nanocrystal in a dendron box. This encapsulation addresses both of the main causes of instability. The linking of the ligand molecules to one

another prevents dissociation of individual ligands form the surface, and the inter- and intra-chain tangling coupled with the formation of the global network of connected molecules creates a more impenetrable barrier to aggressive agents.[39] Peng *et al* created globally cross-linked boxed nanocrystals from generation-3, allyl terminated dendrimers via a Grubbs catalysed, ring closing metathesis (RCM) polymerisation reaction. Polymer encapsulated CdSe/CdS dots were produced using 2nd generation Grubbs catalyst in a highly dilute system **Figure 21**.[46]

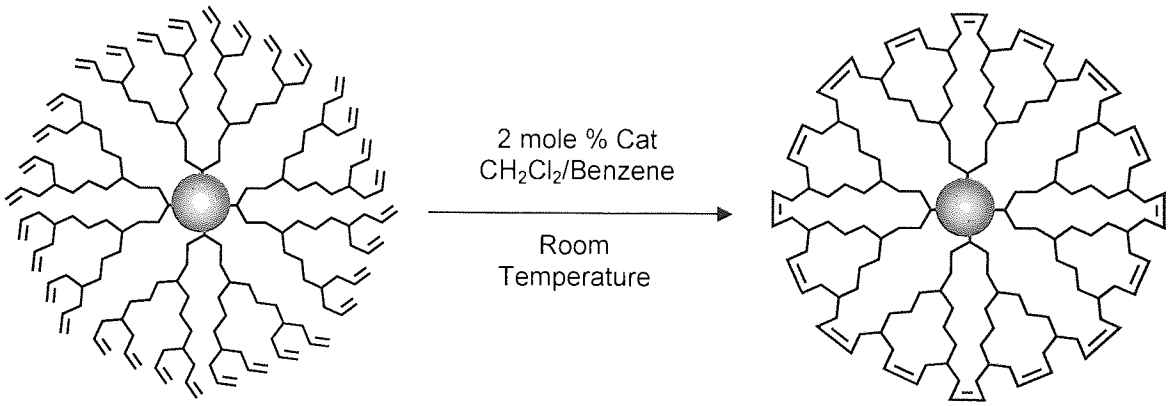

Figure 21: A schematic representation of the global cross-linking of ligands surrounding a central nanoparticle.

The formation of this thin but highly cross linked layer improved the stability of the encapsulated nanocrystals towards a wide range of conditions. Evaluation of the boxed nanocrystals revealed superior stability upon exposure to strong acid and strong oxidant, even improved stability during thermal sintering when compared with none cross-linked dendron nanocrystals.[39, 101]

Although dendron ligands are ideal for creating cross-linked boxes, their production often involves multi step syntheses and as mentioned previously the thickness of the layer they provide may be detrimental to the final application of the nanocrystal. It is

possible to produce globally cross-linked networks with more compact ligands. Ligands that possess two or three bonding sites coupled with a flexible interior (chain entangling) are ideal candidates for producing thin but impenetrable layers.[39]

Feldheim *et al*[100] designed and synthesised a tripodal alkene terminated alkylthiolate ligand in order to maximise intermolecular cross-linking on the surface of a nanocrystal **Figure 22.**

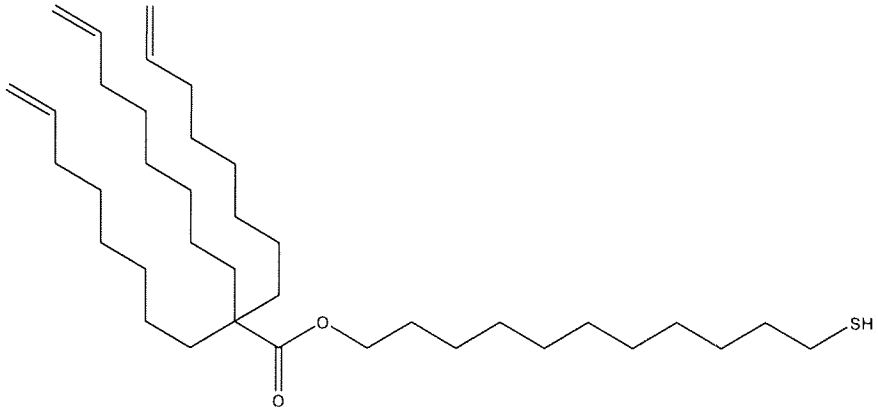

Figure 22: Structure of a tripodal alkene terminated alkylthiolate ligand

The tripodal ligand was extensively cross-linked via Grubb's catalyst mediated RCM to produce an extensively cross-linked network on the surface of gold nanocrystals, etching of these particles yielded spherical, structurally rigid hollow polymer capsules **Figure 23.**

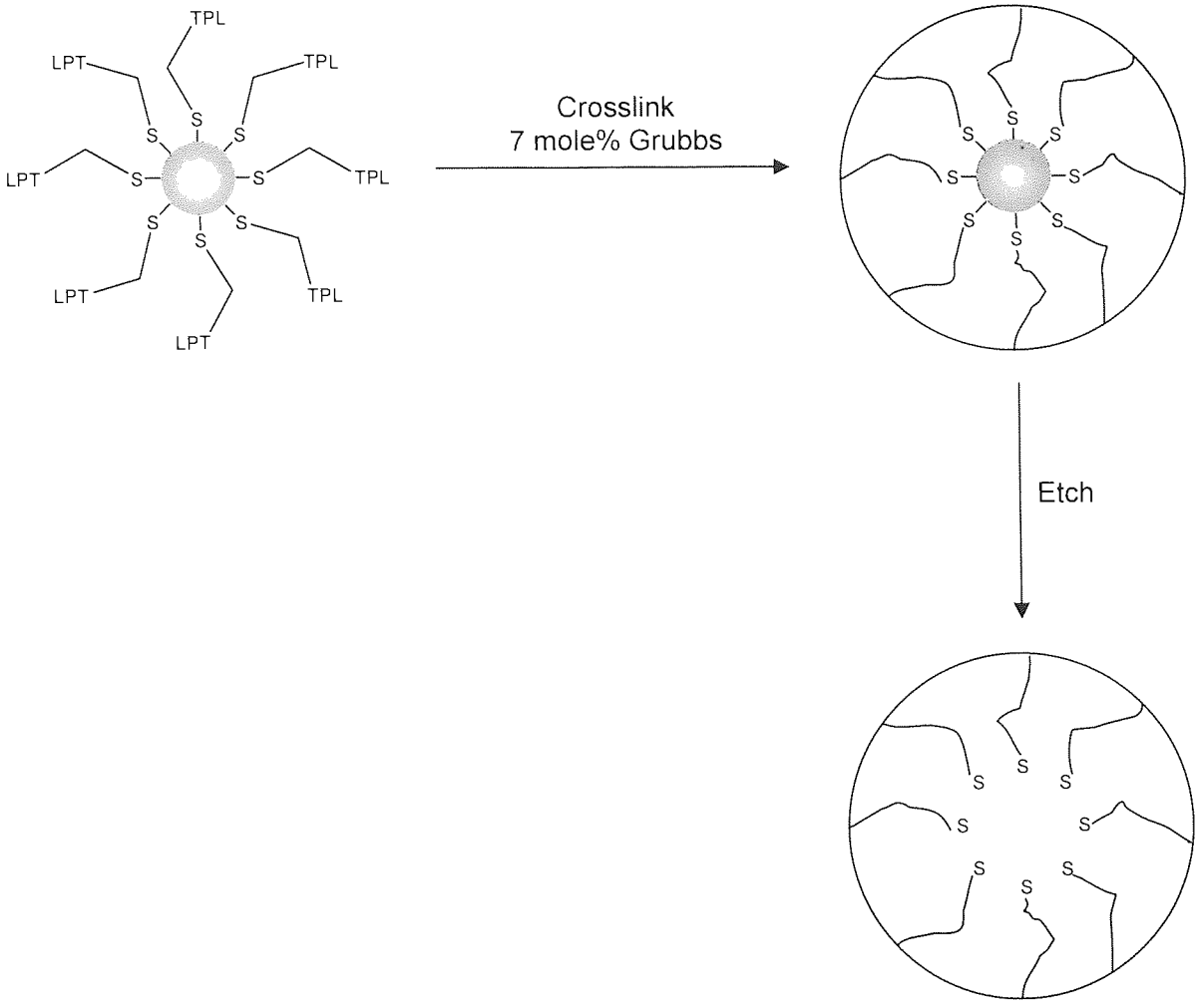

Figure 23: **A schematic representation of the formation of a cross-linked polymer encapsulated nanoparticle followed by removal of the nanoparticle to produce a hollow polymer capsule *via* acid etching**

1.3 Olefin Metathesis

Olefin metathesis was initially observed in the 1950's by industrial chemists working in the petrochemical sector with a variety of multi-component homogeneous and heterogeneous catalyst systems. These systems were poorly defined and consisted of high valent transition metal salts combined with main group alkylating agents that were sometimes deposited on solid supports.[101, 102] In 1956 Herbert. S. Eleuterio, a chemist working for DuPont produced a propylene-ethylene copolymer by passing propylene over molybdenum supported on alumina. In 1960 Peters and Evering of the Standard Oil Company of Indiana reported the production of ethylenes and butenes from propylene after exposure to molybdenum oxide on alumina treated with triisobutyl aluminium. The same disproportionation of propylene after treatment with molybdenum hexacarbonyl supported on alumina was observed in 1964 by Banks and Bailey while working for Phillips Petroleum.[103] Unfortunately these useful and versatile double bond scrambling reactions remained baffling up until 1967.

These reactions could not be explained any of the standard and accepted reactions involving olefins at that time. The process was finally explained by a group of researchers working at Goodyear Tire and Rubber who initially recognised that ring opening polymerisation (ROMP) and cross metathesis (CM) were essentially the same reaction. This realisation led Calderon *et al* to introduce the term olefin metathesis to encompass and describe both reactions.[101, 104, 105]

Today olefin metathesis refers to a number of seemingly different reactions in which a transition metal complex catalyses the redistribution of groups around a carbon-carbon

double bond.[101] **Figure 24** demonstrates the different applications of olefin metathesis.[103]

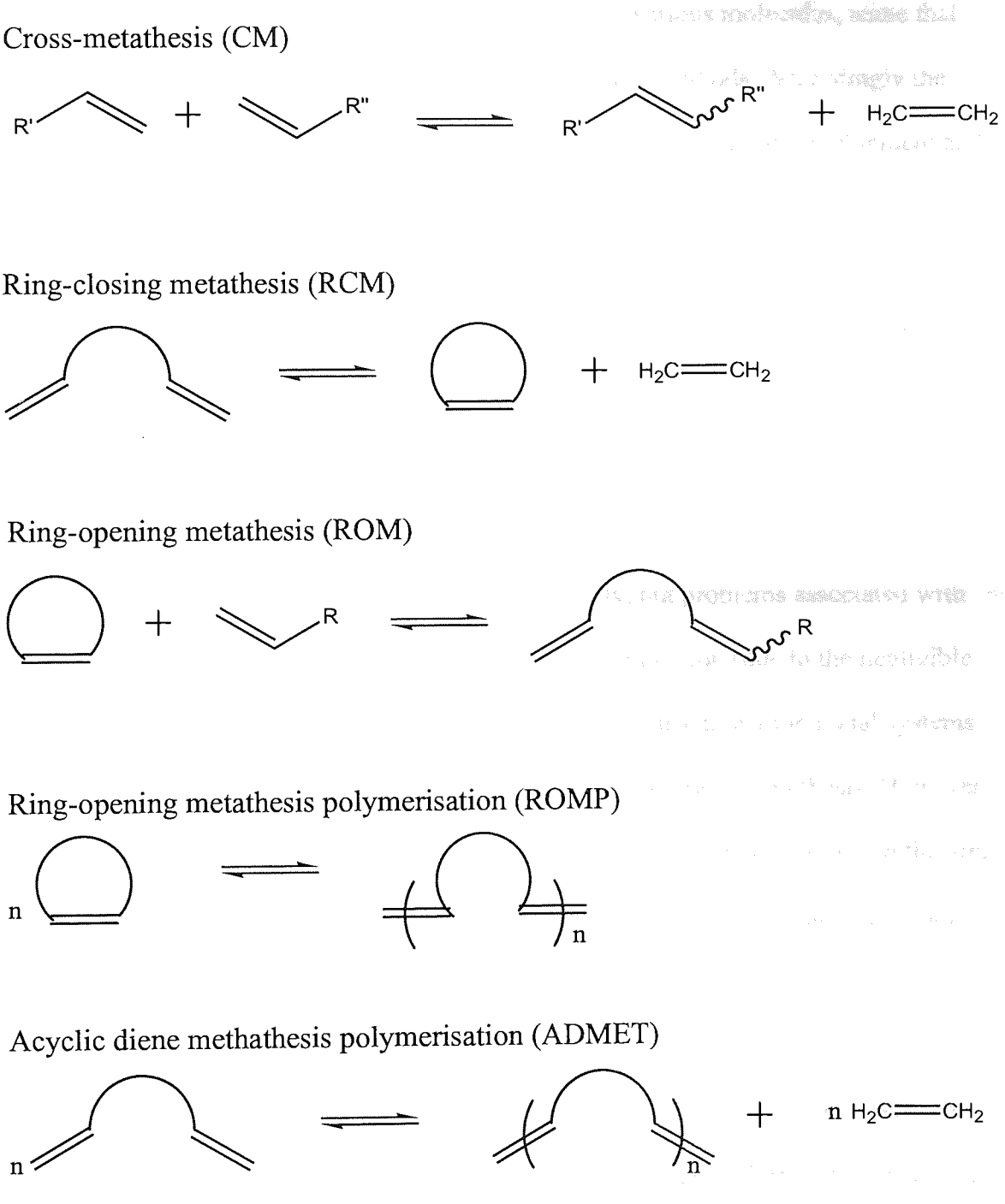

Figure 24: **A schematic depicting the different types of olefin metathesis reactions available**

Carbon-carbon bond forming reactions are some of the most important reactions in organic chemistry, they make it possible to build up the desired carbon skeleton of target compounds. The utilisation of olefin metathesis in synthetic and industrial chemistry has provided novel and reproducible routes to various molecules, some that would prove extremely challenging to synthesise via other methods. Accordingly the scope and versatility of olefin metathesis has expanded vastly with the development and improvement of the catalytic systems available.[101]

The first catalytic systems that were used in the petrochemical industry when metathesis was observed initially were low cost and easy to prepare. Although these early systems are of little use in organic synthesis, they were and continue to be invaluable in the petrochemical and plastics industry. The advantages olefin metathesis could provide synthetic chemistry were envisaged almost immediately, but problems associated with low functional group tolerance and lack of control over initiation (due to the negligible amount of the active species formed) associated with the early transition metal systems hampered the adoption of olefin metathesis in conventional organic synthesis. However the potential synthetic advantages of this method maintained research interest in the area which finally came to fruition in the late 80's early 90's with the development of more complex and selective catalysts.[103, 103]

The design and development of efficient and selective transition metal complexes that catalyse olefin metathesis posed an interesting challenge to researchers. Observation of early multi-component catalysts demonstrated that many different transition metals could be employed to successfully accomplish metathesis. An obvious first step in catalyst design would be to ascertain if certain metals were 'better' than others.

However a lack of understanding relating to the nature of the active species, the involvement of additional components and the overall mechanism of metathesis made evaluation of individual metals impossible.[101]

Prior to the publication of the generally accepted mechanism proposed by Chauvin, various schemes with widely differing intermediates were suggested. Calderon *et al* predicted a cyclobutane intermediate that is complexed to the metal present **Figure 25.**[106, 103]

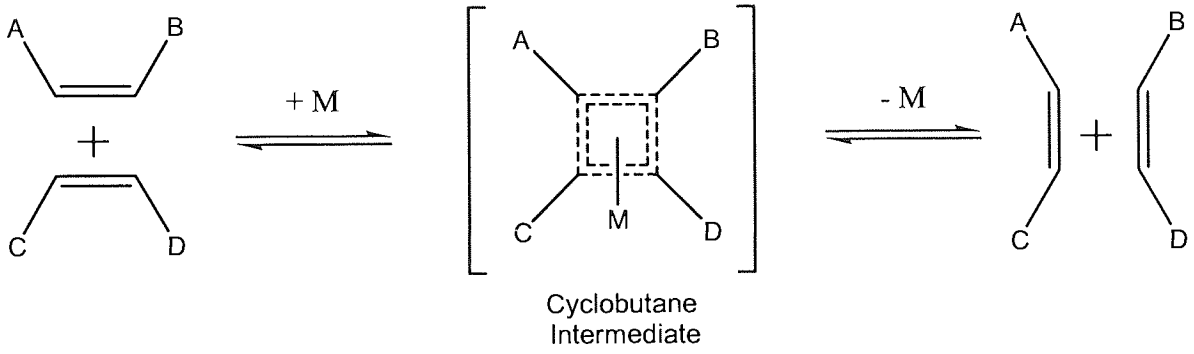

Figure 25: A schematic of the formation of the cyclobutane intermediate predicted by Calderon

Before this mechanism was dismissed it became known as the conventional mechanism. Doubts about this theory arose from three observations, firstly the introduction of cyclobutanes into olefin metathesis systems does not yield alkenes, secondly cyclobutanes are not products formed from olefin metathesis and thirdly cyclobutane has no accessible valencies for bonding to metals.[103, 113]

Grubbs proposed several theories that were later disproved, to account for the observed products of metathesis. The first of these hypotheses involved a rearranging

metallacyclopentane intermediate and resulted from the observation of a tungsten catalysed metathesis reaction **Figure 26.**[107]

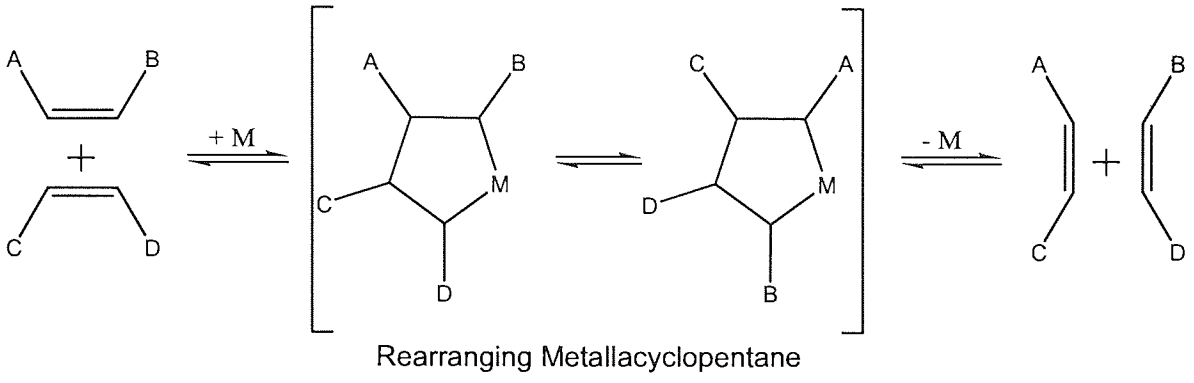

Figure 26: A schematic of the formation of the metallacyclopentane intermediate predicted by Grubbs

The second theory proposed by Grubbs involved a pair-wise exchange of alkylidenes (metal carbenes) through a *quasi*-cyclobutane intermediate similar to that proposed by Calderon **Figure 27.**[108]

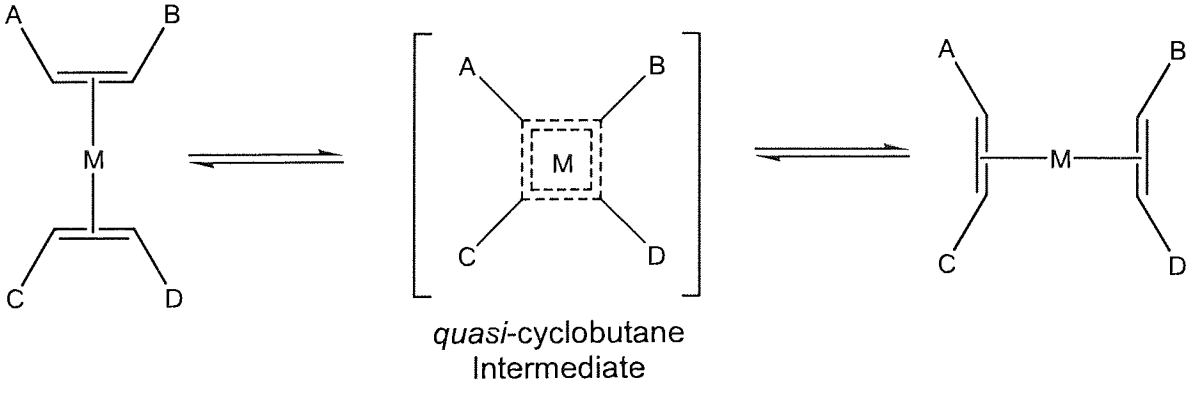

Figure 27: A schematic of the formation of the *quasi*-cyclobutane intermediate predicted by Grubbs

Finally in 1971 just prior to Chauvin's revelation, Pettit suggested a tetramethylene complex was responsible for the redistribution of groups in the metathesis process **Figure 28**.[103, 109]

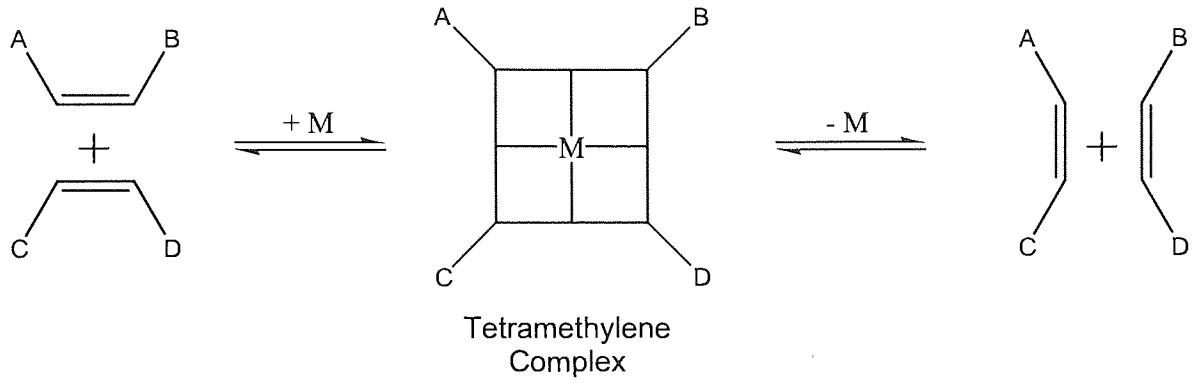

Figure 28: A schematic of the formation of the tetramethylene complex predicted by Pettit

In 1971 Chauvin and Herisson studied the metal catalysed co-reactions of cyclic and acyclic olefins and proposed that the mechanism of metathesis involved the interconversion of a metal alkylidene (metal carbene) and an olefin via the formation of a metallocyclobutane **Figure 29**.[101, 110]

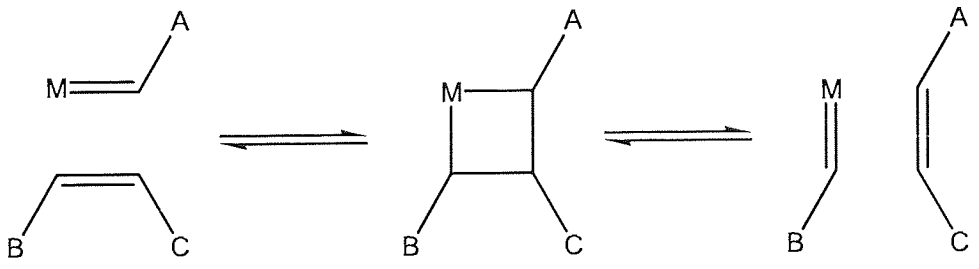

Figure 29: A schematic representation of the mechanism of olefin metathesis proposed by Chauvin and Herisson

Chauvin and Herisson came to the above mechanistic conclusions following analysis of the products produced from the reaction of cyclopentene and 2-pentene. The metal catalysed metathesis reaction of cyclopentene and 2-pentene produces three different sized products, C_9, C_{10} and C_{11} in the ratio of 1:2:1. The conventional mechanism accepted at the time predicted the formation of only the C_{10} product and was unable to account for the complete exchange of the double bonds. The formation of three products could not be explained using a cyclobutane intermediate but was easily explained via Chauvin and Herisson's suggestion **Figure 30** below.

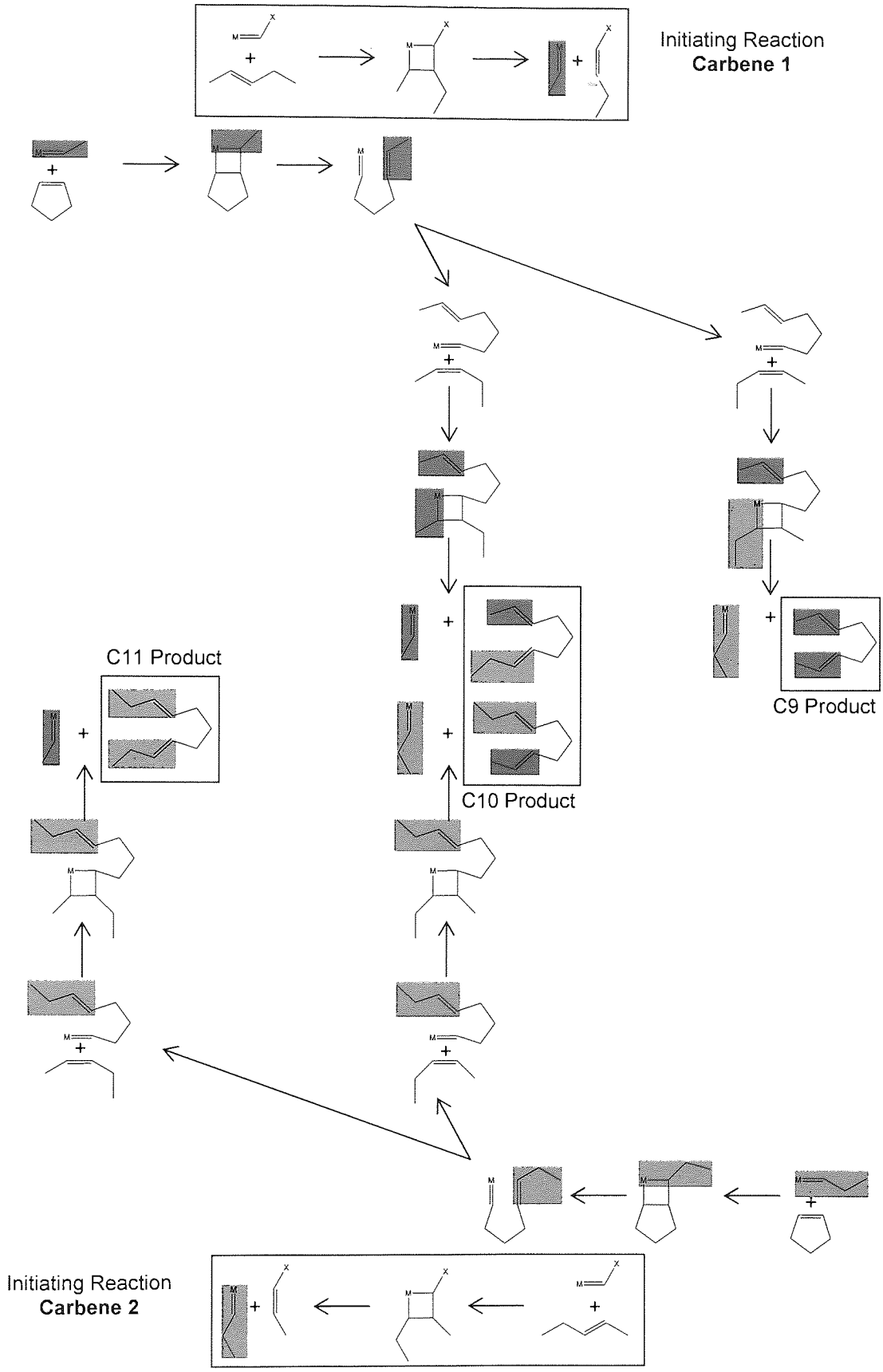

Figure 30: Chauvin and Herisson explanation for the metal catalysed reaction between cyclopentene and 2-pentene

This mechanism finally became generally accepted and was consistent with subsequent experimental evidence. However, this process took several years and a large number of other supporting publications.[101] A large part of the argument against acceptance of this mechanism resulted from the fact that although it explained the previously unexplainable it was unable to exclude existing mechanisms. An example of this discrepancy can be found in the metathesis reaction of cyclooctene and pentene. The Chauvin and Herisson's metal carbene mechanism predicts the formation of three products see **Figure 32**, but only one product is formed experimentally and this is the sole product predicted by the conventional mechanism **Figure 31**.[103, 106]

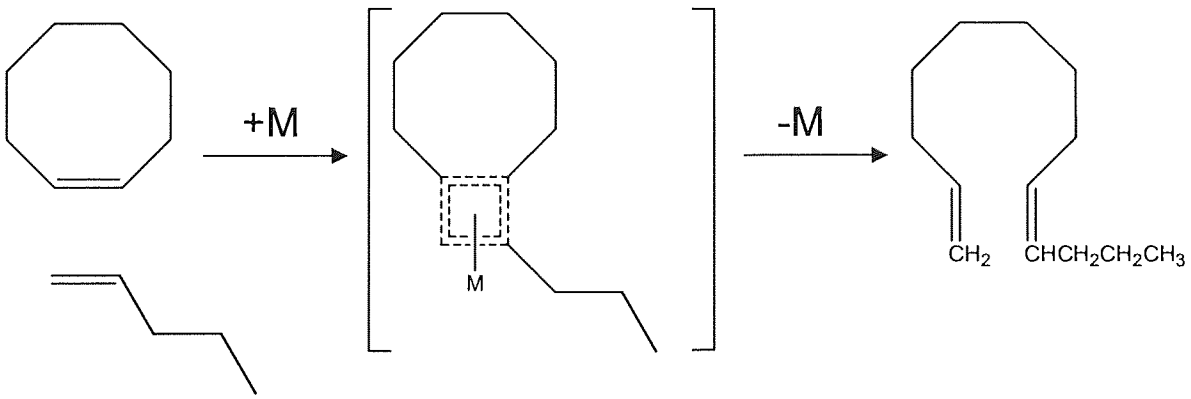

Figure 31: A schematic representation of the conventional mechanism

This discrepancy continued to cause confusion until the publication of a paper in 1975 by Thomas J. Katz.[111] This paper discussed the products of olefin metathesis reaction from the point of view of the kinetics involved. Katz explained that the products formed from the metathesis reactions of cyclic and acyclic olefins depends on the relative stability of the carbenes formed. The individual stability of the two carbenes involved in the reaction effects the kinetics of the alkene displacement stage of the reaction.

Formation of a stable carbene promotes rapid displacement of the alkene and carbene from the intermediate complex. Conversely if the carbene formed is less stable then rate of dissociation of the alkene and carbene from the intermediate complex is slow in comparison **Figure 32** (highlighted route).

Applying this 'relative stability of carbenes' hypothesis to Chauvin and Herisson's mechanistic prediction of the products from the reaction of cyclooctene and pentene, modifies the prediction suggesting the sole experimentally observed product. Katz methodology predicts that carbene **Y** is more stable than carbene **X Figure 32.** Therefore the dissociation of the alkene from the intermediate metal complex to form carbene **X** is slow in comparison to the alkene dissociation to form carbene **Y**. The rapid kinetics of the steps involving carbene **Y** compared to that of carbene **X** dominate the reaction and the C13 product is formed in a vast majority via the single mechanistic pathway highlighted in **Figure 32.**

Katz stated that if the groups on either side of the double bond of the acyclic olefin are very different then kinetic factors will mean that one carbene will be formed more quickly than the other and only one final product will be formed selectively. Conversely if the groups are similar then the role of kinetics is not so pronounced and three products are formed.[103] Shortly after the Katz paper Grubbs published a paper coming to the same conclusion as Katz but explaining the exchange of groups using topically labelled alkenes rather than differently substituted olefins.[101]

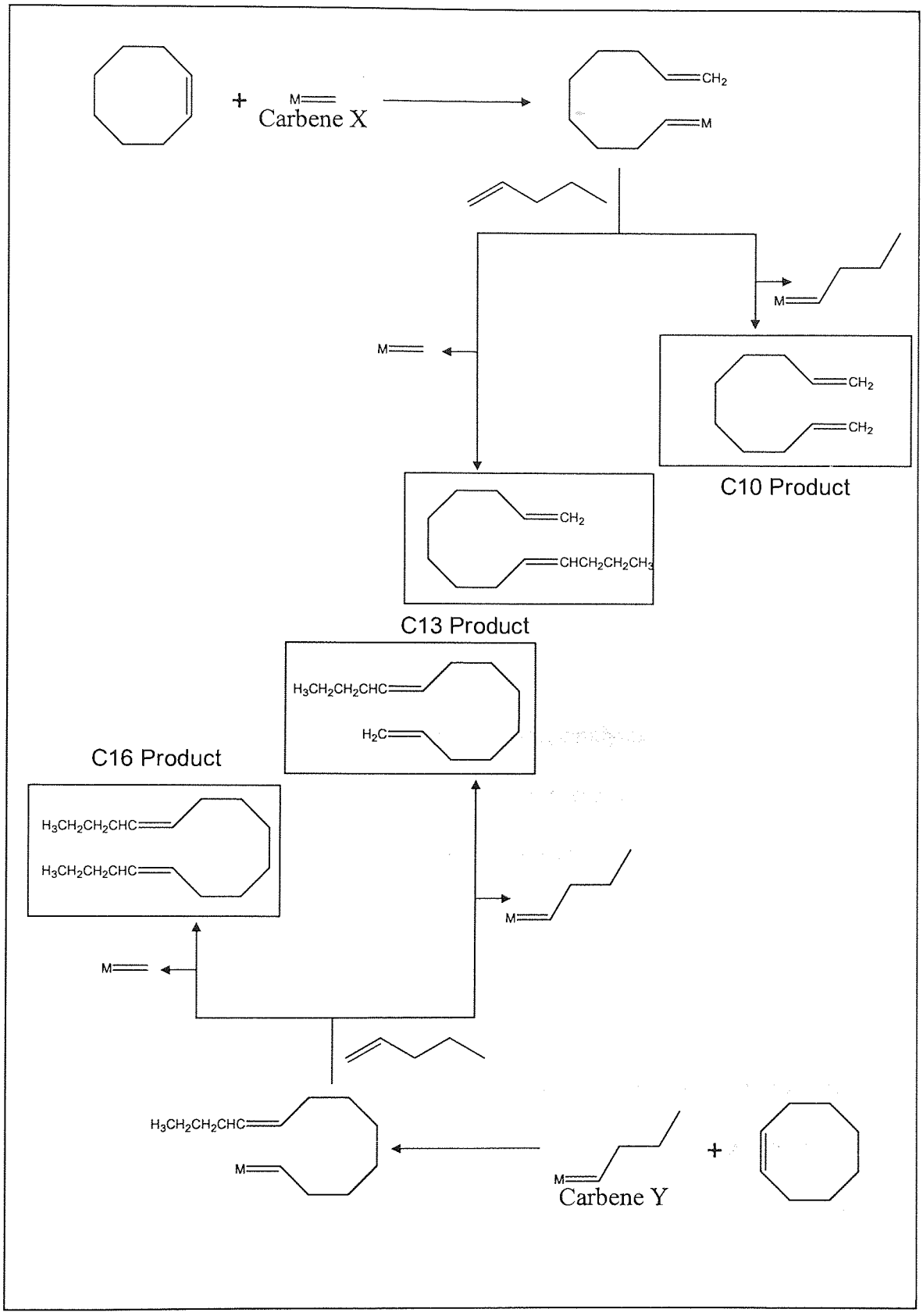

Figure 32: **Katz's explanation for the ratio of products formed from the metal catalysed reaction of cyclooctene and pentene**

The publication of the Katz paper heralded a new and interesting era in olefin metathesis. Katz proposed that the new generation of catalysts used in olefin metathesis should comprise of metal alkylidenes since these were the initiators of the reaction. This design rational directed subsequent efforts to synthesise suitable metal alkylidenes and lead to the discovery of the first single component homogeneous catalysts.

The first single component homogeneous catalysts were comprised of a wide variety of transition metals complexed to various ligands including the all important alkylidene. This diversity gave researchers the opportunity to study the relationship between structure and activity in much greater detail than ever before. The new complexes showed much improved initiation and activity under significantly milder conditions making them far more suited for use in synthetic organic chemistry. Although greatly improved the situation was still far from perfect. The catalysts exhibited differing functional group tolerance that ranged from moderate to poor, this coupled with severe sensitivity to moisture and oxygen made them awkward to use and far from the ideal universal catalyst.[101]

Research in this area continued and began to focus on the area of functional group tolerance. In any catalytic system the presence of functional groups other than those directly involved in the reaction can detrimentally interfere with the activity of the catalyst. More functional groups can be present both in the reactants and in the solvent used. Additionally impurities such as water or oxygen may have detrimental effects on certain catalytic systems and these groups can affect the catalytic activity of the highly reactive metal centres by either binding competitively to or irreversibly destroying the active species. Improved functional group tolerance can be achieved by designing

catalysts that react preferentially with the desired functionality. **Table 2** shows the functional group tolerance of transition metals commonly used in metathesis catalysts. The reactivity of the metal towards the functional group increases from bottom to top, however the catalytic activity decreases.[101]

TITANIUM	TUNGSTEN	MOLYBDENUM	RUTHENIUM
Acids Alcohols & Water Aldehydes Ketones Esters & Amides OLEFINS	Acids Alcohols & Water Aldehydes Ketones OLEFINS Esters & Amides	Acids Alcohols & Water Aldehydes OLEFINS Ketones Esters & Amides	OLEFINS Acids Alcohols & Water Aldehydes Ketones Esters & Amides

Table 2: **A table comparing the functional group tolerance of four transition metals**

Ruthenium reacts with preferentially with olefins and tolerates the presence of alcohols, carboxylic acids, aldehydes, ketones, esters and amides. However ruthenium was not immediately considered a viable candidate for the catalysis of metathesis due to problems associated with the synthesis of well defined ruthenium alkylidene species.[101] The slow initiation times and low activity of the available ruthenium complexes resulted in researchers concentrating on the less selective but more reactive systems based on molybdenum and tungsten. Richard R. Schrock developed a catalytic system based on molybdenum that exhibited very high reactivity coupled with some selectivity in

reacting with olefins over other functional groups. This system began to be utilised by organic chemists and later became known as the Schrock catalyst **Figure 33**.[103]

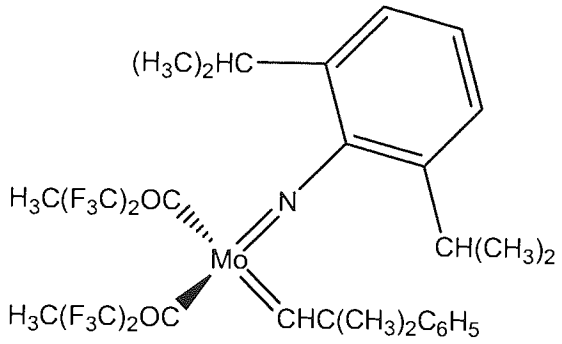

Figure 33: Structure of Schrock Catalyst

Some protection of various functional groups was still required when using the Schrock catalyst but this catalyst began to enable the routine use of olefin metathesis in everyday synthetic organic chemistry.

The next breakthrough in catalytic design was made by Robert H. Grubbs who applied methodology relating to the synthesis of tungsten alkylidenes to the synthesis of the corresponding ruthenium complex. This species showed excellent functional group tolerance but unfortunately suffered from low activity. Grubbs continued research into this species and four years later produced the first catalyst that eventually became known as Grubbs catalyst **Figure 34**.[103]

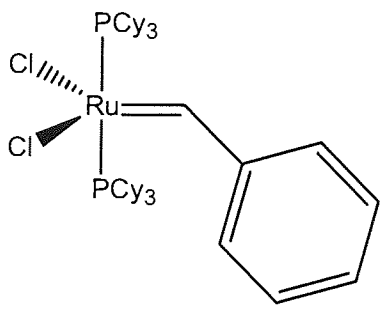

Figure 34: Structure of Grubbs Catalyst (first generation)

This catalyst showed excellent selectivity and was more stable than the Schrock catalyst but still suffered a significantly lower reactivity when compared to the molybdenum system.[112] Grubbs did not stop refining his catalyst and research involving the exchange of the ligands around the ruthenium yielded the release of the much improved second generation Grubbs catalyst[103] **Figure 35**. Second generation Grubbs catalyst is prepared from Grubbs catalyst by the substitution of one of the PCy_3 ligands with an *N*-heterocyclic carbene. This modification of the parent catalyst produces dramatically higher activity with olefins and thus a greater stability.[108, 113] The emergence of the *N*-heterocyclic ruthenium complex has closed the reactivity gap between the molybdenum and ruthenium systems without sacrificing functional group compatibility.[112]

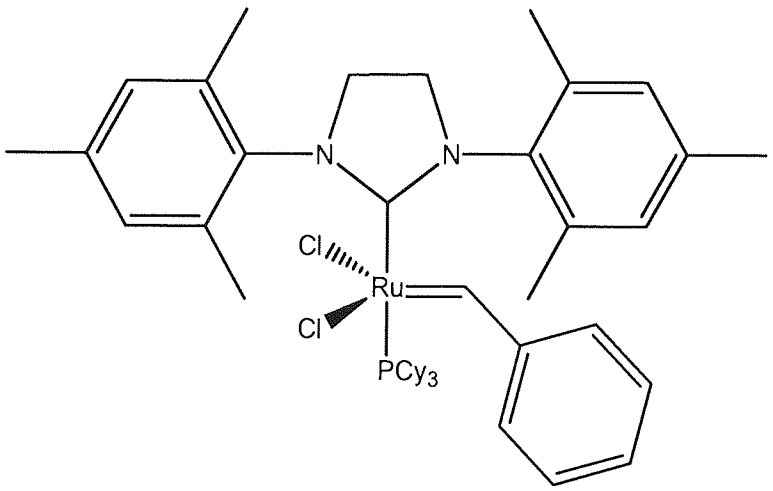

Figure 35: Structure of Grubbs second generation Catalyst

The increased reactivity of the second generation Grubbs catalyst compared with that of Grubbs catalyst can be explained by examination of the mechanism responsible for ruthenium-complex mediated olefin metathesis. Both generations of catalyst participate

in the same catalytic cycle shown in **Figure 36**[112, 113, 114], however differences associated with their rates of initiation and propagation lead to differences in reactivity.[112]

The catalytic cycle is initiated when a ruthenium complex enters the cycle by the dissociative loss of a phosphine resulting in a 14 electron intermediate. This intermediate can now follow one of two paths, it can rebind to a phosphine and leave the cycle reforming the starting alkylidene or it can bind to an olefin and continue through the cycle propagating the metathesis reaction.[112, 114]

The differences in reactivity of the two types of Grubbs catalyst relate to their behaviour in these initial stages. Grubbs catalyst undergoes rapid loss of the phosphine ligand, however this rapid initiation also results in rapid trapping of the intermediate by free phosphine leading to competive binding between the phosphine and substrate olefin. Second generation Grubbs catalyst does not undergo initiation as efficiently and looses its phosphine much less readily, re-uptake of the phosphine is also slow. This difference in the rate of initiation allows the 14 electron intermediate formed by the second generation catalyst to cycle through multiple olefin metathesis reactions before being deactivated to the starting alkylidene by rebinding to a phosphine.[112, 113, 114]

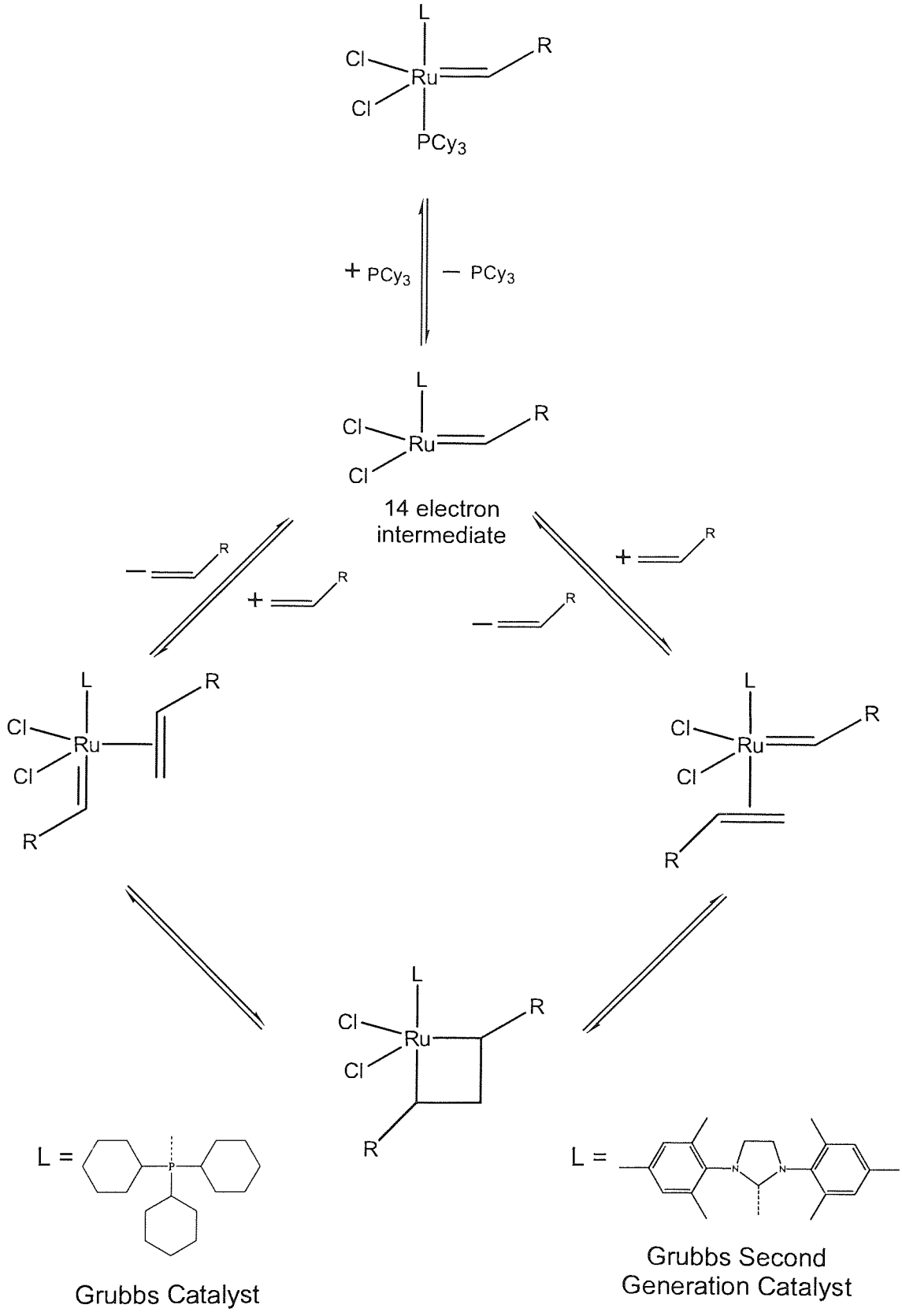

Figure 36: A schematic of the Grubbs catalytic cycle

Schrock and Grubbs will likely be remembered as the two chemists most responsible for the development of metathesis catalysts. Their work in this area ultimately led to the utilisation and acceptance of olefin metathesis.[103] Both catalytic systems are in wide use today giving a choice depending on the type of reaction desired. Grubbs catalyst is more commonly used since it tolerates standard organic techniques (vac line and inert atmosphere) and can be handled easily.[108] If a higher reactivity is required for example in systems possessing sterically demanding or electron deficient olefins Schrock catalyst can be utilised by employing more stringent conditions (vac line and a dry box).[108, 112]

1.4 Diffusion ordered Spectroscopy

Nuclear magnetic resonance spectroscopy (NMR) is valued as one of the most powerful tools utilised by chemists for structure elucidation. Standard NMR spectroscopic techniques require pure samples in order to produce a spectrum where the signals of one chemical species dominate. However recent advances in NMR techniques are now permitting its use for the analysis of mixtures.[115]

Diffusion ordered spectroscopy (DOSY) is the result of one such advance and is a technique that can facilitate the virtual separation of mixtures of compounds. DOSY is a non-invasive two dimensional NMR experiment that produces spectra that account for chemical shift in one dimension and diffusion behaviour in another.[116]

The ability to separate the signals is a product of the relationship between the individual properties of a molecule and its self diffusion behaviour. Self diffusion or translational motion is dependent on various physical parameters. The size and shape of the molecule, the temperature of the system and the viscosity of the surrounding media all affect the self diffusion of a species.[117]

Self diffusion is a consequence of the thermal energy of a molecule that results in constant motion of that molecule in solution.[118, 119] Different molecules comprising a mixture experience the same environment but differ in size and shape. This inhomogenity in geometry produces differences in diffusion behaviour. The self diffusion of each species can be measured resulting in individual diffusion coefficients for each component of the mixture.[115, 118, 119]

Assuming a spherical shape for the molecules in solution, the diffusion coefficient can be described by the Stoke-Einstein equation **Equation 1**.[115, 116, 117, 118 & 119]

$$D = k T / 6 \pi \eta r_h \qquad \textbf{Eqn 1}$$

Where

D	is the diffusion coefficient	($m^2 s^{-1}$)
K	is the Boltzman constant	($J K^{-1}$)
T	is the temperature	(K)
η	is the viscosity of the solvent	($N s m^{-2}$)
r_h	is the hydrodynamic radius	(m)

Pulsed field gradient NMR spectroscopy can be used to measure the translational motion of molecules.[119] Diffusion coefficients can be obtained by measuring the displacement of a molecule over a given time. The relationship between the distance a molecule can travel in a single specified direction during a pre-set length of time can be represented by **Equation 2**.

$$z = (2 D t_d)^{1/2} \qquad \textbf{Eqn 2}$$

where

z	is the distance travelled	(m)
D	is the diffusion coefficient	($m^2 s^{-1}$)
t_d	is the diffusion time	(s)

Since not every molecule will travel this distance during t_d, z is composed of an ensemble of averages of many particles and is known as the mean square distance.[118, 120]

Plotting values of the root mean square distance travelled against the square root of the diffusion time results in a straight line, the gradient of which is the diffusion coefficient of the molecule in question.[118, 120]

DOSY interrogates the diffusion behaviour of different species by spatially labelling molecules in solution. Following excitation a gradient pulse encodes the exact position of molecules by producing a spatially dependent phase angle. The system is then allowed to evolve over a pre-determined time (diffusion occurs). If the molecules have moved their new positions are decoded by the second gradient pulse. By collating diffusion data at several different gradient strengths diffusion coefficients relating to each component can be produced.[119, 120]

This powerful technique has only recently been developed and is currently finding applications in many areas of chemistry and biology. It has proved useful in the analysis of zeolites, polymers, liquid crystals, surfactants, combinatorial chemistry and in particular can be used to provide invaluable information about the structure and activity of molecular transport.[118]

CHAPTER 2

RESULTS AND DISCUSSION

2.1 Synthesis of functionalised phosphine oxides and sulphides

Quantum dots are usually produced with a simple non-functionalised capping agents such as trioctylphosphine oxide (TOPO) **1** or hexadecylamine (HDA) **3**. As discussed in the introduction the nature of these surface ligands is directly related to the behaviour and compatibility of the quantum dots with a specific environment. Exchange of the original capping ligand with alternative suitable functionalised ligands provides a useful route to tailoring the properties of the quantum dots to a particular application. Many examples of modified nanocrystals bearing 'designer ligands' can be found in the literature. **Figure 37** contains some examples of the breadth of designer ligand structures that have been reported.[37, 38, 41, 42, 43, 46, 47, 97, 98, 150]

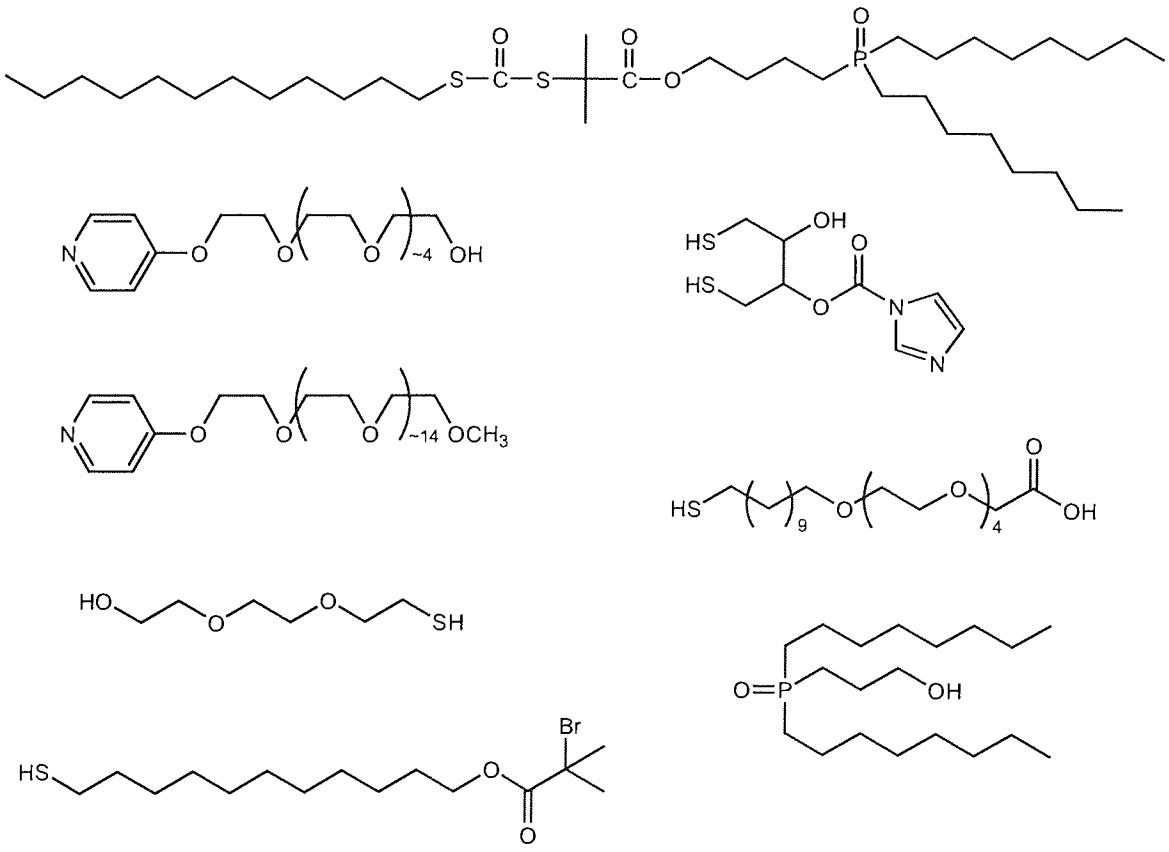

Figure 37: Structures of existing designer ligands published in the literature

Commonly the desired functionality is incorporated into ligands that mimic well established surface ligands **Figure 38**. Ligand dioctyl(octene)phosphine oxide (DOOPO) **6** mimics TOPO **1** closely the only difference in their structures being the addition of a polymerisable functionality at the end of one of the alkyl chains in ligand **6**. The P=O group anchors the ligand to the surface of the dot and is thus remote from the double bond. It is unlikely the double bond will interfere with ligand quantum dot complexation and therefore it is anticipated that ligand **6** should complex quantum dots as well as ligand **1**. A range of 'designer ligands' with different functionalities were synthesised for evaluation and surface modification of quantum dots for a variety of different applications.

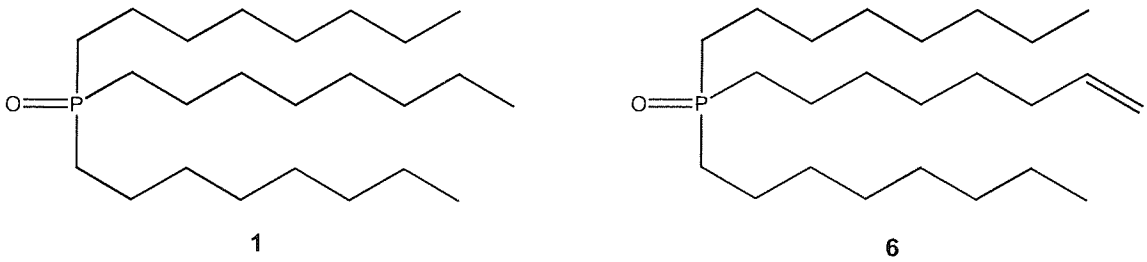

1 6

Figure 38: Structure of TOPO and DOOPO

Initial work involved the design and synthesis of several different symmetrical phosphinic acids produced from the reaction between dibutyl phosphite **13** with various functionalised and non-functionalised Grignard reagents.[38, 121, 122, 123, 124, 125] Further reaction of these phosphinic acids with different functionalised reagents produced a range of symmetrical and unsymmetrical tertiary phosphine oxides.[38]

2.1.1 Dioctlyphosphinous acid (DOPA) 14[38, 121, 122, 123, 124, 125]

Synthesis of the phosphine oxides began with the production of a simple straight chain phosphinous acid intermediate that possessed no extra functionality. DOPA **14** was synthesised from the reaction of dibutyl phosphite **13** with three equivalents of the corresponding Grignard reagent derived from 8-bromooctane **15 Scheme 1**.

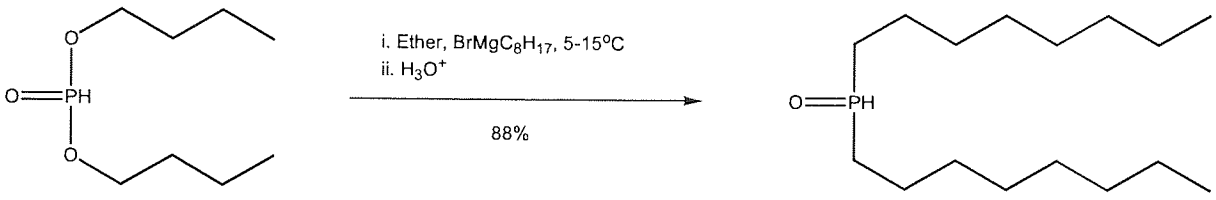

13 **14**

Scheme 1: Synthesis of DOPA

The in-situ formation of the Grignard reagent is mildly exothermic and careful drop-wise addition of the 8-bromooctane **15** solution was required to ensure gentle reflux was maintained. Upon completion of the addition extra heating was undertaken to ensure complete formation of the Grignard reagent prior to the cooling necessary during the addition of dibutly phosphite **13**. The reaction between the Grignard reagent and the phosphite is assumed to be fairly rapid, evident from the fact that longer reaction times did not significantly increase the yield of the final product. Acidification of the reaction mixture was required to form the DOPA **14**. Neutralisation, followed by an aqueous work up that occasionally required the addition of brine or sodium chloride (NaCl) to assist with the separation resulted in the production the crude product as a fluffy white solid in a good yield of 88%.

Unfortunately attempts to monitor the progress of the reaction using thin layer chromatography (TLC) failed due to the inability to visualise DOPA **14** and 8-bromooctane. A range of different stains including ammonium molybate in sulphuric acid, iodine, concentrated sulphuric acid and molybdic acid in ethanol and plate types including silica gel with and without organic binding agents were evaluated without success.

A small portion of the crude product was recrystallised from hexane providing a white powdery solid in a modest yield of 48%. Both the crude and recrystallised products were characterised, comparison of the two sets of data revealed that the aqueous work up was sufficient for purification in future.

All of the analytical data obtained for the product of this reaction **Scheme 1**, was in agreement with data previously reported for DOPA **14**.[121, 124, 125] However since DOPA **14** was intended to serve not only as a direct precursor for a large number of closely related ligands but also as a model for the synthesis of functionalised phosphinous acids it was deemed necessary to assign all of the spectroscopic data obtained for DOPA **14** as thoroughly and unambiguously as possible.

Both the low resolution and high resolution mass spectroscopic analysis show the presence of a molecule with the correct mass consistent with that of the product. The infra red spectrum was also entirely consistent with the expected product. A medium to strong peak at 2356 cm^{-1} corresponds to the P-H functionality, a second strong peak at 1467 cm^{-1} characteristic of the P-CH_2 moiety and a third strong peak at 1160cm^{-1} is indicative of the P=O function. Also the absence of a strong peak in the region of 1050-

1030cm^{-1} that would imply the presence of P-O suggests that the reaction had been successful.

The ^{1}H and ^{13}C NMR spectra of organophosphorus compounds exhibit extra complexity resulting from splitting of the NMR signals of atoms proximate to the phosphorus nucleus. ^{31}P comprises 100% of the natural abundance of phosphorus and possesses a spin of a ½, consequently it is capable of splitting the NMR signals of neighbouring atoms. The magnitude of the splitting observed is affected by a number of factors such as the charge or covalency of the phosphorus nucleus, the other groups attached to the phosphorus and the distance of the affected nucleus from the phosphorus atom. Although the complexity of the spectra can be increased, the splitting of the signals can provide extra information that can prove useful in structure elucidation.[124, 126]

The ^{1}H NMR spectra of DOPA **14** is consistent with the structure of the desired product. The signals present exhibit the predicted chemical shifts, integrate as expected and possess coupling constants within the acceptable ranges reported for compounds of this type.[123, 124, 126] The triplet centred at ∂ 0.87 ppm with a coupling constant of 6.7 Hz corresponds to the two terminal methyl groups. Overlap of the individual signals of the CH_2 groups comprising the two alkyl chains produces a broad multiplet from ∂ 1.10-1.80 ppm. Unfortunately overlap and broadening of the signals in this region prevents any useful interpretation of individual ^{31}P-^{1}H or ^{1}H-^{1}H spin couplings. The most interesting aspect of this spectrum arises from the widely separated doublet centred at ∂ 6.75 ppm. This doublet corresponds to the unique proton directly attached to the phosphorus atom and has a very large coupling constant of 445 Hz. The magnitude of this value is consistent with previously published couplings of this type in similar

compounds such as diethylphosphinous acid ($^1J_{P-H}$=468 Hz), *diiso*propylphosphinous acid ($^1J_{P-H}$=468 Hz) and dibutylphosphinous acid ($^1J_{P-H}$=458 Hz).[123, 127, 128]

Analysis of the ^{13}C NMR spectrum reveals that it is in accordance with the intended structure of DOPA **14**. Examination of the spectrum reveals that it is composed of eleven signals **Figure 39**.

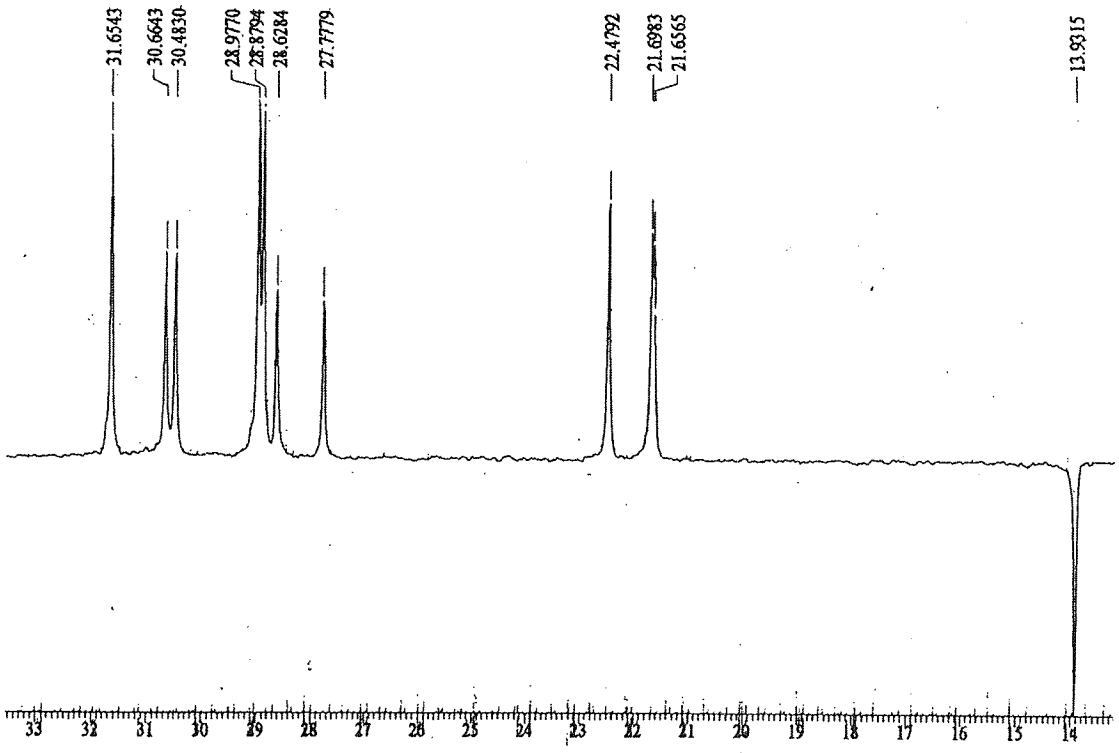

Figure 39: ^{13}C **spectrum of DOPA 14**

The increased number of signals, over the 8 that might be initially be expected is due to the previously discussed ability of the phosphorus atom to split the NMR signals of neighbouring atoms.[126] Unfortunately the factors influencing P-C couplings are quite complex, investigations into this area have discovered that electronegative and steric effects are reflected in the P-C couplings.[129] Despite this complexity and variation in the

magnitudes of the couplings, various trends have been observed. Assignment of the signals is made possible due the regular shielding and coupling patterns exhibited by phosphine oxides. As expected the coupling constant of the signals corresponding to the carbon C-1 to the phosphorus are the largest **Figure 40**.

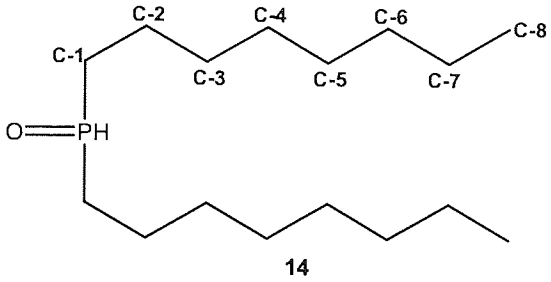

Figure 40: Numerically labelled structure of DOPA 14

The carbon at the C-2 position presents as a doublet with a small coupling and finally the coupling for the signals produced by the carbon in the C-3 position is characteristically large.[124, 130] The position of the signals and the values calculated for the P-C couplings in the ^{13}C spectrum of DOPA **14** are in accordance with those found in the literature.[124] Coupling of the phosphorus to the first three carbons in the chain is evident, the assignments are based on chemical shift, magnitude of coupling constant and intensity.

Referring to the ^{13}C spectrum of DOPA **14 Figure 39** it can be observed that the two peaks of similar intensity at ∂ 27.8 ppm and ∂ 28.6 ppm are in fact a doublet corresponding to C-1 centred at ∂ 28.2 ppm with a large coupling constant of $^{1}J_{PC}$=63.8 Hz. The carbon at position C-2 is responsible for the two closely positioned signals at ∂ 21.6 ppm and ∂ 21.7 ppm that are centred at ∂ 21.7 ppm. The P-C coupling constant for this doublet is $^{2}J_{PCC}$= 3.1 Hz and is small. The two signals for the final carbon coupled

to the phosphorus can be found at ∂ 30.5ppm and ∂ 30.7ppm with a relatively large coupling constant of $^{3}J_{PCCC}$=13.6 Hz. It is possible that the phosphorus is coupled to the carbons further down the alkyl chain since a coupling of $^{4}J_{PCCCC}$=1.4 Hz has been reported for the terminal methyl of phosphine oxide possessing a butyl chain.[130] However the signals corresponding to the carbons at positions C-4 and C-5 of this molecule are very close to one another at ∂ 28.9 ppm and ∂ 29.0 ppm respectively. Thus any further couplings present are likely to be small and obscured by overlap on a spectrum recorded on a 75MHz machine such as the one at Aston.[124, 131]

The mechanism of the reaction proceeds via the formation of a dialkyloxyphosphinylmagnesium halide **Figure 41**. This is formed by the abstraction of the proton directly attached to the phosphorus producing the diethyloxyphosphinylmagnesium bromide and octane as a by-product. The diethyloxyphosphinylmagnesium bromide then undergoes alkyl-de-alkoxy-substitution with the remaining two equivalents of Grignard reagent. Finally the phosphinous acid is formed by protonation with excess acid.[121, 125,132, 133]

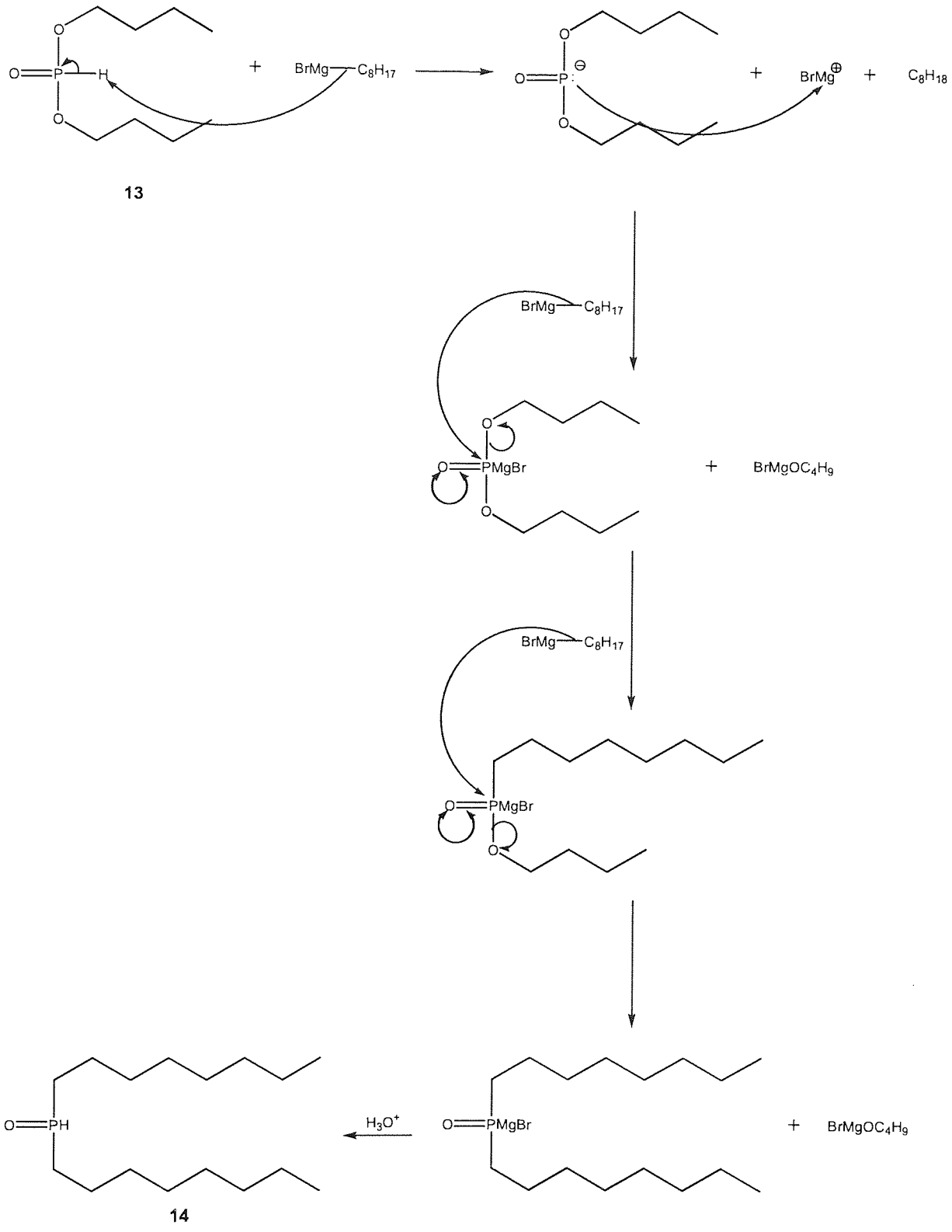

Figure 41: Mechanism for the formation of DOPA 14

2.1.2 Dioctyl(decan-1-ol)phosphine oxide (DODPO) 16[38, 124]

The first tertiary phosphine oxide to be synthesised from DOPA **14** possessed an alky chain terminating in an -OH functionality. The molecule was designed for use in a collaboration with a group at Trinity College Dublin who were working towards attaching a biocompatible molecules to the surface of nanoparticles. It was assumed that the biocompatible molecule could be attached via reaction with the OH group. The collaborating group were supplied with a sample of DODPO **16** and a sample of DODPO coated NanoDots™.

The alcohol-functionalised phosphine oxide **16** was successfully prepared by the reaction of DOPA **14** with *tert*-butyl-dimethylsilylprotected-10-bromodecanol **18** under basic conditions immediately followed by deprotection with tertiary butyl ammonium fluoride (TBAF)[38, 134, 135] **Scheme 2.**

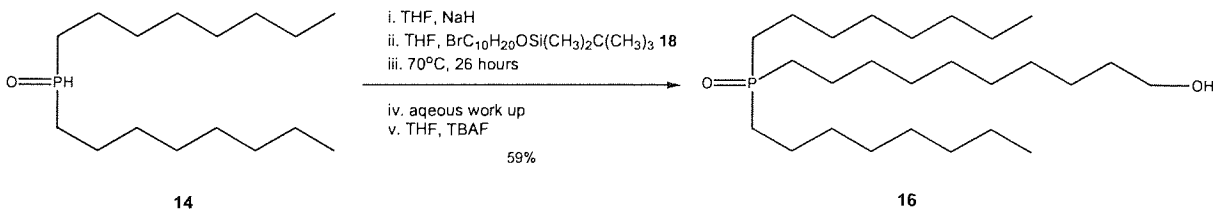

Scheme 2: Synthesis of DODPO 16

Prior to the reaction in **Scheme 2** 10-rromo-1-decanol **17** was protected by the formation of a silyl ether. 10-Bromo-1-decanol **17** was reacted with *tert*-butyldimethylsilyl-chloride (TBDMSi-Cl) in the presence of imidazole and DMF. The formation of the protected alcohol was monitored by TLC (20% ethyl acetate in hexane v/v). Aqueous work-up provided the product that was used without further purification

in a 77% yield. Analysis by IR, LRMS, ^{1}H NMR spectroscopy and ^{13}C NMR spectroscopy confirmed the protection had been successful **Scheme 3**.[134]

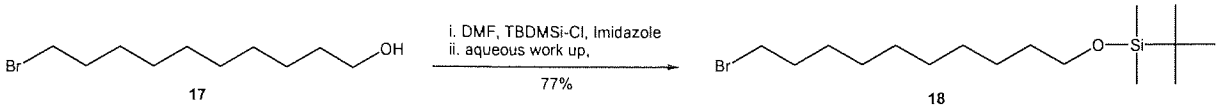

Scheme 3: Synthesis of TBDMSi-protected-10-bromodecanol 18

The mechanism for the protection of alcohols *via* silylation proceeds *via* formation of the conjugate acid of the *N-tert*-butyl-silyl-imidazole produced in the reaction between *tert*-butyl-silyl-chloride and imidazole **Figure 42**. The DMF present in the reaction mixture serves two purposes, the first is to act as a solvent and the second is to help deprotonate the alcohol making it more reactive towards the silylating agent **Figure 43**. The protection stage of the reaction occurs with the attack of the silicon atom of conjugate acid of the *N-tert*-butyl-silyl-imidazole by a lone pair remaining on the oxygen of the alcohol to be protected **Figure 43**. The imidazole is reformed and removed along with the other impurities in the aqueous work up.

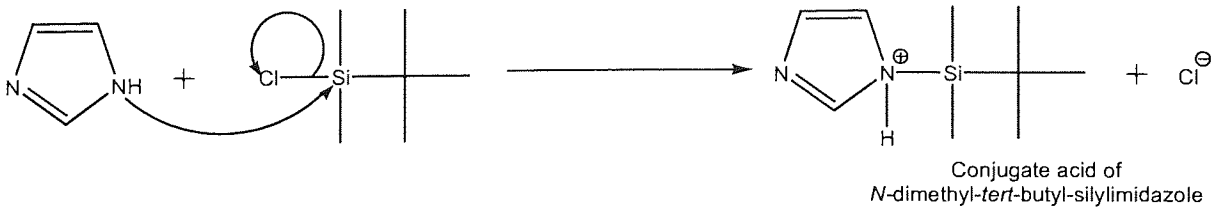

Figure 42: Mechanism for the formation of conjugate acid of *N*-dimethyl-*tert*-butyl-silylimidazole

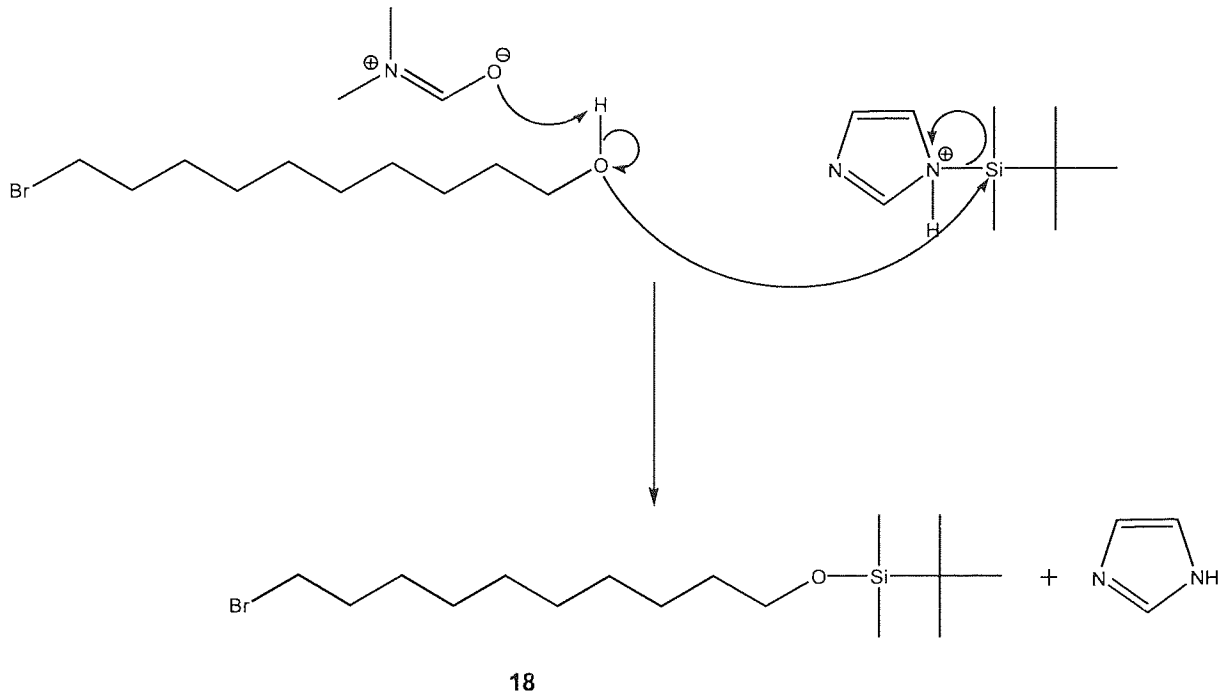

18

Figure 43: Mechanism of the addition of the silyl ether protecting group to 10-bromodecanol

DOPA **14** was deprotonated *in situ* under basic conditions via treatment with 1.5 equivalents sodium hydride (NaH).[38, 124] A solution of *tert*-butyl-dimethyl-silyl-protected-10-bromodecanol **18** in THF was then slowly added to the anion formed initially. After reflux for 26 hours, analysis by TLC (50% ethyl acetate and 2.5% MeOH in hexane v/v) indicated the reaction had gone to completion by the appearance of a new compound and the disappearance of the protected bromoalcohol **18** from the reaction mixture. Unfortunately visualisation of DOPA **14** on the TLC plate was not possible. An aqueous work-up provided the product as a yellow oil in 95% yield. Characterisation was not attempted at this stage instead the oil was treated with a solution of TBAF in THF in a deprotection step to cleave the silyl ether and restore the OH functionality. A second aqueous work-up isolated the product as a dark golden oil. Subsequent

purification via flash column chromatography (50% ethyl acetate and 2.5% MeOH in hexane v/v) furnished the final product of DODPO **16** in a good yield of 59%.

Analysis of the pure product by IR spectroscopy confirmed the presence of the OH functionality (broad, 3346 cm^{-1}) as well as the retention of the P=O group (1148 cm^{-1}). The ^{1}H NMR spectrum supported the formation of the OH functionalised tertiary phosphine oxides by the presence of a triplet at ∂ 3.48 ppm that corresponds to the two protons on the carbon α to the OH group. A broad signal at ∂ 3.10 ppm is most likely the proton directly attached to the oxygen. Finally disappearance of the widely spaced doublet indicative of the unique proton attached to the phosphorus atom in DOPA **14** suggests the coupling reaction was successful.

The ^{13}C NMR spectrum shows the presence of P-C coupling in the signals of carbons C-1, C-2 and C-3 along with the characteristic pattern in the observed coupling constants of $^{1}J_{PC}$=64.3 Hz, $^{2}J_{PCC}$=2.8 Hz and $^{3}J_{PCCC}$=13.8 Hz respectivley.[124, 129] The coupling constants recorded are similar to those observed earlier for DOPA **14** and those reported for compounds possessing similar structures. This observation along with the appearance of a new peak with a chemical shift of ∂ 62.5 ppm characteristic of the carbon directly attached to the OH function implies the successful formation of DODPO **16**. Finally both the low resolution and high resolution mass spectroscopic analysis confirm the presence of a molecule with the correct mass consistent with that of the product.

The mechanism of the addition of the *tert*-butyl-dimethyl-silyl-protected-10-bromodecanol **18** to DOPA **14** begins with the formation of a dialkylphosphosphinous

ion by deprotonation under basic conditions **Figure 44**. The resultant anion displaces the bromine atom of *tert*-butyl-dimethyl-silyl-protected-10-bromodecanol **18**, in an S_N^2 reaction that results in the formation of a new P-C bond. Finally the TBDMS protecting group is removed by treatment with TBAF.[133, 134, 135]

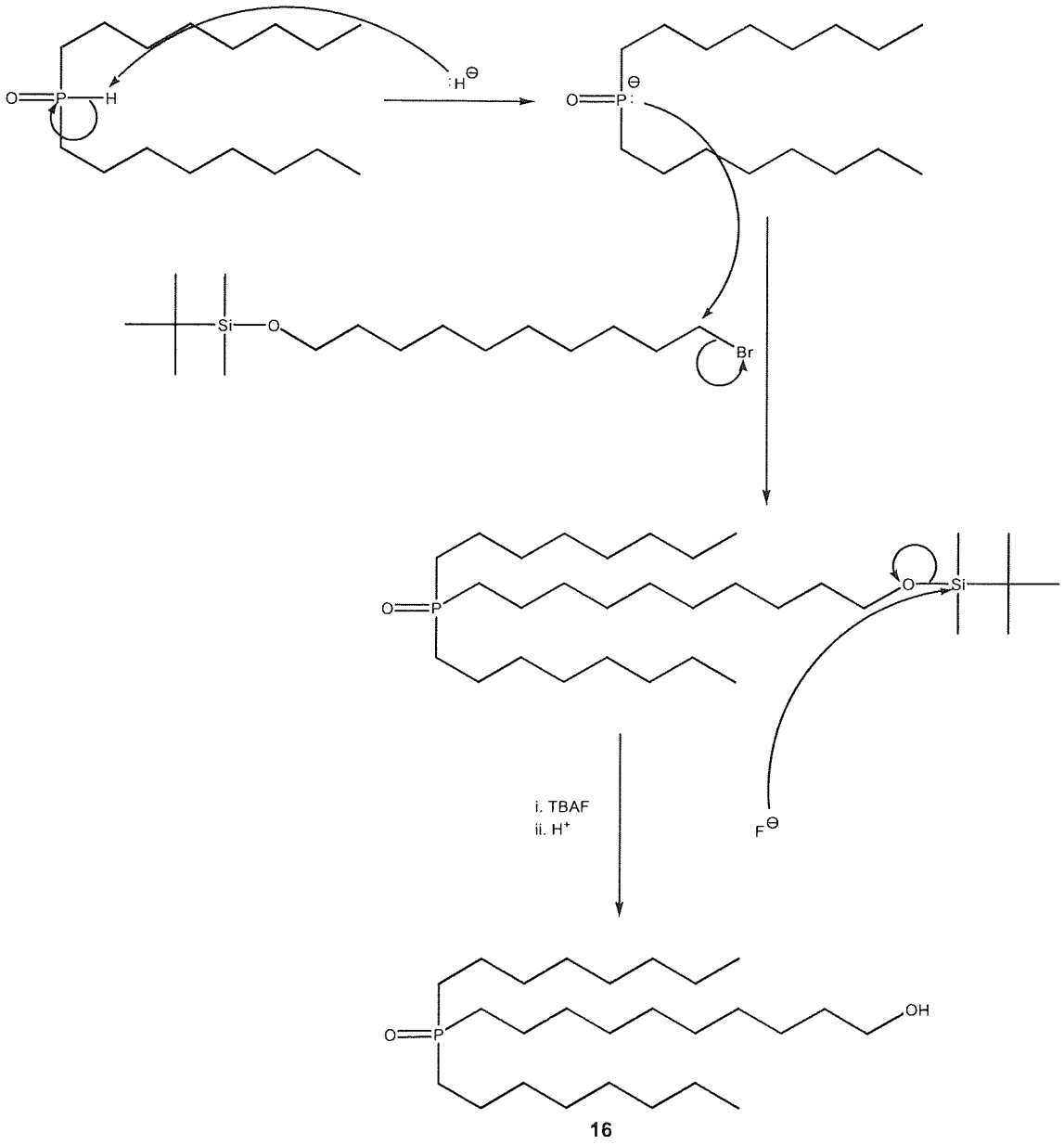

Figure 44: **Mechanism of the sodium hydride mediated formation of a tertiary phosphine oxide followed deprotection with TBAF**

Previous attempts to synthesise DODPO **16**, in a shorter procedure involving the reaction of DOPA **14** with 10-bromo-decanol **17**, failed despite the addition of 2.5 equivalents of base to facilitate the deprotonation of both the DOPA **14** and the bromodecanol **17**. Thin layer chromatography (TLC) (50% ethyl acetate in hexane) was used to monitor the progress of the reaction. Since the DOPA **14** could not be visualised on the plate the disappearance of the bromoalcohol **17** accompanied by the appearance of a new compound was used to indicate success. Analysis by TLC in this manner indicated that the reaction did not proceed either at room temperature or when the mixture was refluxed overnight at 70°C.

2.1.3 Dioctyl(octene)phosphine oxide (DOOPO) 6 and Dioctyl(undecene)phosphine oxide (DOUPO) 19

The second type of functionality added to DOPA **14** was an alkene function. An olefinic group was chosen for two reasons. The first was that it provided a functionalised tertiary phosphine oxide in a one step reaction, no protection and subsequent deprotection was required. The second concerned the introduction of a polymerisable unit that could potentially be used to covalently incorporate the NanoDots™ into the matrices of various polymeric materials. Two similar tertiary phosphine oxides containing an olefinic function were synthesised. DOOPO **6 Scheme 4** and DOUPO **19 Scheme 5** differ only in the chain length that contains the terminal alkene, eight carbons and eleven respectively. The synthesis of the two is essentially the same and the molecules behaved in a similar manner in the procedure used to work-up the reactions.

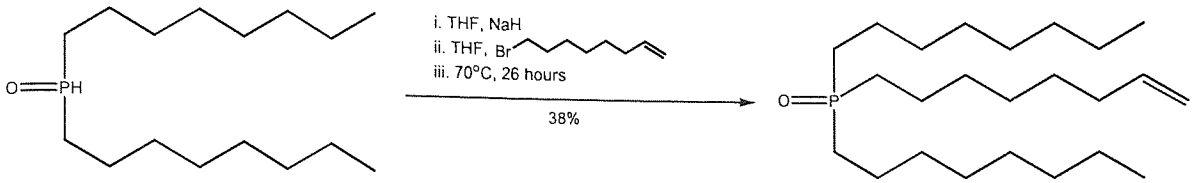

14 6

Scheme 4: Synthesis of DOOPO 6

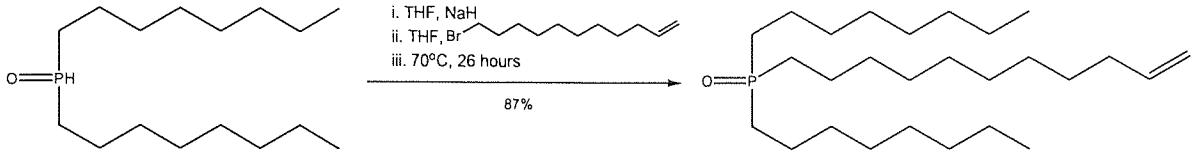

14 19

Scheme 5: Synthesis of DOUPO 19

In both the syntheses DOPA **14** was deprotonated *in situ* under basic conditions via treatment with 1.5 equivalents sodium hydride (NaH).[38, 124] A solution of the relevant bromoalkene dissolved in THF was added to the resultant anion and the reaction mixtures were refluxed for 26 hours. In both cases analysis by TLC (50% ethyl acetate and 2.5% MeOH in hexane v/v) indicated that the reactions had gone to completion by the appearance of new compounds at Rf=0.5 and Rf=0.1 for DOOPO **6** and DOUPO **19** respectively. The additional disappearance of the bromoalkene from the reaction mixture also indicated the reactions had been successful. Unfortunately visualisation of DOPA **14** on the TLC plate was not possible. Both the reactions underwent an aqueous work up that was unfortunately problematic due to the formation of emulsions. In both cases the emulsions were broken by the addition of brine or solid sodium chloride and crude products were obtained.

A pure sample of DOOPO **6** was isolated in 38% yield from recrystallisation of the crude product in hexane. The same recrystallisation conditions provided DOUPO **19** in an 87% yield. Infra-red analysis of both the products revealed the presence of the expected functional groups, the important band for the olefinic function (3074 cm^{-1}), the P-CH_2 (1461 cm^{-1}) group and the P=O functionality (1151 cm^{-1}) feature prominently in both spectra. The LRMS and HRMS recorded for each compound suggest that the desired products are present in both cases.

Examination of the ^1H NMR spectra obtained from the two compounds reveal that they are similar, differing only as expected in the broad multiplet corresponding to the protons of the alkyl chains. The multiplet integrates to 38 protons in the spectrum of DOOPO **6** and 44 protons in the spectrum of DOUPO **19**. The triplets (∂ 0.83 ppm) in both cases integrate to six protons and are assigned to the two terminal methyl groups in each molecule. By far the most interesting signals in these spectra correspond to the protons adjacent to and encompassing the double bond **Figure 45**. Since the spectra are identical at this region analysis of only the DOUPO **19** spectra will be discussed.

Due to the lack of free rotation about a double bond the protons labelled **Ha** and **Hb** cannot be treated as equivalent. Their different positions in space result in individual and unequal splitting by the adjacent proton **Hc**. Referring to **Figure 45** the positions on the double bond of the protons labelled **Ha** and **Hb**, relevant to the position of the proton labelled **Hc** are *trans* and *cis* respectively. The standard magnitude of both *cis* and *trans* couplings of this nature is well established, cis couplings fall in the range of 7-11 Hz and trans in the range of 12-18 Hz .[136, 137, 138]

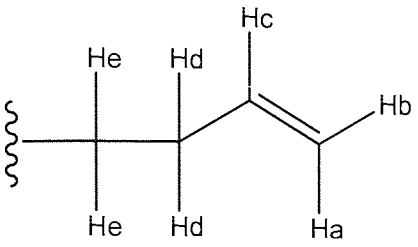

Figure 45: Structure and labelling of the protons encompassing and adjacent to the double bond

Examination of the spectra indicates the presence of two partially superimposed doublet signals centred at ∂ 4.89 ppm and ∂ 4.95 ppm **Figure 46**. The chemical shift and the coupling constants, calculated to be 10.2 Hz and 16.9 Hz respectively, suggest that **Ha** and **Hb** are responsible for the existence of these signals. **Figure 47** is a splitting diagram that represents the observed pattern arising from the observed signals for **Ha** and **Hb**. Referring to **Figure 47** it is clear that the doublet centred ∂ 4.89ppm with a coupling constant of 10.2 Hz is the smaller of the two and falls with in the range of values for a *cis* coupling. This doublet centred at ∂ 4.89 ppm therefore corresponds to the proton labelled **Hb** coupled to **Hc**. It follows then that the second doublet centred at ∂ 4.95ppm corresponds to the proton labelled **Ha**. The coupling constant of 16.9 Hz reflects this and suggest that this signal arises from the *trans* coupling of **Ha** to **Hc**.

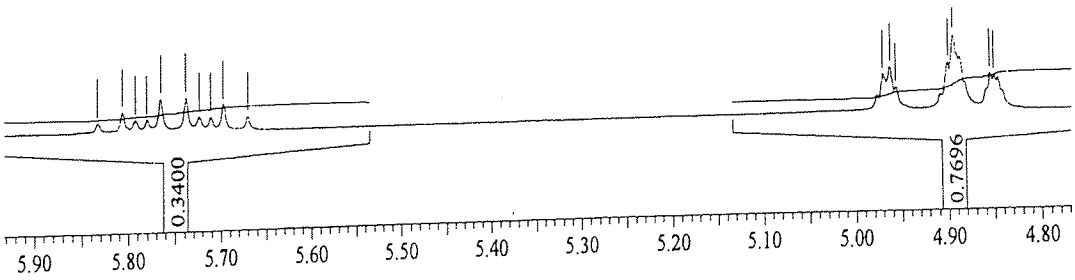

Figure 46: ^{1}H NMR spectrum of DOUPO 19 expansion of the olefinic resonances between ∂ 5.90 ppm & 4.80 ppm

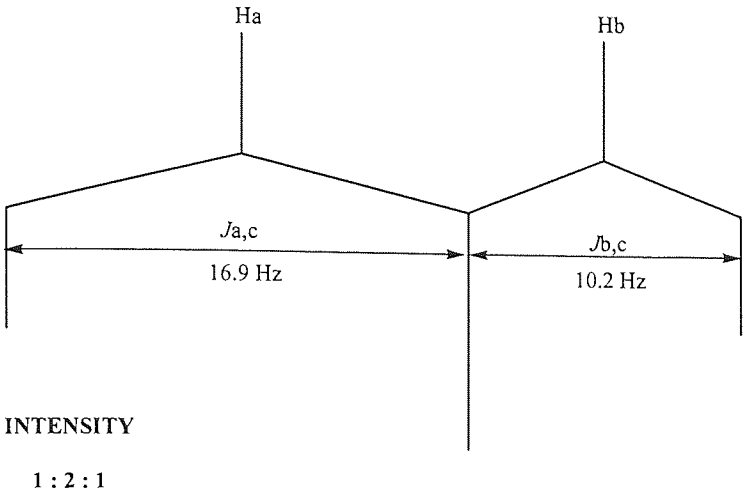

Figure 47: Splitting pattern produced by the coupling the protons labelled Ha & Hb to Hc

The splitting pattern arising for the coupling of **Hc** to the adjacent protons initially appears very complex. **Figure 45** shows that **Hc** should be coupled to **Ha**, **Hb** and **Hd,** theoretically this would produce a doublet doublet triplet pattern comprising of 16 signals all of the same intensity. However examination of the olefinic region of the ^{1}H NMR spectrum of DOUPO **19 Figure 46** shows a multiplet centred ∂ 5.75 ppm containing 10 peaks of differing intensities. The chemical shift of this signal is consistent with similar signals of this type reported in the literature. [138] This pattern results from the overlap of split signals, resulting in the observation of fewer peaks composed of multiple intensities. The signal pattern produced for **Hc** can be explained by examination of the splitting diagram produced for the splitting of **Hc** by the protons labelled **Ha**, **Hb** and **Hd Figure 48**.

Figure 45 demonstrates that **Hc** is coupled to **Ha**, this results in the signal for **Hc** being split by 16.9 Hz. The resulting doublet is then split by 10.2 Hz to account for the

coupling of **Hc** to **Hb**. The resulting four signals are then split into triplets by coupling to **Hd**, overlap of this splitting increases the intensity of some of the observed peaks. The intensity pattern of the peaks is of the form 1 : 2 : 1 : 1 : 3 : 3 : 1 : 1 : 2 : 1, the sum of these intensities is 16 and this correlates to the predicted number of single intensity signals expected. The coupling of **Hc** to **Hd** is 6.7 Hz and this is a typical value for couplings of this nature.[136]

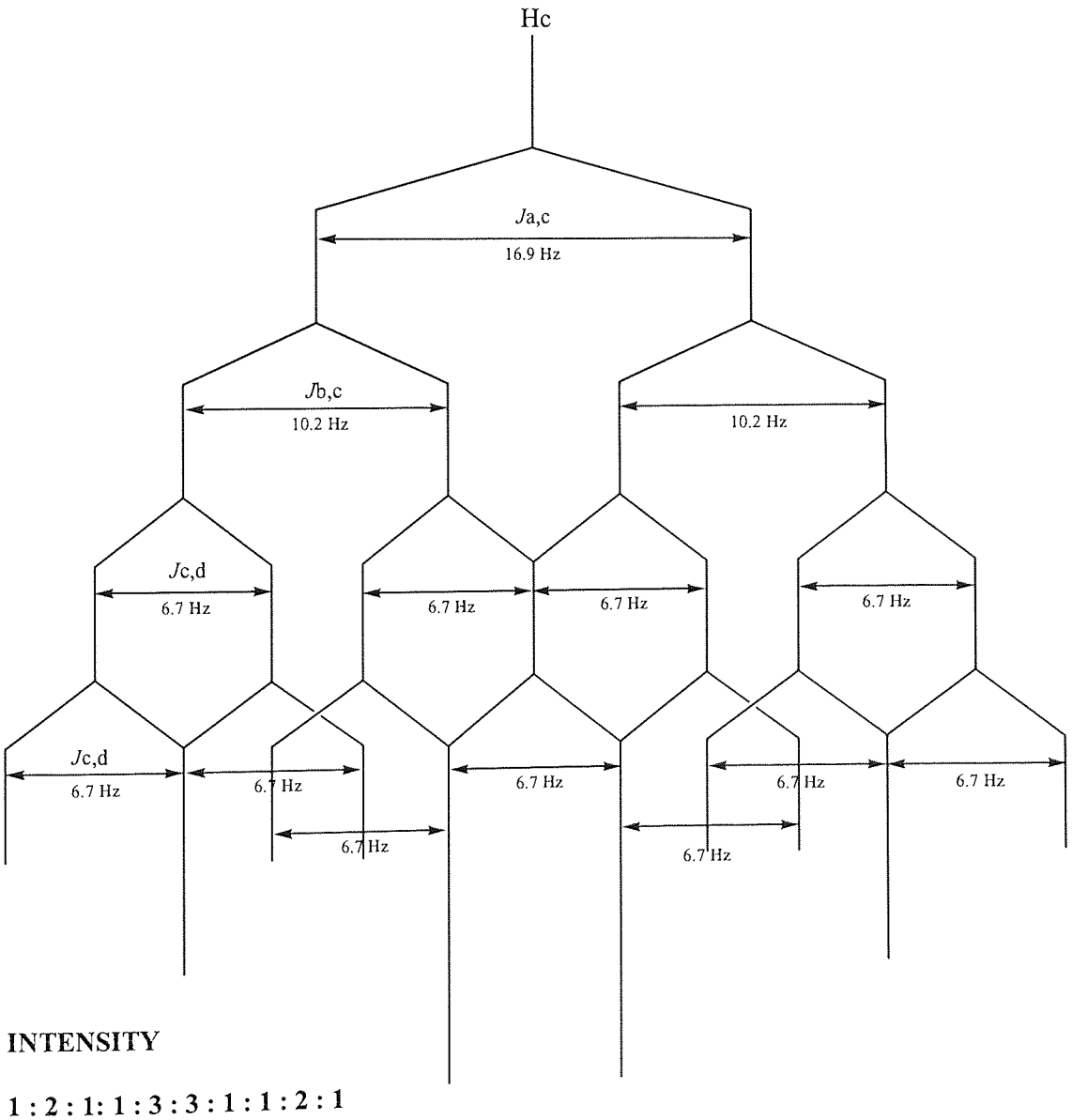

Figure 48: Splitting pattern produced by the coupling the protons labelled Ha, Hb & Hd to Hc

The final signal relating to the protons surrounding the olefinic group is the signal corresponds to **Hd**. This signal is centred at ∂ 1.98ppm is composed of 4 peaks with the relative intensity 1 : 3 : 3 : 1. This pattern and intensity is due to the splitting of 6.7 Hz resulting from the coupling with **Hc**, and a coupling of 7.0 Hz from the interaction of **He** and **Hd**.

The chemical shift and coupling constants recorded from the spectra of DOOPO **6** and DOUPO **19** correlate to those of similar molecules that have been reported previously.[127, 139] Finally the disappearance of the signals corresponding to the proton attached to the phosphorus indicates complete reaction of the starting materials.

The ^{13}C NMR spectrum of DOOPO **6** shows the presence of P-C coupling in the signals of carbons C-1 and C-3, unfortunately poor resolution prevented the elucidation of the coupling constant for the C-2. Three new signals at ∂ 138.8 ppm, ∂ 114.3 ppm and ∂ 33.6 ppm are present in the spectrum that are not present in the spectrum recorded for DOPA **14**. The chemical shifts of these signals are consistent with the CH_2, CH signals of the double bond and the CH_2 adjacent to the olefinic group respectively.

2.1.4 Dioctyl(methylstyrene)phosphine oxide (DOMSPO) 7

The addition of a styrenic functionality to DOPA **14** was undertaken to produce a tertiary phosphine oxide that would be more compatible with the conventional resin synthesis undertaken previously in the group **Scheme 6**. The ultimate goal of this ligand was to irreversibly and covalently incorporate the NanoDots™ into the matrix of resin

beads.[37] Successful accomplishment of this would be the first stage towards the production of quantum dot encoded beads for potential use in combinatorial synthesis.

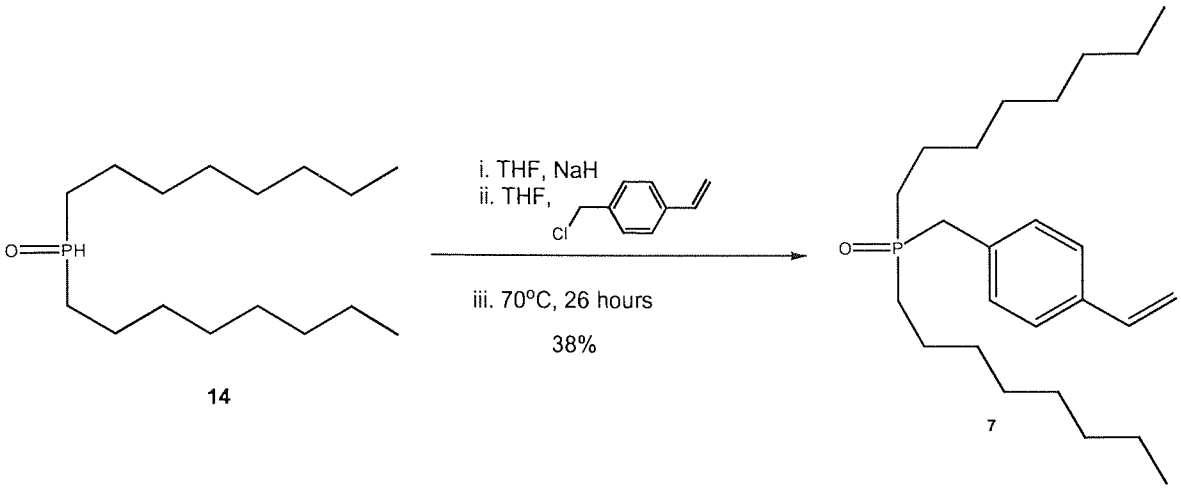

Scheme 6: Synthesis of DOMSPO 7

As with the previous syntheses of mono-functionalised tertiary phosphine oxides, DOPA **14** was deprotonated *in situ* under basic conditions via treatment with 1.5 equivalents sodium hydride (NaH).[38, 124] A solution of chloromethylstyrene (CMS) **10** in THF was then slowly added to the anion formed in the deprotonation step and the resultant mixture refluxed. Analysis by TLC (50% ethyl acetate and 2.5% MeOH in hexane v/v) indicated that the reaction had gone to completion by the appearance of a new compound that was visible under UV light, and the disappearance of the CMS **10** from the reaction mixture. Unfortunately visualisation of DOPA **14** on the TLC plate was not possible. An aqueous work up produced the product as an orange oil in 68% yield. Recrystallisation from ice cold hexane provided white powdery crystals in a 38% yield.

Analysis by IR and LRMS supported the formation of the styrenically-functionalised tertiary phosphine oxide. The IR spectrum contained peaks corresponding to the P=O

functionality at 1171cm^{-1}, and three bands at 1640 cm^{-1}, 1628 cm^{-1} and 1134 cm^{-1} that correlate to the presence of a 1,4 disubstituted aromatic ring. A small peak at 3040cm^{-1} suggests that the double bond of the styrenic unit is still intact. Finally the absence of the band corresponding to the P-H (2236 cm^{-1}) functionality strongly suggests that intended product had been formed. In addition the LRMS provides evidence of a molecule of the correct mass to be DOMSPO **7**.

The ^{1}H NMR spectrum of DOMSPO **7** indicates that the formation of the tertiary phosphine oxide proceeded successfully as indicated by the previous analysis discussed. Broad signals that integrate as expected are present for the two octyl chains. The signal for the protons on the carbon directly attached to the phosphorus appears as a doublet centred at ∂ 3.07ppm **Figure 49,** C-9. This is the first observation of splitting of protons on a carbon directly attached to the phosphorus atom. In the structures discussed previously these $^{2}J_{PCH}$ couplings have been obscured by overlap from other CH_2 proton signals in the alkyl chain.[126] The coupling of $^{2}J_{PCH}$=14.8 Hz is observed in this case because the CH_2 group C-9 is also attached to an aromatic ring. The aromatic ring withdraws electron density from the CH_2 group, deshielding the protons of the CH_2 groups. The result of which pulls the signal downfield and out of the complex multiplet composed of the CH_2 signals from the alkyl chain. The magnitude of the splitting is of the same order as $^{2}J_{PCH}$ couplings recorded in the literature.[126, 127, 131] For example $^{2}J_{PCH}$=12.8 Hz is recorded for $(CH_3)_3P{=}O$[127] and $^{2}J_{PCH}$=16.3 Hz is recorded for $(CH_3CH_2)_3P{=}O$.[126]

The remaining signals correspond to the protons present in the styrene unit. Two doublets centred at ∂ 5.20ppm and ∂ 5.70ppm are the signals for the protons on the

carbon labelled C-15 in **Figure 49**. The protons on C-15 are *cis* and *trans* coupled respectfully to the proton on C-14 that is responsible for the doublet doublet centred at ∂ 6.66ppm. The signals for the aromatic protons on carbons C-11 and C-12 are coupled to each other and can be found as two doublets centred at ∂ 7.17ppm and ∂ 7.33ppm.

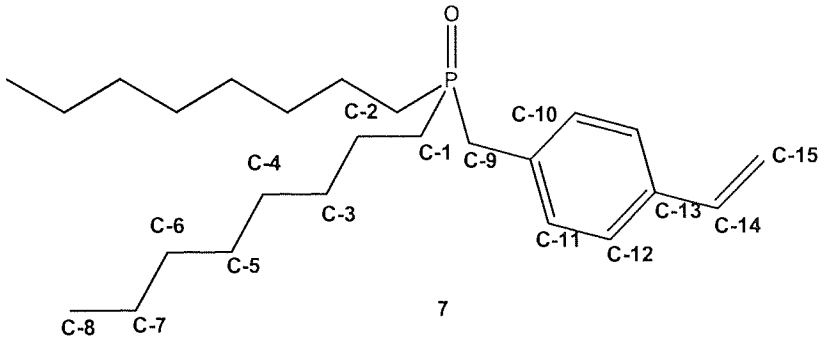

Figure 49: Numerically labelled structure of DOMSPO

The ^{13}C spectra of DOMSPO **7** shares many of the features with that of DOPA **14** the signals for carbons C-1 to C-8 are all present and at anticipated chemical shifts. Again the signals for carbons C-1 to C-3 in the alkyl chain are coupled to phosphorus in the familiar pattern $^{1}J_{PC}$=65.2 Hz, $^{2}J_{PCC}$=3.7 Hz and $^{1}J_{PCCC}$=13.8 Hz, where the splitting for C-2 is larger than that of C-3. As expected the carbon labelled C-9 directly attached to the phosphorus is also split with a coupling constant of $^{1}J_{PC}$=58.1 Hz that is comparable to that of C-1 and is in agreement with the same coupling reported for a related molecule in the literature.[124]

The signal for C-10 at ∂ 136.0ppm should be split with a coupling constant similar to that of C-2 but unfortunately poor resolution prevented the calculation of the coupling constant. Evidence of coupling to the phosphorus is present all the way to C-5 but unfortunately poor resolution has hindered the calculation of all the coupling constants.

However all the signals for carbons C-9 to C-15 are present and assigned at the expected chemical shift values.

Unfortunately as this work was being undertaken a report utilising a similar approach was published by the Emrick group.[38] The analysis obtained for styrenic compound **7** is consistent with that of the published data for the same structure, however a comparison of the coupling constants could not be made as the published literature data excluded them.[38]

2.1.5 Dimethylstyrylphosphinous acid (DMSPA) 20

The successful syntheses of tertiary phosphine oxides from the DOPA **16** provided ligands with the required functionality for various different applications. However these ligands suffered from the disadvantage that they are all mono-functionalised in nature, unfortunately each ligand only possessed one chain with the chosen functionality. This restriction arose from the synthetic protocol used in their construction. Accordingly it was decided that a tertiary phosphine oxide that contained more than one functionalised chain would prove to be more versatile. The synthesis of a functionalised phosphinous acid intermediate would not only immediately increase the amount of functionality per ligand, but also make the synthesis of mutli-functionalised ligands possible.

Other findings within the group suggested that the styrenic functionalised ligand was more compatible than the olefinic functionalised ligand with the conditions employed in

polystyrene bead production.[37] It was therefore decided to synthesis a dimethylstyrene-functionalised phosphinous acid intermediate **Scheme 7**.

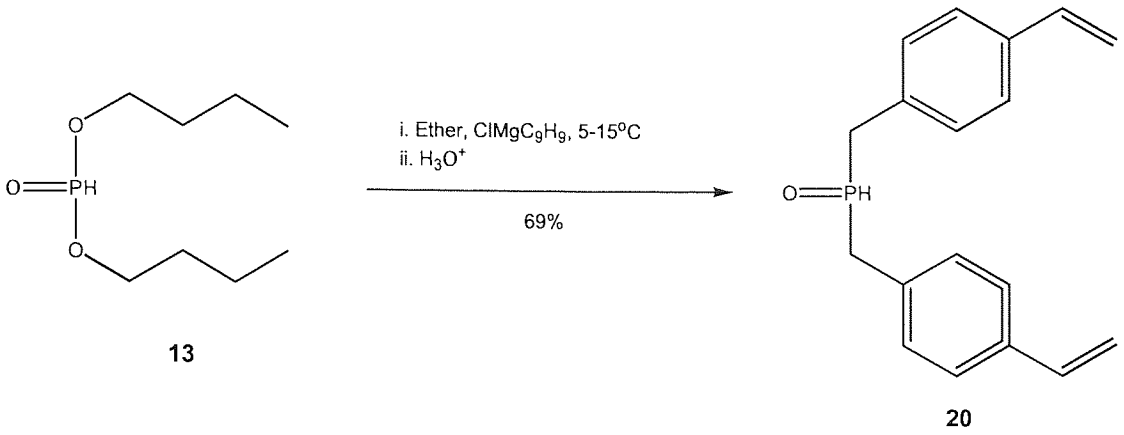

Scheme 7: Synthesis of DMSPA 20

DMSPA **20** was synthesised from the reaction of dibutyl phosphite **13** with three equivalents of the corresponding Grignard reagent derived from CMS **10**. The *in situ* formation of this particular Grignard reagent is violently exothermic and very careful drop-wise addition of the CMS **10** solution was required during its generation. The reaction between the Grignard reagent and the phosphite appears to be very rapid as evidenced by the immediate formation of a gel like precipitate upon addition of the dibutyl phosphite **13**. After aqueous work-up, the crude product was obtained as a bright green/yellow waxy solid in a yield of 92%. Several triturations in ice cold ether produced the pure product as an off white powdery solid in a good yield of 69%.

All of the spectroscopic analysis undertaken on this product is fully consistent with the structure of DMSPA **20**. Both the LRMS and the HRMS show the presence of a molecule of the correct mass to be the desired phosphinous acid. The infra red spectrum

shows the presence of several anticipated functional groups and the absence of functionality associated with the starting material. A medium to strong peak at 2326 cm^{-1} that corresponds to the P-H functionality, a medium peak at 1406 cm^{-1} characteristic of P-CH_2 and a strong peak at 1194 cm^{-1} indicative of the P=O function are all present. Finally the absence of a strong peak in the region of 1050-1030 cm^{-1} that would imply the presence of P-O suggests that the reaction had been successful.

The ^1H NMR spectra of DMSPA **20** is consistent with the structure of the desired product **Figure 50**.

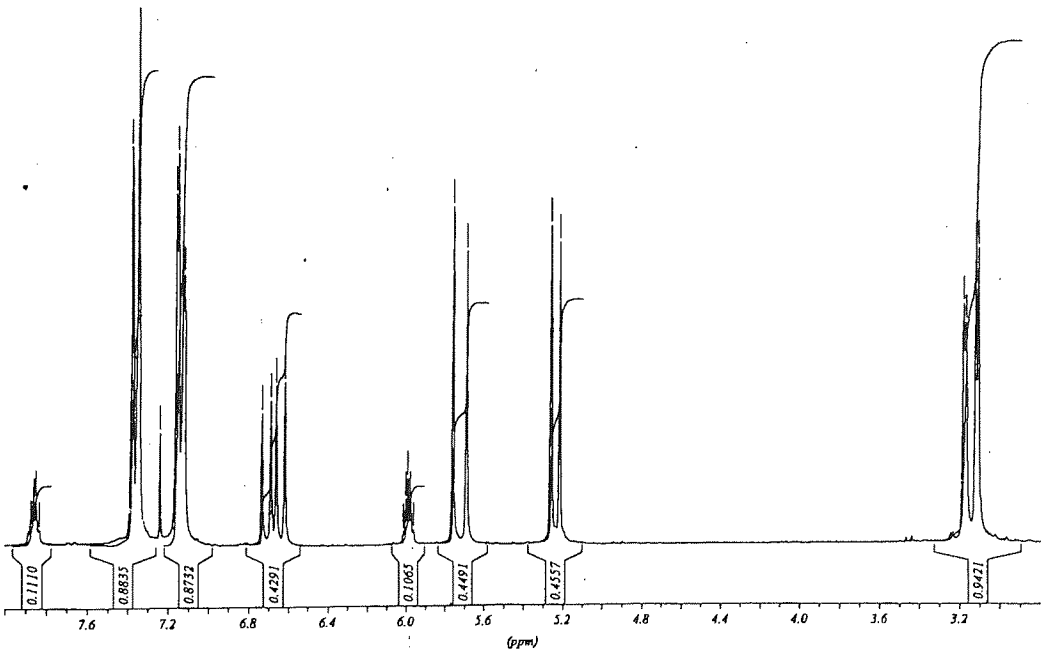

Figure 50: ^1H NMR spectrum of DMSPA 20

The signals present exhibit the predicted chemical shifts, integrate as expected and posses coupling constants that correlate to those reported in the literature. An attractive feature of this spectrum is the doublet pentet centred at ∂ 6.92 ppm, the large coupling

to the phosphorus atom has a $^{1}J_{PH}$=468.7 Hz. The magnitude of this value is consistent with literature published couplings of this nature in similar compounds such as diethylphosphinous acid ($^{1}J_{P\text{-}H}$=468 Hz), diisopropylphosphinous acid ($^{1}J_{P\text{-}H}$=468 Hz) and dibutylphosphinous acid ($^{1}J_{P\text{-}H}$=458 Hz).[123, 140, 141] The smaller splittings of 3.0 Hz correspond to couplings between the proton on the phosphorus and those on C-1 **Figure 51**.

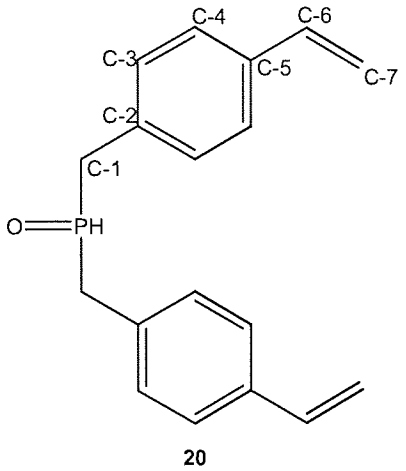

20

Figure 51: Numerically labelled structure of DMSPA 20

The large coupling of this unique proton to the phosphorus and the smaller characteristic splitting by the four protons on **C-1** are represented in **Figure 52.** The doublet doublet centred at ∂ 3.15 ppm corresponds to the four protons on the carbons (**C-1**) directly attached to the phosphorus. The coupling constants of 15.3 Hz reflect the coupling between the protons on **C-1** and the phosphorus whereas the coupling of 3.0 Hz results from coupling of the protons on **C-1** and the proton directly attached to the phosphorus. Both the values are consistent with evidence of a similar splitting reported in the literature for dimethylphosphinous acid that has $^{2}J_{PCH}$=14 Hz and $^{3}J_{HPCH}$=3.5 Hz.[123, 142] The two doublets centred at ∂ 5.23ppm and ∂ 5.77ppm are signals corresponding to the two protons on carbon **C-7**, these are coupled to the proton on **C-6**

with a *cis* and *trans* coupling of 10.9 Hz and 17.9 Hz respectively. It follows then that the proton on **C-6** gives rise to a doublet doublet signal with couplings of 10.9 Hz (*cis* proton on **C-7**) and 17.6 Hz (*trans* proton on **C-7**). The protons of the aromatic ring are coupled to each other and appear as two doublets.

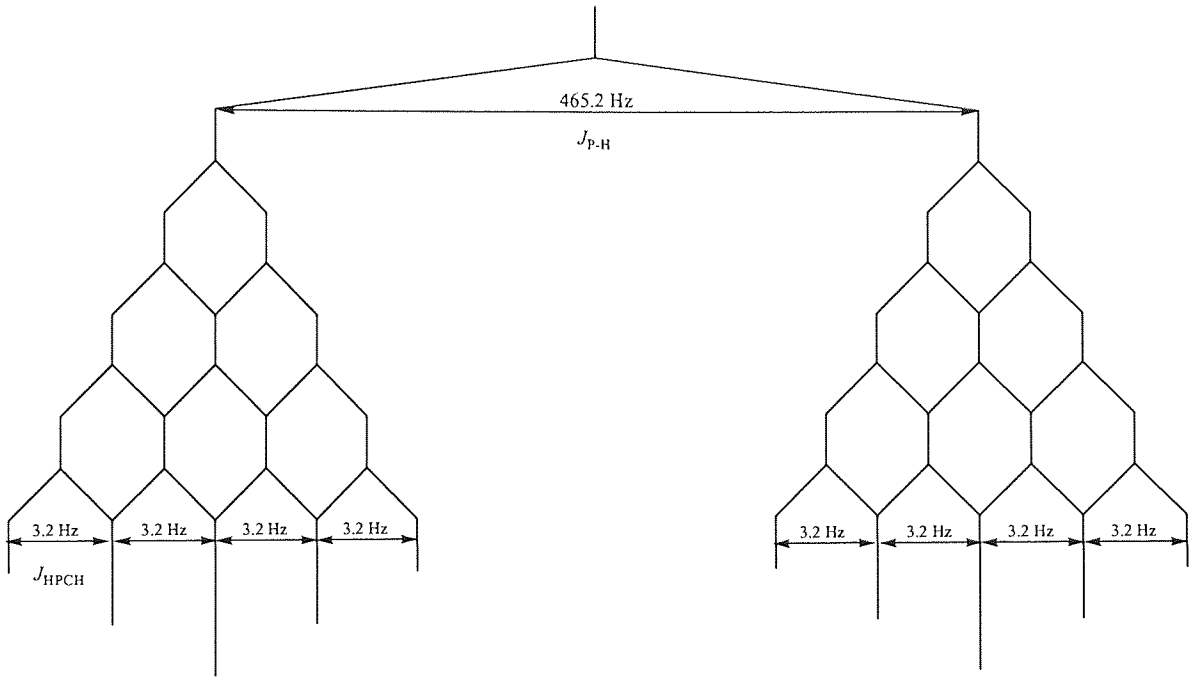

Figure 52: Splitting diagram for the unique proton attached directly to the phosphorus in DMSPA 20

A D_2O shake revealed that the proton directly attached to the phosphorus atom is not rapidly exchangeable. However evidence in the literature suggests that upon standing over time protons of this type can exchange.[123]

Analysis of the ^{13}C NMR spectrum reveals that it is in accordance with structure of DMSPA **20**. Examination of the spectrum reveals that it is composed of 12 signals **Figure 53 and 54**. The increased number of signals is due to short and long range

coupling of the phosphorus atom.[126] However unlike the straight chain compounds previously discussed splitting of signals is evident all the way to carbon **C-5 Figure53.**

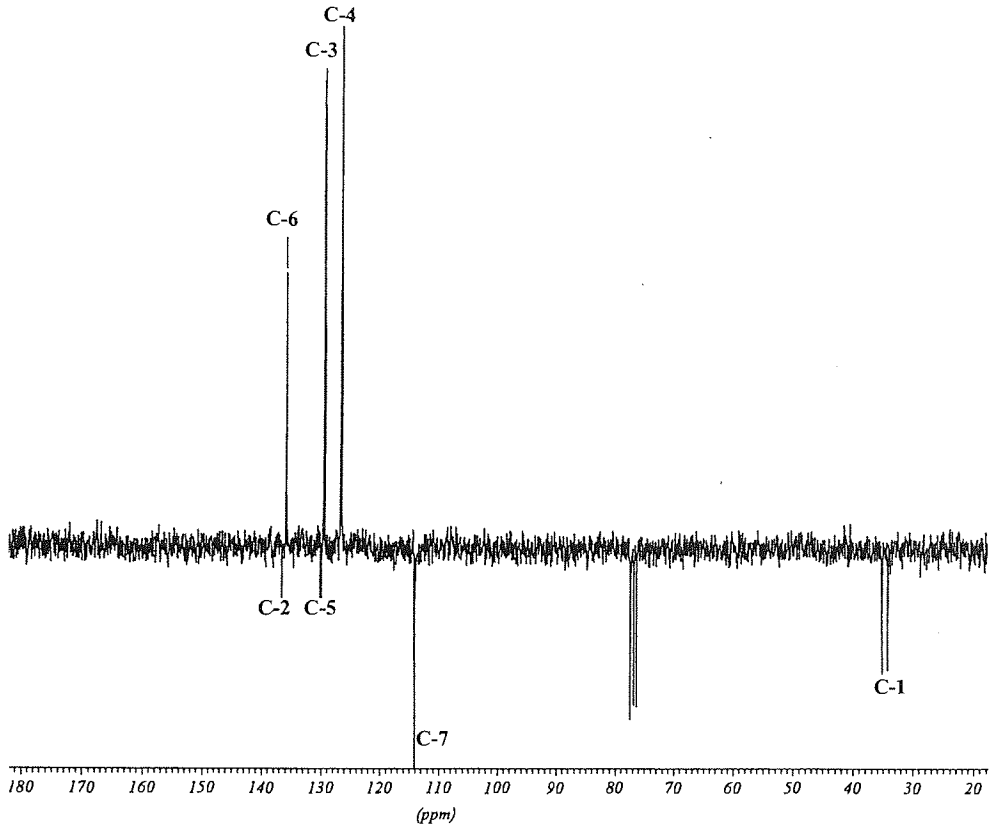

Figure 53: **^{13}C PENDANT NMR spectrum of DMSPA 20**

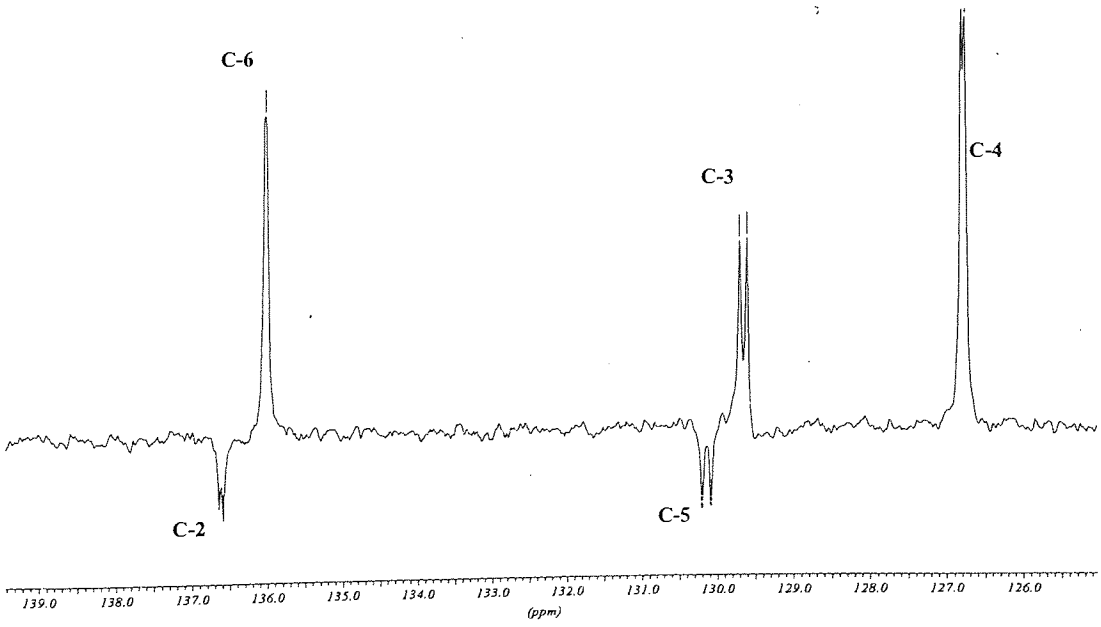

Figure 54: **^{13}C PENDANT NMR spectrum of DMSPA 20 expansion between ∂ 126 and 139 ppm**

Carbon **C-1** appears as a doublet centred at ∂ 34.8 ppm, as expected this coupling exhibits the larges splitting of $^{1}J_{PC}$=59.7 Hz and is in very good agreement with couplings of this nature reported in the literature. The chemical shifts of the carbons correlate well with those reported for similar compounds.[124, 143] The coupling in this system is present all the way to carbon **C-5**, the coupling constants calculated are significantly smaller that of **C-1**. Couplings of $^{2}J_{PCC}$=3.7 Hz, $^{3}J_{PCCC}$=6.5 Hz, $^{4}J_{PCCCC}$=2.8 Hz and $^{5}J_{PCCCCC}$=7.4 Hz were recorded.

2.1.6 Dimethylstyryl(decane)phosphine oxide (DMSDPO) 21 and Dimethylstyryl(octane)phosphine oxide (DMSOPO) 22

The synthesis of a tertiary phosphine oxide with the maximum possible number of polymerisable units seemed to be the logical step to maximise the irreversible covalent incorporation of quantum dots into a polystyrene-based solid support. Since the styrenic-functionality appeared to be the most compatible with resin synthesis the addition of a third methyl styrene unit was attempted **Scheme 8**.

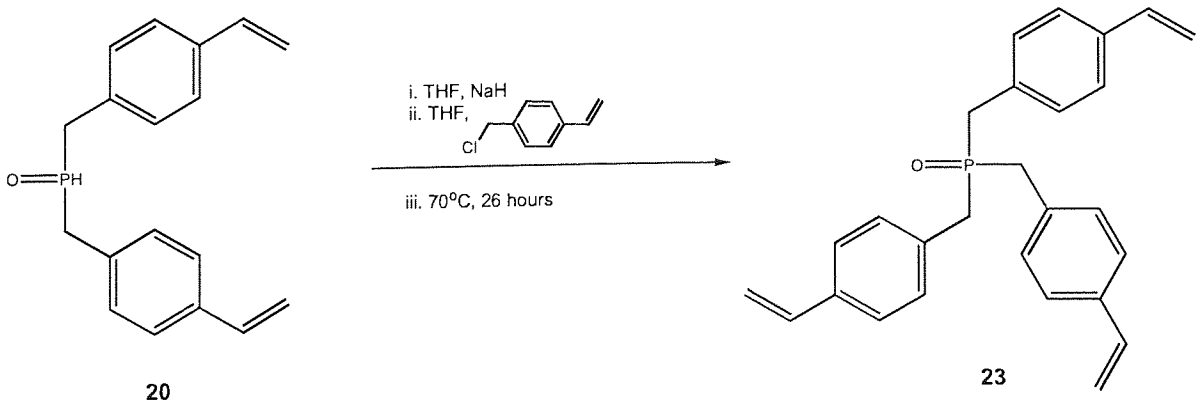

20 23

Scheme 8: Synthesis of TMSPO 23

Trimethylstyrylphosphine oxide (TMSPO) **23** was synthesised by the same procedure described previously, sodium hydride was used to deprotonate the phosphinous acid, followed by drop-wise addition of the CMS moiety. The progress of the reaction was monitored by TLC and aqueous work-up produced the product as a golden brown solid. Unfortunately all attempt at purifying this product failed presumably due to the very low solubility exhibited by the compound. A LRMS of the compound confirmed the presence with a molecule of the correct mass to be consistent with the desired product. This evidence coupled with a crude ^{1}H NMR that showed the complete disappearance of the unique doublet pentet of the proton attached directly to the phosphorus suggested success in the synthesis. The insoluble nature of this compound not only prevented its purification and complete characterisation but led to the assumption that this characteristic would be detrimental to the purpose it was designed for. Therefore further work involving this compound was abandoned.

Instead the design of the structure was modified to improve solubility by the replacement of the third styrenic unit with an alkyl chain. An eight and a ten carbon un-functionalised alkyl chain was added **Scheme 9**. Again DMSPA **20** was deprotonated and the relevant length alkyl halide added in a drop-wise manner. Both reactions were monitored with TLC, the disappearance of the DMSPA **20** and the formation of a new compound in the reaction mixture was used to indicate completion since visualisation of the alkyl hailide proved impossible.

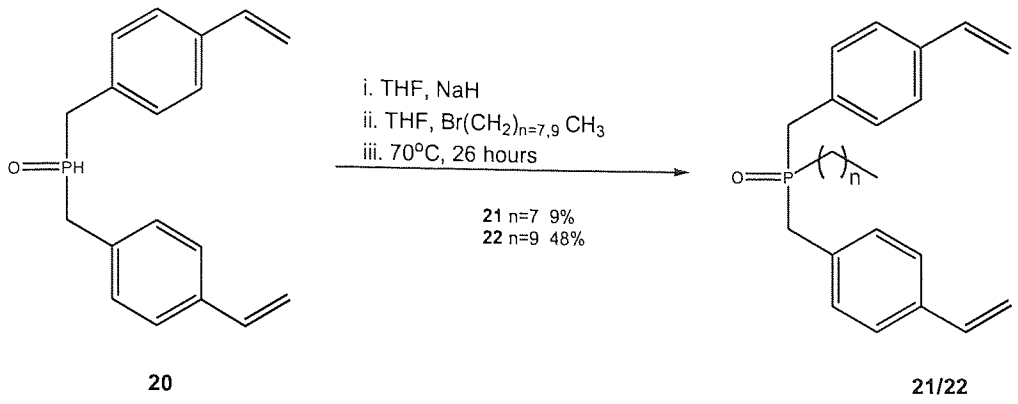

20 21/22

Scheme 9: Synthesis of DMSOPO 21 and DMSDPO 22

The aqueous work-up for both compounds was difficult due to the frequent formation of emulsions. The addition of brine and ethanol was used to aid in the separation. DMSOPO **21** was subsequently purified via flash column chromatography, but unfortunately this reduced the yield to 9%. Alternatively DMSDPO **22** was purified by trituration in ice cold ether followed by Recrystallisation from a mixture of ethyl acetate and hexane to furnish an off-white solid in a better yield of 48%.

The ^{1}H NMR spectra for both the compounds appeared as expected. In each case the signal corresponding to the terminal methyl and the complex multiplet integrated correctly. Both spectra possessed doublet doublets at ~3.0ppm, that correspond to the protons on **C-1 Figure 55** that are split by phosphorus with similar couplings of $^{2}J_{PCH}$=14.8 Hz for DMSOPO **21** and $^{2}J_{PCH}$=14.2 Hz for DMSDPO **22**.These values for coupling to the phosphorus correlates well with similar couplings published in the literature.[139] The remaining signals correspond to the protons of the aromatic ring and double bond. All the signals integrate as expected and exhibit the previously discussed splitting patterns. Finally no signal for the proton attached to the phosphorus was observed in either spectrum.

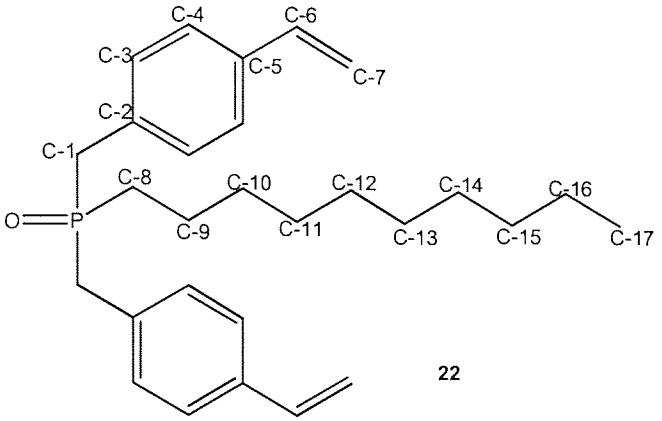

22

Figure 55: Numerically labelled structure of DMSDPO 22

Both ^{13}C NMR spectra also show the splitting patterns discussed previously. The carbons at **C-1** and **C-8** show the largest splitting. Coupling of the phosphorus to carbon **C-5** in the styrenic group and to **C-10** in the alkyl chain is also observed in both spectra, this is consistent with data obtained from molecules of this type described earlier and those reported in the literature.[124] Analysis by LRMS, HRMS and IR spectroscopy also supported the successful formation of both products. The addition of the alkyl chain vastly improved the solubility of the compounds compared with the tristyrenic derivative **23** in a wide range of solvents.

2.1.7 Diundecenephosphinous acid (DUPA) 24

The next functionalised intermediate that was synthesised possessed two olefinic groups. This intermediate was synthesised to provide tertiary phosphine oxide ligands for applications other than in resin synthesis. It was hypothesised that olefinic functionalised ligands could be used to produce protective polymer layers close to the surface of quantum dots. Once a successful strategy for this had been achieved the

possibility of incorporation of other functionalities to this layer could be envisaged, ultimately producing protected quantum dots that are individually functionalised.

To facilitate this protection and functionalisation strategy the DUPA **24** intermediate was synthesised for immediate evaluation and for the synthesis of tertiary phosphine oxides possessing useful functional groups **Scheme 10**. DUPA **24** was synthesised in the same method as the other two phosphinous acid intermediates **14** and **20**, via the addition of the appropriate Grignard reagent to dibutyl phosphite followed by acidification and aqueous work up. The product was isolated in a reasonable 53% yield and all characterisation undertaken suggested a successful synthesis.

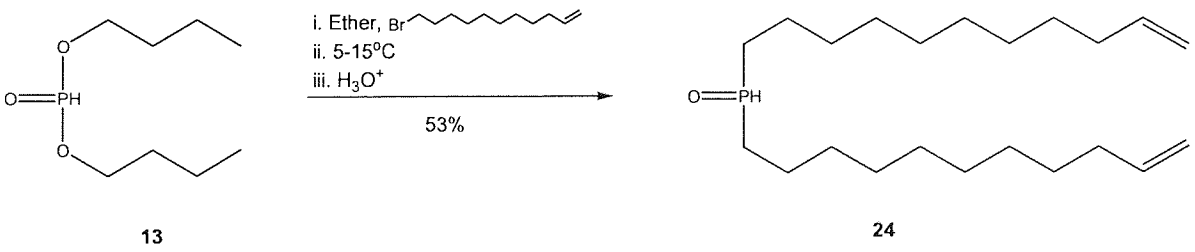

13 24

Scheme 10: Synthesis of DUPA 24

The IR spectrum showed the presence of peaks corresponding to the olefinic group (3078 cm^{-1}, =C-H), the P-H function (2356 cm^{-1}) and the P=O group (1160 cm^{-1}). Also the appearance of a new peak for the P-CH_2 stretch at 1642 cm^{-1} that is not present in the starting materials is evidence of the formation of the product. The LRMS and HRMS gave molecular ion peaks consistent with the correct size for the desired product.

The ^1H NMR spectrum was consistent with the structure of DUPA **24**. The broad multiplet (∂ 1.10-1.80 ppm) integrated to 36 the expected number of protons for the CH_2

groups of the alkyl chains. The doublet triplet (∂ 5.70 ppm) corresponding to the protons of the carbon directly adjacent to the double bond was present and integrated as expected. The three characteristic signals for the olefinic protons were also present, integrated correctly and possessed the previously explained splitting patterns. Finally the widely split doublet corresponding to the proton of the phosphorus was present centred at ∂ 6.67ppm with a coupling to the phosphorus of ^{1}J=445.1 Hz. Again the magnitude of the coupling was in the range anticipated for compounds of this type.[123, 127, 128]

The ^{13}C spectra is similar to that of DOPA **14**, with the addition of the signals for the carbons in the olefinic group. All the peaks present exhibit the anticipated chemical shifts and the two coupling constants for **C-1** and **C-3 Figure 56** are comparable to that of similar molecules of this type. Unfortunately poor resolution prevented the calculation of a coupling constant for **C-2**. However all the analysis was in agreement with the successful formation of the intermediate DUPA **24** and this intermediate was used in the synthesis of multi functionalised tertiary phosphine oxides.

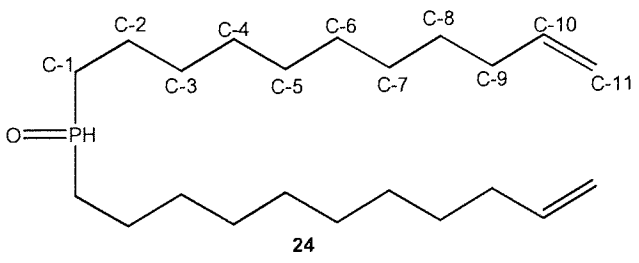

Figure 56: Numerically labelled structure of DUPA 24

2.1.8 Triundecenephospine oxide (TUPO) 25

This tertiary phosphine oxide was synthesised to provide the maximum number of polymerisable units per ligand **Scheme 11**. Since this phosphine oxide is composed of three undecene chains attached to the central phosphorus atom it does not suffer from the solubility problems that were prevalent in TMSPO **23**. TUPO **25** was designed exclusively for the individual polymer encapsulation of quantum dots. Long mobile chains with the potential for global cross-linking around the entire surface of the dot.

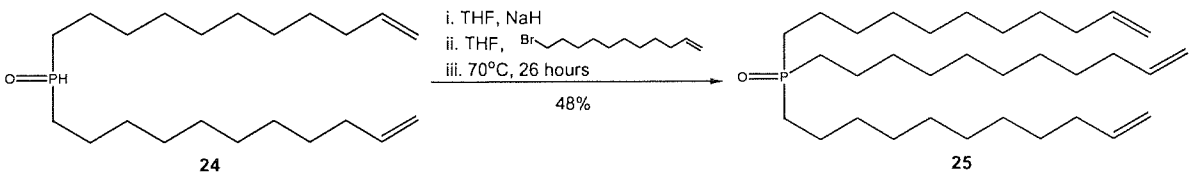

Scheme 11: Synthesis of TUPO 25

TUPO **25** was synthesised via the base deprotonation of DUPA **24** followed by the drop-wise addition of 11-bromo-1-undecene. The reaction was monitored by TLC, disappearance of both of the starting materials and formation of a new product was used to indicate the progress of the reaction since DUPA **24** does not suffer the same visualisation problems as DOPA **14**. Slow crystallisation in ice cold hexane provided the product in 48% yield and analysis confirmed the formation of tertiary phosphine oxide **25**.

The ^{1}H NMR spectrum presented as anticipated from the previous analysis in this thesis and that in the literature of similar compounds containing this functionality.[138] The integration of the signals corresponded with the structure of the tertiary phosphine oxide

and no trace of a signal for the proton attached to the phosphorus in the intermediate phosphinous acid remained. Examination of the coupling of the protons in and adjacent to the double bond revealed that the splitting patterns were identical to those of the same form discussed previously.

The ^{13}C spectrum also supported the formation of the desired product. The first three carbons in the chain were coupled to the phosphorus. The pattern of the coupling was consistent with those of phosphine oxides of this nature described earlier and those reported in the literature.[124, 130] The presence of the signals correlating to the carbons of the olefinic groups suggested successful synthesis without deterioration of the functional group. The ^{31}P NMR spectrum contained a sharp singlet at 48.8ppm, this chemical shift is indicative of tertiary phosphine oxides.[129, 137, 138, 139, 140, 143] Finally analysis by LRMS, HRMS and IR spectroscopy all supported the successful formation of TUPO **25**.

2.1.9 Diundecene(decanol)phosphine oxide (DUDPO) 27

The final tertiary phosphine oxide to be synthesised contained a mixture of alkene and alcohol functionalities. The multi-functionalised ligand was synthesised for development applications in the area of functionalised polymer coating of individual quantum dots. It was theorised that the polymerisation of the alkene groups on the surface of the dot would produce a globally polymerised shell with free hydroxyl groups that could be utilised for future reactions.

DUDPO **27** was synthesised by deprotection of diundecene(decyl-silyl-ether)phosphine oxide intermediate (DUDSPO) **26 Scheme 12**. The protected intermediate was synthesised by the base catalysed deprotonation of DUPA **26** followed by the addition of TBDMSi-protected-10-bromo-1-decanol **18**. The reaction was monitored by TLC, on completion the THF was removed and the solids re-dissolved in DCM. Aqueous workup provided the intermediate product DUDSPO **26** in an excellent yield of 97%. Characterisation of the product was undertaken at this stage since subsequent applications of the ligand may require the continued protection of the hydroxyl group.

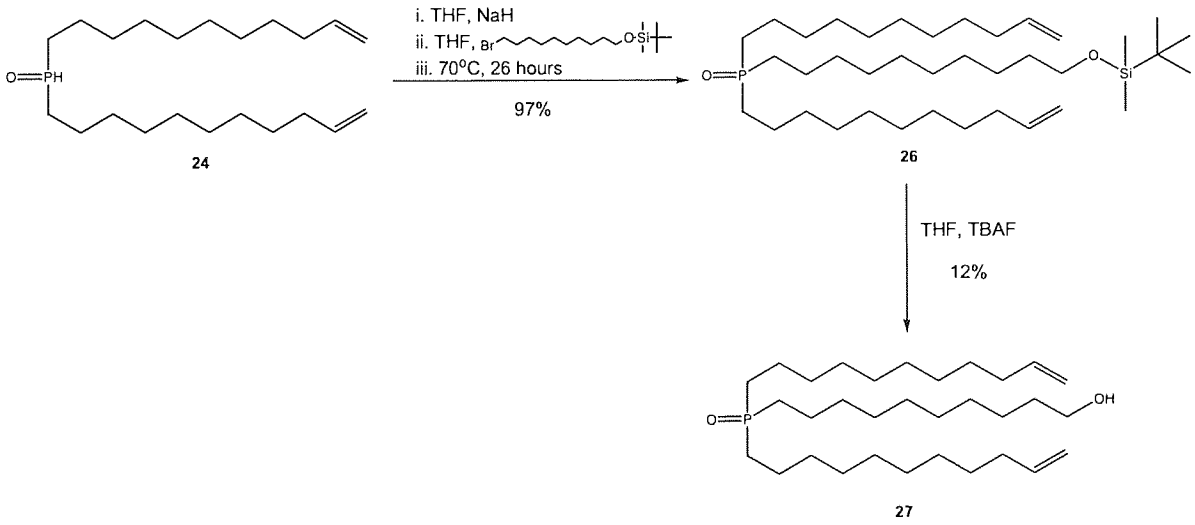

Scheme 12: Synthesis of DUDPO 27

Examination of the IR spectrum revealed all the anticipated peaks of the functional groups present in the intermediate. The most significant peaks included =C-H bond at 3076 cm^{-1} and $SiO\text{-}CH_2$ at 1099 cm^{-1}, these imply that the double bond and the protecting group remain unchanged after reaction. The LRMS detected a species of the correct mass for the structure of the protected intermediate. The ^{1}H and ^{13}C NMR spectra contained all of the previously discussed signals for the functional groups

present. The integration and coupling patterns of the ^{1}H spectrum corresponded to the desired structure and there was no trace of the unique proton attached to the phosphorus that is present in the starting material, DUPA **24**.

The silyl protecting group was removed by treatment of the intermediate **26** with TBAF and the process monitored by TLC. After an aqueous work-up, a pure sample of the product was obtained from crystallisation at below 0°C, the initial filtration provided a 12% yield. This reaction was not repeated and thus this yield is totally unoptimised, based on the TLC analysis it is anticipated that the yield can be improved considerably.

All analysis on the pure sample obtained indicated that deprotection had occurred and that the OH functionality had been restored successfully. The IR spectra exhibited a broad peak (3347 cm^{-1}) for the OH functionality and the =C-H peak remained (3078 cm^{-1}). The ^{1}H NMR spectra showed no trace of signals correlating to the silyl protecting group and all the integration and the previously discussed splitting patterns presented as anticipated. The ^{13}C NMR showed peaks at the expected chemical shift and the coupling of the first three carbons followed the pattern seen for the phosphine oxides described earlier. Unfortunately the carbons towards the centre of the alkyl chain formed a complex multiplet and as a result individual assignment was not possible. Finally the LRMS and HRMS detected species of the correct mass to be the desired multi-functionalised phosphine oxide **27**.

2.1.10 Trioctlyphosphine sulphide (TOPS) 28

The P=O moiety was chosen as the anchoring group for all of the previously described ligands because of the nature of the metal phosphine bond. X-ray data has shown that metal---O bonds have multiple bond character,[144] where as metal---S bonds are single bonds formed simply by the donation of a pair of electrons from the sulfur atom to the metal. However P=S groups have been shown to exhibit bridging behaviour.[144, 145] Since the outer shell of the NanoDots™ are composed of ZnS the possibility of forming sulphur bridges between the shell and a ligand with a P=S anchoring group existed. Several phosphine sulphides were synthesised to explore this theory.

The first phosphine sulphide to be synthesised was trioctylphosphine sulphide (TOPS) **28** since it was the closest mimic to TOPO **1**. The initial transformation of TOPO **1** to TOPS **28** involved the use of the thionating reagent commonly known as Lawesson's reagent[146] (LR) **29 Figure 57**.

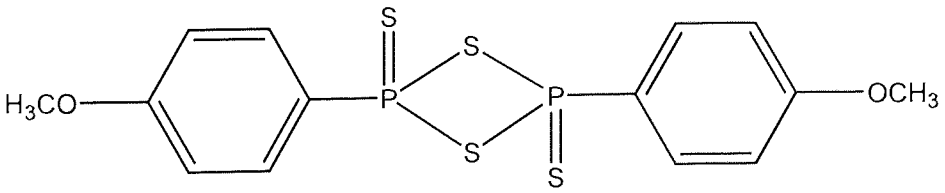

29

2,4-Bis-(4-methoxy-phenyl)-[1,3,2,4]dithiadiphosphetane 2,4-disulfide

Figure 57: Structure of Lawesson's Reagent

TOPO **1** was reacted with 0.5 equivalents of LR at 110°C for two hours. Aqueous work up followed by filtration of an insoluble by-product produced a sticky oil with a foul odour **Scheme 13**. The oil was analysed by LRMS that confirmed the transformation

had been successful. Unfortunately, however all attempts to remove the unreacted LR from the product failed.

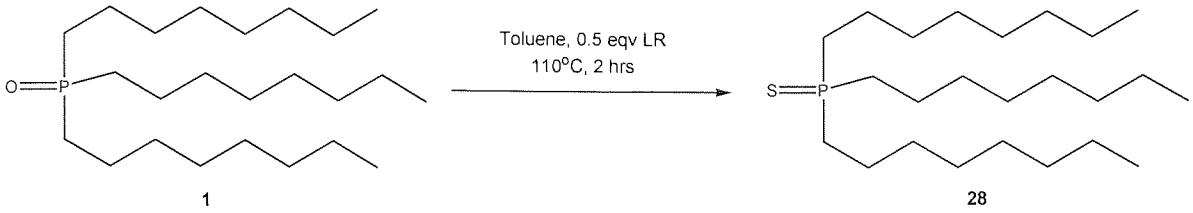

Scheme 13: Synthesis of TOPS 28 using LR

The problems in purification resulted in the employment of an alternative synthetic strategy for the production of TOPS **28.** The utilisation of a polymer supported thionating reagent (PS-TR) that could be removed by simple filtration was investigated as a means of avoiding any contamination of the product. PS-TR **30**[147] was synthesised from commercial *N*-2-(aminomethyl)aminomethyl polystyrene **31** via treatment with ethyldichlorothiophosphate (EDCTP) using methodology reported recently[147] **Scheme 14**. The diamine resin was suspended in pyridine and kept at 0°C during the drop-wise addition of EDCTP, the temperature was then allowed to rise to ambient and the flask agitated gently for 24 hours. The resulting bright orange resin was filtered and dried under vacuum to a constant weight. The successful synthesis of the polymer-supported thionating reagent was assumed from the distinct colour change and the correlation of the IR spectrum to the IR data provided in the literature.[147]

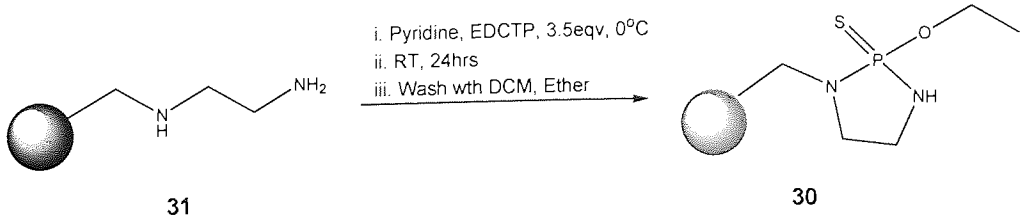

Scheme 14: Preparation of PS-TR 30

The conversion of TOPO **1** to TOPS **28** was achieved in a 86% yield by the treatment of TOPO **1** with 6.8 equivalents of PS-TR **30** followed by 38 hours of heating at 90°C **Scheme 15**.[147] The reaction was monitored by TLC and LRMS, upon completion the reaction mixture was filtered through a pad of silica and concentrated under reduced pressure. Analysis of the sticky oil with LRMS confirmed that the conversion had occurred. A peak at *m/z* 403 (100%) corresponded to the protonated mass of TOPS **28** and there was no sign of any peak at or around *m/z* 387 that would be the protonated mass of TOPO **1**. The IR spectrum also supported the complete conversion with the disappearance of the strong P=O at 1146cm^{-1} and the appearance of a strong band at 734cm^{-1} that corresponds to P=S.[127, 136, 148]

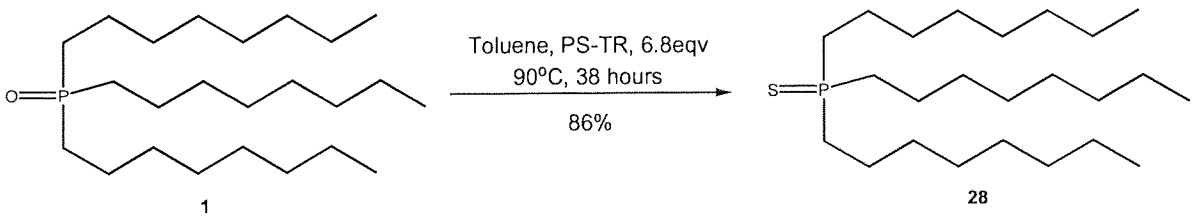

Scheme 15: Synthesis of TOPS 28 using PS-TR

The ^{1}HNMR spectrum was very similar to that of TOPO **1**, however the large multiplet between ∂ 1.10 and 1.80ppm, corresponding to the CH_2 protons of the alkyl chains, appears to have been pulled slightly further downfield compared with that in the spectrum of TOPO **1**. This suggests a difference in the coupling of the protons of the CH_2 groups neighbouring the phosphorus atom.[139] Unfortunately as in the phosphine oxide-containing compounds overlap prevents the elucidation of individual couplings.[126]

Examination of the ^{13}C NMR spectrum also supports the complete transformation of the P=O to P=S. The chemical shifts of the peaks for the first few carbons away from the phosphorus have shifted slightly downfield compared those in TOPO **1**. However the most compelling evidence of conversion from this spectrum is the decrease in the coupling constant of the carbon labelled **C-1 Figure 58**.

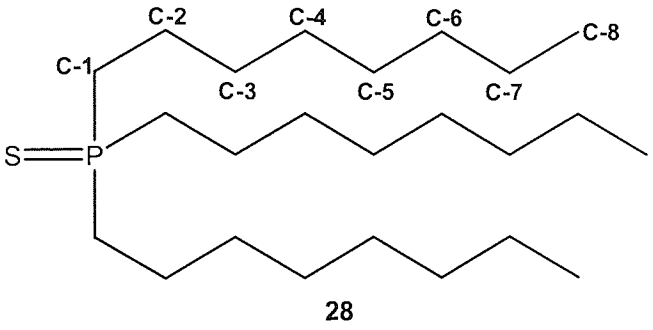

28

Figure 58: Numerically labelled structure of TOPS 28

The coupling of **C-1** to the phosphorus in TOPS **28** is calculated at $^{1}J_{PC}$=49.6 Hz where as the analogous carbon in TUPO **1** is split $^{1}J_{PC}$=65.0 Hz[124] by the phosphorus. The couplings for **C-2** and **C-3** also differ by slightly increased coupling in TOPS **28** compared to TOPO **1**. The observed coupling constants correspond to couplings of the same nature in similar systems such as tributylphosphine sulphide found in the literature.[129]

The mechanism for the thionation reaction involving the PS-LR **30** most likely proceeds via a wittig-type intermediate in a similar manner to that of the thionation with LR **29** **Figure 59**.

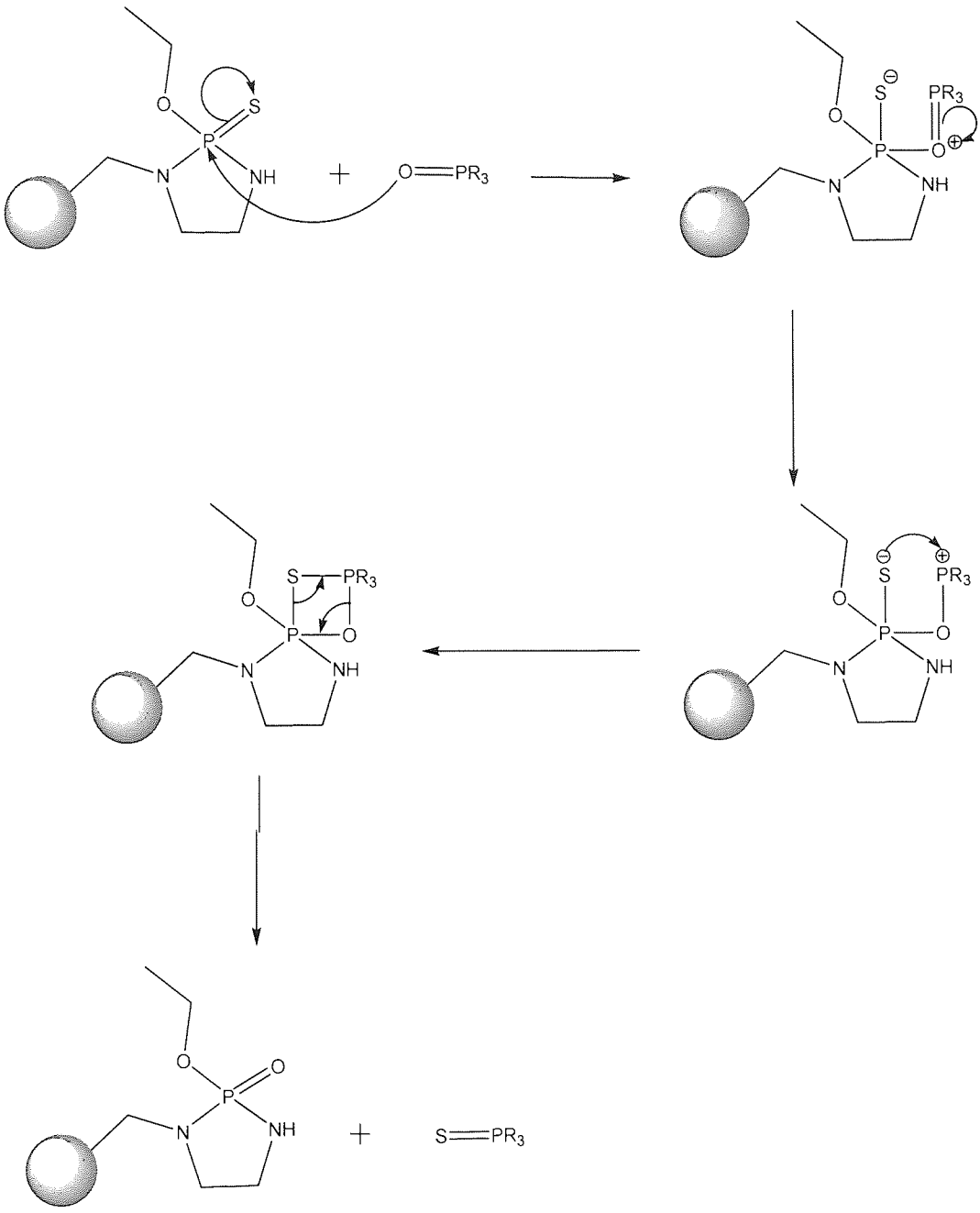

Figure 59: **Mechanism of thionation by polymer supported thionating reagent 30**

2.1.11 Diundecenephosphosulfinous acid (DUPSA) 33[147]

Following the successful synthesis of TOPS **28** the conversion of other functionalised phosphine oxides was attempted. The transformation of the intermediate DUPA **24** to DUPSA **33** was achieved by treatment of the phosphinous acid **24** with PS-TR **30**. DUPSA **33** was synthesised in an excellent yield of 91% by heating to 90°C in the presence of 3 equivalents of PS-TR **30 Scheme 16**. The reaction was monitored by TLC and LRMS.

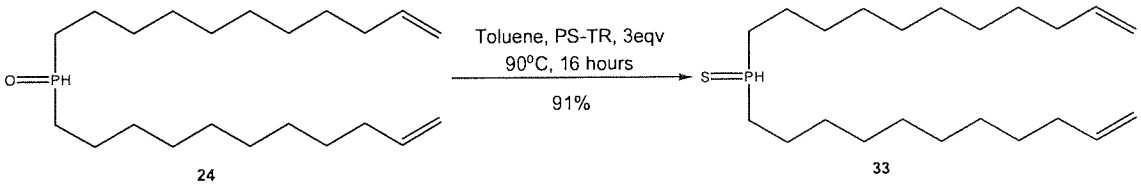

Scheme 16: Synthesis of DUPSA 33

The LRMS contained a peak for the protonated product of the P=S derivative and the IR spectrum as for TOPS **28** again showed the disappearance of the peak at 1160 cm^{-1} for P=O and replacement with P=S at 735 cm^{-1}. [127, 136, 148] The ^{13}C NMR spectrum is complex due to overlap of signals but the distinctive drop in the size of the coupling constant of the carbon directly attached to the phosphorus compared to the same coupling in the oxide is again present and the value is consistent with similar couplings reported in the literature.[129]

As with TOPS **28**, the ^{1}H NMR of the sulfide **33** was very similar to that of the corresponding oxide **24**, the coupling of the protons in and adjacent to the double bond are identical to those previously discussed. However the most noticeable difference

concerns the position of the doublet produced by the proton directly attached to the phosphorus. In the spectrum of DUPA **24** the doublet is centred at ∂ 6.76ppm, with one of the signals (∂ 5.86 ppm) positioned to the left of the ddt signal at ∂ 5.70ppm **Figure 60.**

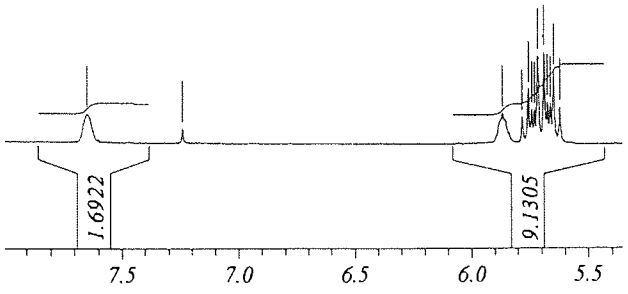

Figure 60: **^{1}H NMR spectrum of DUPA 24 expansion between ∂ 5.45 ppm & ∂ 8.00 ppm**

In contrast the spectrum of DUPSA **33** the doublet has shifted upfield and is centred at ∂ 6.51ppm, with one of the signals (∂ 5.65 ppm) to the right of the ddt signal centred at ∂ 5.78ppm **Figure 61.**

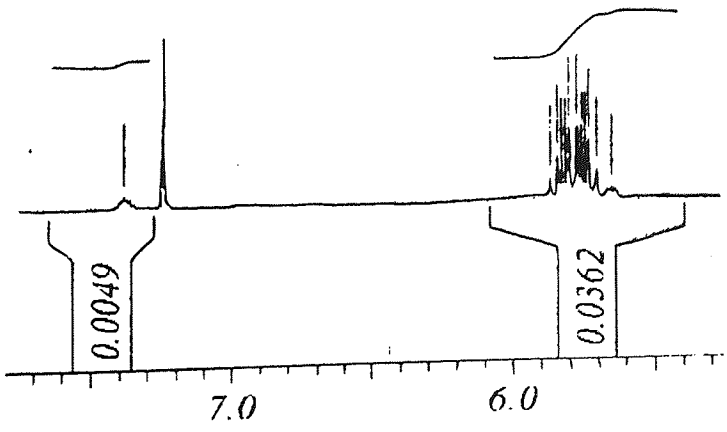

Figure 61: **^{1}H NMR spectrum of DUPSA 33 expansion between ∂ 5.20 ppm & ∂ 7.80 ppm**

The magnitude of the coupling of this proton to the phosphorus is also different in sulfide **33** compared with oxide **24**. The coupling in oxide **24** is $^{1}J_{PH}$=445.1 Hz compared with $^{1}J_{PH}$=433.2 Hz for sulfide33. This decrease is consistent with similar data reported in the literature.[140]

2.1.12 Dimethylstyrylphosphosulfinous acid (DMSPSA) 34[146]

Due to the successful synthesis of the DUPSA **33** intermediate it was decided to synthesise the DMSPSA **34** intermediate. The synthesis was initially attempted with the PS-TR **30**, however the reaction failed to go to completion on a number of occasions. Elevated temperature and increased equivalents of the polymer supported reagent had no effect. Contra to our expectations, the conversion could however be taken to completion via reaction with LR **29 Scheme 17**.

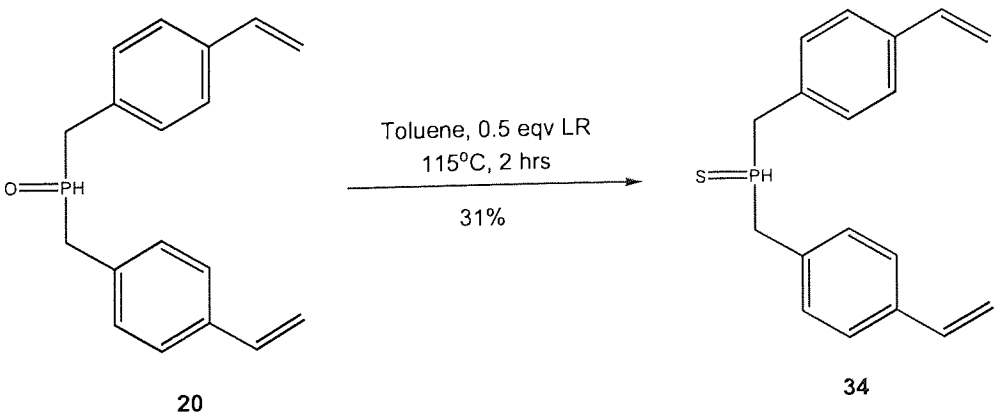

Scheme 17: Synthesis of DMSPA 34

DMSPA **20** was heated to 115°C with 0.5 equivalents of LR **29** and the reaction monitored by TLC. Aqueous work up in DCM followed by filtration to remove an insoluble by-product furnished the crude product as a mixture of white and yellow

crystals. The crude product was then dissolved in a mixture of acetone and DCM and passed through a pad of silica. The solvent was again removed and the resulting solid triturated in ether producing the pure product as lustrous white crystals in a moderate yield of 31%.

Both LRMS and HRMS supported the complete transformation of the DMSPA **20** to DMSPSA **34**. The IR spectrum also supported the formation of sulfide **34** with the disappearance of the P=O peak at 1194cm^{-1} and the appearance of a peak at 712cm^{-1} that is in the correct region for P=S. The ^{13}C NMR spectrum is almost identical to that of DMSPA **20**, but the decrease in coupling constant from $^{1}J_{PC}$=59.7 Hz in oxide **20** to $^{1}J_{PC}$=45.5 Hz in sulfide **34** is evidence of transformation.

The ^{1}H NMR spectrum of the sulfide **34** possess the same coupling patterns as seen in DMSPA **20** intermediate and the majority of the chemical shifts are comparable. The doublet pentet corresponding to the proton attached to the phosphorus is shifted upfield compared with that of oxide **20**. One of the doublet pentet signals is now under the doublet that corresponds to the *trans* coupled proton of the double bond, whereas this doublet pentet signal is well separated and upfield of the *trans* coupled proton signal in DMSPA **20**. The transformation to the sulfide **34** is also accompanied by a drop in the coupling constant of the proton attached and coupled to the phosphorus, from 468.7 Hz for the oxide to 451.2 Hz for the sulfide.

The mechanism of thionation with LR **29** is thought to proceed via a highly reactive dithiophosphine ylide **35 Figure 62**. Speculation on the formation of this reactive species leads to two similar mechanistic pathways that both involve Wittig-type

intermediates for the thionation reaction. Neither pathway is mutually exclusive and it is most likely that a combination of both lead to successful thionation. The first resulted from the investigation by Lawesson of the behaviour of LR **29** in solution by means of ^{31}P NMR spectroscopy. Examination of the spectrum implied the presence of low concentrations of a dipolar species. Lawesson concluded that this species was that of the dithiophosphine ylide **35** and thionation initiated by this species would proceed as show in **Figure 62.**[149]

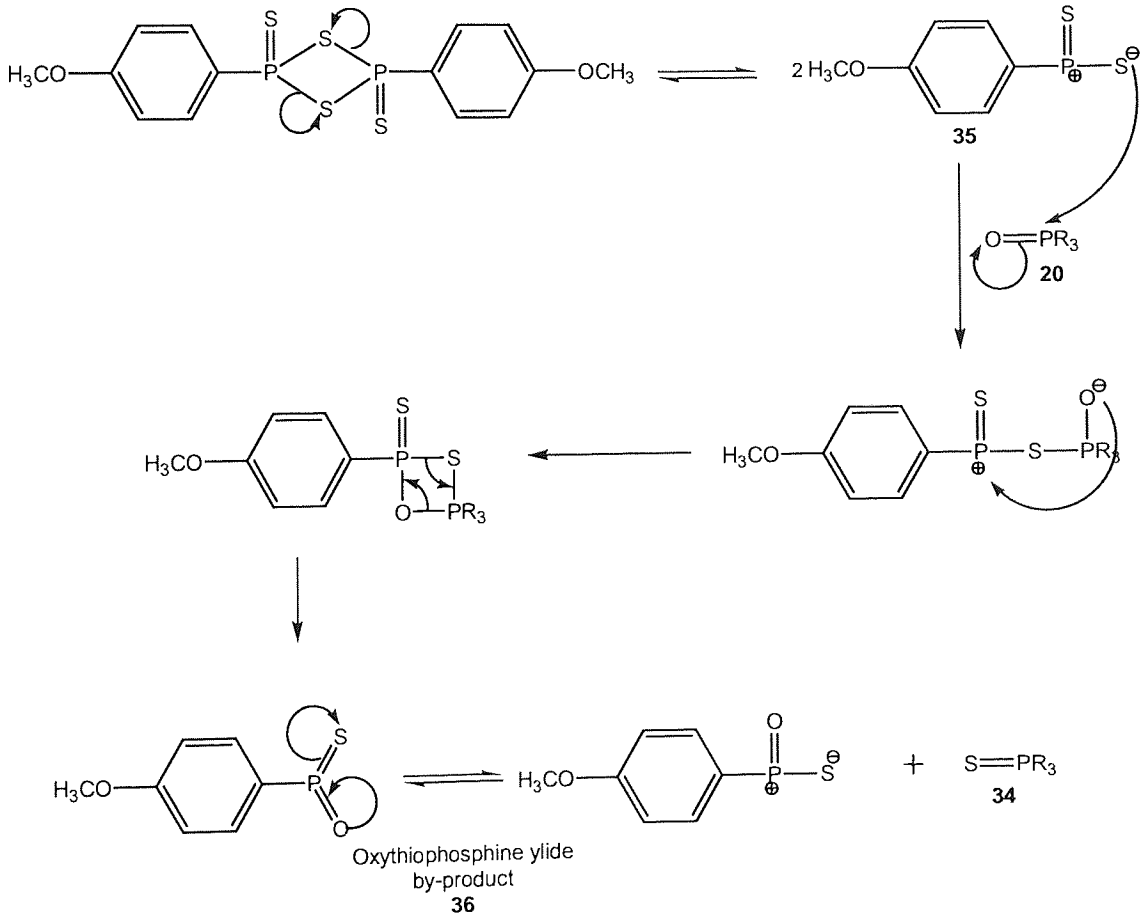

Figure 62: Mechanism of LR mediated thionation of phosphine oxide 20

The alternate possibility for formation of the dithiophophine ylide results from an initial attack by the oxygen of the group to be transformed on the one of the phosphorus atom of LR **29 Figure 63.**

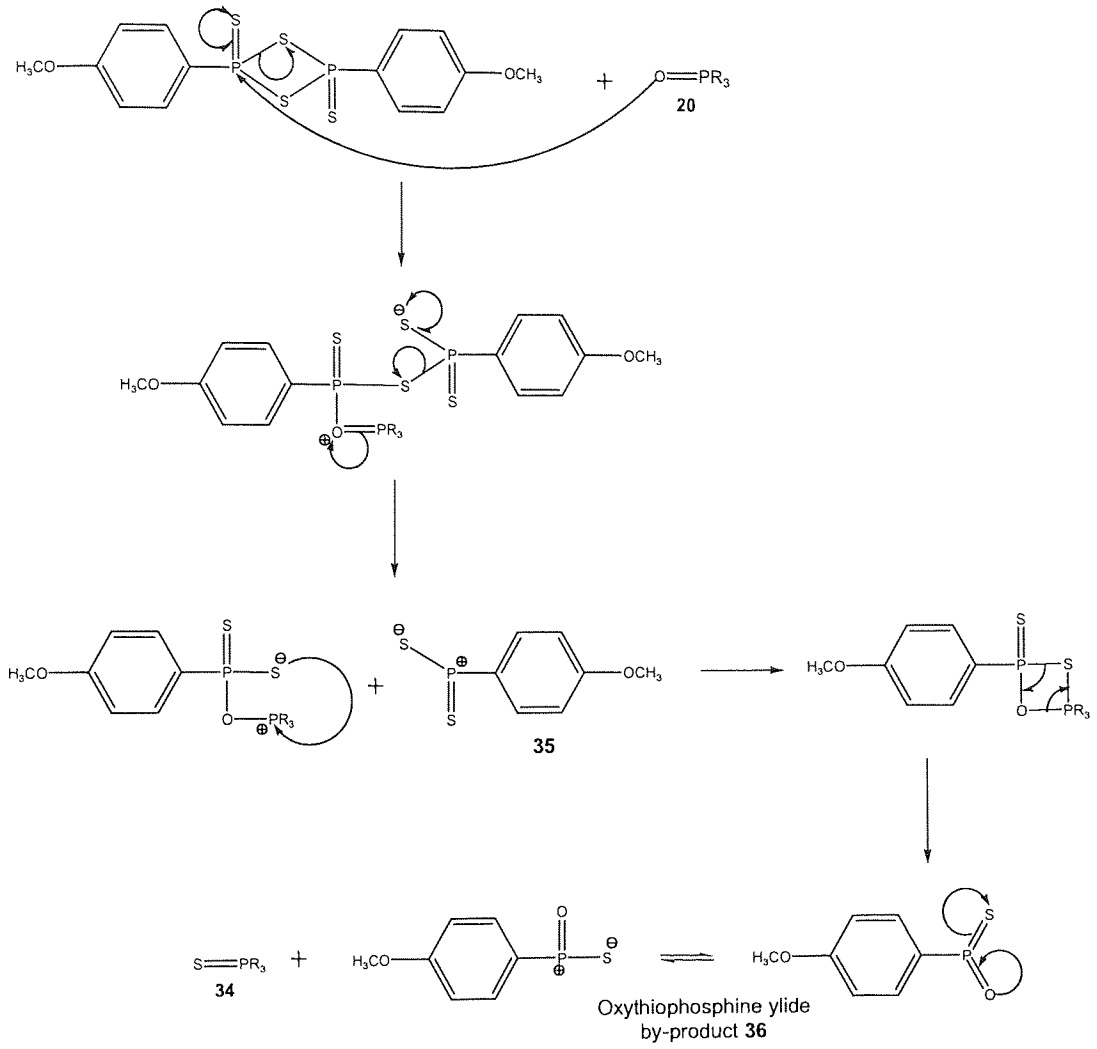

Figure 63: Alternative mechanism of LR mediated thionation of phosphine oxide 20

This mechanism results in the production of a dithiophosphine ready to follow the pathway shown in **Figure 62** and the same oxythiophosphine ylide by-product **36**. Both possible mechanisms produce an oxythiophosphine ylide by-product **36** that forms a highly insoluble trimer **37 Figure 64**. It is possible that this trimer **37** accounts for the insoluble powder encountered in the work-up, although this was not confirmed by analysis.

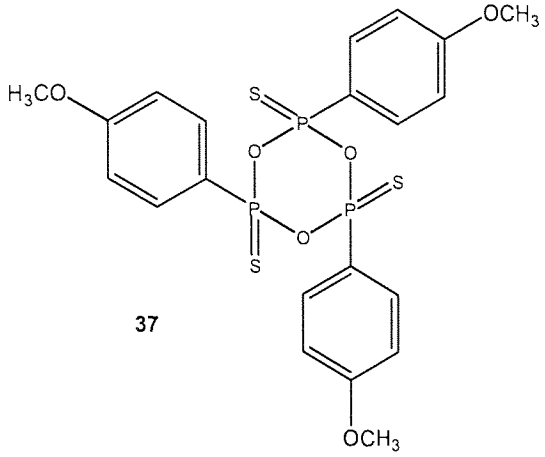

37

Figure 64: Structure of the trimer 37 formed by the intermolecular reaction of the oxythiophosphine ylide by-product

2.2 – Investigation of HDA Coated NanoDots ™

The quantum dots used in this body of work were supplied by Nanoco™ Technologies Limited and are composed of CdSe/ZnS. The NanoDots™ were supplied with an organic capping layer of HDA **3** **Figure 65**, that could be displaced by the functionalised ligands discussed in section 2.1.[15] A range of different coloured NanoDots™ were used and it was discovered that their behaviour both in terms of photoemissive and their chemical properties varied slightly from batch to batch.

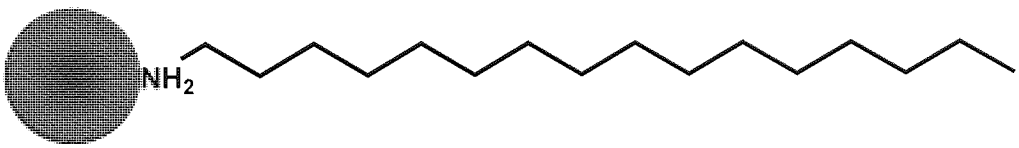

Figure 65: Schematic representation of HDA 3 capped nanoparticle

Analysis of the NanoDots™ by ^{1}H NMR revealed almost identical spectra in each case. The spectra resembled that of HDA **3**, a triplet at ∂ 0.86ppm followed by a broad multiplet between ∂ 1.00-1.70ppm. The triplet corresponds to the protons of the terminal methyl and the multiplet corresponds to the protons of the alkyl chain of HDA **3**. Interestingly the signal for the two protons on the carbon adjacent to the nitrogen that is shifted downfield out of the multiplet in a sample of pure HDA **3** is absent in all the spectra obtained from HDA **3** coated NanoDots™. The absence of this signal may be a consequence of the interaction of the molecule with the surface of the nanoparticle.

A sample of NLP121 that was composed of CdSe/ZnS NanoDots™ was analysed by combustion analysis. Examination of the results shows that less than half the material comprising the NanoDot™ is organic, the majority of the mass comes from the core

shell structure. A combustion analysis of the same NanoDots™ after rigorous washing with methanol was also undertaken. Comparing the ratio of nitrogen to cadmium in the non-washed and washed NanoDots™ revealed that 50% of the HDA **3** capping ligand can be removed in this way **Table 3**.

	Sample	Cd	N
Combustion analysis	Non-washed	68.50 %	1.29%
	Washed	67.35%	0.75%
Molar ratio	Non-washed	1 mole	0.15 moles
	Washed	1 mole	0.08 moles

Table 3: Table of the percentage composition and molar ratio of Cd and N of washed and non-washed batches of NanoDots™

An investigation into the stability of HDA **3** coated NanoDots™ under a range of conditions was undertaken. Their ability to withstand strong acid was evaluated by serial dilution of a stock solution of NanoDots™ with strong hydrochloric acid. The resistance to acid etching was monitored by the intensity of the photoluminescence (PL) spectra recorded for each solution at the different dilutions **Figure 66**. The photoluminescence of the NanoDots™ decreases as the concentration of acid increases.

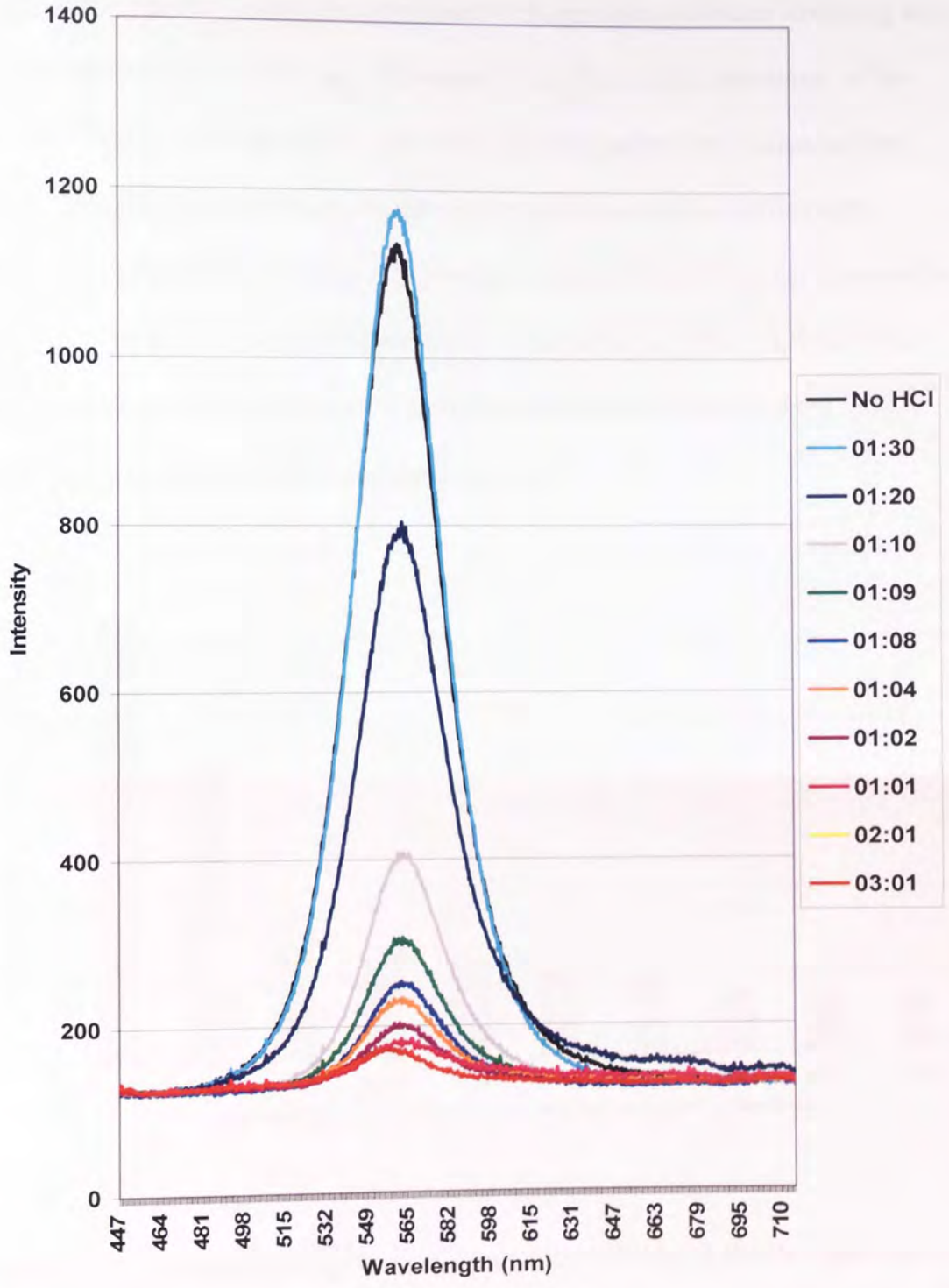

NB – The serial dilutions in **Figure 66** correspond to the volumetric ratio of pH 1.5 HCl acid solution to NanoDot™ stock solution respectively.

Figure 66: PL Spectra of HDA 3 coated NanoDots™ upon exposure to increasing volumes of concentrated acid

Figure 67 is a graph showing the percentage of PL emission maximum remaining for a sample after exposure to HCl (aq) with respect to the PL emission maximum of the sample where no acid was added. Examination of this graph makes it clear that the HDA **3** capped NanoDots™ can tolerate weakly acidic conditions. Sufficient PL remains when the acid concentration is less than 1 part in 20, doubling the concentration to 1 part in 10 reduces the photoluminescence to below 40%. Further increase in the concentration of acid steadily reduces the photoluminescence down to about 15%, at which point no more deterioration appears to occur.

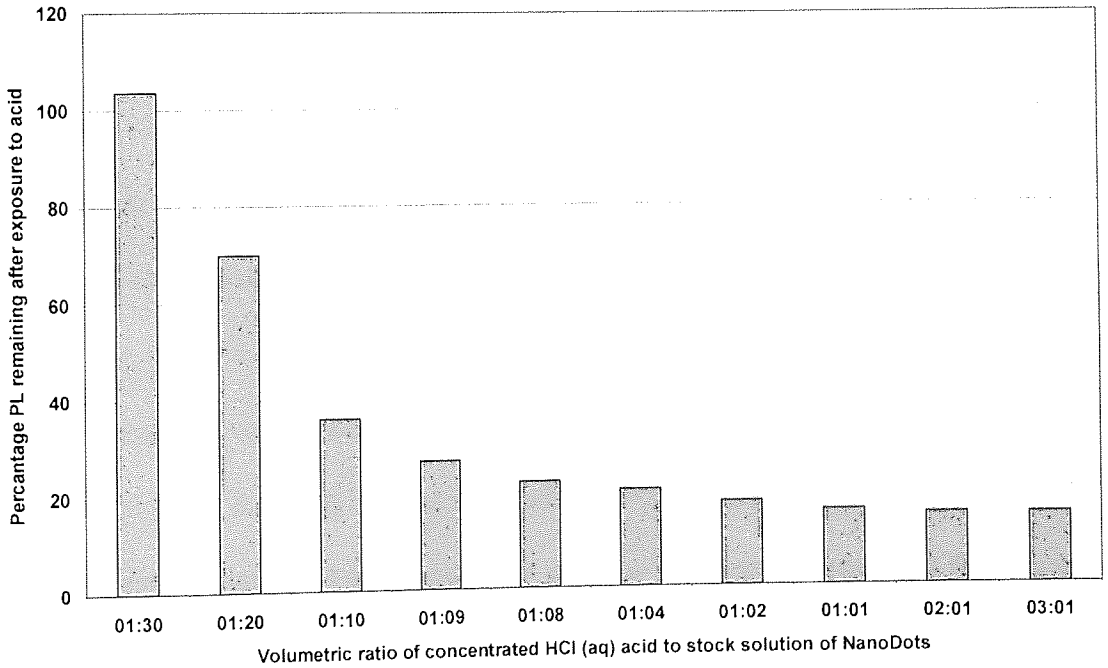

Figure 67: Graph showing the percentage deterioration in the PL emissions of a stock solution of HDA coated NanoDots™ exposed to increasing amounts of concentrated HCl (aq)

The resistance to deterioration of HDA **3** capped NanoDots™ to the activity of azobis-*iso*-butyronitrile (AIBN) was examined by heating 10mg of NanoDots™ with 0.1mg,

0.2mg and 0.4mg of AIBN. The PL spectra were recorded after 4 hours at 72°C was consistent with previous findings reported in the literature and showed almost complete deterioration in all cases (Appendix A, **Figure 68**).[38, 150]

Further investigation into the stability of HDA **3** coated NanoDots™ involved the exposure of two different batches of NanoDots™ to a variety of commonly encountered reagents. Stock solutions of two batches of nanoparticles and reagents were prepared. Aliquots of the NanoDot™ solutions were exposed to solutions containing the different reagents. The resilience of the NanoDots™ to the various reagents were monitored by comparison of the PL spectra before and after addition. **Figure 69** and **Figure 70** show a compilation of PL spectra after exposure to reagents for NanoDot™ batches MC610 and MC556 respectively.

In order to enable a comparison to be made upon the effect of each reagent on the stability of the two different batches of NanoDots™, the PL spectra recorded after the addition of each reagent had were compared with the PL spectrum obtained from each NanoDot™ sample prior to exposure to any reagents. Comparing the PL emission maximum of an aliquot of the NanoDots™ before treatment to the PL emission maximum after treatment allows a calculation of the percentage PL remaining after the exposure to each reagent.

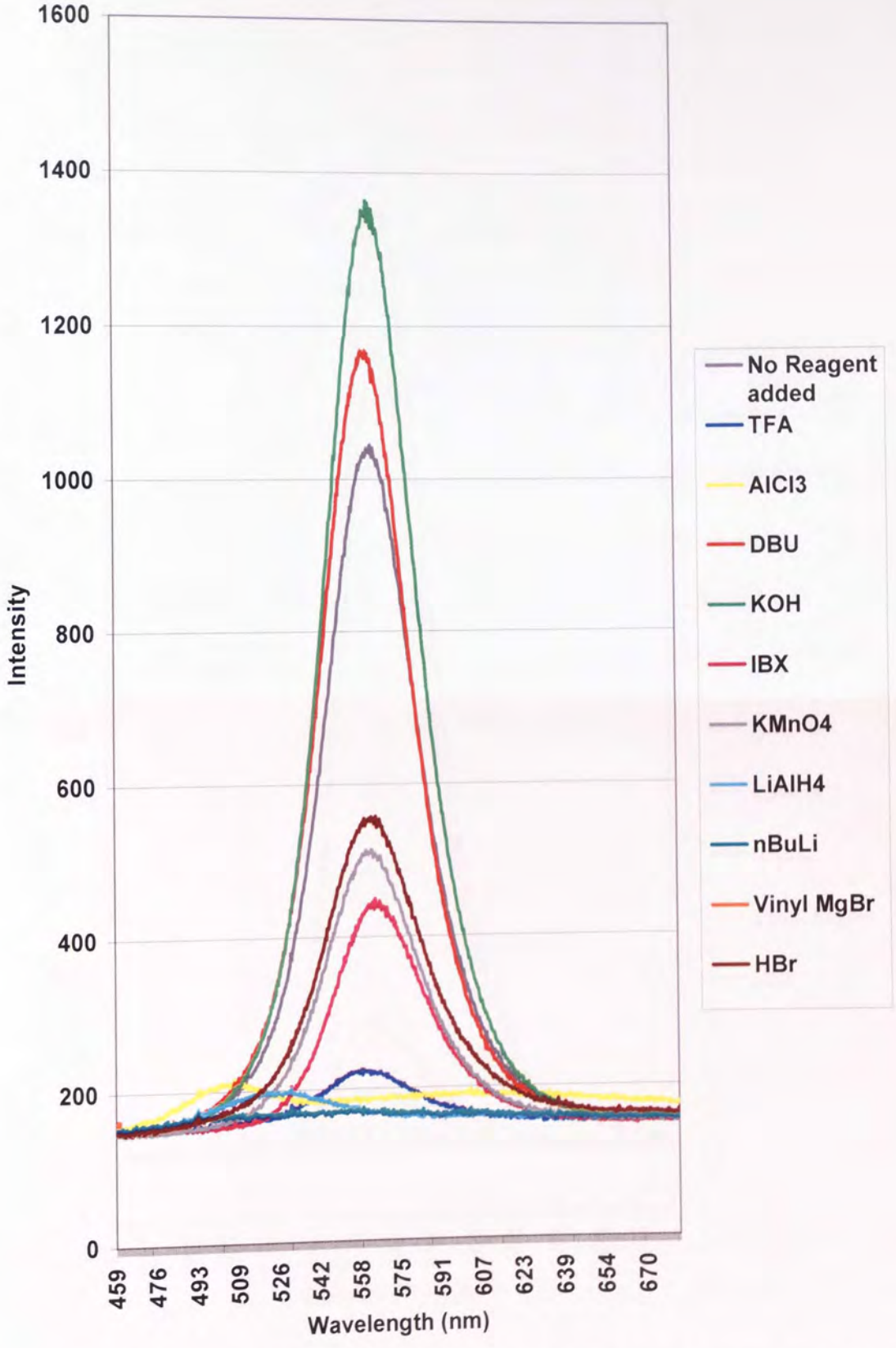

Figure 69: PL spectra of HDA coated NanoDot ™ batch MC610 upon exposure to a variety of reagents

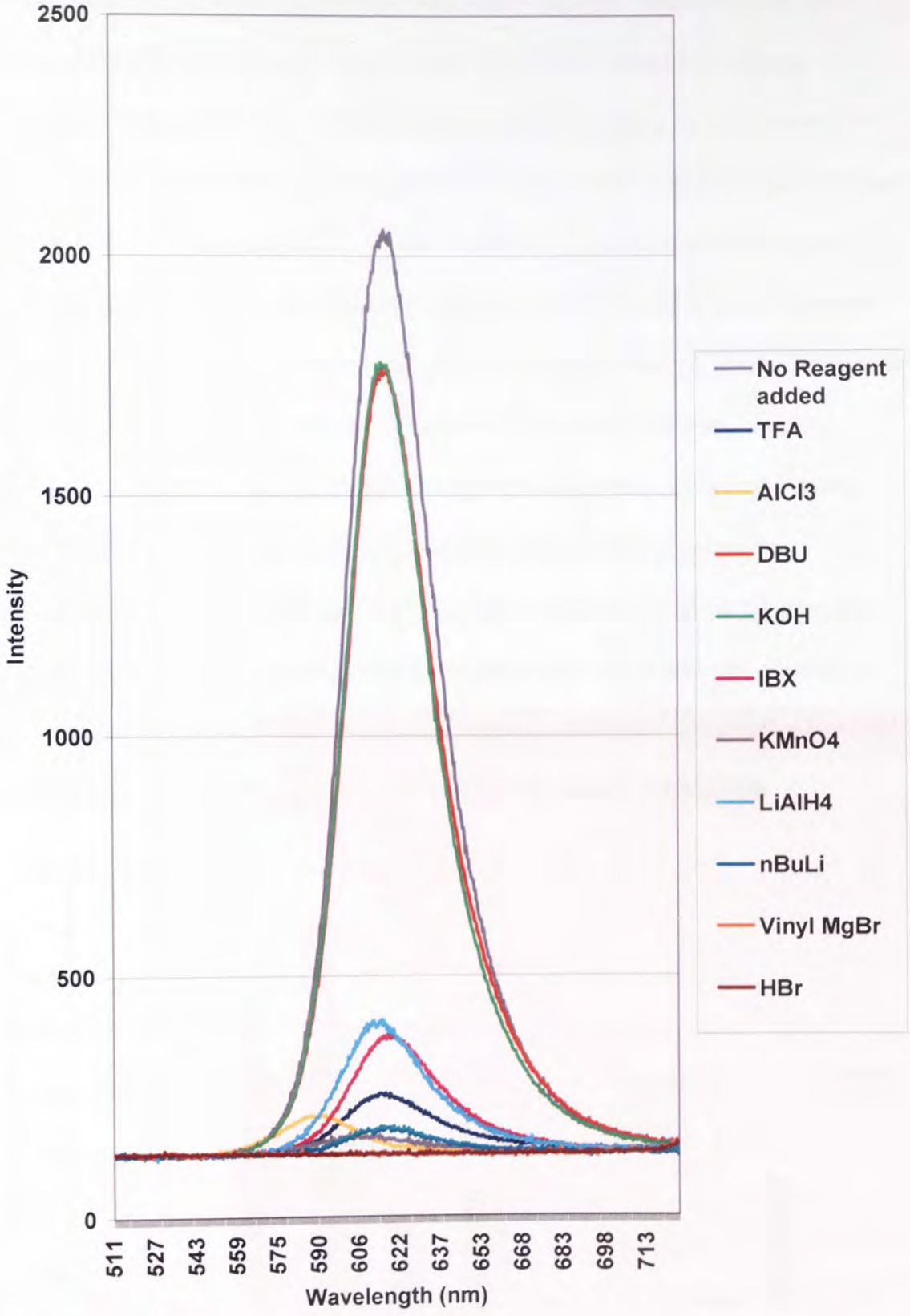

Figure 70: **PL spectra of HDA coated NanoDot ™ batch MC556 upon exposure to a variety of reagents**

A comparison of the remaining percentage PL emissions after treatment with the various different reagents is represented below for MC610 and MC556 **Figure 71**. Immediately noticeable is that both batches are affected similarly by exposure to the same reagent. Overall batch MC610 appears to be more resilient to the range of reagents than MC556. 1,8-diazabicyclo[5.4.0]undec-7-ene (DBU) and potassium hydroxide (KOH) do not have a seriously detrimental effect on the PL of either batch. However exposure to trifluroacetic acid (TFA), aluminium trichloride ($AlCl_3$), lithium aluminium hydride ($LiAlH_4$), *N*-butyl lithium (*N*-BuLi) and vinyl magnesium bromide (vinyl MgBr) reduce the PL of the NanoDots™ to such an extent that they would become useless in identification applications. Iodobenzoic acid (IBX) and potassium permanganate ($KMnO_4$) also have a negative effect on the PL emission however these reagents are marginally less destructive than those previously mentioned. Finally, it is apparent that whilst the addition of hydrogen bromide (HBr) has completely destroyed the PL emission of MC556, just under 50% of the PL remains for MC610.

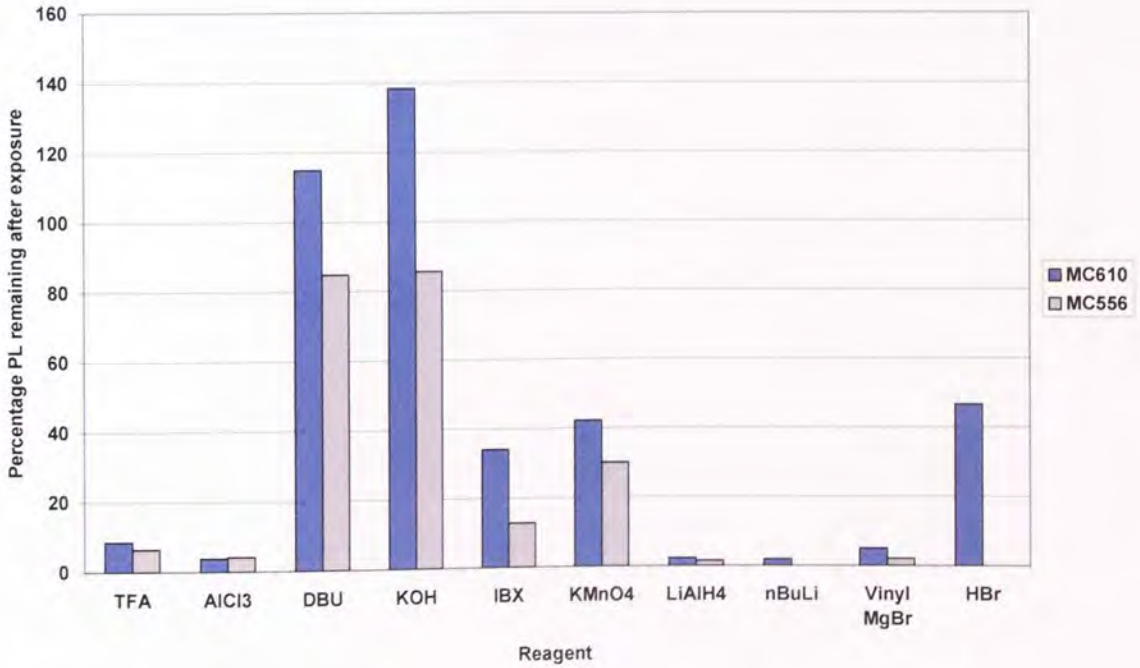

Figure 71: Bar graph depicting the remaining percentage PL of two batches of NanoDots™ upon exposure to a variety of reagents

Examination of these results suggests that although the stability of the NanoDots™ follows the same general trends when exposed to different reagents other factors also participate. Differences in the synthesis and subsequent treatment of the NanoDots™ could affect their behaviour and interaction with conditions they encounter. Further research and development into this area is required.

2.3 – Ligand Displacement

Exchange of the HDA **3** capping layer for the functionalised phosphine oxides previously discussed enabled the properties of the NanoDots™ to be tailored for particular applications. The first ligand exchange involved the two functionalised phosphinous acids DMSPA **20** and DUPA **24**. In solution the structures of these two molecules are in equilibrium between the pentavalent and trivalent forms **Figure 72**. It was hypothesised that the introduction of the NanoDots™ would bias the equilibrium towards the pentavalent form where the surface binding through the P=O would be assumed to be stronger than that through the lone pair on the phosphorus.[133, 144]

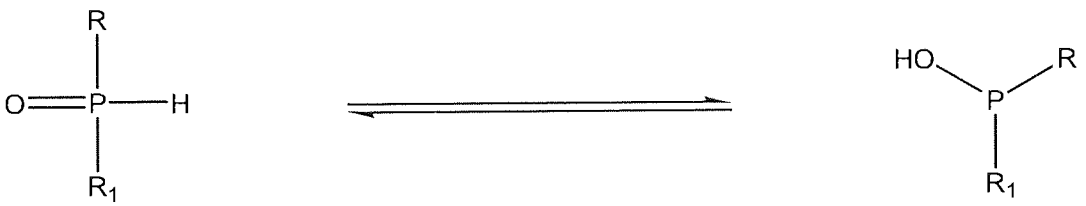

Figure 72: Scheme depicting the pentavalent and trivalent interconversion of phosphinous acids

The HDA **3** ligand surrounding the NanoDots™ was displaced by agitated incubation of the NanoDots™, as received, with a large excess of the desired surface ligand in a dichloromethane (DCM) solution. Precipitation by the addition of a polar solvent such as methanol (MeOH), followed by centrifugation provided the newly capped NanoDots™ as a pellet that could be analysed by ^{1}H NMR spectroscopy. The ^{1}H NMR spectra of displaced dots are composed of the signals for the new ligand and that of residual HDA **3** since the displacement is based upon equilibria and is not a complete

replacement. Integration of signals comprising the ^{1}H NMR spectrum allows an approximate quantification of the success of the displacement.

The ^{1}H NMR spectrum for the displacement with DMSPA **20** is the most straightforward to quantify since there is no overlap between the signals of the DMSPA **20** and HDA **3** **Figure 73**. Using the integration of signals corresponding to DMSPA **20** it is possible to produce a numerical value for the integration relating to a single proton of DMSPA **20**. The same can be produced for HDA **3** using the integration of the signals for corresponding to HDA **3**. Converting the integration for a single proton of each molecule to a percentage of the total integration of the two protons results in an approximate evaluation of the displacement of HDA **3** with DMSPA **20**. The approximate displacement of HDA **3** with DMSPA **20** was calculated at 14% HDA **3** to 86% DMSPA **20**.

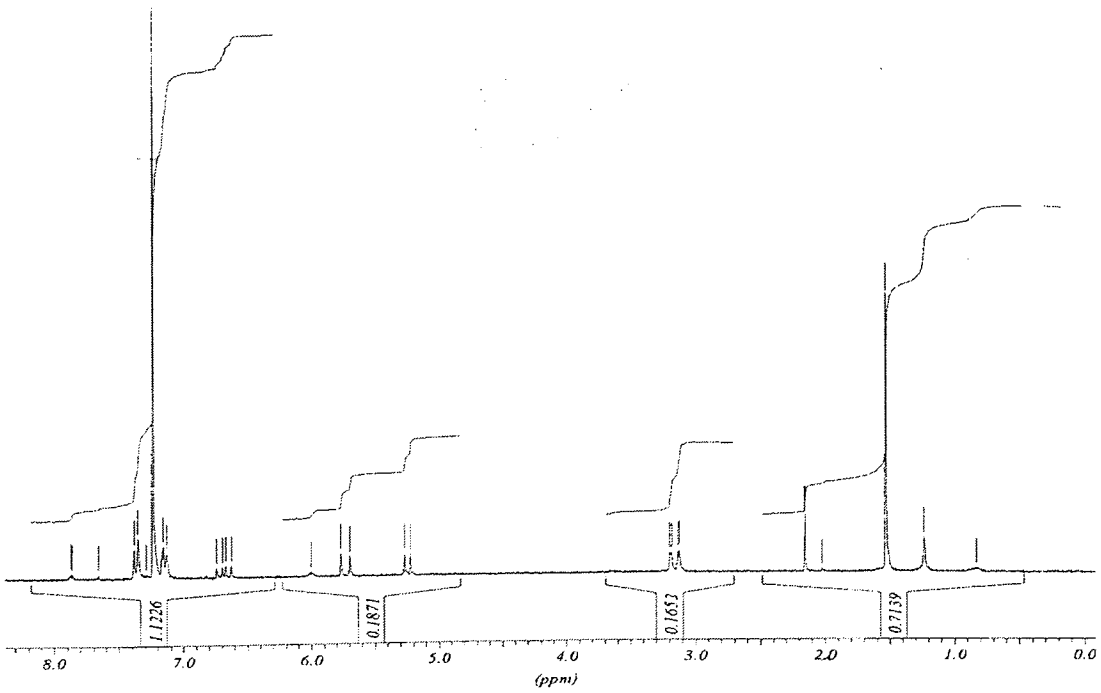

Figure 73: **^{1}H NMR Spectrum of HDA 3 coated NanoDots™ displaced with excess DMSPA 20**

The same type of calculation can be done for the displacement of HDA **3** with DUPA **24**. This spectra is complicated slightly by the overlap of the signals comprising the protons of the alkyl chains. Discrete signals for each are still present, the integration relating one proton of DUPA **24** can be calculated from the signals of the double bond and the terminal methyl group can be used for the integration for one proton of HDA **3**. These calculations resulted in an approximate displacement of 67% HDA **3** to 33% DUPA **24**.

Both the phosphinous acids appeared to displace HDA sufficiently but unfortunately the surface modified NanoDots™ could not be stored in solution as they gradually precipitated out of solution over time. This was tentatively attributed to be a consequence of the flux between the 5 and 3 coordination as this type of behaviour was not apparent with the tertiary phosphine oxides.

The evaluation of the displacement of HDA **3** with the tertiary phosphine oxides is slightly more challenging that with the secondary phosphine oxides, this is due to overlap of the signals. However an approximate evaluation of displacement is still possible since signals correlating to the functionality of the new ligands are usually well separated and discrete. Obtaining a value for the integration of a single proton of the functionalised ligand can then be used to subtract that ligands contribution to the area of the overlapped peaks.

For instance DMSDPO **21** contains a ten carbon alkyl chain, the signal of which overlaps with both the terminal methyl and the broad multiplet of the alkyl signals of HDA **3**. Fortunately though the signals for the two methylene groups of the styrenic

moieties styrene groups also attached to the phosphorus are well separated. Examination of the signals for these methylene groups allow the integration corresponding to one proton of DMSDPO **21** to be calculated at 2.25mm.

The signal for the terminal methyl group integrates to 12mm and is composed of three protons from DMSDPO **21** and three protons of HDA **3**, an equation describing this would take the form of **Equation 3**.

$$(3\mathbf{a}+3\mathbf{b}) = 3\mathbf{a} + 3\mathbf{b} \qquad \textbf{Eqn 3}$$

where $(3\mathbf{a}+3\mathbf{b})$ is the integration of the terminal methyl signal

a is the integration corresponding to one proton of DMSDPO **21**

b is the integration corresponding to one proton of HDA **3**

Insertion of the known values for $(3\mathbf{a}+3\mathbf{b})$ and **a** obtained directly from the ^{1}H NMR spectrum of DMSDPO **21** gives **Equation 3i**.

$$12\text{mm} = (3 \times 2.25\text{mm}) + 3\mathbf{b} \qquad \textbf{Eqn 3i}$$

Solving **Equation 3i** provides a value for **b**.

$3\mathbf{b} = 12\text{mm}-6.75\text{mm} = 5.25\text{mm}$

$\mathbf{b} = 5.25\text{mm} / 3 = 1.75\text{mm}$

The integration corresponding to a single proton of HDA **3** is calculated as 1.75mm. provides a value for the integration corresponding to a single proton of HDA **3**. Finally comparing the integration for a single proton of each molecule by converting them to a percentage results in an approximate displacement of 50% to 50% for DMSDPO **21** and HDA **3** respectively.

A check of the method, a similar calculation using the broad multiplet resulting from the protons of the alkyl chains is also possible. The following equation relates to this.

$(18\mathbf{a} + 30\mathbf{b}) = 18\mathbf{a} + 30\mathbf{b}$ **Eqn 4**

where $(18\mathbf{a}+30\mathbf{b})$ is the integration of broad multiplet signal

a is the integration corresponding to one proton of DMSDPO **21**

b is the integration corresponding to one proton of HDA **3**

Solving this equation gives a value of 1.70mm for the integration of a single proton of HDA **3** that correlates well to the values calculated using the terminal methyl signal.

Percentage displacement calculations were completed in a similar manner for each of the surface modifications undertaken. The results of these are summarised below **Table 4**.

Ligand	Percentage new ligand after displacement	Percentage residual HDA after displacement
DODPO **16**	60	40
DOOPO **6**	11	89
DUDSPO **26**	26	74
DOMSPO **7**	50	50
TUPO **25***	38 58 66	62 42 34

* several batches of different coloured NanoDot™

Table 4: Summary of percentage ligand composition of the surface of NanoDots™ after displacement with various designer ligands

The calculations are approximate indications of the amount of new ligand present on the surface of the NanoDot™ and were undertaken as a guide to the efficiency of the displacement. The structure of the ligand does affect the extent to which HDA **3** is displaced, however it is likely many other factors, such as batch of NanoDots™ used etc, may also be involved.

The ligand displacement techniques described in the literature vary greatly. In each case the new ligand, nanocrystal and ligand to be displaced vary in each case. Many groups repeatedly wash and precipitate the newly coated nanocrystals in suitable solvents to remove unbound ligand.[38, 46] The ligand displacement technique employed by the Sutherland group does not involve an extra washing procedure. This step was precluded following some preliminary findings that suggest extra washing can remove bound ligand resulting in deterioration in the performance of the nanocrystal.

The first indication of deterioration in the properties of the NanoDots™ resulted from insolubility of washed NanoDots™ that had been exchanged with DOMSPO **7**. NanoDots™ that were ligand exchanged and precipitated once with methanol remained soluble and underwent no deterioration. Conversely NanoDots™ that were exchanged in an identical manner but resuspended and precipitated a second time became insoluble. Upon discussion with the NanoCo™, the NanoDot™ suppliers, it became apparent that this phenomenon had been encountered before with over-washing of HDA **3** coated NanoDots™ subsequent to their synthesis. It was suggested that the interaction of the ligands with the surface of the NanoDot™ was not permanent, rather that it was an equilibrium between bound and free ligand.[151]

Further evidence to suggest over-washing can remove desired ligand from the surface of the NanoDot™ comes from the analysis of washed and unwashed NanoDots™ by diffusion ordered ^{1}H NMR spectroscopy. Two samples of TUPO **25** coated NanoDots™, one precipitated just once following the ligand exchange procedure (i.e. not washed), the other resuspended (after the precipitation step of the ligand exchange procedure) and precipitated a second time (i.e. washed) were analysed using the DOSY technique. The spectrum of the un-washed NanoDots™ was consistent with that of a nanoparticle with a surface composed of HDA **3** and TUPO **25**. No evidence of un-bound HDA **3** or TUPO **25** was present. Conversely the DOSY spectrum of the washed NanoDot™ consisted of solely bound HDA **3**. These findings resulted in the conclusion that a single precipitation was sufficient to remove any excess ligand without any detrimental effect on the properties of the NanoDot™.

2.4 – Investigation into the Optimisation of HDA Displacement

The displacement of HDA **3** from the surface of NanoDots™ is influenced by a number of factors. Identification and investigation of these factors should lead to a greater control over the displacement ultimately resulting in a greater degree of control over the surface chemistry.

The examination of the approximate displacement efficiency of TUPO **25** on batches of different coloured NanoDots™ suggested that different NanoDots™ did not behave in a uniform manner towards displacement. An investigation into the extent of this difference in behaviour between various batches of NanoDots™ was undertaken. The displacement of HDA **3** with DMSPA **20** on five batches NanoDots™ was evaluated by ^{1}H NMR spectroscopy. Each batch of NanoDots™ were identically incubated with DMSPA **20**, precipitated with methanol and dried to constant mass. Analysis of each solution by ^{1}H NMR allowed the percentage displacement of HDA **3** by DMSPA **20** to be calculated for each batch of NanoDot™ **Figure 74** (Appendix A, **Table 5**)

The approximate displacement of HDA **3** with DMSPA **20** varies quite substantially between the batches NanoDot™. The best displacement with DMSPA **20** is 50% and the worst 9%. The variations could be inherent to each type of NanoDot™ or they could be due to differences in the treatment of the samples in the synthesis or work-up of the samples before they are supplied. The results do suggest that each batch is individual and that it is useful to evaluate the efficiency of the ligand displacement procedure on a batch by batch basis prior to employing the NanoDots™ in their intended application.

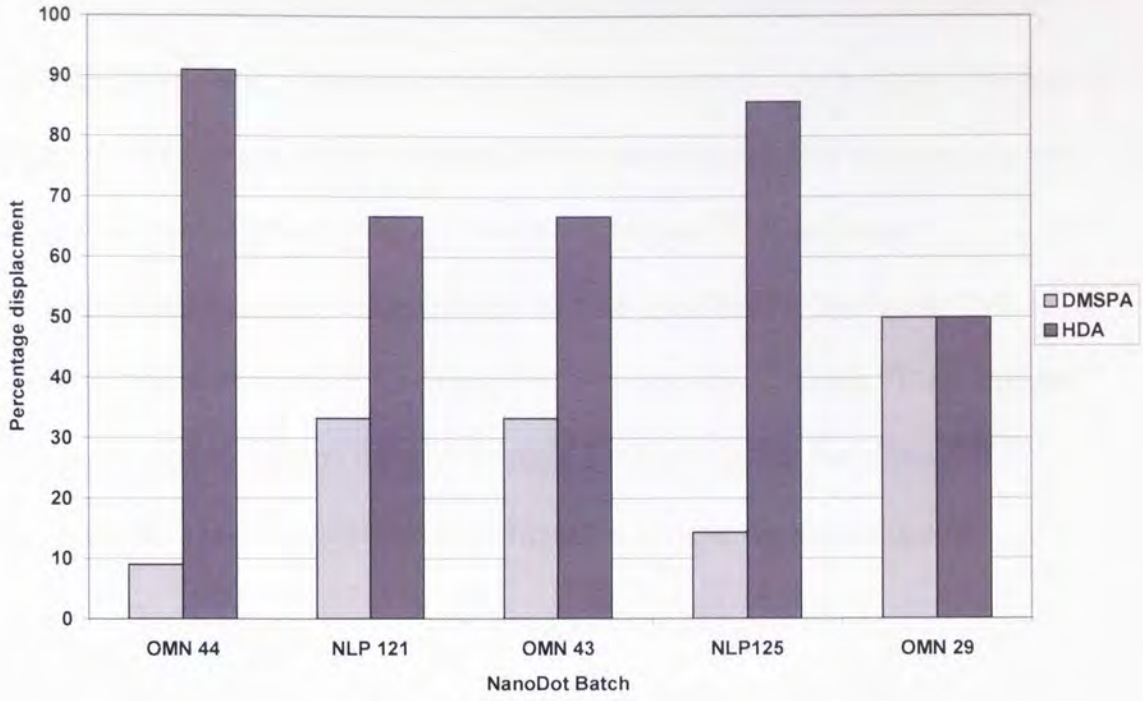

Figure 74: Graph comparing the percentage ligand composition of five different batches of NanoDots™ following displacement with DMSPA 20

The displacement of HDA **3** from the surface of NanoDots is achieved by incubation with a large excess of the replacement ligand. A series of displacements with increasing excesses of ligand were set up in parallel to determine the optimum excess require for the maximum possible displacement of HDA **3**. The excess of ligand used is quantified in terms of weight for weight equivalents. This study was completed with both a secondary phosphine oxide, DMSPA **20** and a tertiary phosphine oxide, commercially available triphenylphosphine oxide (TPhPO) **38**.

Excesses of 5, 10, 20 and 40 weight for weight equivalents were investigated, and a control containing solely 40 equivalents of ligand were set up in both cases. Following incubation the samples were precipitated with methanol and analysed by ^{1}H NMR

spectroscopy. In addition a control experiment with DMSPA **20** and TPhPO **38** were also included in this study. These involved incubation of maximum weight equivalent of each ligand in the absence of the NanoDots™ in order to ensure that the precipitation technique was capable of removing all the unbound ligand. The percentage displacement of each sample was calculated for both the DMSPA **20 Figure 75** (Appendix A, **Table 6**) and TPhPO **38 Figure 76** (Appendix A, **Table 7**). The spectra of both the controls showed no trace of the ligand suggesting that the volume of methanol used for the precipitation was sufficient to remove the excess ligand.

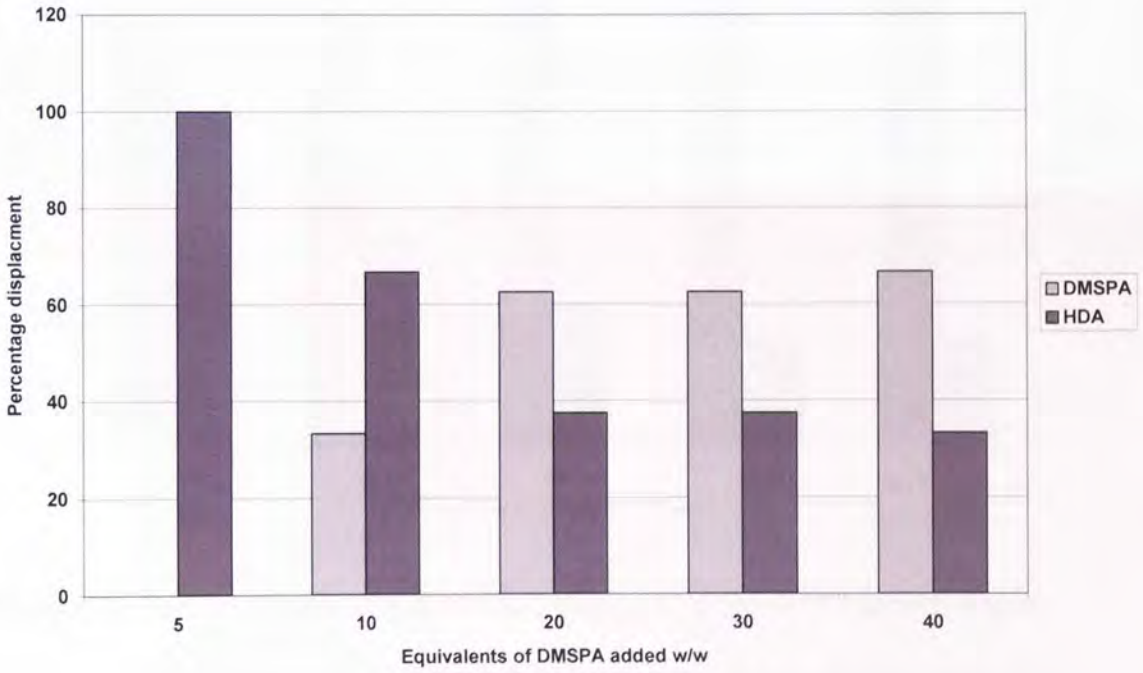

Figure 75: Graph showing the percentages of NanoDot™ binding ligands DMSPA 20 and HDA 3 following displacement procedures with increasing excesses of DMSPA 20

No evidence of displacement is present with 5 equivalents of DMSPA **20**, increasing to 10 equivalents to results in about half of the total displacement possible. In order to

achieve the maximum displacement possible with DMSPA **20** an excess of greater than 20 equivalents is required. However significantly increasing the equivalents of ligand **20** used to greater than 20 does not increase the amount of HDA **3** that is displaced. DMSPA **20** is one of the phosphinous acid-based ligands and it is possible that the plateauing effect observed in Figure **73** may be related to the equilibrium between the 3 and 5 coordination of DMSPA **20** in solution.

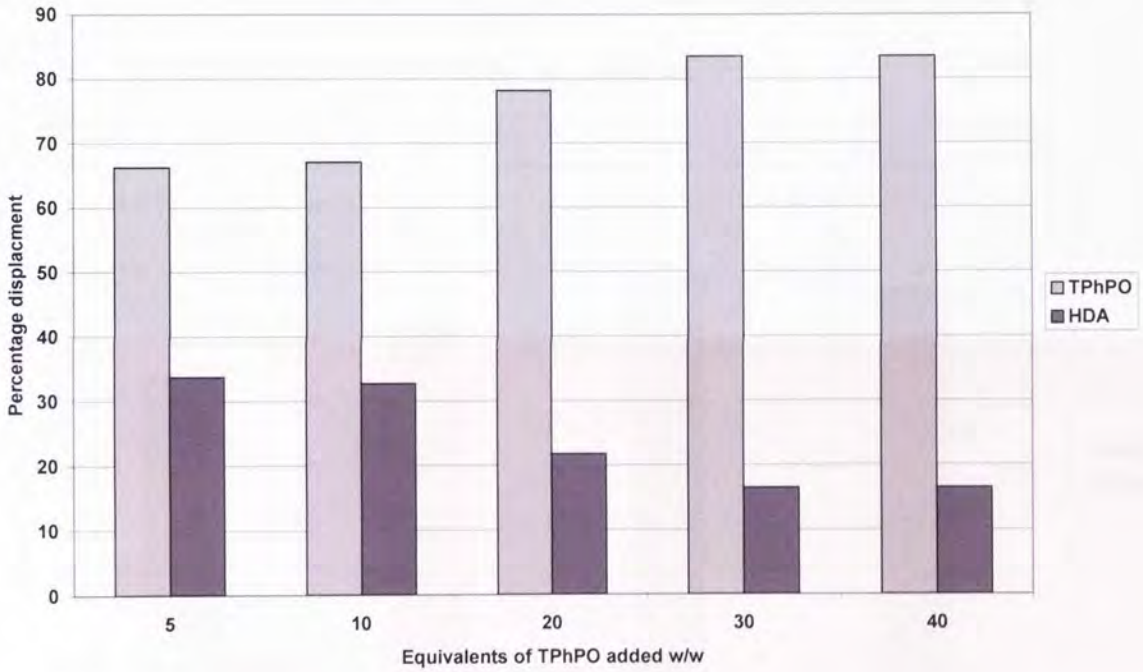

Figure 76: Graph showing the percentages of NanoDot™ binding ligands TPhPO 38 and HDA 3 following displacement procedures with increasing excesses of TPhPO 38

Examination of the percentage displacement of HDA **3** by the tertiary phosphine oxide, TPhPO **38**, suggests that fewer equivalents are required to achieve sufficient displacement of the HDA **3** ligand. The pattern in displacement suggests that the addition of greater that 30 equivalents of ligand does not lead to greater displacement of

HDA **3**. If all tertiary phosphine oxides are assumed to behave in the manner the data suggests that displacement should be attempted with greater than 20 equivalents of ligand where possible.

Another factor that may affect the displacement of HDA **3** by the new ligand is that of incubation time. Investigation into the length of incubation time required for maximum displacement was completed over a 12 day period. Again each sample was precipitated with methanol, analysed by ^{1}H NMR spectroscopy and the percentage displacement calculated for each **Figure 77** (Appendix A, **Table 8**).

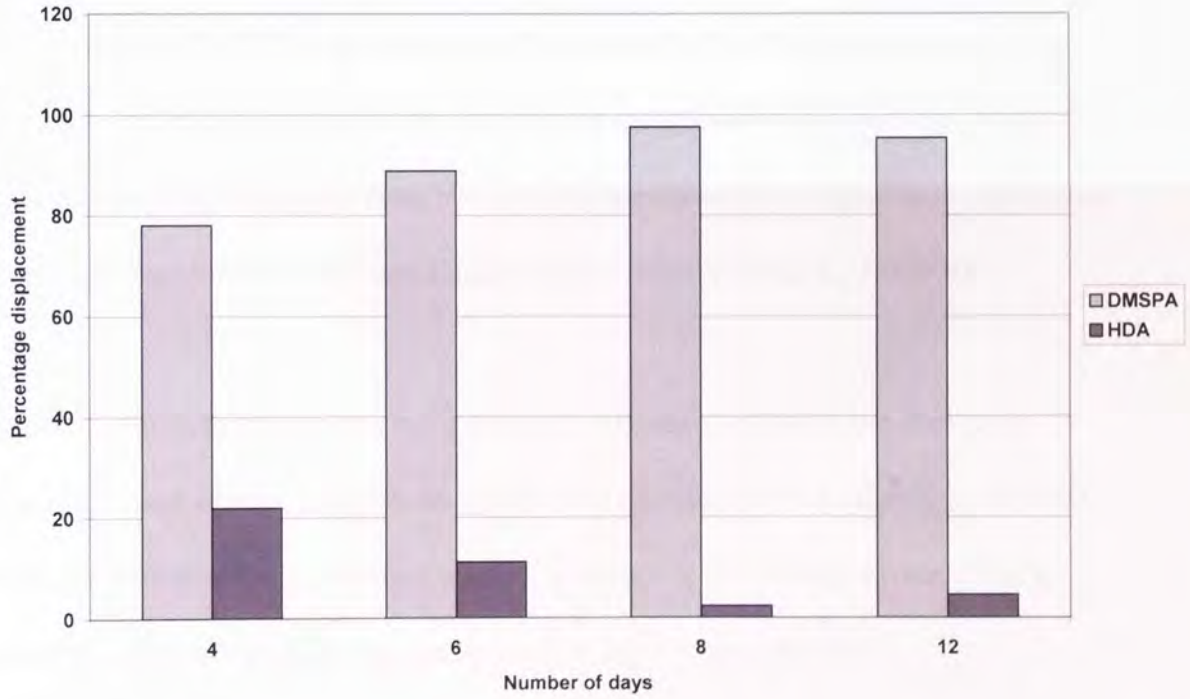

Figure 77: Graph showing the percentage of NanoDot™ binding ligand DMSPA 20 over time

The longer the incubation time the greater the displacement of HDA **3** by DMSPA **20**. The percentage displacement of HDA **3** with DMSPA **20** can be increased to almost 100% by extending the displacement time to 8 days. The data suggests that between 6

and 8 days would be ideal to maximise displacement, but 4 days is adequate to produce sufficient displacement for the majority of applications.

The final factor affecting the displacement of HDA **3** to be investigated was that of the anchoring group. The P=O head group was compared with the P=S head group in a non-competitive and a competitive study. As previously mentioned since the outer shell of NanoDots ™ are composed of ZnS it was theorised that P=S anchoring groups may participate in sulphur bridging to the sulphur atoms on the surface of the nanoparticle resulting in better NanoDot™ complexation. This theory was investigated firstly by a non-competitive study involving the displacement of HDA **3** by DUPA **24**, DUPSA **33**, DMSPA **20** and DMSPSA **34** where the efficiency of HDA **3** displacement of each ligand was evaluated separately. Precipitation of the solutions in a mixture of acetone and methanol followed by analysis by ^{1}H NMR spectroscopy resulted in the following percentage displacements for each ligand **Figure 78** (Appendix A, **Table 8**).

Figure 78 shows that there was not a dramatic difference between the choice of anchoring group chosen. DUPSA **33** appeared to displace HDA **3** slightly better than DUPA **24**, however the same trend was not apparent in the methyl styrene derived ligands where the P=S anchoring group performed relatively poorly.

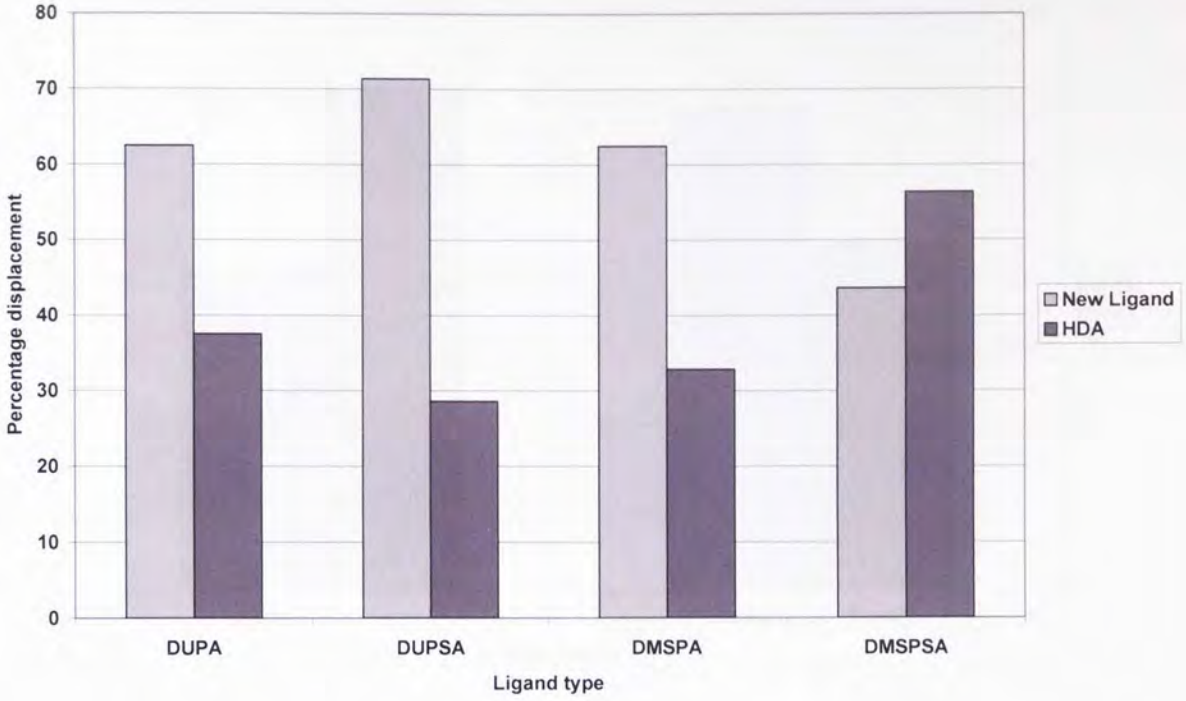

Figure 78: Graph demonstrating the effect of anchoring group on percentage displacement of HDA 3 ligand

The second study investigating the effect of the anchoring group involved a competitive displacement of HDA **3**. Two displacements procedures were undertaken. Each procedure employed a mixture of P=O and P=S ligands, one displacement mixture contained TPhPO **38** and TOPS **28** whereas the other contained TPhPS **39** and TOPO **1**. Both displacement procedures were carried out under identical conditions prior to analysis by ^{1}H NMR to produce the percentage displacement for each pair **Figure 79**.

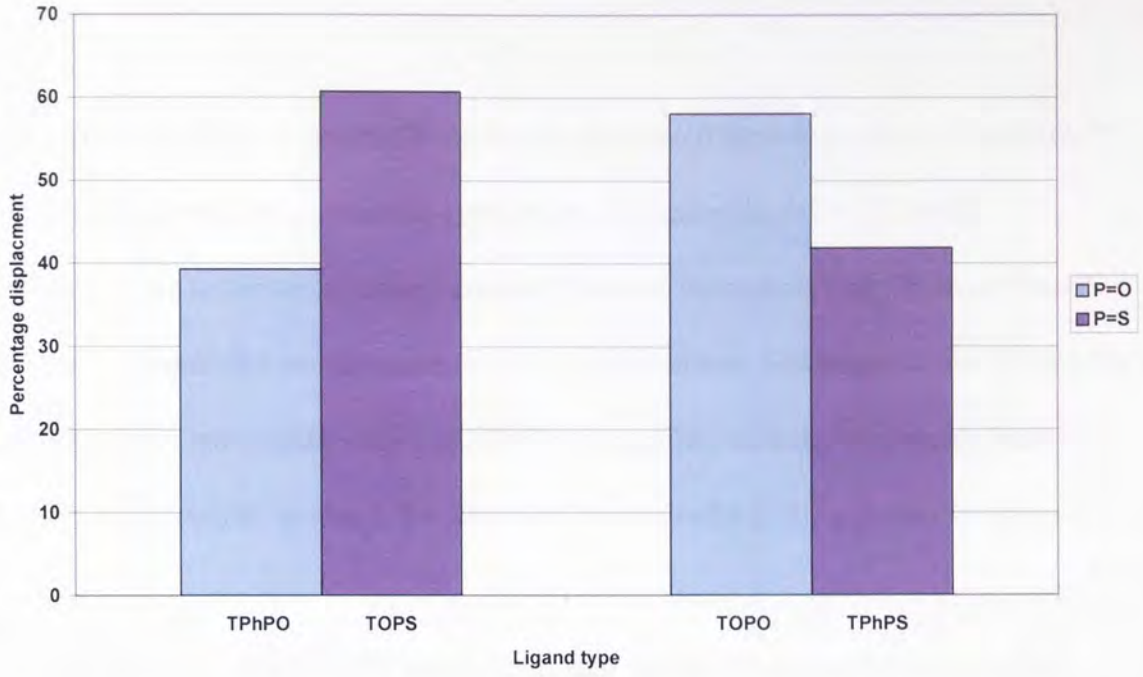

Figure 79: Graph demonstrating competitive displacement of HDA 3 with ligands containing either P=O head groups or P=S head groups

Again these findings suggest that the choice of anchoring group does not exert as much influence over the extent of HDA **3** displacement as the actual structure of the ligand. In both studies it would appear that the more aliphatic-containing ligands perform better at displacing HDA **3** than the aromatic containing ones. A possible explanation for this may be in the rigidity of the structures, the aliphatic ligands are more flexible than the aromatic ones and it is possible that this results in easier packing on the surface of the NanoDot™ with either themselves or the residual HDA **3**.

2.5 – Encoded Resin

Exchange of the HDA **3** capping layer for functionalised ligands produces NanoDots™ specifically tailored for a particular application. For example, HDA **3** coated NanoDots™ are not soluble in the monomer phase of commonly used in cross-linked polystyrene suspension polymerisation reaction procedures. Exchange of the HDA **3** for DOMSPO **7** not only renders the NanoDot™ compatible with the monomer phase but also adds functionality to attach the NanoDot™ covalently to the polymer backbone.[37]

This application of NanoDots™ was investigated within the group for the specific intention of producing quantum dot-containing polystyrene beads as a first step towards the optical encoding of solid supports for the specific use in SPOC **Figure 80**. Previous quantum dot-containing resins reported in the literature had been produced for use in biological based assays[71] and were unlikely to withstand the rigours associated with SPOC since the individual beads were prepared by embedding the quantum dots into the outer layer of 1-2μ resin beads and simply sealing them inside with a coat of silica.

In contrast, the method developed within the Sutherland group resulted in the NanoDots™ being incorporated covalently into the polymer matrix throughout each bead. Initial work began with the synthesis of non-functionalised, non-quantum dot containing resins to ensure that the resins could be produced successfully in small and large scales following standard protocols. Small scale production was accomplished using a 12 place carrousel™, both 2% and 20% cross-linked beads were synthesised in this way. Large scale synthesis was achieved with a large enclosed vessel fitted with an

overhead propeller stirrer, a test batch of CMS functionalised polystyrene beads were produced satisfactorily by this method.

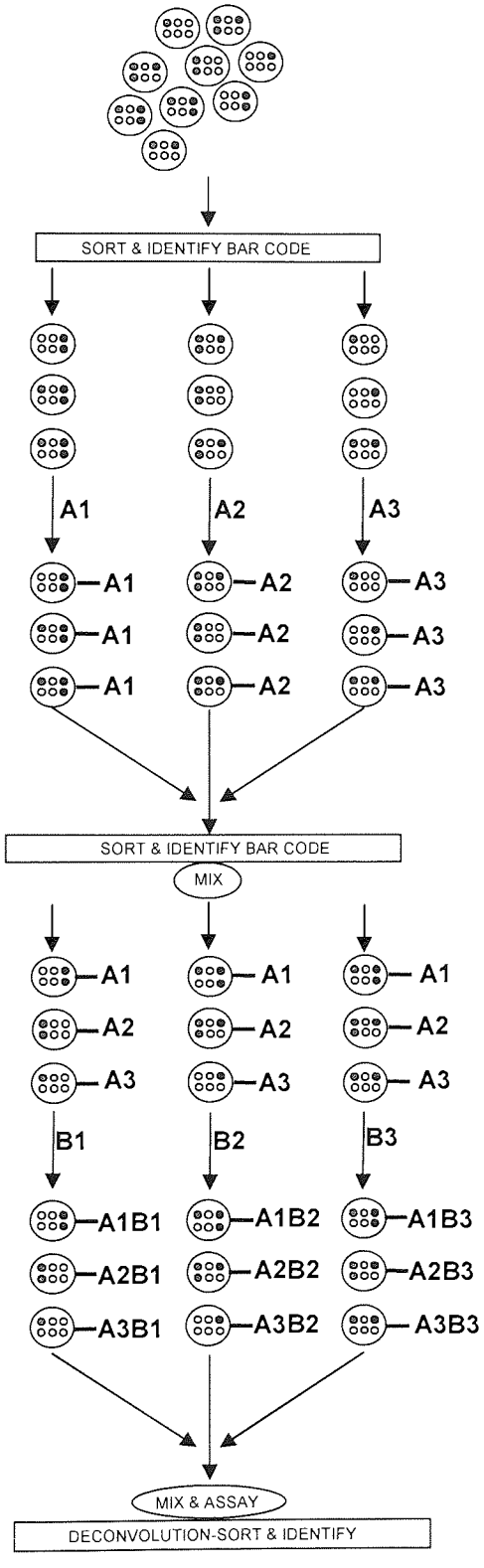

Figure 80: Schematic of quantum dot encoded 'split and mix' synthesis

Following the successful production of resins on small and large scale the synthesis of quantum dot-containing resin was attempted. DOMSPO 7 coated NanoDots™ were added to the monomer phase of a large scale standard non-functionalised, highly cross-linked styrene suspension polymerisation reaction. The quantum dot containing monomer mixture was added to the aqueous phase and the mixture stirred vigorously for 30 minutes before the temperature was raised to 72°C for 12 hours. Cold washing of the resin first with water then with solvent revealed highly coloured resin beads. The resin was dried to a constant weight and the PL spectrum evaluated **Figure 81**.

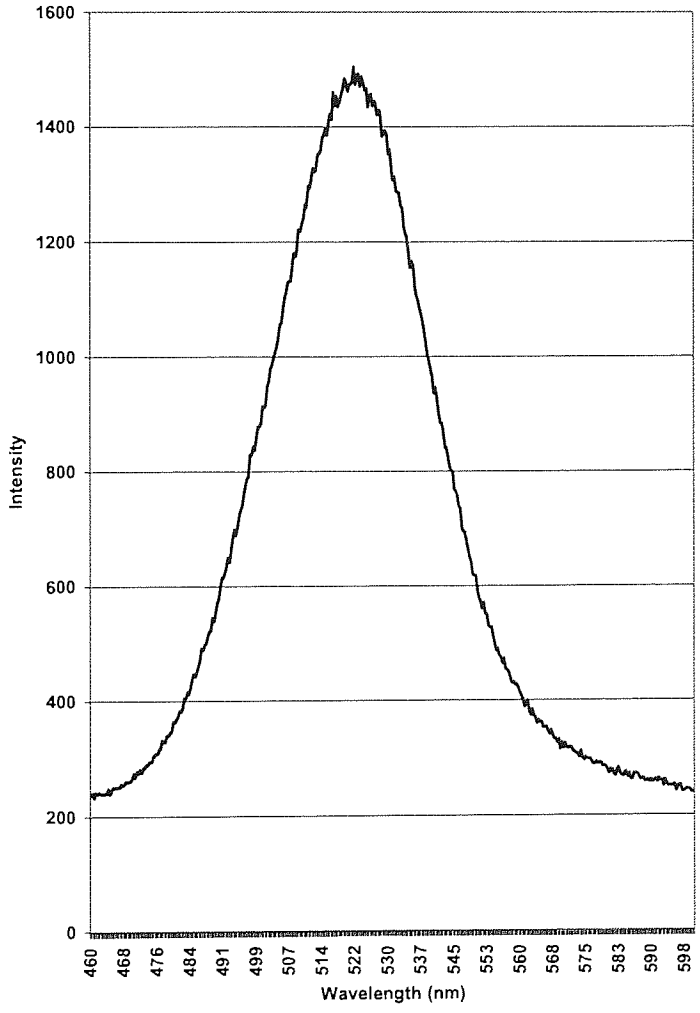

Figure 81: PL spectrum of resin containing covalently incorporated DOMSPO 7 coated NanoDots™

The yellow colour of the resin indicated that the NanoDots™ had been incorporated and this was confirmed with the observation of a strong emission in the PL spectrum that corresponded directly with that of the DOMSPO **7** capped NanoDots™ before polymerisation reaction. The irreversibility of the incorporation of the NanoDots™ was investigated preliminarily by Soxhlet extraction of the resin for 8 hours in dichloromethane. It was theorised that since the NanoDots™ were very highly soluble in dichloromethane any non-covalently incorporated crystals would be washed out. The resin remained yellow throughout the Soxhlet extraction procedure and no significant colour change of the washing solvent was observed. Finally the PL spectrum recorded after drying confirmed that the NanoDots™ were retained by the polymer structure of the resin.

Other quantum dot-containing resins generated following the same procedure within the group were additionally investigated by both fluorescent emission fingerprinting and combustion analysis.[37] The fluorescent emission fingerprinting spectroscopy of these NanoDot ™ containing materials showed that two different regions of the same bead gave essentially identical emission spectra that strongly indicated uniform incorporation of the NanoDots™ **Figure 82**. The data obtained from combustion analysis of the resin prior to and post to extended Soxhlet extraction in dichloromethane was yet more evidence supporting irreversible incorporation of the NanoDots ™ within the matrices of the resin beads (Appendix B, **Table 10**).

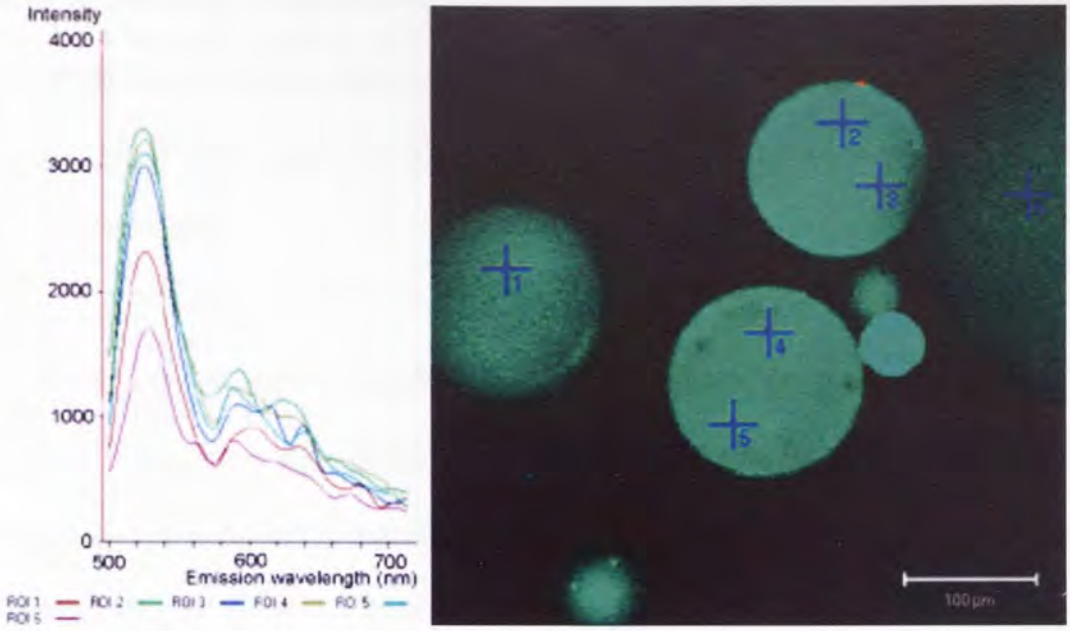

Figure 82: Fluorescent emission fingerprinting spectroscopy of macroporous resin beads containing covalently incorporated NanoDot ™

Following the successful irreversible incorporation of NanoDots ™ into non-functionalised resin it was decided that generating chemically functionalised beads was the next logical step towards the production of quantum dot encoded resin for use in SPOC. The addition of functionality would allow the performance of the encoded resin in standard SPOC to be evaluated alongside that of standard commercially available resins. Initial attempts within the group to produce a CMS-functionalised NanoDot™-containing resin were unsuccessful. It was believed that the addition of the CMS to the monomer mixture had a detrimental effect on the PL emission of the NanoDots™.

The idea of individually polymer coating NanoDots™ prior to their addition to the suspension polymerisation was initially proposed as a possible method to retard the deterioration that occurred with the addition of functionalised monomers into the suspension polymerisation reactions used to generate functionalised resins. Subsequent

discussion involving the addition of a polymer coat to the NanoDots™ suggested that this approach could also be additionally advantageous as it might also serve to protect the NanoDots™ from aggressive reagents that permeate the polymer matrices of the beads during SPOC.

In addition to the discussion regarding the potentially protective function of these coatings it was suggested that polymerisation of a ligand containing both a polymerisable, and non-polymerisable function could produce individually coated *and* functionalised NanoDots™. These materials could potentially prove useful as luminescent probes in biological assays. However initial focus was directed at the production of the protective coating around individual quantum dots.

2.6 – Polymerisation *via* Acyclic Diene Metathesis Polymerisation

2.6.1 Polymerisation in the absence of NanoDots™

TUPO **25** was designed specifically as a ligand not only to mimic the quantum dot binding nature of TOPO **1**, but also to provide the maximum number of polymerisable groups per ligand with the intention of creating a globally cross-linked network of polymer on the surface of the NanoDot™. Metathesis was chosen as the method of polymerisation due to the success of this procedure in the production of globally cross-linked networks around other nanoparticles that had reported in the literature.[99, 100] It was assumed that the metathesis of TUPO **25** would produce a polymeric network *via* acyclic diene metathesis polymerisation (ADMET). However the possibility of some metathesis transformations *via* a ring closing metathesis mechanism were also expected, leading to the design of the tripodal structure of TUPO **25**. Three terminal olefin chains ensured that if two reacted inter molecularly there was a remaining one to react intra molecularly to form the desired network.

The mechanism proposed for the ADMET polymerisation **Figure 83** and RCM **Figure 84** reaction of olefins by Grubbs 2nd generation catalyst **42** proceeds via an initial dissociative pathway. Loss of the PCy_3 produces a four co-ordinate 14 electron intermediate, that performs multiple olefin metathesis events before recoordinating with the PCy_3.[113, 114, 152]

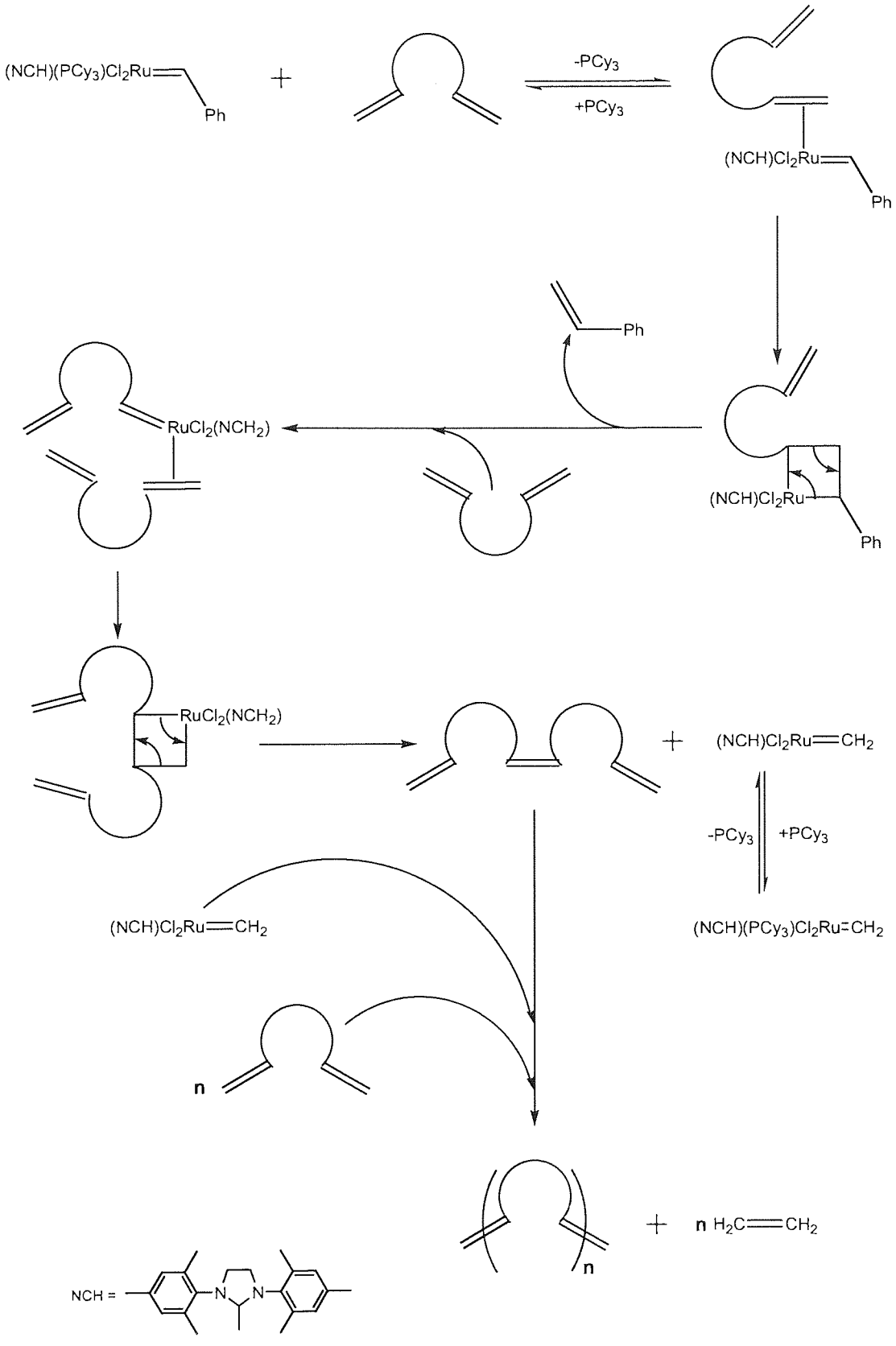

Figure 83: Mechanism proposed for the ADMET polymerisation reaction of olefins by Grubbs 2nd generation catalyst 42

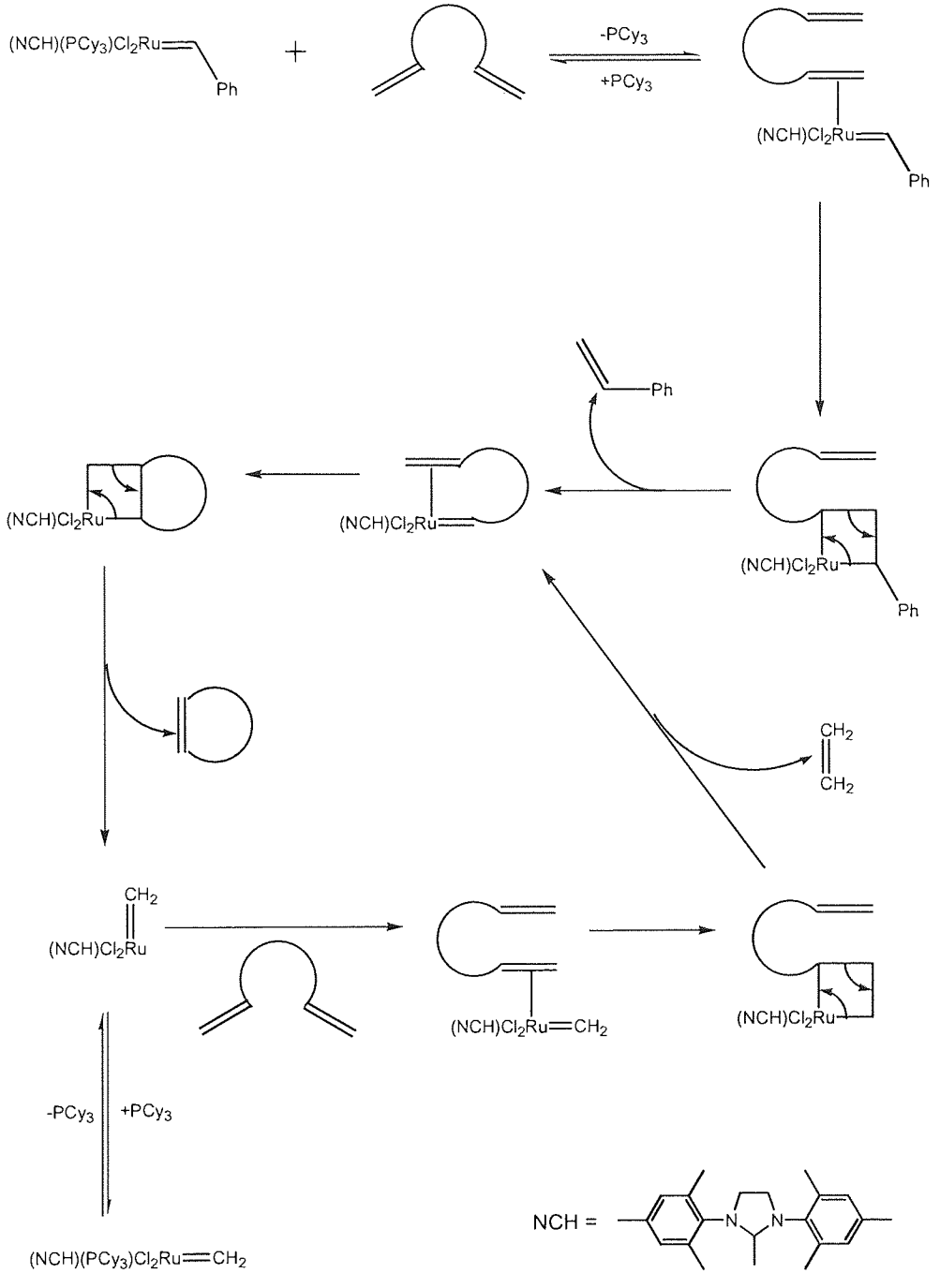

Figure 84: Mechanism proposed for the RCM reaction of olefins by Grubbs 2nd generation catalyst 42

A series of control experiments were performed in the absence of NanoDots™ by injection of 5, 10 and 15 mole percent solutions of Grubbs 2nd generation catalyst **42** into three Carousel™ tubes containing TUPO **25** dissolved in DCM **Scheme 18**. The

polymerisations reactions were allowed to proceed for three days at 40°C before the solvent was removed under reduced pressure and the products isolated as flaky brown solids $\mathbf{40_{5\%}}$, $\mathbf{40_{10\%}}$ & $\mathbf{40_{15\%}}$. Each solid was dispersed in $CDCl_3$ and the soluble components analysed by ^1H NMR spectroscopy.

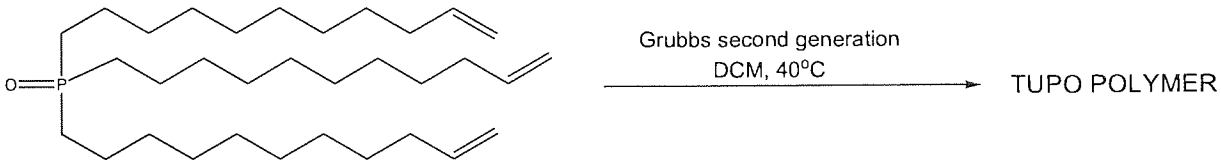

Scheme 18: Synthesis of TUPO polymer

Examination of the spectra of the products from the reaction using only 5 mole percent Grubbs 2nd generation catalyst **42** did not proceed to completion. Evidence of the olefinic superimposed *cis* and *trans* doublets and doublet doublet triplet resonances associated with the double bond function of the monomer TUPO **25** remained **Figure 85** (signals a and c). The olefinic region of the spectra however also contained a new olefinic resonance that presented as a broad signal at ∂ 5.33 ppm (signal b). The chemical shift of these resonances corresponded well with the signals observed for the RCM product of a similar molecule that had been reported in the literature.[100]

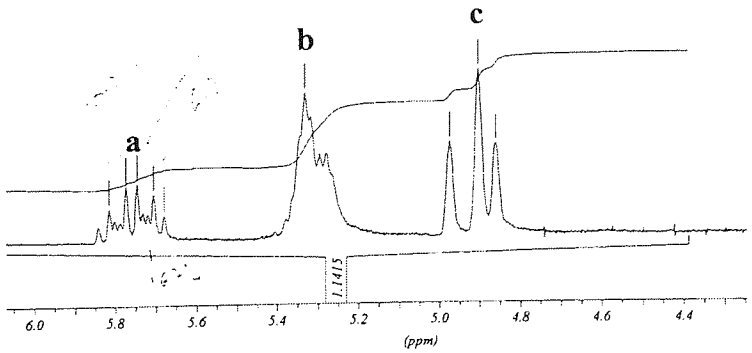

Figure 85 ^1H NMR spectrum of TUPO polymer $40_{5\%}$ expansion between ∂ 4.4 ppm & ∂ 6.0 ppm

The analysis of the reaction mixtures that involved 10 and 15 mole percent equivalents of the catalyst **42** by ^{1}H NMR spectroscopy showed the appearance of the new broad alkene resonance at ∂ 5.33 ppm accompanied by complete disappearance of the two olefinic signals associated with the monomer at ∂ 4.90 ppm and ∂ 5.76 ppm **Figure 86.**

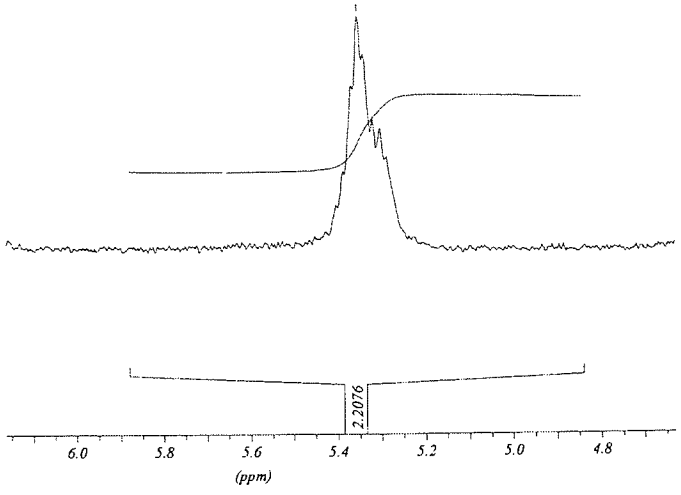

Figure 86 **^{1}H NMR spectrum of TUPO polymer $40_{10\%}$ expansion between ∂ 4.4 ppm & ∂ 6.0 ppm**

Further analysis of all three phosphine oxide polymer products $\mathbf{40_{5\%}}$, $\mathbf{40_{10\%}}$ & $\mathbf{40_{15\%}}$ by MALDI-tof and LRMS were attempted at Aston but unfortunately the soluble oligomers that provided the ^{1}H NMR spectrum were insoluble in the more polar solvents systems required for compatibility with either technique. Finally a sample of the polymer $\mathbf{40_{10\%}}$ produced by 10 mole percent of the catalyst **42** was sent to Birmingham University for analysis to verify that no spectra could be obtained from this sample by Mr Peter Ashton, a highly experienced mass spectroscopist. Again, unfortunately it did not prove possible to obtain a spectrum and this was attributed to the lack of solubility of the sample.[153]

Finally the polymeric material $\mathbf{40_{10\%}}$ was examined by ^{31}P NMR spectroscopy **Figure 87** The ^{31}P spectrum exhibited 8 peaks at ∂ 58.3, 50.9, 50.1, 50.2, 49.3, 40.2, 36.3, 34.3 ppm, whereas the ^{31}P spectrum for monomer only possessed one at ∂ 48.8 ppm. Unfortunately the structure of Grubbs catalyst **42** contains a phosphorus in the PCy_3 ligand **Figure 88**, that dissociates from the catalyst to form the active species during the polymerisation reaction. The ^{31}P NMR spectrum of Grubbs catalyst was obtained from an overnight NMR experiment. The extended time of the NMR experiment was to allow the solution-phase structure of the catalyst to equilibrate. This ^{31}P NMR spectrum possessed 5 peaks at the following chemical shifts ∂ 50.7, 40.6, 32.3, 29.8, 29.8 ppm. By comparison of these three spectra it is possible to subtract the peaks from the spectrum of $\mathbf{40_{10\%}}$. Although this approach is far from ideal interpretation in this manner suggests that two or three of the peaks in the ^{31}P NMR spectrum of polymeric material $\mathbf{40_{10\%}}$ could potentially arise from polymeric entities within the sample.

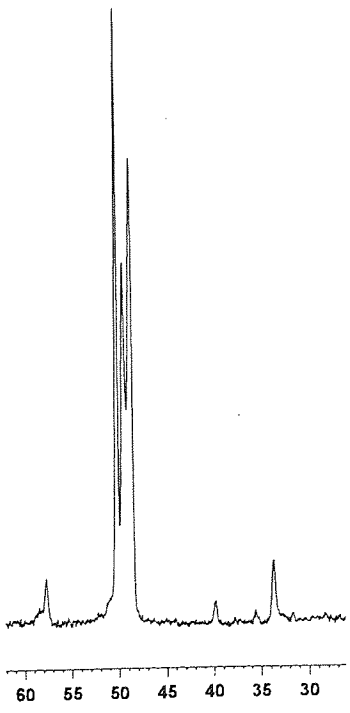

Figure 87: ^{31}P NMR spectrum of TUPO polymer $40_{10\%}$ expansion between ∂ 30.0 ppm & ∂ 60.0 ppm

To circumvent the problem of detecting species associated with the Grubbs 2nd generation catalyst **42** the RCM polymerisation of TUPO **25** was repeated using an alternative metathesis catalyst that contained no phosphorus atoms. Hoveyda-Grubbs 2nd generation catalyst **43** exhibits similar activity to that of Grubbs 2nd generation catalyst **42** but the structure contains no phosphorus **Figure 88**. The polymerisation of TUPO **25** was repeated following the same procedure as before substituting the alternative Grubbs-Hoveyda catalyst **43**, and again the polymeric products were isolated as rubbery solids $\mathbf{41}_{5\%}$, $\mathbf{41}_{10\%}$ & $\mathbf{41}_{15\%}$. The analysis by ^{1}H NMR spectroscopy paralleled the analysis of the product obtained with Grubbs 2nd generation catalyst **42** in that there was a complete disappearance of the olefinic signals of TUPO **25** coupled with the appearance of the new alkene signal at ~∂ 5.30 ppm. However one difference was observed, the Grubbs-Hoveyda catalyst **43** appeared to be more active since the reaction containing 5 mole percent appeared to proceed to completion. Again, unfortunately analysis of the material by mass spectroscopy proved unsuccessful.

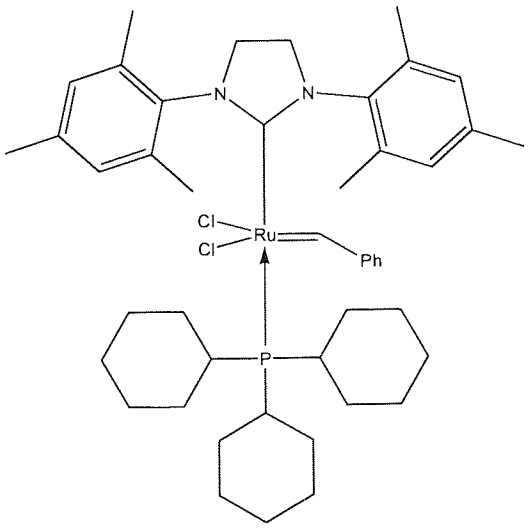

Grubbs Catalyst 2nd Generation **42**
(1,3-Bis-(2,4,6-trimethylphenyl)
-2-imidazolidinylidene)dichloro(phenylmethylene)
(tricyclohexylphosphine)ruthenium

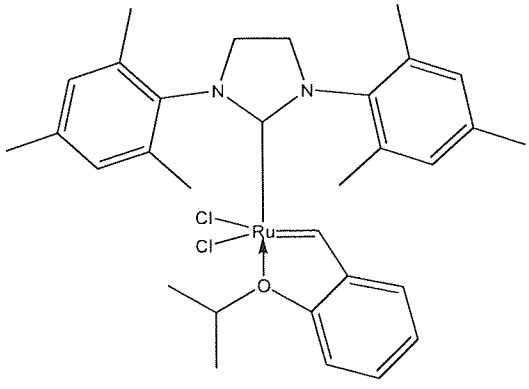

Hoveyda-Grubbs Catalyst 2nd Generation **43**
(1,3-Bis-(2,4,6-trimethylphenyl)
-2-imidazolidinylidene)dichloro
(o-isopropoxyphenylmethylene)ruthenium

Figure 88: Structure of Grubbs 2nd generation and Grubbs-Hoveyda 2nd generation catalyst

As anticipated, the ^{31}P NMR spectra were less complicated since the peaks present could only be reactant or product. The ^{31}P NMR spectrum of the polymeric material $\mathbf{41}_{10\%}$ contained four peaks at ∂ 49.4, 49.6, 51.0, 58.3 ppm **Figure 89**, it is possible that one of these peaks is monomer, however this contradicts the evidence from the ^{1}H NMR spectrum that suggests no monomer remains. Comparison of the two spectra obtained for $\mathbf{40}_{10\%}$ and $\mathbf{41}_{10\%}$ suggests that the signals above 45 ppm in $\mathbf{40}_{10\%}$ related to polymeric material. The signals at ~∂58 ppm are particularly characteristic of polymeric material due to their broad appearance.[154]

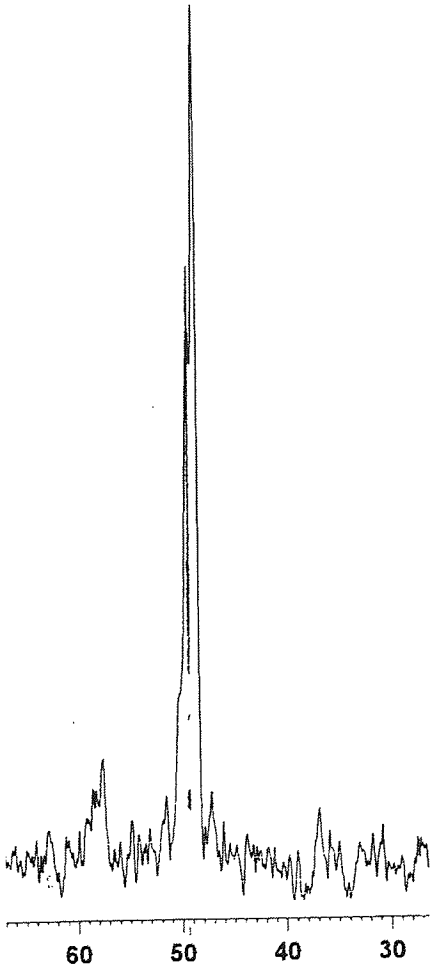

Figure 89: **^{31}P NMR spectrum of TUPO polymer $41_{10\%}$ expansion between ∂ 30.0 ppm & ∂ 70.0 ppm**

Although the characterisation of the polymeric products **40** and **41** is limited the highly soluble monomer TUPO **25** has been converted to a rubbery solid of diminished solubility. This change in physical morphology coupled with the differences observed in the ^{31}P NMR spectrum of the product compared with that of the monomer indicates that Grubbs 2nd generation and the Grubbs-Hoveyda mediated ADMET reactions of TUPO **25** had been successful. Furthermore the ^{1}H NMR evidence in the olefinic region of the various spectra obtained closely correspond to changes reported in same region of a similar cross-linked product, formed by the metathesis of a tri-alkene functionalised monomer, strongly suggests the successful formation of a highly cross-linked polymer by means of ADMET.[100]

2.6.2 Polymerisation on the surface of NanoDots™

These reaction conditions were then used to adapt an existing procedure to facilitate the surface global cross-linking of TUPO **25** capped NanoDots™. The desired outcome of this reaction would be the production of discrete polymer coated particles where the ADMET polymerisation reaction occurs on the surface of individual particles and not between particles. Accordingly to avoid the formation of polymer connected agglomerates suitably high dilution conditions needed to be employed.

The global cross-linking of TUPO **25** on the surface of various different NanoDots™ was attempted a number of times following the modified protocol for the production of globally cross-linked dendron nanocrystals (BN) **Figure 23**.[99] However a major difference concerning solubility of the end product produced from the ADMET

polymerisation of TUPO **25** coated NanoDots™ compared with that of the BN hampered efforts to analyse the materials formed.

The literature described catalyst removal *via* filtration following the addition of DMSO and silica. The BN were then recovered from solution by precipitation and centrifugation with a suitable solvent. The BN were then dried under high vacuum before being redissolved in D_6-DMSO to facilitate the analysis by ^{1}H NMR spectroscopy. The use of deuterated DMSO to dissolve the TUPO-polymeric coated NanoDots™ (TPN) was the first concern since HDA coated NanoDots™ were highly insoluble in DMSO. However it was decided that a range of solvents could be evaluated to find a suitable replacement.

The first time the ADMET-mediated global cross-linking of TUPO **25** coated NanoDots™ was attempted following the modified protocol the product adsorbed irreversibly to the silica added to remove the deactivated catalyst. All attempts to resuspend the NanoDots™ in a range of solvents failed. The reaction repeated without the addition of the silica and the NanoDots™ were precipitated from solution with methanol and dried under high vacuum. The solubility of the resulting powder was then investigated with the use of a wide range of solvents either alone or in conjunction with prolonged sonication. Unfortunately all attempts at resolubilising the powder failed.

Initial thoughts on the insolubility of the material from the ADMET-mediated process were directed towards the continued action of the catalyst as the reaction volume was decreased before precipitation. However after various attempts to deactivate and remove the catalyst made no difference to the insolubility of the final product. A further

investigation focused on the idea that the reaction volumes were too low resulting in aggregation during the formation of the polymer. Consequently a series of reactions in increasingly dilute solution was evaluated to ascertain if this was the cause of the observed insolubility. Each reaction was precipitated in an identical manner with methanol and all after drying under high vacuum produced insoluble pellets.

Finally it was deemed most likely that the insolubility of the product from the ADMET-mediated process was as a direct result of interparticle interactions. This conclusion was drawn following the observation that the material was highly soluble while it remained in solution and that the insolubility only occurred after the material was dried under high vacuum, since was possible to immediately redissolve the TPN after removal of the solvent to 'just dryness' under reduced pressure.

The inability to remove the solvent from the product to complete dryness resulted in the necessity for a different approach for the analysis of the materials produced in this manner. It was therefore decided to monitor the polymerisation reaction as it occurred using ^{1}H NMR spectroscopy, this was made feasible simply by exchanging the reaction solvent for the deuterated equivalent.

2.6.3 Analysis by ^{1}H NMR Spectroscopy

TUPO **25** coated NanoDots™ were suspended in $CDCl_3$ and stirred under nitrogen for 15 minutes before 5 mole percent of 2nd generation Grubbs catalyst **42** was injected. The reaction temperature was then increased to 40°C and the mixture stirred for the duration

of the reaction. Examination of the progress of the reaction began on day 2 by the removal of a sample for immediate analysis by ^{1}H NMR Spectroscopy. Comparison of the relative size of monomer signals at ∂ 4.90 ppm and ∂ 5.76 ppm to that of the signal associated with the polymeric material at ∂ 5.28 can be used as a means to investigate the progress of the polymerisation reaction.

Other samples were removed and analysed on days 3, 6 and 7, the spectrum obtained on day 7 indicated that the reaction had not proceeded any further since the previous analysis on day 6 and so another 5 mole percent of catalyst **42** was added at this stage and the reaction continued. The reaction was monitored daily from this point and the spectrum recorded on day 10 suggested that the polymerisation reaction had proceeded to completion with approximately 80% of the monomer being polymerised.

The integration of the two monomer signals and one polymeric resonance were converted to a percentage for each spectrum recorded in order to quantify the extent of the polymerisation reaction **Figure 90**. The graph shows the steady decline in the contribution of the monomer signals accompanied by the increase in the contribution from the polymeric signal as the reaction proceeds.

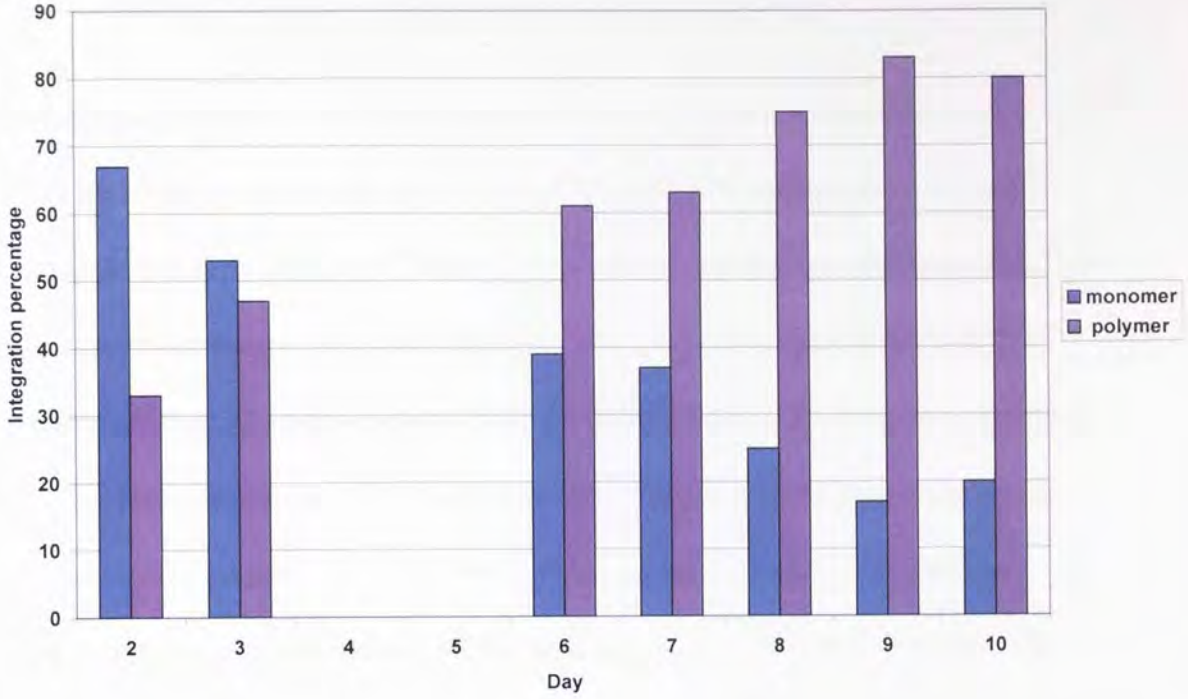

Figure 90: Graph showing the decline in the percentage of monomer signal and an incline in the percentage of polymer signal

From the ^{1}H NMR evidence collected, the reaction was assumed to have worked and the product was believed to be polymer coated NanoDots™. The reaction mixture was then split into two portions in an effort to ascertain if the insolubility previously observed was an inherent property of this type of product. One half of the reaction mixture was filtered through a pad of silica and the other was precipitated with ethanol. The behaviour of the product was identical to the previous observations. Again the polymer coated NanoDots™ stuck irreversibly to the silica. It should be noted that this is behaviour is unique to the NanoDots™ post polymerisation as both TUPO **25** and HDA **3** coated NanoDots™ do not adhere to silica under identical reaction conditions. The ethanol-mediated precipitation of the remaining half of the mixture also produced the anticipated insoluble pellet after drying under vacuum. Again this observation was consistent with results previously seen.

2.6.4 Analysis by ^{31}P NMR Spectroscopy

Following the previous success of monitoring the progress of the polymerisation reaction by NMR spectroscopy it was decided to attempt a similar series of NMR experiments this time using the ^{31}P nucleus to indicate the changes that occurred. Two sets of experiments were completed, the first with 10 mole percent Grubbs 2nd generation catalyst **42** and the second with 10 mole percent of the non-phosphorus-containing Hoveyda-Grubbs 2nd generation catalyst **43**. Both reactions were set up identically by the preparation of two bulk stock solutions, made up in deuterated solvent, that following the addition of the relevant catalyst provided two NMR tube scale samples to enable the polymerisation reaction to be monitored at 40°C in the NMR instrument. The bulk reactions were continued in the laboratory in tandem with the NMR reactions, the Grubbs 2nd generation bulk reaction was continued for 17 days whilst as the Hoveyda-Grubbs bulk reaction was terminated after 10 days.

The series of spectra produced by the reactions in the NMR tubes were unfortunately of little analytical use since necessarily high dilutions of the reaction mixtures resulted in spectra with poor resolution. Despite this short coming the Grubbs catalyst **42** NMR scale experiment was allowed to run to completion, however due to the poor resolution it was decided that the Hoveyda-Grubbs **43** NMR scale experiment should be terminated after 36 hours. The realisation that a more concentrated sample of both reactions was necessary for the procurement of reasonable quality results utilising ^{31}P NMR spectroscopy, led to the concentration and subsequent analysis of the entire bulk reactions for both catalysts.

The ^{31}P spectrum of the concentrated reaction with Grubbs 2nd generation catalyst **42** gave a complex ^{31}P NMR spectrum as anticipated from earlier findings, presenting the following peaks ∂ 34.5, 40.7, 50.2, 51.4, 53.9, 59.6, 60.0-67.6 ppm (overlapping broad signals) **Figure 91**. The olefinic region of the ^{1}H NMR spectrum still showed evidence of a small amount of unreacted terminal alkene so the broad set of peaks at 50.2-53.9 can not be assigned as either polymer or monomer. One of the peaks observed in Grubbs catalyst **42** also appears in this area so assignment will not be made. However the broad spiked cluster of peaks from ∂ 59.6 to 67.6 ppm are indicative of polymeric signals[154] and are not present in either the ^{31}P spectra of the monomer or catalyst **42**. A similar cluster of signals were also observed in the TUPO-polymer $\mathbf{40_{10\%}}$ ^{31}P NMR spectrum **Figure 87**.

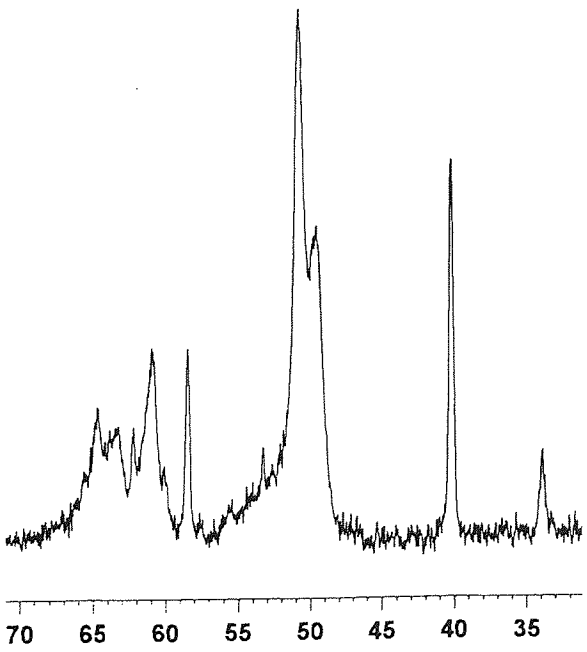

Figure 91: **^{31}P NMR spectrum of TUPO coated NanoDots™ after extended exposure to the ADMET polymerisation procedure with Grubbs 2nd generation catalyst, expansion between ∂ 30.0 ppm & ∂ 70.0 ppm**

The ^{31}P spectrum of the concentrated reaction with Hoveyda-Grubbs **43** again produced the expected simplified spectra consisting of two regions of signals at ∂ 49.5 (broad), 63.0-66.0 (overlapping broad signals) **Figure 92**. The signals are reminiscent of those seen in the ^{31}P spectrum of the TUPO-polymer $\mathbf{41}_{10\%}$ **Figure 89,** but unfortunately the signal at ∂ 49.5 cannot be assigned as polymeric with confidence since it is at a similar chemical shift to that of the monomer. This sample also suffers from a poorly resolved olefinic region of the ^{1}H NMR, the peaks present were extremely small and of little use in assessing the extent of reaction reliably.

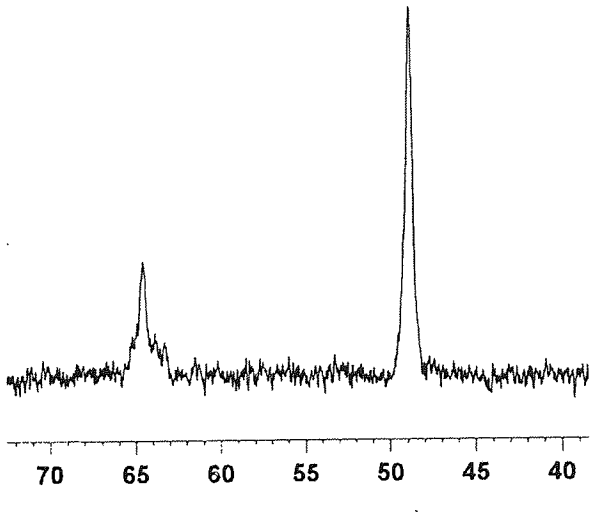

Figure 92: **^{31}P NMR spectrum of TUPO coated NanoDots™ after extended exposure to the ADMET polymerisation procedure with Hoveyda-Grubbs 2nd generation catalyst, expansion between ∂ 40.0 ppm & ∂ 70.0 ppm**

There are two possible explanations that can be proposed for the information obtained from the spectra. The first is that the reaction has not been particularly successful

however, the other is the complete opposite. Unfortunately if the reaction of coating the NanoDots™ is 100% successful it is highly likely that the signals arising from the resultant polymer would not be visible in the NMR spectra. Since the polymeric network since the structure would be too rigid and move too slowly in solution on the NMR time-scale to be detected.[155]

The information obtained from the ^{31}P NMR spectroscopy investigation of the discussed polymer coated NanoDots™ could not be used solely as proof that the reaction has occurred as predicted. However, if presented as part of a body of evidence in support of a significant change in the material after it has been exposed to the polymerisation reaction conditions, there are significant findings that indicate a process has occurred and that possibly this process is one of surface polymerisation.

The evidence discussed so far for the formation of a polymer coating on the surface of a NanoDot™ all suffers from the same discrepancy concerning the fact that there is very little proof the polymerisation is actually occurring on the surface of the NanoDots™. The same results could have been generated in good faith from monitoring the occurrence of the polymerisation in solution. The following NMR experiments, carried out in collaboration with Prof. G. A. Morris at the University of Manchester were designed to investigate whether the polymerisation reaction was occurring on the surface of the nanoparticle or simply in solution.

2.6.5 Analysis by DOSY ^{1}H NMR Spectroscopy

Polymer-coated NanoDots™ were prepared, as discussed previously by the addition of 10 mole percent Grubbs 2nd Generation catalyst **42** to TUPO **25** coated NanoDots™ suspended in $CDCl_3$. The reaction was allowed to proceed for three weeks at 40°C, then the reaction volume was decreased to ~1ml under reduced pressure. Aggregation of the product during the metathesis was ruled out as the material passed through a 20nm filter before analysis by DOSY ^{1}H NMR spectroscopy.

Analysis of the reduced reaction mixture by DOSY ^{1}H NMR spectroscopy was important for two reasons, the first being that it can be used to identify where the polymerisation is occurring. The second involves the fact that the material to be analysed is a mixture of compounds and the DOSY technique is in part, specifically designed to analyse and identify the different components present in a mixture. As discussed previously, DOSY identifies components of a mixture by relating their individual diffusion coefficients to the NMR resonances they produce. Large molecules have large diffusion coefficients and occur towards the top of the spectrum whereas smaller molecules diffuse more quickly and appear at the bottom of the DOSY diffusion grid.

Examination of the DOSY spectrum of polymer-coated NLP121 NanoDots™ shows the different diffusion coefficients of the various different species present in the mixture **Figure 93**.

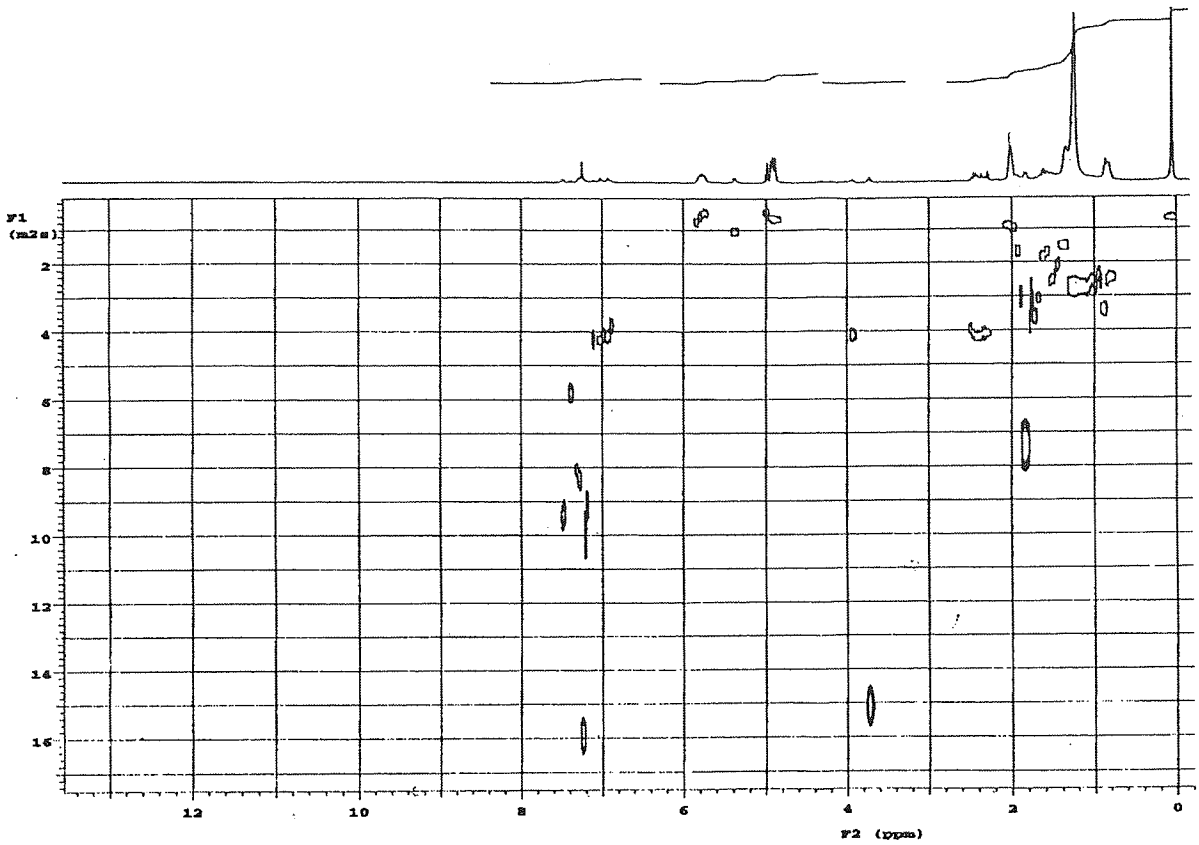

Figure 93: **DOSY ^{1}H NMR spectrum of TUPO coated NanoDots™ after extended exposure to the ADMET polymerisation procedure with Grubbs 2nd generation catalyst, expansion between ∂ 0.0 ppm & ∂ 11.0 ppm**

Two common examples of molecules that possess vastly different diffusion coefficients are $CDCl_3$ and silicone grease. The self diffusion coefficient corresponding to each of these can be read directly from the DOSY spectrum underneath the signals they produce in the one dimensional ^{1}H NMR spectrum. $CDCl_3$ is small and the self diffusion coefficient it produces reflects this with a value of 15.9×10^{-10} m^2s^{-1}. Silicone grease on the other hand is polymeric in nature and composed of large molecules resulting in slow diffusion with a coefficient of 0.8×10^{-10} m^2s^{-1}. The self diffusion coefficient for each

species can be related directly to the dynamic size of the molecule in solution by employment of the Stokes-Einstein equation **Equation 1**. It is this element of the technique that allows it to be of use in the determination of the nature of the polymerisation detected in one dimensional ^{1}H NMR spectroscopy.

$$D = k T / 6 \pi \eta r_h \qquad \textbf{Eqn1}$$

Where

D is the diffusion coefficient

k is the Boltzman constant

T is the temperature

η is the viscosity of the solvent

r_h is the hydrodynamic radius

Using the diffusion coefficient of the signal corresponding to the new olefin produced by the ADMET polymerisation of the surface ligands, the effective radius of the material that the resonance is associated with (i.e. polymer and NanoDot™) can be calculated. The initial calculation will be completed assuming a spherical shape, however this can be corrected if necessary using dimensional information obtained from a TEM image of the polymer coated NanoDot™ **Figure 94**.

Rearrangement of **Equation 1** produces **Equation 1i** allowing the effective radius of the species relating to the polymeric signal at ∂ 5.28 ppm to be calculated.

$$r_h = k T / 6 \pi \eta D \qquad \textbf{Eqn1i}$$

Where

$D = 1.1 \times 10^{-10}\ m^2\ s^{-1}$ (from DOSY spectrum)

$k = 1.38 \times 10^{-23}\ J\ K^{-1}$

$T = 298\ K$

$\eta = 0.569 \times 10^{-3}\ N\ s\ m^{-2}$ (viscosity of $CDCl_3$)

$r_h = (1.38 \times 10^{-23}) \times (298) / 6\pi\ (0.569 \times 10^{-3}) \times (1.1 \times 10^{-10})$

$r_h = 3.427 \times 10^{-9}$ m

Units

$r_h = k\ T / 6\ \pi\ \eta D$ $= J\ K^{-1}\ K / N\ s\ m^{-2}\ m^2\ s^{-1}$ = J/N

however J = Nm

Therefore units Nm/N = m

The effective radius of the species associated with the polymeric resonance was calculated to be 3.4×10^{-9} m, conversion of this to nanometres gives a radius of 3.4 nm with a diameter of 6.8 nm. The TEM image of the polymer coated sample suggests nanoparticles with average dimensions of approximately 3.6 nm x 5.8 nm **Figure 94**. Since these particles are not spherical they will experience a different hydrodynamic drag as they pass through the solvent compared with that of a spherical molecule with the same volume. It is possible to calculate a correction factor that relates the hydrodynamic radius of a sphere to that of a prolate ellipsoid of the same volume by accounting for the different frictional coefficients. This correction factor known as Perrins factor can then be applied to the radius of the sphere calculated using the information from the DOSY, converting it from that of a sphere to that of the effective radius of a prolate ellipsoid.

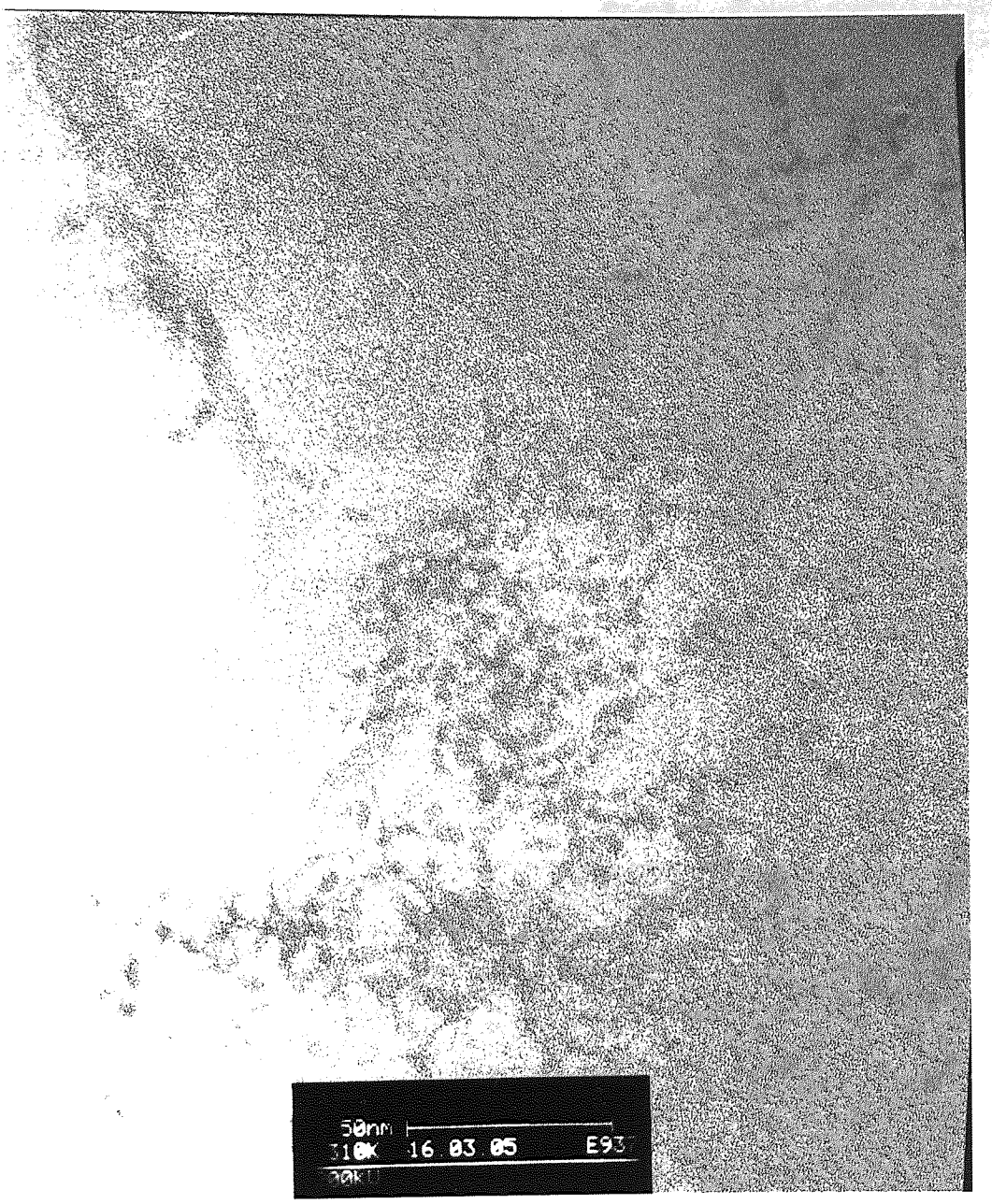

Figure 94: TEM image of Polymer coated NanoDots™

To calculate the correction factor the dimensions of the nanoparticles obtained from several averages observed from the TEM image are assumed to relate to that of a rod with a length of 5.8nm and a diameter of 3.6nm. The length and diameter of the idealised rod can then be related to the ratio of dimensions **a** and **b** of a prolate ellipsoid using **Equation 3**.[156]

$$a/b = (2/3)^{1/2} L/d \qquad \textbf{Eqn 3}$$

where L is the length and d id the diameter of the rod

Therefore $a/b = (2/3)^{1/2} \times (5.8/3.6)$

$a/b = 1.3$

The ratio of **a/b** for the prolate ellipsoid can now be used to obtain Perrins factor (**f/fo**), the diffusion frictional coefficient ratio for a prolate ellipsoid when **a/b** = 1.3 **Figure 95.**[155, 156] is a plot of the inverse of **f/fo** against **a/b**, therefore when a/b = 1.3, Perrins factor is equal to 1/1.005.

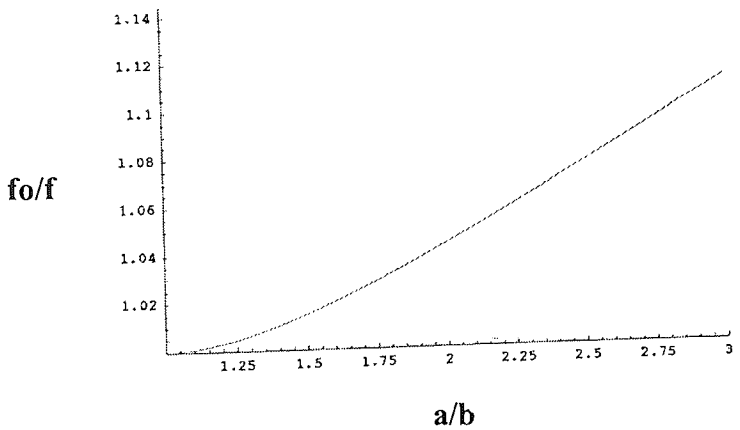

Figure 95: Plot of the inverse of f/fo against a/b (expanded from original source by Pr. G. A. Morris)

Multiplying Perrins factor by the radius of the sphere obtained from data from the DOSY spectrum converts it to the effective radius of a prolate ellipsoid **Equation 4.**

$$r_{eff} = r_h \times 1/(f/f_o) \qquad \textbf{Eqn 4}$$

$r_{eff} = 3.427 \times 10^{-9} \times (1/1.005)$

$r_{eff} = 3.427 \times 10^{-9} \times 0.995$

$r_{eff} = 3.427 \times 10^{-9} \times (1/1.005)$

$\mathbf{r_{eff} = 3.410 \times 10^{-9}\ m}$

The correction factor does not make a significant difference to the calculated size of this sample, however the methodology has been included here for completeness since the accuracy of future applications of this technique may depend on employment of an analogous correction factor.

The same set of calculations can be completed using the DOSY spectrum of TUPO **25** monomer coated NLP121 to give a comparison of the size before and after polymerisation. The diffusion coefficient corresponding to the olefinic signals on the same batch of TUPO coated NLP121 used in the polymerisation reaction was obtained from the DOSY spectrum as $0.4 \times 10^{-10}\ m^2\ s^{-1}$. Using **Equation 1i** the radius of the species corresponding to the monomeric signal was calculated at 9.4nm. This calculation suggests that the diameter of the monomer coated NanoDots™ are 18.8nm.

Comparing the calculated size of the monomer coated NanoDot™ to that of the polymer coated NanoDot™, 18.8nm and 6.8nm respectively suggests that polymerisation shrinks the ligand layer on the surface of the particle. A possible explanation of this may be that before polymerisation the ligand layer was composed of a thick multi layer of ligands most likely comprising a mixture of TUPO **25** and HDA **3**. Following the polymerisation reaction procedure it is possible that the NanoDot™ ligand layer is composed of a thinner layer consisting mainly of polymer. The high dilution, elevated

reaction temperature and extended reaction times make it likely that the majority of the HDA **3** ligand simply diffuses away from the surface of the NanoDots™. No firm experimental evidence has been evidence has yet been obtained to support this hypothesis since it is difficult to establish this from the DOSY spectra obtained as the aliphatic signals result from a mixture of species. However the diffusion coefficient for the terminal methyl protons does appear to be slightly lower down diffusion grid in the polymer coated DOSY **Figure 93** than that in the monomer coated DOSY **Figure 96.** This may suggest that less of the HDA is bound to the surface of the NanoDot™ subsequent to the polymerisation process.

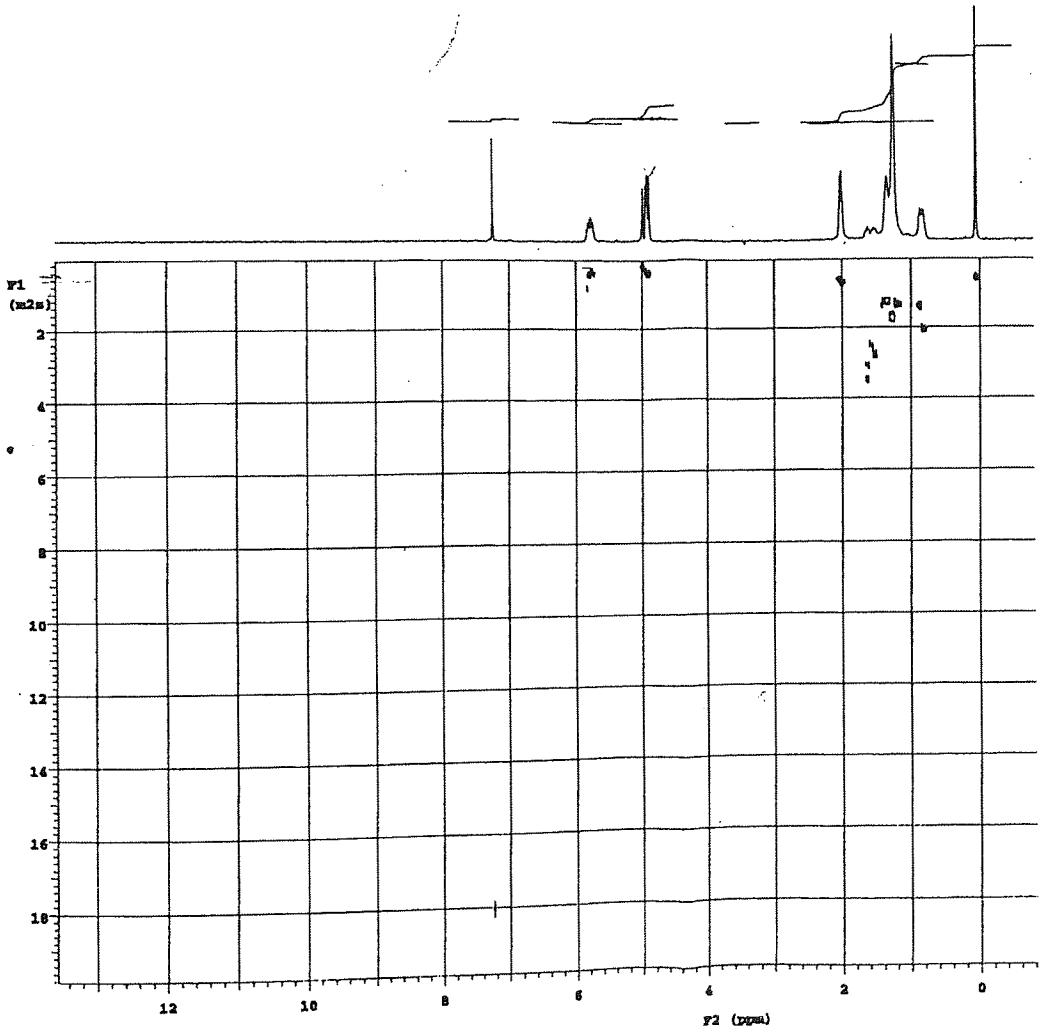

Figure 96: **DOSY ^{1}H NMR spectrum of TUPO coated NanoDots™, expansion between ∂ -0.10 ppm & ∂ 13.0 ppm**

These findings are the results of a preliminary DOSY investigation conducted in collaboration with Pr. Morris at the University of Manchester to extend the analysis of the coated particles produced. The subsequent interpretation of the diffusion coefficient for the polymeric species obtained from the DOSY spectrum does however strongly support the theory that the polymer coating resides on the NanoDot and is not simply in solution. At the time of writing, to the best of the authors knowledge no other study providing such unambiguous evidence in support of this fact has been reported. The calculation of the correction factor was included for the polymer coated NanoDots™, however the poor quality of the TEM image may also have affected the accuracy of this method. Nevertheless the important result of this initial investigation should remain that the calculation of the size of the polymer coated NanoDots™ is certainly comparable with that obtained from the TEM image **Figure 94**.

Encouraged by the positive results obtained from the initial DOSY experiments it was the intention to improve upon this investigation by further purification of this sample and the preparation of several others. The ADMET polymerisation of TUPO **25** coated SD396, TUPO **25** coated MC556 and TUPO **25** coated MC610 were each completed with 10 mole percent Grubbs 2nd generation catalyst at 40°C for three weeks. An attempt was made to remove residual impurities before subjecting the second batch of samples to analysis by DOSY ^{1}H NMR at the University of Manchester.

It was decided that it would be possible to remove the impurities by dialysis of the sample in deuterated chloroform using a cellulose membrane. The initial dialysis was attempted using a standard cellulose dialysis tubing mainly utilised in biological applications. The specifications of this tubing and the suppliers suggested that both the

membrane and the clips supplied were chloroform compatible. However upon exposure to chloroform both leached impurities into the solvent. Subsequent dialysis was attempted using ultra pure chloroform compatible D-tubes (supplied by Novagen for use in organic and aqueous based solvents). A D-tube is a small polypropylene vessel that incorporates two cellulose membrane windows through with impurities are removed, the samples can be added with a standard laboratory pipette and are sealed inside by a polypropylene screw cap top. Unfortunately the use of D-tubes also caused additional contamination of the samples dialysed within them.

Despite the purification and contamination problems encountered three samples of polymer coated NanoDots ™ were analysed ^{1}H DOSY again at the University of Manchester. Unfortunately all the diffusion coefficients obtained for the analysis of the polymer coated and non-polymer coated NanoDots™ were larger than expected. Consequently the calculations to obtain the size of the particles from the recorded diffusion coefficients were much smaller than anticipated, the full calculations for each nanoparticle investigated are included in **Appendix C**. For example, the diameter of the polymer coated MC556 was calculated to be 1.5nm and the diameter of the NanoDots ™-MC556 before polymerisation were calculated at 3.0nm. The fact that both the diffusion coefficients for non-polymer coated and polymer coated NanoDots™ were affected suggests that either there was a difference in the set of parameters used in the second batch of DOSY experiments, or that the different types of NanoDots™ used in this second study were not behaving as expected in solution. Due to the time constraints on the use of the equipment and on this body of work no further investigation into these findings could be completed. However, although in its infancy this type of analysis

holds important potential for the characterisation of NanoDots™ and requires further investigation for its application to the study of ligand/polymer coated nanoparticles.

2.6.6 Combustion Analysis

A sample of TUPO monomer coated NanoDots ™ and the corresponding sample of TUPO polymer coated NLP121 NanoDots ™ were washed and precipitated twice with excess methanol before being analysed by combustion analysis **Table 11**. Calculating the molar ratio of phosphorus to the molar ratio of cadmium in each sample allows a direct comparison between the amount of ligand layer remaining after the washing of both samples. The polymer coated sample of NanoDots™ has twice as much phosphorus remaining adhered to the surface after washing compared with that of the monomer coated NanoDots™ **Table 11**. This is more evidence in support of the formation of a polymer network that resists removal by washing and precipitation with methanol.

	Sample	Cd	P
Combustion analysis	non-polymerised-washed	40.12 %	0.33%
	polymerised-washed	33.99%	0.54%
Molar ratio	non-polymerised-washed	1 mole	0.03 moles
	polymerised-washed	1 mole	0.07 moles

Table 11: Table of the percentage composition and molar ratio of Cd and P in a samples of TUPO-coated and TUPO-polymer-coated NanoDots™

2.6.7 Evaluation of Enhanced Stability

The following investigation was designed to evaluate the effect of the polymer shell on the overall stability of the NanoDots™. The study involved the exposure of a batch of polymer coated MC566 NanoDots™ to a variety of commonly encountered chemical reagents. An identical investigation was carried out on a batch of TUPO **25** monomer coated MC566 NanoDots™ as a means of evaluating the effectiveness, in terms of the enhanced chemical stability of the coated NanoDots™. Stock solutions of the two batches of nanoparticles were prepared in THF. Standard solutions of each reagent were prepared in THF (10ml) according to **Table 12**.

Reagent	Amount (g)	Amount (ml)
Trifluroacetic acid (TFA)	0.0285	0.019
Aluminium trichloride (AlCl3)	0.0325	-
1,8-Diazabicyclo[5.4.0]undec-7-ene (DBU)	0.0380	0.037
Potassium hydroxide (KOH)	0.0140	
Iodobenzoic acid (IBX)	0.0700	
Potassium permanganate (KMnO4)	0.0390	
Lithium aluminium hydride (LiAlH4)*	-	0.250
n-Butyl lithium (nBuLi)*	-	0.250
Vinyl magnesium bromide (Vinyl MgBr)*	-	0.025
Hydrogen Bromide (HBr)	-	0.040

* 1M in THF

Table 12: Amounts of each reagent used to prepare stock solutions in THF for the investigation into stability

0.5ml aliquots of the NanoDot™ solutions were exposed to 0.5ml of the solutions containing the different reagents. The resilience of the NanoDots™ to the various different reagents was monitored by comparison of the PL spectra before and after addition of the reagents. **Figure 97** and **Figure 98** show a compilation of PL spectra

recorded after exposure to reagents for monomer and polymer coated NanoDots™ respectively.

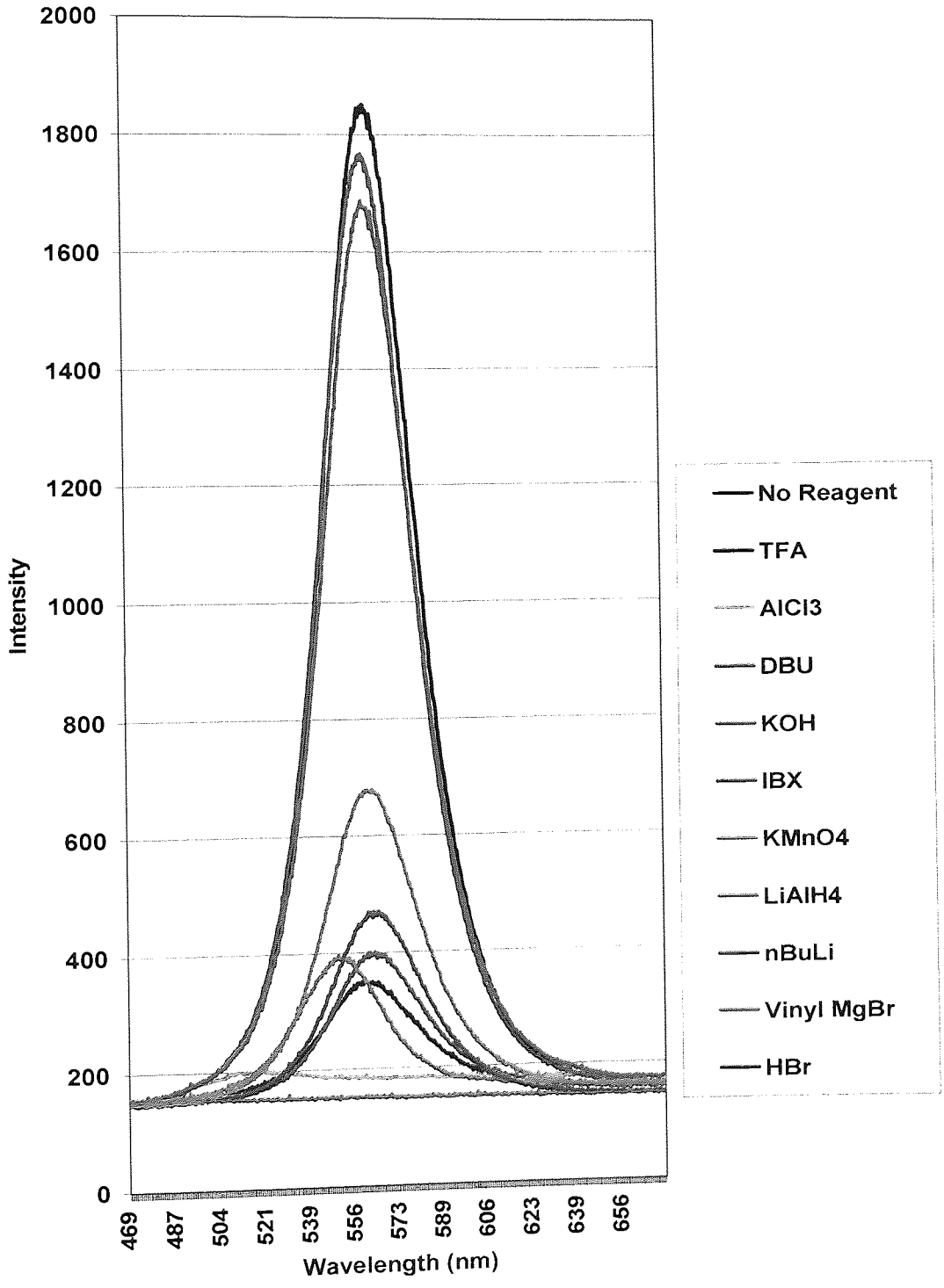

Figure 97: **PL spectra of TUPO-coated NanoDot ™ batch MC556 upon exposure to a variety of reagents**

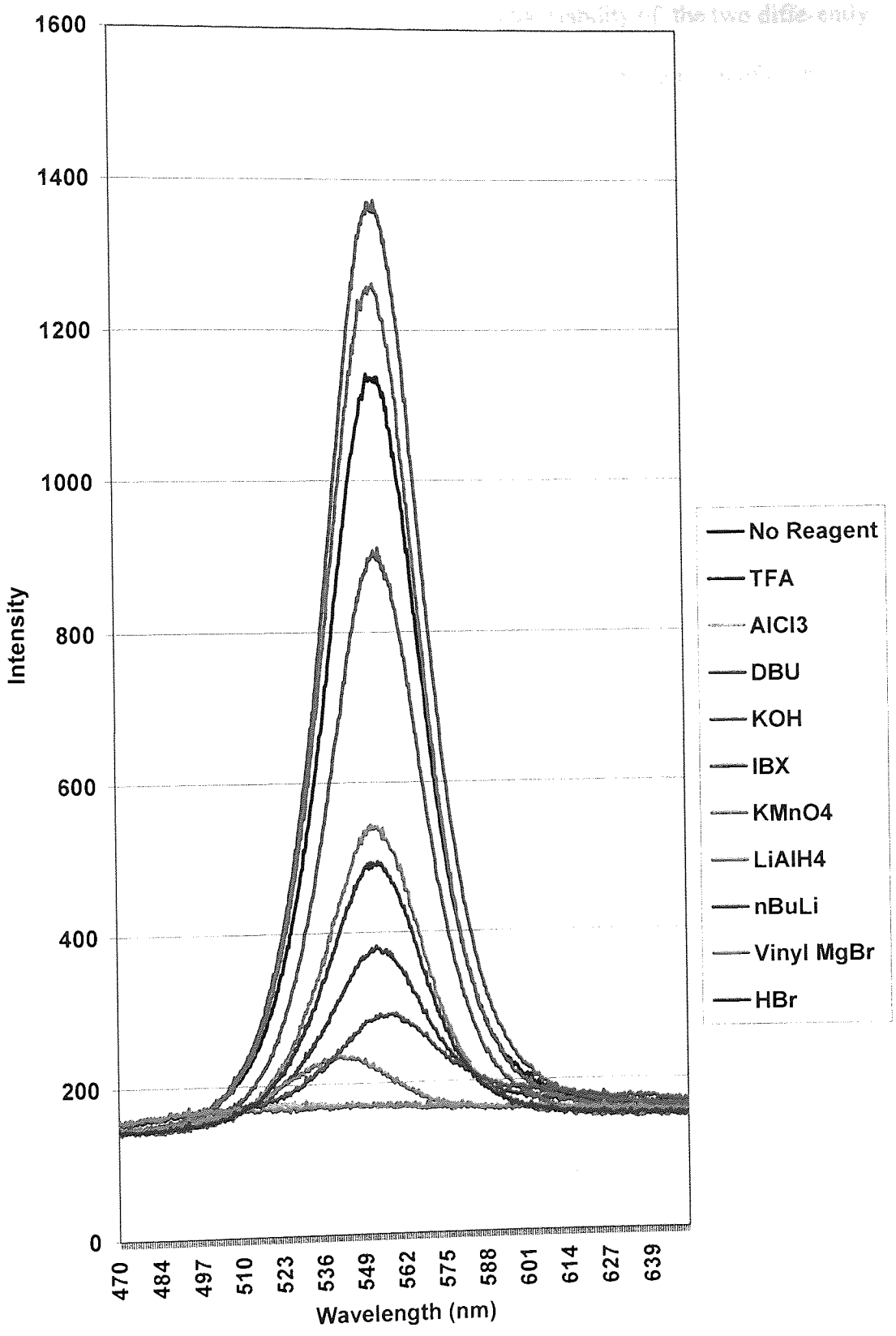

Figure 98: PL spectra of TUPO-polymer-coated NanoDot ™ batch MC556 upon exposure to a variety of reagents

In order to compare the effect of each reagent upon the stability of the two differently capped batches of NanoDots™ the PL spectra recorded after the addition of each reagent had to be compared with the corresponding PL spectrum where no reagent had been added. Comparing the PL emission maximum of an aliquot of the NanoDots™ before treatment with the PL emission maximum after treatment allows a calculation of the percentage PL remaining after the exposure to each reagent to be made. A comparison of the remaining percentage PL after treatment with the various different reagents is represented below for both monomer and polymer coated NanoDots™ **Figure 99**.

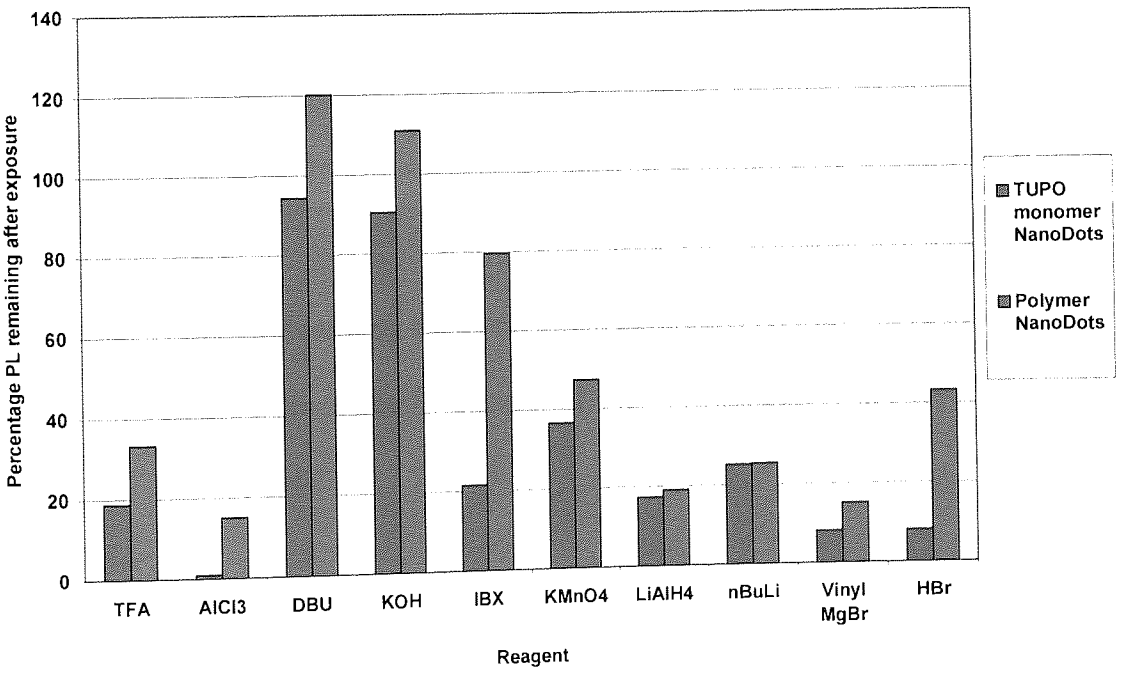

Figure 99: Graph comparing the percentage of residual PL maximum emission of the monomer and polymer coated NanoDots™

The polymer coated NanoDots™ were consistently more stable than their monomer coated counterparts upon exposure to all the reagents in the investigation.

This extra resilience was quantified by the calculation of percentage stability enhancement directly resulting from the presence of the polymer coating **Figure 100**.

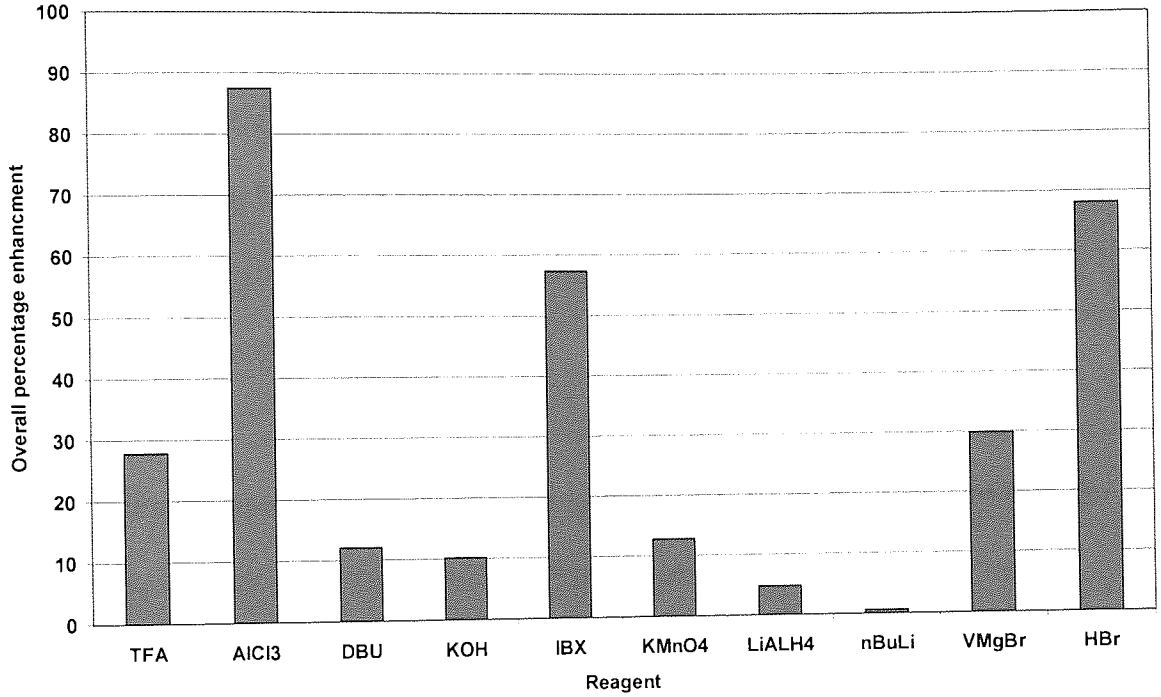

Figure 100: Graph depicting the percentage enhanced stability of the polymer-coated NanoDots™ compared with the monomer-coated NanoDots™

Both the monomer and polymer coated NanoDots™ appeared stable in the presence of DBU and KOH. Exposure to $KMnO_4$ was tolerated by both monomer and polymer coated NanoDots™, with the that latter performing marginally better with about 13% enhancement. Exposure to TFA and Vinyl MgBr destroyed the PL emissions of both the monomer and coated NanoDots™ to below 50% of the untreated PL maximum emission, but again the polymer-coated dots performed about 30% better than the monomer-coated NanoDots™ in both cases. Treatment with $LiAlH_4$, nBuLi and $AlCl_3$ had a severely detrimental effect on the emissions PL property of both, however in the

case of $AlCl_3$ the presence of the polymer coating protected the residual PL of the NanoDots™ significantly compared with the monomer coated NanoDots™. The polymer coated NanoDots™ also showed impressive resistance to the effects of IBX and HBr. IBX destroyed the PL emission of the monomer-coated NanoDots™ by almost 80% where as, the polymer coated dots suffered only a 20% decrease in the intensity of the PL emission maximum. Finally exposure to HBr destroyed the PL of the polymer-coated NanoDots™ by just over half however, this is a marked improvement compared with only 10% of the PL emission maximum remaining in the case of the monomer coated NanoDots™.

The exhibition of improved stability by the polymer coated NanoDots ™ is possibly the strongest demonstration that the NanoDots ™ have been modified favourably by the RCM procedure. This extra stability coupled with the previously discussed pieces of evidence strongly suggest the presence of a protective polymer coating on the surface of the NanoDots™. However further investigation and development into the nature of this coating is still required.

2.7 – Incoporation of coated NanoDots™ into Functionalised Resin

Polymer coating NanoDots™ was proposed initially as a method to retard the deterioration of the PL emissions of NanoDots™ incorporated into CMS **10** functionalised solid supports. Accordingly evaluation of the addition of the polymer coating in this application was investigated by the production two batches of 1mmol/g CMS functionalised 20% cross-linked resin, one containing polymer coated NanoDots™ and the other containing DOMSPO **7** coated NanoDots™.

The resins were prepared in series with use of a 12 station Carousel™ workstation, and the PL spectra of each sample was evaluated before and after 8 hours of Soxhlet extraction in DCM. **Figure 101** displays the PL spectra before and after Soxhlet of the DOMSPO **7** and polymer-coated NanoDots™ respectively following incorporation into the functionalised resin. Contrary to previous results produced in the Sutherland group the CMS does not appear to have had a severely detrimental effect on the PL of the DOMSPO **7** coated NanoDots™. However in this single example incorporation of the polymer coated NanoDots™ has not been nearly as successful. Comparing the PL emissions spectra of the two resins, it is apparent that the beads containing the polymer coated NanoDots™ have a much reduced PL emissions maximum.

There are a number of possibilities that could account for this, the first being that the polymer coating reduces the stability of the NanoDots™ to the reactive agents in the polymer mixture. Another possibility could be that the residual double bonds remaining on the surface of the polymer coated NanoDots™ are not reactive towards AIBN and as

a result the polymer coated NanoDots™ were not incorporated as efficiently into the polymer matrix.

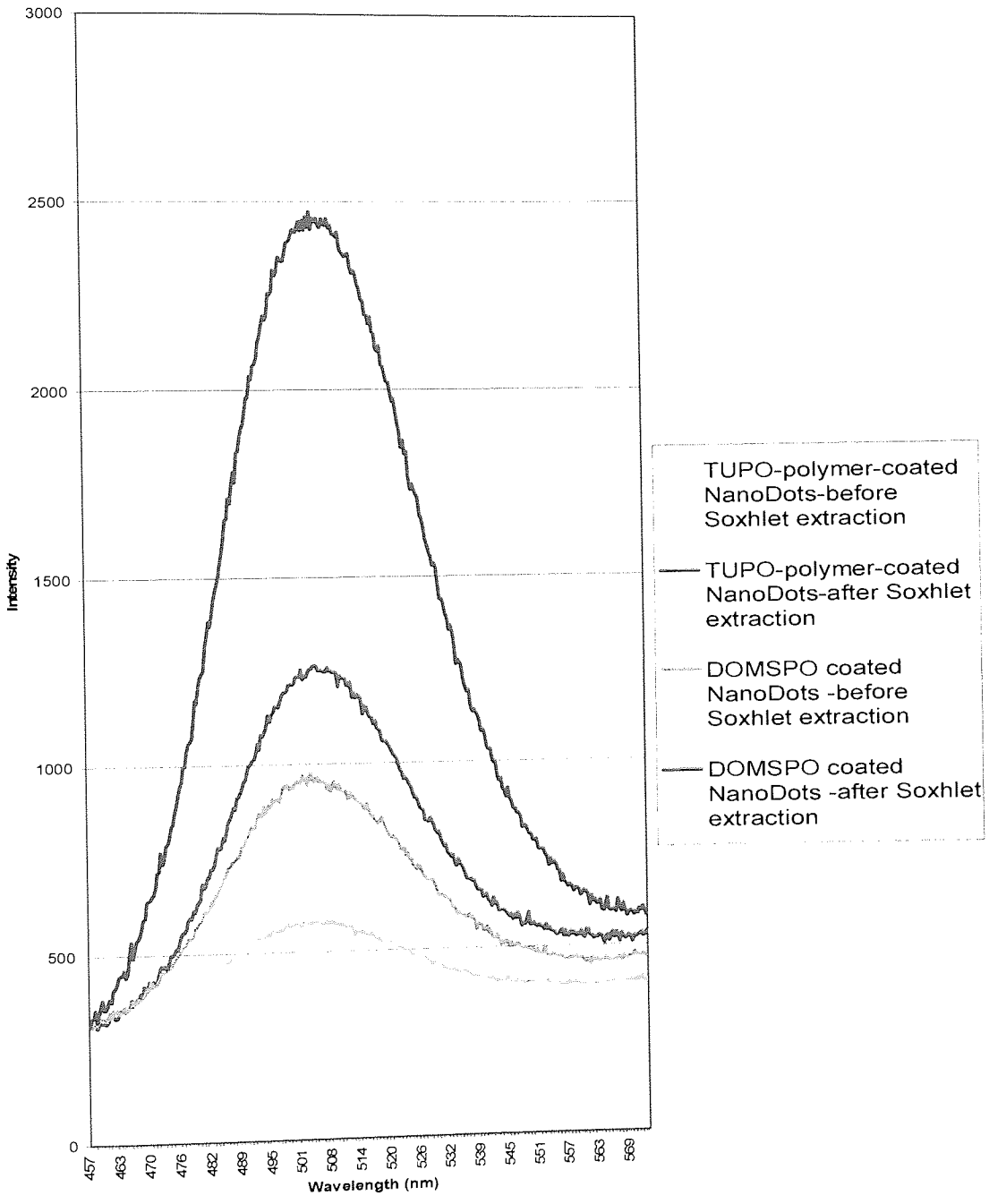

Figure 101: PL spectra before and after Soxhlet extraction of resins containing DOMSPO 7-coated NanoDots™ and TUPO-polymer-coated NanoDots™

Working on the assumption that any NanoDot™ incorporated into the polymer matrix of a resin produced for use in SPOC may benefit from extra protection from aggressive reagents the production of a more compatible polymer coat was discussed. To this end the DMSDPO **21** ligand that contains two syrenic units was considered for the ADMET polymerisation on the surface NanoDots™.

Unfortunately preliminary studies on the metathesis of ligand **21** without the presence of NanoDots™, suggested that the two double bonds of the ligand react together preferentially in a RCM reaction rather than following an ADMET polymerisation pathway. The metathesis reaction of DMSDPO **21** was attempted with 5 and 10 mole percent of both Grubbs 2nd generation and Hoveyda-Grubbs 2nd generation catalysts. Examination of the ^{1}H NMR produced from the products obtained in both cases showed the same resonances. The signals relating to the all three protons of the terminal olefin disappeared and were replaced by a singlet at ∂ 7.0 ppm. The logical modification to this ligand would be to mimic the tri-functionalised nature of TUPO **25** and add a third styrene unit. Accordingly synthesis of this ligand was attempted but as mentioned earlier the inherent insoluble nature of the product meant it was of little use.

Future work in this area is required to assess the stability, to reaction conditions commonly encountered in SPOC, of covalently incorporated NanoDots™ residing in the polymer matrices of the beads. If extra protection is required the design of a more soluble trifunctionalised styrenic based ligand with improved stability may be necessary to both allow covalent incorporation into the beads and to protect the NanoDots™ from aggressive reagents.

CHAPTER 3

CONCLUSION

3. Conclusion

A series of functionalised phosphine oxides and sulfides ligands based on the structure of TOPO **1** have been successfully synthesised. Initial design and synthesis of the ligands began with the production of a range of non-functionalised and functionalised phosphinous and phosphosulfinous acid intermediates. Optimised procedures enabled the production in multi-gram scales, of intermediates possessing aliphatic, olefinic and styrenic groups. All attempts to synthesise an intermediate bearing a hydroxyl function failed regardless of the presence of protecting groups on the hydroxyl functionality.

The intermediate acids were converted to the corresponding tertiary phosphine oxides *via* a deprotonation process employing sodium hydride. Initial attempts at deprotonation with sodium amide were abandoned due to the slower reaction times and impurities that remained in the final products. Difficulties encountered in the purification of these compounds *via* column chromatography, resulted in often time consuming purification of the majority of the products *via* crystallisation in different solvents at different temperatures. Analysis of the ligands by ^{1}H NMR spectroscopy was complicated by the presence of the phosphorus atom, however the resulting splitting patterns aided in the production of invaluable structural information.

The ligands produced were evaluated initially for their ability to displace HDA on the surface of NanoDots™, and subsequently for their suitability in the various applications they had been designed for. The synthesis of the phosphine sulphides is limited mainly due

to the fact that they showed no significant improvement over the phosphine oxides, however the unpleasant syntheses coupled with the awkward handling characteristics of the reagents employed in their construction was also an important factor.

An investigation into the nature and behaviour of the NanoDots™ supplied by Nanoco™ was undertaken to obtain a better understanding of the limits of the materials supplied prior to their modification and application. An evaluation of the stability of the HDA capped NanoDots™ to various different reagents and conditions was completed. It was discovered that the properties of NanoDots™ varied considerably from batch to batch and that the surface ligand can be removed by excessive washing resulting finally in the material becoming insoluble.

Observation of the behaviour and interactions of the NanoDots™ with the designer ligands was undertaken and it was discovered that the structure of the ligand was an important factor in the success of the HDA **3** displacement procedure. Attempts were also made to evaluate and optimise the displacement procedure. A procedure that could be generalised to the majority of displacement procedures was elucidated, however the individual characteristics of the different batches of the NanoDots™ coupled with the effect of the structural differences between the displacement ligands continually needed to be considered. A common issue affecting all the displacement procedures was the potential for over-washing and thus stripping the surface ligand from the surface of the NanoDots™ resulting in either no desired ligand residing on the surface or in extreme cases insolubility. It was discovered that a single post displacement precipitation process in polar solvent was

sufficient to remove excess ligand following the displacement procedure without compromising the solubility of the NanoDots™.

Finally the production of a polymer shell initially developed for protection of the NanoDots™ but with the possibility of adaptation to provide surface functionalisation of individual dots was investigated. The ADMET polymerisation of surface bound TUPO **25** was successfully achieved on several different batches of NanoDots™

Difficulties encountered with the solubility of the final product resulted in the employment of a different approach to the analysis of products produced *via* the ADMET polymerisation reaction procedure. The reactions were completed in $CDCl_3$ and direct analysis of the reaction mixture produced evidence in support of the successful surface polymerisation. The growth of the polymeric resonance with the corresponding diminishing resonances of the monomer olefin was monitored by ^{1}H NMR spectroscopy. The reaction was pushed to 80% completion by the addition of a total of 10 mole percent Grubbs 2nd generation catalyst.

Changes observed by ^{31}P NMR spectroscopy that mirrored changes present in the polymerisation of the monomer in the absence of NanoDots™ were recorded with both non-phosphorus and phosphorus containing catalysts. Evidence demonstrating the inability to wash the polymer shell from the surface of the NanoDots™ was produced by comparing the combustion analysis results of washed samples of polymer and monomer coated

NanoDots™ also strongly suggested the formation of a surface bound cross-linked polymer.

Analysis by ^{1}H DOSY NMR spectroscopy confirmed the presence of surface bound polymer. The diffusion coefficient relation to the polymer resonance was used to calculate the sizes of the species the resonance was associated with and this figure compared well with a TEM image obtained for the same batch of NanoDots™. Finally consistently improved stability exhibited by polymer coated NanoDots ™ over their monomer coated counterparts upon exposure to a variety of different reagents provided physical evidence of the presence of a polymeric shell. Future work is still required to solve compatibility problems associated with the addition of these protected NanoDots™ to suspension polymerisation reactions.

CHAPTER 4

EXPERIMENTAL

4.1 General Information

All reactions involving moisture sensitive reagents were conducted in oven dried (120°C) glassware using dried solvent. All reagents were used as received from Sigma-Aldrich, Fischer Scientific, Acros Organics, Alfa Aesar, BHD, Avocado Organics or Lancaster unless otherwise stated. The N(2-aminomethyl)aminomethyl polystyrene resin was purchased from Novabiochem. The NanoDots™ were received from NanoCo and stored under nitrogen and away from any light sources.

4.1.1 Solvents

Deuterated Chloroform 99.8at.%D over molecular molecular sieves was purchased from Goss scientific Instrumentation Ltd. All solvents were purchased from Fischer Scientific. Dichloromethane, toluene, pyridine and dimethylformamide were distilled to dryness over calcium hydride. Diethyl ether and Tetrahydrofuran were distilled to dryness over a mixture of sodium wire and benzophenone. Ethanol, ethyl acetate, hexane and methanol were used as received.

4.1.2 Reagents

1-Bromodecane

Supplied by:	Sigma-Aldrich
Purity/grade:	98%
Special storage requirements:	None

10-Bromo-1-decanol

Supplied by:	Sigma-Aldrich
Purity/grade:	>95%
Special storage requirements:	None

11-Bromo-1-undecene

Supplied by:	Avocado Organics
Purity/grade:	96%
Special storage requirements:	None

1-bromooctane

Supplied by:	Sigma-Aldrich
Purity/grade:	99%
Special storage requirements:	None

8-Bromo-1-octene

Supplied by:	Sigma-Aldrich
Purity/grade:	97%
Special storage requirements:	None

Azobis-iso-butyronitrile

Supplied by:	Fischer Scientific
Purity/grade:	>97%
Special storage requirements:	<20°C

Benzophenone

Supplied by:	Avocado Organics
Purity/grade:	99%
Special storage requirements:	None

Calcium hydride

Supplied by:	Acros Organics
Purity/grade:	93%
Special storage requirements:	None

Chloromethylstyrene

Supplied by:	Sigma-Aldrich
Purity/grade:	90%/Tech
Special storage requirements:	<5°C
Purified by distillation before use	

Dibutylphosphite

Supplied by:	Sigma-Aldrich
Purity/grade:	96%
Special storage requirements:	None

Divinylbenzene

Supplied by:	Sigma-Aldrich
Purity/grade:	80%/Tech
Special storage requirements:	<5°C

Ethyldichlorothiophosphate

Supplied by:	Sigma-Aldrich
Purity/grade:	95%
Special storage requirements:	Under N_2

Grubbs 2nd generation catalyst

Supplied by:	Sigma-Aldrich
Purity/grade:	Not given
Special storage requirements:	Under N_2

Hoveyda-Grubbs 2nd generation catalyst

Supplied by:	Sigma-Aldrich
Purity/grade:	Not given
Special storage requirements:	Under N_2

Imidazole

Supplied by:	Alfa Aesar
Purity/grade:	99%
Special storage requirements:	None

Iodine

Supplied by:	Sigma-Aldrich
Purity/grade:	99.8
Special storage requirements:	None

Lawessons Reagent

Supplied by:	Sigma-Aldrich
Purity/grade:	97%
Special storage requirements:	Under N_2

Magnesium turnings

Supplied by:	Sigma-Aldrich
Purity/grade:	98%
Special storage requirements:	Under N_2/over silica gel

N(2-aminomethyl)aminomethyl polystyrene resin

Supplied by:	Novabiochem
Purity/grade:	3.0mmol/g
Special storage requirements:	>20°C

Poly(vinylalcohol)

Supplied by:	Sigma-Aldrich
Purity/grade:	87-89% hydrolysed
	Average M_w 85,000-146,000
Special storage requirements:	None

Sodium

Supplied by:	BDH
Purity/grade:	99.9%
Special storage requirements:	Under mineral oil

Sodium hydride

Supplied by:	Avocado Organics
Purity/grade:	60% dispersed in mineral oil
Special storage requirements:	None

Styrene

Supplied by:	Acros Organics
Purity/grade:	99.5%
Special storage requirements:	<5°C

Tert-butylamonium fluoride

Supplied by:	Avocado Organics
Purity/grade:	1M solution in THF
Special storage requirements:	Under N_2

Tert-butyldimethylsiliyl chloride

Supplied by:	Avocado Organics
Purity/grade:	97%
Special storage requirements:	None

Trioctylphosphine oxide

Supplied by:	Lancaster
Purity/grade:	90%/Tech
Special storage requirements:	None

Triphenylphosphine oxide

Supplied by:	Lancaster
Purity/grade:	99%
Special storage requirements:	None

Triphenylphosphine sulfide

Supplied by:	Lancaster
Purity/grade:	99%
Special storage requirements:	None

All reactions were stirred magnetically or agitated gently and conducted under an atmosphere of nitrogen unless otherwise stated. Where possible reactions were monitored by thin layer chromatography (TLC) using Merck silica gel 60 F_{254} precoated glass plates, that were visualised with UV light and then developed using either iodine or a solution of phosphomolybdic acid in ethanol.

The majority of ^{1}H NMR and ^{13}C NMR spectra were recorded on a Brucker AC300 spectrometer, using $CDCl_3$ as a solvent. Chemical shift values (∂) were reported in parts per million (ppm) relative to the residual signal of the solvent (∂ 7.24 for ^{1}HNMR and ∂ 77.00 for ^{13}C NMR) and coupling constants were reported in hertz. Carbon spectra were recorded using the PENDENT program.[153] Diffusion order ^{1}H NMR spectra were recorded with assistance from the Department of Chemistry at the University of Manchester (Varian Inova 400 MHz spectrometer). Low-resolution mass spectra (LRMS) were recorded on a Finnigan LCQ ion-trap spectrometer using atmospheric pressure chemical ionisation (APCI). High-resolution mass spectra were recorded by Mr

Peter Ashton (School of Chemistry, Birmingham University) using a micromass LCT mass spectrometer. Infra-red spectra were recorded on a Perkin Elmer Paragon 1000 FT-IR spectrometer as a thin film between two sodium chloride plates or suspended in a potassium bromide disk. Elemental analyses were performed by Medac Ltd.

4.2 Synthesis of phosphinous acids and phosphine oxides

4.2.1 Dioctylphosphinous acid (DOPA) 14 [38, 119, 120, 121, 122]

Magnesium turnings (2.952g, 0.123 mol, 3eqv) and a crystal of iodine were heated with a heat gun. Upon sublimation and subsequent condensation of the iodine, diethyl ether (75ml) was added and the mixture heated to reflux. Reflux was then maintained by the addition of a solution of 8-bromooctane **15** (23.739g, 21.2ml, 0.123mol, 3eqv) in diethyl ether (25ml). The reaction mixture was then heated to 40°C and refluxed for 10 minutes to complete the formation of the Grignard reagent. The reaction mixture was then cooled to between 5-15°C and a solution of dibutylphosphite **13** (8.000g, 8.0ml, 0.041mol, 1 eqv) in diethyl ether (25ml) added drop-wise over 2 hours. The reaction mixture was refluxed for 60 minutes to complete the formation of the product. The reaction mixture was then cooled to 5°C in an ice bath and this temperature maintained while a solution of 25% sulphuric acid (50ml) added drop-wise over 1 hour. The reaction mixture was then transferred to a separating funnel using diethyl ether (100ml) and distilled water (80ml). Once in the separating funnel diethyl ether (100ml) was added to dissolve some precipitate that had formed. The aqueous layer was then removed and the organic layer washed with distilled water (3 x 100ml). The organic phase was then neutralised with an aqueous solution of 15% w/v K_2CO_3 (2 x 100ml) and extracted with distilled water (3 x 100ml) and finally with a saturated solution of sodium chloride (1 x 100ml). The organic phase was dried over anhydrous sodium sulphate, filtered and concentrated under reduced pressure to provide the crude product. The crude product was isolated as a white powder (9.9060g, 88%) and used without subsequent purification. 1.000g was recrystallised from hexane to furnish a white powdery solid (0.4822g, 48%), Mp 73-74°C, that was used for characterisation purposes

and for comparison with the crude product. IR (thin film, NaCl plate): ν_{max}/cm^{-1} 2954s (C-H aliphatic), 2911s (C-H aliphatic), 2850s (C-H aliphatic), 2356s/m (P-H), 1467s (P-CH_2), 1378w, 1238m, 1159s (P=O), 1081w, 1037w, 1003w, 976m, 948m, 916w, 896w, 845w, 780m, 762m, 724s. ^{1}H NMR (300 MHz, $CDCl_3$): ∂_H 0.78 (t, J=6.7 Hz, 6H), 1.10-1.80 (m, 28H), 6.75 (d, $^1J_{PH}$=445.0 Hz, 1H). ^{13}C NMR (75 MHz, $CDCl_3$, PENDANT): ∂_C 13.9 (s, CH_3), 21.7 (d, $^2J_{PCC}$=3.1 Hz, CH_2), 22.5 (s, CH_2), 28.2 (d, $^1J_{PC}$=63.8 Hz, CH_2), 28.9 (s, CH_2), 29.0 (s, CH_2), 30.6 (d, $^3J_{PCC}$=13.6 Hz, CH_2), 31.7 (s, CH_2). LRMS (APCI+): *m/z* 275 (100%, $[M+H]^+$). HRMS (EI): *m/z* 297.2329 ($[M+Na]^+$); calculated for $C_{16}H_{35}ONaP$ 297.2323.

4.2.2 *tert*-Butyl-dimethylsilylprotected-10-bromodecanol 18

TBDMSi-Cl (2.700g, 18.0mmols, 1.2eqv) and imidazole (2.600g, 37.5mmols, 2.5eqv) were added to a solution of 10-bromo-1-decanol **17** (3.500g, 2.4mmols, 1eqv) in DMF (1.0ml, 2ml/g alcohol). The reaction mixture was stirred under an atmosphere of nitrogen at room temperature overnight. Thin layer chromatography analysis (20% ethyl acetate in hexane) indicated that the reaction was complete. The mixture was then poured into diethyl ether (25ml) and washed with 2 x 20ml of distilled water and 5 x 25ml of saturated sodium chloride solution. The organic phase was dried over anhydrous sodium sulphate, filtered and concentrated under reduced pressure to provide the crude product. The crude product was isolated as a golden oil (4.0659g, 77%) and used without further purification. IR (thin film, NaCl plate): ν_{max}/cm^{-1} 2929s (C-H aliphatic), 2855s (C-H aliphatic), 1463w/m (Si-CH_3), 1388w, 1360w, 1255m (CH_2-Br), 1099m (SiO-CH_2), 1006w, 909s, 836m, 776m, 735s, 672w . ^{1}H NMR (250 MHz, $CDCl_3$): ∂_H 0.01 (s, 6H), 0.84 (s, 9H), 1.20-1.60 (m, 14H), 1.80 (p, $^3J_{HCCH}$=7.1 Hz, 2H),

3.34 (t, $^{3}J_{HCCH}$=6.9 Hz, 2H), 3.55 (t, $^{3}J_{HCCH}$=6.5 Hz, 2H). ^{13}C NMR (62.5 MHz, $CDCl_3$, PENDANT: ∂_C -5.4 (CH_3), 18.2 (C), 25.7 (CH_2), 25.9 (CH_3), 28.1 (CH_2), 28.7 (CH_2), 29.3 (CH_2), 29.4 (CH_2), 29.7 (CH_2), 32.8 (CH_2), 33.7 (CH_2), 63.1 (CH_2). LRMS (APCI+): m/z 352 ($[M+H]^+$), 338 (100%), 337 ($[Br(CH_2)_{10}OSi(CH_3)_2C(CH_3)_2+H]^+$), 322 ($[Br(CH_2)_{10}OSi(CH_3)_2C(CH_3)+H]^+$), 295 ($[Br(CH_2)_{10}OSi(CH_3)_2+H]^+$), 272 ($[(CH_2)_{10}OSi(CH_3)_2C(CH_3)_3+H]^+$), 221 ($[Br(CH_2)_{10}+H]^+$), 207 ($[Br(CH_2)_9+H]^+$), 179 ($[Br(CH_2)_7+H]^+$), 158 ($[(CH_2)_7OSi(CH_3)+H]^+$), 157 ($[(CH_2)_{10}O+H]^+$), 115 ($[(CH_3)_3CSi(CH_3)_2+H]^+$), 113 ($[(CH_2)_8+H]^+$).

4.2.3 Dioctyl(decanol)phosphine oxide (DODPO) 16

A solution of DOPA **14** (0.800g, 2.9mmols, 1eqv) in THF (30ml) was added slowly to sodium hydride (0.17, 4.35mmols, 1.5eqv) in THF (20ml). The mixture was then stirred under nitrogen for 35 minutes at room temperature. A solution of TBDMSi-protected 10-bromo-1-decanol (0.100g, 0.36ml, 2.9mmols, 1eqv) in THF (10ml) was then added drop-wise over 20 minutes. The temperature was then raised to 70°C and the mixture refluxed for 26 hours. Thin layer chromatography analysis (50% ethyl acetate, 47.5% hexane and 2.5% methanol) suggested that the reaction had gone to completion. The THF was then removed under reduced pressure and the resultant brown solids re-dissolved in DCM (100ml) and extracted with distilled water (4 x 200ml) and saturated sodium chloride solution (2 x 150ml). The organic phase was then dried over anhydrous magnesium sulphate and concentrated under reduced pressure to give the product as a yellow oil (3.6237g, 95%). The crude product was not characterised at this stage and was used without further purification. The crude oil was dissolved in THF (100ml) and

placed under an atmosphere of nitrogen. A one molar solution of TBAF was added (15ml, 15.1mmols, 2.2eqv) and the mixture stirred at room temperature for 3.5 hours. The progress of the reaction was monitored by Thin layer chromatography analysis (85% ethyl acetate in hexane, v/v). The THF was removed under reduced pressure and the resulting oil was dissolved in diethyl ether (300ml). The organic phase was washed with distilled water (2 x 200ml), saturated ammonium chloride (2 x 100ml), saturated sodium chloride solution (2 x 200ml) and finally dried over anhydrous sodium sulfate. The organics were filtered and concentrated to a constant mass under reduced pressure, the crude product was isolated as a dark golden oil (3.0264g, 103%). Flash column chromatography (50% ethyl acetate, 45% hexane and 5% methanol v/v) gave the product as a golden oil (1.7538g, 59%, Rf=0.1). IR (thin film, NaCl plate) ν_{max}/cm^{-1} 3346w,b (-OH), 2924s (C-H aliphatic), 2853s (C-H aliphatic), 1465w (P-CH_2), 1408, 1378, 1148w/m (P=O), 1062. ^{1}H NMR (250 MHz, $CDCl_3$): ∂_H 0.78 (t, $^3J_{HCCH}$=6.5 Hz, 6H), 1.10-1.70 (m, 46H), 3.00 (s, broad, 1H), 3.47 (t, $^3J_{HCCH}$=6.6 Hz, 2H). ^{13}C NMR (62.5 MHz, $CDCl_3$, PENDANT): ∂_C 14.0 (s, CH_3), 21.5 (d, $^2J_{PCC}$=2.8 Hz, CH_2), 22.5 (s, CH_2), 25.7 (s, CH_2), 27.7 (d, $^1J_{PC}$=64.3 Hz, CH_2), 28.9 (s, CH_2), 29.2 (s, CH_2), 29.3 (s, CH_2), 29.4 (s, CH_2), 31.0 (d, $^3J_{PCC}$=13.8 Hz, CH_2), 31.7 (s, CH_2), 32.7 (s, CH_2), 62.5 (s, CH_2). LRMS (APCI+): *m/z* 431 (100%, $[M+H]^+$). HRMS (EI): *m/z* 453.3827 ($[M+Na]^+$); calculated for $C_{26}H_{55}O_2NaP$ 453.3837.

4.2.4 Dioctyl(octene)phosphine oxide (DOOPO) 6

Sodium hydride (60% in mineral oil 0.400g, 11mmols, 1.5eqv) was washed with hexane (2 x 20ml), suspended in THF (10ml) and placed under an atmosphere of nitrogen. A solution of DOPA **14** (2.000g, 7.3mmols, 1eqv) in THF (80ml) was slowly added and

the mixture stirred for 30 minutes at room temperature. A solution of 8-bromo-1-octene (1.3960g, 1.2ml, 7.3mmols, 1eqv) in THF (40ml) was then added drop-wise over 30 minutes. The temperature was then raised to 70°C and the mixture refluxed for 26 hours. Thin layer chromatography analysis (50% ethyl acetate, 47.5% hexane and 2.5% methanol v/v, Rf_{DOOPO}=0.5) suggested that the reaction had gone to completion. The THF was then removed under reduced pressure and the brown solids re-dissolved in DCM (200ml) and extracted with distilled water (4 x 200ml) and saturated sodium chloride solution (2 x 200ml). The organic phase was then dried over anhydrous sodium sulphate and concentrated under reduced pressure to give the crude product as an off white powdery solid (2.2515g, 83%). 0.500g was recrystallised from hexane to furnish a white powdery solid (0.1890g, 38%), Mp 27°C. IR (thin film, NaCl plate) ν max/cm-1 3074w (=C-H), 2926s (C-H aliphatic), 2854s (C-H), 2215m, 1839w, 1641w (=C-H), 1464m (P-CH2), 1410w, 1376w, 1224w, 1151m/s (P=O), 909s, 809w, 733s. ^{1}H NMR (250 MHz, CDCl3): ∂_H 0.83 (t, $^3J_{HCCH}$=6.4 Hz, 6H), 1.00-1.80 (m, 38H), 2.00 (m, (poor resolution), 2H), 4.95 (d, $^3J_{HCCH}$=17.1$_{trans}$ Hz, 1H), 4.89 (d, $^3J_{HCCH}$= 10.2$_{cis}$ Hz, 1H), 5.75 (ddt, $^3J_{HCCH}$=10.2$_{cis}$, 16.8$_{trans}$, 6.7 Hz, 1H). ^{13}C NMR (62.5 MHz, CDCl3, PENDANT): ∂ 14.0 (s, CH_3), 21.6 (d, $^2J_{PCC}$=poor resolution, CH_2), 22.5 (s, CH_2), 27.9 (d, $^1J_{PC}$= 64.3 Hz, CH_2), 28.5 (s, CH_2), 29.0 (s, CH_2), 30.8 (s, CH_2), 31.1 (d, $^3J_{PCCC}$=13.8 Hz, CH_2), 31.2 (s, CH_2), 32.6 (s, CH_2), 114.3 (s, CH_2), 138.8 (s, CH). LRMS (APCI+): *m/z* 385 (100%, [M+H]+). HRMS (EI): *m/z* 407.3427 ([M+Na]+); calculated for $C_{24}H_{49}ONaP$ 407.3427.

4.2.5 Dioctyl(undecene)phosphine oxide (DOUPO) 19

Sodium hydride (60% in mineral oil 0.8800g, 11mmols, 2.0eqv) was washed with hexane (2 x 15ml), suspended in THF (5ml) and placed under an atmosphere of nitrogen. A solution of DOPA **14** (3.000g, 11.0mmols, 1eqv) in THF (100ml) was slowly added and the mixture stirred for 35 minutes at room temperature. A solution of 11-bromo-1-undecene (1.3960g, 1.2ml, 7.3mmols, 1eqv) in THF (50ml) was then added drop-wise over 30 minutes. The temperature was then raised to 70°C and the mixture refluxed for 26 hours. Thin layer chromatography analysis (50% ethyl acetate, 47.5% hexane and 2.5% methanol v/v, Rf_{DOUPO}=0.1) suggested that the reaction had gone to completion. The THF was then removed under reduced pressure and the brown solids re-dissolved in DCM (300ml) and extracted with distilled water (2 x 200ml) saturated sodium chloride solution was added to break up the emulsion formed. Finally the organic layer was washed with saturated sodium chloride solution (2 x 200ml). The organic phase was then dried over anhydrous sodium sulphate and concentrated under reduced pressure to give the crude product as a golden oil (4.1330g, 88%). recrystallisation from hexane gave a golden waxy solid (3.5896, 87%). IR (thin film, NaCl plate) ν_{max}/cm^{-1} 3422w, 3075w (=C-H), 2924s (C-H aliphatic), 2853s (C-H), 1640w (=C-H), 1465m (P-CH_2), 1412w, 1377w, 1222w, 1156m (P=O), 993w, 908w, 908w, 722w. ^{1}H NMR (250 MHz, $CDCl_3$): ∂_H 0.82 (t, $^3J_{HCCH}$=6.5 Hz, 6H), 1.00-1.70 (m, 44H), 1.98 (dtt, $^3J_{HCCH}$= 6.7, 7.0 Hz, 2H), 4.95 (d, $^3J_{HCCH}$=16.9$_{trans}$ Hz, 1H), 4.89 (d, $^3J_{HCCH}$= 10.2$_{cis}$ Hz, 1H), 5.75 (ddt, $^3J_{HCCH}$=10.2$_{cis}$, 16.9$_{trans}$, 6.7 Hz, 1H). LRMS (APCI+): *m/z* 427 (100%, $[M+H]^+$).

4.2.6 Dioctyl(methylstyrene)phosphine oxide (DOMSPO) 7

Sodium hydride (60% in mineral oil 0.8400g, 21.0mmols, 1.5eqv) was washed with hexane (2 x 40ml), suspended in THF (20ml) and placed under an atmosphere of nitrogen. A solution of DOPA **14** (4.000g, 14.0mmols, 1eqv) in THF (70ml) was slowly added and the mixture stirred for 30 minutes at room temperature. A solution of chloromethylstyrene **10** (2.1400g, 1.97ml, 14.0mmols, 1eqv) in THF (30ml) was then added drop-wise over 30 minutes. The temperature was then raised to 70°C and the mixture refluxed for 26 hours. Thin layer chromatography analysis (50% ethyl acetate, 47.5% hexane and 2.5% methanol v/v, Rf_{DMSPA}=0.3) indicated that the reaction had gone to completion. The THF was then removed under reduced pressure and the brown solids re-dissolved in DCM (200ml) and extracted with distilled water (4 x 150ml) and saturated sodium chloride solution (2 x 150ml). The organic phase was then dried over anhydrous sodium sulphate and concentrated under reduced pressure to give the crude product as an orange oil (3.7318g, 68%). 0.500g was recrystallised from ice cold hexane to furnish a white powdery solid (0.1890g, 38%), Mp 57-58°C. IR (thin film, NaCl plate) ν_{max}/cm^{-1} 3090w (C-H aromatic), 3040 w (C-H vinyl), 2925s (C-H aliphatic), 2851s (C-H aliphatic), 1640w (=C-H), 1628w (C=C ring), 1510w, 1464m (P-CH_2), 1406w, 1376w, 1254w, 1171m/s (P=O), 1134m (1,4 disubstituted), 904w, 902w, 861w, 839w, 783w, 753w, 714w. ^{1}H NMR (250 MHz, $CDCl_3$): ∂_H 0.85 (sb, 6H), 1.00-1.70 (m, 28H), 3.07 (d, $^2J_{PCH}$= 14.8 Hz, 2H), 5.20 (d, $^3J_{HCCH}$=10.6_{cis} Hz, 1H), 5.70 (d, $^3J_{HCCH}$= 17.9_{trans} Hz, 1H), 6.66 (dd, $^3J_{HCCH}$= 10.9_{cis}, 16.7_{trans} Hz, 1H), 7.17 (d, $^3J_{HCCH}$= 6.7 Hz, 2H), 7.33 (d, $^3J_{HCCH}$=7.2 Hz, 2H). ^{13}C NMR (62.5 MHz, $CDCl_3$, PENDANT): ∂_C 14.0 (s, CH_3), 21.4 (d, $^2J_{PCC}$=3.7 Hz, CH_2), 22.5 (s, CH_2), 27.3 (d, $^1J_{PC}$=65.3 Hz, CH_2), 28.9 (s, CH_2), 29.0 (s, CH_2), 31.0 (d, $^3J_{PCCC}$=13.8 Hz, CH_2), 31.8 (s, CH_2), 36.0 (d, $^1J_{PC}$=58.8 Hz, CH_2), 113.6 (s, CH_2), 126.5 (s, poor resolution, CH), 129.5 (d, $^3J_{PCCC}$=4.6 Hz, CH),

131.9 (d, $^{5}J_{PCCCCC}$=6.4 Hz, C), 136.0 (s, poor resolution, C), 136.2 (s, CH). LRMS (APCI+): *m/z* 391 (100%, $[M+H]^+$), 291 ($[C_{17}H_{27}PO+H]^+$).

4.2.7 Dimethylstyrylphosphinous acid (DMSPA) 20

Magnesium turnings (1.400g, 59mmols, 3eqv) and a crystal of iodine were heated with a heat gun. Upon sublimation and subsequent condensation of the iodine, diethyl ether (30ml) was added and the mixture heated to reflux. Reflux was then maintained by the addition of a solution of distilled 1-chloromethyl-4-vinylbenzene **10** (9.000g, 8.30ml, 59.0mmols, 3eqv) in diethyl ether (40ml). The reaction mixture was then heated to 40°C and refluxed for 40 minutes to complete the formation of the Grignard reagent. The reaction mixture was then cooled to between 5-15°C and a solution of di-n-butylphosphite **13** (4.0740g, 4,1ml, 21.0mmols, 1eqv) in diethyl ether (40ml) added drop-wise over 2 hours. The reaction mixture was refluxed for 2 hours and monitored by thin layer chromatography (50% ethyl acetate, 47.5% hexane and 2.5% methanol v/v). The reaction mixture was then cooled to 5°C in an ice bath and acidified by slow drop-wise addition of an aqueous solution of 25% sulphuric acid. The mixture was then transferred to a separating funnel using diethyl ether (200ml) and distilled water (100ml). The aqueous layer was then removed and the organic layer washed with distilled water (3 x 100ml). The organic phase was then neutralised with an aqueous solution of 15% w/v k_2CO_3 (2 x 50ml) and extracted with distilled water (4 x 100ml) and finally with a saturated solution of sodium chloride (1 x 300ml). The organic phase was dried over anhydrous sodium sulphate, filtered and concentrated under reduced pressure to provide the crude product. The crude product was isolated as a yellow/green solid (5.4999g, 92%). The crude product was triturated in ice cold diethyl ether and

filtered to furnish the purified product as an off white solid (4.0806g, 69%) (TLC 2.5% MeOH and 45.5% ethyl acetate in hexane v/v, Rf_{DMSPA}=0.25). Mp >250°C. IR (KBr disk): ν_{max}/cm^{-1} 3077w (C-H aromatic), 3040w (C-H aromatic), 3010w (=C-H), 2989w (=C-H), 2933w (=C-H), 2368w, 2326w/m (P-H), 1736w, 1718w, 1627w (C=C), 1510m (C=C), 1406m (P-CH_2), 1364w ,1249w, 1194s (P=O), 1149m (1,4 disubstituted), 1110w, 991m, 942w/m, 906m, 856s, 790w, 705w, 673w. ^{1}H NMR (250 MHz, $CDCl_3$): ∂ 3.15 (dd, $^2J_{PCH}$=15.3, $^3J_{HPCH}$=3.0 Hz, 4H), 5.23 (d, $^3J_{HCCH}$=10.9$_{cis}$, 2H), 5.77 (d, $^3J_{HCCH}$= 17.6$_{trans}$ Hz, 2H) , 6.68 (dd, $^3J_{HCCH}$=10.9$_{cis}$, 17.6$_{trans}$ Hz, 2H), 6.92 (dp, $^1J_{PH}$=468.4, $^3J_{HCPH}$=3.3 Hz, 1H), 7.14 (dd, $^3J_{HCCH}$=8.0, J=2.0 Hz, 4H), 7.36 (d, $^3J_{HCCH}$=8.0 Hz, 4H). D_2O Shake ∂ 3.15 (dd, $^2J_{PCH}$=14.9, $^3J_{HPCH}$=split 3.0 Hz, 4H), 5.23 (d, $^3J_{HCCH}$=10.9$_{cis}$, 2H), 5.77 (d, $^3J_{HCCH}$= 17.6$_{trans}$ Hz, 2H) , 6.68 (dd, $^3J_{HCCH}$=10.9$_{cis}$, 17.6$_{trans}$ Hz, 2H), 6.92 (dp, $^1J_{PH}$=468.7, $^3J_{HCPH}$=3.1 Hz, 1H), 7.14 (dd, $^3J_{HCCH}$=8.0, J=2.0 Hz, 4H), 7.36 (d, $^3J_{HCCH}$=8.0 Hz, 4H). ^{13}C NMR (62.89 MHz, $CDCl_3$, PENDANT): ∂ 34.8 (d, $^1J_{PC}$=59.7 Hz, CH_2), 114.1 (s, CH_2), 126.8 (d, $^4J_{CCCC}$=2.8 Hz, CH), 129.7 (d, $^3J_{PCCC}$=6.4 Hz, CH), 130.1 ($^5J_{PCCCCC}$=7.4 Hz, C), 136.0 (s, CH), 136.6 (d, $^2J_{PCC}$=3.7 Hz, C). LRMS (APCI+): *m/z* 283 (100%, $[M+H]^+$), 117 ($[CH_2CHC_6H_4CH_2+H]^+$). HRMS (EI): *m/z* 305.1067 ($[M+Na]^+$); calculated for $C_{18}H_{19}ONaP$ 305.1067.

4.2.8 Dimethylstyryl(octane)phosphine oxide (DMSOPO) 21

Sodium hydride (60% in mineral oil 0.2100g, 5.3mmols, 1.5eqv) was suspended in THF (10ml) and placed under an atmosphere of nitrogen. A solution of DMSPA **20** (1.0000g, 3.5mmols, 1eqv) in THF (15ml) was slowly added and the mixture stirred for 30 minutes at room temperature. A solution of 1-bromooctane (0.6755g, 0.6ml, 3.5mmols, 1eqv) in THF (15ml) was then added drop-wise over 60 minutes. The mixture was then

stirred for 16 hours at room temperature. Thin layer chromatography analysis (50% ethyl acetate, 47.5% hexane and 2.5% methanol v/v) suggested that the reaction had gone to completion. The THF was then removed under reduced pressure and the brown solids re-dissolved in DCM (100ml) and extracted with distilled water (4 x 100ml) and saturated sodium chloride solution (2 x 100ml). The organic phase was then dried over anhydrous sodium sulphate and concentrated under reduced pressure to give the crude product as a brown wax (1.2604g, 91%). Flash column chromatography (50% ethyl acetate, 47.5% hexane and 2.5% methanol v/v, Rf_{DMSOPO}=0.2) gave a small amount of product as an off white solid (0.0850g, 8%). IR ν_{max}/cm^{-1} 3086w (C-H aromatic), 3050w (C-H aromatic), 2999w (=C-H), 2951m (=C-H), 2933w, 2921s (C-H aliphatic), 2850s (C-H aliphatic), 1627m (C=C ring), 1511m/s (C=C ring), 1667w (C=C ring), 1407m (P-CH_2), 1237m, 1178s (P=O), 1129m (1,4 disubstituted), 1100w, 989m, 908w/m, 859s, 786w, 765w, 722w. ^{1}H NMR (250 MHz, $CDCl_3$): ∂ 0.84 (t, $^3J_{HCCH}$=6.5 Hz , 3H), 1.10-1.70 (m, 14H), 3.04 (d, $^2J_{PCH}$=14.8 Hz, 4H), 5.21 (d, $^3J_{HCCH}$=10.9_{cis}, 2H), 5.70 (d, $^3J_{HCCH}$= 17.6_{trans} Hz, 2H), 6.66 (dd, $^3J_{HCCH}$=10.9_{cis}, 17.6_{trans} Hz, 2H), 7.14 (dd, $^3J_{HCCH}$=8.0, J=1.8 Hz, 4H), 7.33 (d, $^3J_{HCCH}$=8.0 Hz, 4H). ^{13}C NMR (75 MHz, $CDCl_3$, PENDANT): ∂ 14.0 (s, CH_3), 21.4 (d, $^2J_{PCC}$=3.7 Hz, CH_2), 22.5 (s, CH_2), 26.2 (d, $^1J_{PC}$=66.2 Hz, CH_2), 28.9 (s, CH_2), 29.0 (s, CH_2), 30.9 (d, $^3J_{PCCC}$=13.8 Hz, CH_2), 31.7 (s, CH_2), 35.7 (d, $^1J_{PC}$=58.8 Hz, CH_2), 113.8 (s, CH_2), 126.6 (d, $^4J_{PCCCC}$=1.8 Hz, CH), 129.7 ($^3J_{PCCC}$=4.6 Hz, CH), 131.5 (d, $^5J_{PCCCCC}$=7.4 Hz, C), 136.2 (s, CH), 136.3 (s, poor resolution, C). LRMS (APCI+): *m/z* 294 (100%, $[M+H]^+$).

4.2.9 Dimethylstyryl(decane)phosphine oxide (DMSDPO) 22

Sodium hydride (60% in mineral oil 0.6240g, 26mmols, 1.5eqv) was washed with hexane (2 x 20ml), suspended in THF (10ml) and placed under an atmosphere of nitrogen. A solution of DMSPA **20** (5.0000g, 17.7mmols, 1eqv) in THF (120ml) was slowly added and the mixture stirred for 30 minutes at room temperature. A solution of 10-bromodecane (3.7600g, 3.5ml, 17.7mmols, 1eqv) in THF (30ml) was then added drop-wise over 60 minutes. The mixture was then stirred for 4 hours at room temperature. Thin layer chromatography analysis (50% ethyl acetate, 47.5% hexane and 2.5% methanol v/v, Rf_{DMSDPO}=0.3) indicated that the reaction had gone to completion. The THF was then removed under reduced pressure and the brown solids re-dissolved in DCM (200ml) and extracted with distilled water (4 x 200ml) and saturated sodium chloride solution (2 x 200ml). The organic phase was then dried over anhydrous sodium sulphate and concentrated under reduced pressure to give the crude product as orange wax (7.0750.g, 99%). Trituration in diethyl ether followed by recrystallisation in a mixture of hexane and ethyl acetate gave the product as an off white solid. (3.4050g, 47%). Mp 87-88°C. IR ν_{max}/cm^{-1} 3083w, 3047w, 2998w, 2949m, 2919s, 2850m, 1627w, 1605w, 1511m, 1463w, 1409w, 1235w, 1173w, 1127s, 1102w, 1017w, 988m, 902w, 871w, 855w, 835w. ^{1}H NMR (250 MHz, $CDCl_3$): ∂_H 0.86 (t, $^3J_{HCCH}$=6.65 Hz, 3H), 1.10-1.60 (m, 18H), 3.05(dd, $^2J_{PCH}$=14.2 Hz, J=2.3 Hz, 2H), 5.22 (d, $^3J_{HCCH}$=10.9_{cis}, 2H), 5.71 (d, $^3J_{HCCH}$= 17.6_{trans} Hz, 2H), 6.67 (dd, $^3J_{HCCH}$=10.9_{cis}, 17.6_{trans} Hz, 2H), 7.19 (dd, $^3J_{HCCH}$=8.2, J=1.9 Hz, 4H), 7.34 (d, J=8.1 Hz, 4H). ^{13}C NMR (62.5 MHz, $CDCl_3$, PENDANT): ∂_C 14.1 (s, CH_3), 21.5 (d, $^2J_{PCC}$=4.6 Hz, CH_2), 22.6 (s, CH_2), 26.7 (d, $^1J_{PC}$=66.4 Hz, CH_2), 29.1-29.5 (m, poor resolution, CH_2), 30.8 (d, $^3J_{PCCC}$=poor resolution, CH_2), 31.8 (s, CH_2), 34.2 (d, $^1J_{PC}$=58.1 Hz, CH_2), 113.8 (s, CH_2), 126.6 (d, $^4J_{PCCCC}$=1.8 Hz, CH), 129.5 (s, C), 131.5 (d, $^3J_{PCCC}$=9.2Hz, CH) , 136.0 (s, poor

resolution, C) 136.2 (s, CH). LRMS (APCI+): *m/z* 423 (100%, $[M+H]^+$), 117 ($[CH_2CHC_6H_4CH_2+H]^+$). HRMS (EI): *m/z* 445.2636 ($[M+Na]^+$); calculated for $C_{28}H_{39}ONaP$ 445.2636

4.2.10 Diundecenephosphinous acid (DUPA) 24

Magnesium turnings (0.500g, 21.4mmols, 3eqv) and a crystal of iodine were heated with a heat gun. Upon sublimation and condensation of the iodine, diethyl ether (10ml) was added and the mixture heated to reflux. Reflux was then maintained by the addition of a solution of distilled 11-bromo-1-undecene (5.000g, 4.7ml, 21.4mmols, 3eqv) in diethyl ether (40ml). The reaction mixture was then heated to 40°C and refluxed for 30 minutes to complete the formation of the Grignard reagent. The reaction mixture was then cooled to between 5-15°C and a solution of di-n-butylphosphite **13** (1.3580g, 1.4ml, 7.0mmols, 1eqv) in diethyl ether (40ml) added drop-wise over 1 hours. The temperature was then raised to 40°C and the mixture refluxed for 26 hours. Analysis by thin layer chromatography (50% ethyl acetate, 47.5% hexane and 2.5% methanol v/v) indicated that the reaction was complete. The reaction mixture was then cooled to 5°C in an ice bath and acidified by slow drop-wise addition of an aqueous solution of 25% sulphuric acid. The mixture was then transferred to a separating funnel using diethyl ether (200ml) and distilled water (100ml). The aqueous layer was then removed and the organic layer washed with distilled water (100ml). The organic phase was then neutralised with an aqueous solution of 15% w/v k_2CO_3 (2 x 15ml) and extracted with distilled water (3 x 100ml) and finally with a saturated solution of sodium chloride (1 x 200ml). The organic phase was dried over anhydrous sodium sulphate, filtered and concentrated under reduced pressure to provide the crude product. The crude product

was isolated as a greasy white solid (2.6684g, 107%). The crude product was triturated in ice cold diethyl ether and filtered to furnish the purified product as a white powdery solid (1.3227g, 53%). Mp 65°C. IR (KBr disk): ν_{max}/cm^{-1} 3078w (C-H alkene), 2979w (C-H aliphatic), 2915s (C-H aliphatic), 2848s (C-H aliphatic), 2326w/m (P-H), 1642w (C=C), 1464m (P-CH_2), 1218w, 1160m/s (P=O), 990w, 913w/m, 767w, 720w. ^{1}H NMR (250 MHz, $CDCl_3$): ∂ 1.10-1.80 (m, 32H), 1.93 (dt, $^3J_{HCCH}$=6.9, 7.0 Hz, 4H), 4.87 (d, $^3J_{HCCH}$=10.1_{cis} Hz, 2H), 4.89 (d, $^3J_{HCCH}$=17.1_{trans} Hz, 2H), 5.70 (ddt, $^3J_{HCCH}$=10.2_{cis}, 16.8_{trans}, 6.7 Hz, 2H), 6.76 (d, $^1J_{PH}$=445.1 Hz, 1H). ^{13}C NMR (62.5 MHz, $CDCl_3$, PENDANT): ∂ 21.7 (d, poor resolution, CH_2), 28.2 (d, $^1J_{PC}$=64.0, CH_2), 28.8 (s, CH_2), 29.0 (s, CH_2), 29.1 (s, CH_2), 29.2 (s, CH_2), 29.3 (s, CH_2), 30.6 (d, $^3J_{PCCC}$=13.5 Hz, CH_2), 33.7 (s, CH_2), 114.1 (s, CH_2), 139.1 (s, CH). LRMS (APCI+): *m/z* 355 (100%, $[M+H]^+$), HRMS (EI): *m/z* 377.2945 ($[M+Na]^+$); calculated for $C_{22}H_{43}ONaP$ 377.2945.

4.2.11 Triundecenephosphine oxide (TUPO) 25

Sodium hydride (60% in mineral oil 1.3620g, 40.0mmols, 2.5eqv) was washed with hexane (2 x 30ml), suspended in THF (30ml) and placed under an atmosphere of nitrogen. A solution of DUPA **24** (5.4880g, 16.0mmols, 1eqv) in THF (100ml) was slowly added and the mixture stirred for 30 minutes at room temperature. A solution of 11-bromo-1-undecene (3.7300g, 3.5ml, 16.0mmols, 1eqv) in THF (30ml) was then added drop-wise over 60 minutes. The reaction was then heated to 70°C for 72 hours. Thin layer chromatography analysis (50% ethyl acetate, 47.5% hexane and 2.5% methanol, v/v) indicated that the reaction had gone to completion. The THF was then removed under reduced pressure and the brown solids re-dissolved in DCM (200ml) and extracted with distilled water (4 x 200ml) and saturated sodium chloride solution (2 x

200ml). The organic phase was then dried over anhydrous sodium sulphate and concentrated under reduced pressure to give the crude product as orange oil (7.0750g, 100%). Crystallisation in ice cold hexane produced white crystals. (4.2703g, 48%). Mp 31-32°C. IR (KBr disk): ν_{max}/cm^{-1} 3078w (C-H alkene), 2922s (C-H aliphatic), 2851s (C-H aliphatic), 1654w, 1640w (C=C), 1468m (P-CH_2), 1384w, 1152m/s (P=O), 993w, 910w/m, 812w, 760w, 720w. ^{1}H NMR (250 MHz, $CDCl_3$): ∂ 1.10-1.80 (m, 48H), 1.99 (dt, $^3J_{HCCH}$=6.7, poor resolution, Hz, 6H), 4.88 (d, $^3J_{HCCH}$=10.2$_{cis}$ Hz, 3H), 4.94 (d, $^3J_{HCCH}$=18.6$_{trans}$ Hz, 3H), 5.76 (ddt, $^3J_{HCCH}$=10.2$_{cis}$, 16.8$_{trans}$, 6.7 Hz, 3H). ^{13}C NMR (62.5 MHz, $CDCl_3$, PENDANT): ∂ 21.6 (d, $^2J_{PCC}$=3.7 Hz, CH_2), 27.9 (d, $^1J_{PC}$=64.3 Hz, CH_2), 28.8 (s, CH_2), 29.0 (s, CH_2), 29.1 (s, CH_2), 29.2 (s, CH_2), 29.3 (s, CH_2), 31.1 (d, $^3J_{PCCC}$=13.8 Hz, CH_2) , 33.7 (s, CH_2), 114.1 (s, CH_2), 139.1 (s, CH). ^{31}P NMR (121.5 MHz, $CDCl_3$, Referenced to 85% phosphoric acid) ∂ 48.8. LRMS (APCI+): *m/z* 507 (100%, $[M+H]^+$), HRMS (EI): *m/z* 529.4504 ($[M+Na]^+$); calculated for $C_{33}H_{63}ONaP$ 529.4504

4.2.12 Diundecene(decanolsilylether)phosphine oxide (DUDSPO) 26

Sodium hydride (60% in mineral oil 0.0790g, 3.3mmols, 1.5eqv) was washed with hexane (2 x 5ml), suspended in THF (5ml) and placed under an atmosphere of nitrogen. A solution of DUPA **24** (0.8000g, 2.2mmols, 1eqv) in THF (25ml) was slowly added and the mixture stirred for 10 minutes at room temperature. A solution of TBDMSi-protected-10-bromo-1-decanol **18** (0.7800g, 2.2mmols, 1eqv) in THF (15ml) was then added drop-wise over 20 minutes. The reaction was then heated to 70°C for 16 hours. Thin layer chromatography analysis (50% ethyl acetate, 47.5% hexane and 2.5% methanol v/v, Rf_{DUDSPO}=0.4) indicated that the reaction had gone to completion. The

THF was then removed under reduced pressure and the brown solids re-dissolved in DCM (200ml) and extracted with distilled water (4 x 100ml) and saturated sodium chloride solution (2 x 100ml). The organic phase was then dried over anhydrous sodium sulphate and concentrated under reduced pressure to furnish the crude product as an orange oil (1.3382g, 97%). The crude product was analysed and used with out further purification IR (thin film, NaCl plate): ν_{max}/cm^{-1}. 3076w (C-H alkene), 2925s (C-H aliphatic), 2853s (C-H aliphatic), 1640w (C=C), 1463m (P-CH_2) or (Si-CH_3), 1254w/m, 1154w/m (P=O), 1099m (SiO-CH_2), 992w, 908 w/m, 835m, 775w/m, 721w. ^{1}H NMR (250 MHz, $CDCl_3$): ∂_H 0.00 (s, 6H), 0.85 (s, 9H), 1.10-1.70 (m, 50H), 1.99 (dt, $^3J_{HCCH}$=6.5, 7.4 Hz , 4H), 3.55 (t, $^3J_{HCCH}$=6.5 Hz, 2H), 4.86 (d, $^3J_{HCCH}$=10.8_{cis} Hz, 2H), 4.96 (d, $^3J_{HCCH}$=17.1_{trans} Hz, 2H), 5.76 (ddt, $^3J_{HCCH}$=10.2_{cis}, 16.9_{trans}, 6.7 Hz, 2H). ^{13}C NMR (62.5 MHz, $CDCl_3$, PENDANT): ∂_C -5.3 (s, CH_3), 18.3 (s, C), 21.6 (d, $^2J_{PCC}$=3.7 Hz, CH_2), 25.7 (s, CH_2), 25.9 (s, CH_3), 27.9 (d, $^1J_{PC}$=62.2 Hz, CH_2), 28.8-29.7 (complex multiplet, signals overlap, 9 x CH_2), 31.1 (d, $^3J_{PCCC}$=13.8 Hz, CH_2), 32.8 (s, CH_2), 33.7 (s, CH_2), 63.2 (s, CH_2), 114.1 (s, CH_2), 139.1 (s, CH). LRMS (APCI+): *m/z* 626 (100%, $[M+H]^+$), 627.

4.2.13 Diundecenel(decanol)phosphine oxide (DUDPO) 27

DUDSPO **26** (2.7350g, 4.4mmol, 1eqv) was dissolved in THF (20ml) and placed under an atmosphere of nitrogen. A one molar solution of TBAF was added (9.7ml, 9.7mmols, 2.2eqv) and the mixture stirred at room temperature for 3 days. The progress of the reaction was monitored by Thin layer chromatography analysis (75% ethyl acetate in hexane, v/v, Rf_{DUDPO}=0.1). The THF was removed under reduced pressure and the resulting brown oil was dissolved in diethyl ether (100ml). The organic phase was

washed with distilled water (2 x 100ml), saturated ammonium chloride (2 x 100ml), saturated sodium chloride solution (2 x 100ml) and finally dried over anhydrous sodium sulfate. The organics were filtered and concentrated to a constant mass under reduced pressure, the crude product was isolated as a dark golden oil (1.9440g, 87%). The crude oil was dissolved in ice cold hexane and transferred to the freezer. Golden crystals formed that were cold filtered to furnish a golden oil at room temperature (0.2601, 12%). The yield of pure material can be increased by further cooling and filtering. IR (thin film, NaCl plate) ν_{max}/cm^{-1} 3347w,b (-OH), 3078w (=C-H), 2925s (C-H), 2854s (C-H), 1640w (C=C), 1465w (P-CH_2), 1408w, 1153w (P=O), 1058w, 991w, 909w. ^1H NMR (250 MHz, $CDCl_3$): ∂_H 1.10-1.70 (m, 50H), 2.00 (dt, $^3J_{HCCH}$=6.7, 7.5 Hz, 4H), 2.20 (s, broad, 1H), 3.59 (t, $^3J_{HCCH}$=6.6 Hz, 2H), 4.82 (d, $^3J_{HCCH}$=10.9cis Hz, 2H), 4.88 (d, 17.0_{trans} Hz, 4H), 5.77 (ddt, $^3J_{HCCH}$= 10.3_{cis}, 17.0_{trans}, 6.7 Hz, 2H). ^{13}C NMR (62.5 MHz, $CDCl_3$, PENDANT): ∂_C 21.6 (d, poor resolution, CH_2), 25.7 (s, CH_2), 27.7 (d, $^1J_{PC}$= 64.3 Hz, CH_2), 28.8-29.8 (multiplet from signals overlap, CH_2), 31.1 (d, $^3J_{PCCC}$=13.8 Hz, CH_2), 32.7 (s, CH_2), 33.9 (s, CH_2), 62.9 (s, CH_2), 114.1 (s, CH_2), 139.1 (s, CH). LRMS (APCI+): *m/z* 511 (100%, $[M+H]^+$). HRMS (EI): *m/z* 533.4473 ($[M+Na]^+$); calculated for $C_{32}H_{63}O2NaP$ 533.4473

4.3 Synthesis of phosphosulfinous acids and phosphine sulfides

4.3.1 Preparation of polymer supported thionating reagent (PS-TR) 30[143]

N-(2-aminomethyl)aminomethyl polystyrene resin (3.100g, 9.3mmols, 1eqv) and pyridine (45ml) were placed under an atmosphere of nitrogen and cooled to 0°C in an

ice bath. Ethyldichlorothiophosphate (5.800g, 4.3ml, 32mmols, 3.5eqv) was added drop-wise and the temperature and kept at 0°C during the addition. The mixture was then allowed to warm to room temperature and stirred gently over night. The resin was then transferred to a sintered funnel and washed with DCM (5 x 100ml) and diethyl diethyl ether (5 x 100ml). The resin was then dried to a constant mass under reduced pressure to give a bright orange solid (4.0704g, 99.6%). IR (KBr disk): ν_{max}/cm^{-1} 3447s/b, 3024w, 2962w, 2925w, 2863w, 2361s, 2340m, 1654m, 1635m, 1618m, 1560m, 1542w, 1508m, 1458m, 1262w, 1097w, 1054w, 1022w, 802w, 669m.

4.3.2 Trioctylphosphine sulphide (TOPS) 28

Polymer supported thionating reagent **30** (3.000g, 9.0mmols, 5eqv) was suspended in toluene (10ml) and placed under an atmosphere of nitrogen. A solution of TOPO **1** (0.700g, 1.8mmols, 1eqv) in toluene (5ml) was added and the mixture stirred slowly. The temperature was raised to 90°C for 48 hours, analysis of the reaction mixture by thin layer chromatography indicated that some starting material remained. A further three equivalents of polymer supported thionating reagent **30** (1.800g, 5.4mmols) was added and the mixture again heated to 90°C for 24 hours. Analysis by thin layer chromatography indicated that the reaction was complete (50% ethyl acetate, 2.5% MeOH in hexane v/v, Rf_{TUPS}=0.9). The mixture was allowed to cool before being tipped onto a pad of silica. The silica was then washed through with DCM (50ml). The combined organic washings were dried over anhydrous sodium sulphate, filtered and concentrated under reduced pressure to produce a cloudy sticky oil (0.6208g, 86%). IR (KBr Thin film): ν_{max}/cm^{-1} 2958s, 2925s (C-H), 2855m (C-H), 1465m (P-CH_2), 1408w, 1378w, 1302w, 1219w, 1193w, 1114w, 1031w, 909s, 847w, 798w, 734s (P=S). ^1H

NMR (250 MHz, $CDCl_3$): ∂_H 0.81 (t, $^3J_{HCCH}$=6.4 Hz, 9H), 1.1-1.8 (bm, 42H). ^{13}C NMR (62.5 MHz, $CDCl_3$, PENDANT): ∂_C 13.9 (s, CH_3), 22.3 (d $^2J_{PCC}$=3.7 Hz, CH_2), 22.5 (s, CH_2), 29.0 (s, CH_2), 30.7 (d, $^1J_{PC}$=49.6, CH_2), 30.7 (d, $^3J_{PCCC}$=14.7 Hz, CH_2), 31.7 (s, CH_2). LRMS (APCI+): *m/z* 403 (100%, $[M+H]^+$).

4.3.3 Diundecylphophosulfinous acid (DUPSA) 33

Polymer supported thionating reagent **30** (3.600g, 12.6mmols, 3eqv) was suspended in toluene (10ml) and placed under an atmosphere of nitrogen. A solution of DUPO **24** (1.300g, 3.6mmols, 1eqv) in toluene (10ml) was added and the mixture stirred slowly. The temperature was raised to 90°C for 16 hours, analysis of the reaction mixture by thin layer chromatography indicated that some starting material remained. Another one equivalent of polymer supported thionating reagent **30** (1.200g, 3.6 mmols) was added and the mixture again heated to 90°C for 16 hours. Analysis by thin layer chromatography indicated that the reaction was complete (50% ethyl acetate, 2.5% MeOH in hexane, v/v Rf_{DUPSA}=0.7). The mixture was allowed to cool before being tipped onto a pad of silica. The silica was then washed through with DCM (100ml). The combined organic washings were dried over anhydrous sodium sulphate, filtered and concentrated under reduced pressure to produce a clear sticky oil (1.2243g, 91%). IR (KBr Thin film): ν_{max}/cm^{-1} 3076w (=C-H), 2922w (C-H), 2852s (C-H), 2285w (P-H), 1821w, 1640m (C=C), 1465m (P-CH_2), 1413w, 1368w, 1156w, 992m, 909s, 735s (P=S)m. ^1H NMR (250 MHz, $CDCl_3$): ∂_H 1.10-2.2 (bm, 36H), 4.90 (d, $^3J_{HCCH}$=10.2_{cis} Hz, 2H), 4.96 (dd, $^3J_{HCCH}$=17.1_{trans} Hz, 2H), 5.78 (ddt, $^3J_{HCCH}$=10.2_{cis}, 16.9_{trans}, 6.7 Hz, 2H), 6.51 (d, $^1J_{PH}$=433.2 Hz, 1H). ^{13}C NMR (62.5 MHz, $CDCl_3$, PENDANT): ∂_H 22.3 (d, poor resolution, CH_2), 29.2 (d, $^1J_{PC}$=47.8 Hz, CH_2), 29.1-29.5 (multiplet from signal

overlap, CH_2), 30.7 (d, poor resolution, CH_2), 33.8 (s, CH_2), 114.1 (s, CH_2), 139.1 (s, CH). LRMS (APCI+): *m/z* 371 ($[M+H]^+$), 370 (100%), 355, 151

4.3.4 Dimethylstyrylphosphosulfinous acid (DMSPSA) 34

Lawesson's Reagent **29** (1.4000g, 3.6mmols, 0.5eqv) was suspended in toluene (150ml) and placed under nitrogen. A solution of DMSPA **20** (2.000g, 7.1mmols, 1eqv) was added and the temperature was raised to 115°C for 1.5 hours. Analysis by thin layer chromatography (50% ethyl acetate, 47.5% hexane and 2.5% methanol, v/v Rf_{DMSPSA}=0.7) suggested that the reaction had gone to completion. The reaction was quenched by the addition of distilled water (50ml) and stirred for 30 minutes. The reaction mixture was then transferred to a separating funnel, a further 150ml of distilled water was added and the aqueous extracted with DCM (2 x 200ml). The combined organics were dried over anhydrous sodium sulphate, filtered and concentrated under reduced pressure to give the crude product as a yellow and white solid (1.4000g, 70%). The solid was then dissolved in a mixture of DCM and acetone and filtered through a pad of silica. The solvent was again removed under reduced pressure and the resulting solid triturated in ice cold diethyl ether to furnish the product as lustrous white crystals (0.6200g, 31%). Mpt > 250°C. IR (KBr disk) ν_{max}/cm^{-1} 3081w (C-H), 3049w (C-H), 2951w (C-H), 2360m (P-H), 1624w (C=C), 1509w, 1405(P-CH_2)m, 1150w, 1110m, 995, 944m/s, 908m, 854s, 834w, 774w, 712w (P=S). ^{1}H NMR (250 MHz, $CDCl_3$): ∂_H 3.29 (dd, $^2J_{PCH}$=14.3, $^3J_{HCPH}$= 4.3 Hz, 4H), 5.25 (d, $^3J_{HCCH}$=10.9$_{cis}$, 2H), 5.73 (d, $^3J_{HCCH}$= 17.6$_{trans}$ Hz, 2H), 6.62 (dp, $^1J_{PH}$=451.2, $^3J_{HCPH}$=4.2 Hz, 1H), 6.68 (dd, $^3J_{HCCH}$=10.9$_{cis}$, 17.6$_{trans}$ Hz, 2H), 7.16 (dd, $^3J_{HCCH}$=8.0, *J*=2.0 Hz, 4H), 7.36 (d, $^3J_{HCCH}$=8.0 Hz, 4H). ^{13}C NMR (62.5 MHz, $CDCl_3$, PENDANT): ∂_H 37.6 (d, $^1J_{PC}$=45.5 Hz, CH_2), 115.0 (s, CH_2),

126.8 (d, $^4J_{CCCC}$=3.7 Hz, CH), 129.7 (s, CH), 130.7 (d, but not well resolved, C), 136.1 (s, CH), 137.0 (s, C). LRMS (APCI+): m/z 298 (100%, $[M-H]^+$),117 ($[CH_2CHC_6H_4CH_2+H]^+$). HRMS (EI): m/z 299.1023 ($[M+Na]^+$); calculated for $C_{18}H_{20}ONaP$ 299.1023.

4.4 Investigation of HDA Coated NanoDots™

4.4.1 ^{1}H NMR spectroscopy analysis of NanoDots™

4.4.1i NanoDots™-NLP121

NLP121 (10mg) was dissolved in $CDCl_3$ (~1ml) and analysed by ^{1}H NMR spectroscopy. ^{1}H NMR (200 MHz, $CDCl_3$): ∂ 0.86 (bs, 3H), 1.00-1.70 (m, 30H). PL max = 577nm (Appendix D, **Figure 102**)

4.4.1ii NanoDots™-SD396

SD396 (10mg) were dissolved in $CDCl_3$ (~1ml) and analysed by ^{1}H NMR spectroscopy. ^{1}H NMR (200 MHz, $CDCl_3$): ∂ 0.87 (bs, 3H), 1.00-1.70 (m, 30H). PL max = 504nm (Appendix D, **Figure 103**)

4.4.1iii NanoDots™-MC610

MC610 (10mg) was dissolved in $CDCl_3$ (~1ml) and analysed by DOSY ^{1}H NMR spectroscopy. ^{1}H NMR (400 MHz, $CDCl_3$, DOSY): ∂ 0.80 (t, $^3J_{HCCH}$=6.8Hz, D=3.2-5.2 x $10^{-10}m^2s^{-1}$,3H), 1.00-1.80 (m, D=3.2-5.8 x $10^{-10}m^2s^{-1}$, 30). PL max = 560nm (Appendix D, **Figure 104**)

4.4.1iv NanoDots™-MC556

MC556 (10mg) was dissolved in $CDCl_3$ (~1ml) and analysed by DOSY ^1H NMR spectroscopy. ^1H NMR (400 MHz, $CDCl_3$, DOSY): ∂ 0.89 (bm, D=2.0-3.4 x $10^{-10}m^2s^{-1}$,3H), 1.00-1.80 (m, D=1.7-2.9 & 4.2-5.2 x $10^{-10}m^2s^{-1}$, 30H). PL max = 617nm (Appendix D, **Figure 105**)

4.4.2 Combustion analysis of none washed and washed NanoDots™

HDA capped NanoDots™ -NLP121 (10mg) were placed into a centrifuge tube, DCM (2ml) and MeOH were added and the tube shaken. The NanoDots™ were precipitated with centrifugation, the supernatant discarded and the pellet was washed with MeOH (10ml) added. The pellet was precipitated with centrifugation and the supernatant decanted off, the pellet was dried to a constant mass. The washed NanoDots™ and a sample of none washed NanoDots™ were analysed by combustion analysis.

Combustion analysis: Non-washed 25.51% C, 4.33% H, 1.29% N and 68.50% Cd.

Washed 19.75% C, 3.20% H, 0.75% N and 67.35% Cd.

To quantify the amount of HDA that can be removed by washing and precipitation with methanol the molar ratio of N to Cd for both non-washed and washed samples was calculated.

Non-washed sample

68.50% of the total sample was Cd, therefore in 100g there would be 68.50g of Cd.

The number of moles in 68.50g of Cd

= 68.50/112.4 = 0.61 moles of Cd

1.29% of the total sample was N, therefore in 100g there would be 1.29g of N.

The number of moles in 1.29g of N

= 1.29/14.0 = 0.09 moles of N

Therefore the molar ratio of N to Cd is 0.09 to 0.61

For every one mole of Cd there is 0.15 moles of N in the sample of non-washed NanoDots™

Washed sample

67.35% of the total sample was Cd, therefore in 100g there would be 67.35g of Cd.

The number of moles in 67.35g of Cd

= 67.35/112.4 = 0.60 moles of Cd

0.75% of the total sample was N, therefore in 100g there would be 0.75g of N.

The number of moles in 0.75g of N

= 0.75/14.0 = 0.05 moles of N

Therefore the molar ratio of N to Cd is 0.05 to 0.60

For every one mole of Cd there is 0.08 moles of N in the sample of washed NanoDots™

Comparing the number of moles of N per 1 mole Cd in the washed and non-washed batches a percentage of the N containing ligand removed by washing with methanol can be calculated.

(0.08/0.15) x 100 = 53.3

Therefore 53% of the nitrogen containing ligand was removed by the washing procedure.

4.4.3 Stability of NanoDots™- MC610 on exposure to acid

The stability of HDA coated NanoDots™ to pH 1.5 hydrochloric acid was evaluated by comparing the PL spectrum of a solution of NanoDots™ before the addition of acid with the PL spectra of those after exposure to acid. A stock solution of NanoDots™ MC610 (10mg) in THF (8.0ml) was prepared and the mixture shaken for 10 minutes to ensure complete dissolution. The PL spectrum of 2ml of the NanoDot™ solution was recorded. A series of dilutions with decreasing amounts of acid to NanoDot solution were prepared. Each dilution in **Table 13** was prepared with a total volume of 2ml and shaken for 10 seconds before the PL of the solution recorded in quadruplet.

Ratio of pH 1.5 HCl to NanoDot solution	Volume pH 1.5 HCl (μl)	Volume NanoDot™ (μl)
3:1	1500	500
2:1	1333	667
1:1	1000	1000
1:2	667	1333
1:4	400	1600
1:8	222	1778
1.9	200	1800
1:10	182	1818
1:20	95	1905
1:30	65	1935
0:1	0	2000

Table 13: Serial dilution of NanoDot™ stock solution with pH 1.5 HCl aq

Table 14 provides the PL maximum emission of the solutions of NanoDots™ after exposure to strong acid. The actual spectra can be viewed in (Appendix D, **Figure 66**)

Ratio of acid to NanoDot™ solution	Mean intensity of the photoluminescence of the solutions at PL max (nm)
3:1	170.75
2:1	171.25
1:1	181.25
1:2	203.00
1:4	233.50
1:8	254.00
1.9	305.50
1:10	408.25
1:20	795.50
1:30	1177.00
0:1	1136.50

Table 14: PL maximum emission of the NanoDot™ solutions after exposure to pH1.5 HCl aq

4.4.4 Stability of NanoDots ™ to AIBN

Four samples of NLP121 (0.0100g) were dissolved in toluene (10ml), transferred to a carousel tubes labelled **A-D** and stirred for 10 minutes under nitrogen. AIBN was then added to tubes labelled **B-D**, (0.0001g, 0.0002g and 0.0004g respectively). No AIBN was added to tube **A**. The temperature was then raised to 72°C and the tubes stirred for four hours before the photoluminescence of each tube was evaluated. (Appendix A, **Figure 68**)

4.4.5 Stability of NanoDots™-MC610 upon exposure to a range of reagents

The stability of HDA 3 coated NanoDots™ (MC610) to a variety of different reagents was evaluated by comparing the PL spectra of a solution of NanoDots™ (MC610) before the addition of any reagent with the PL spectra recorded after exposure to the reagent. A stock solution of NanoDots™ MC610 (10mg) in THF (8.0ml) was prepared and the mixture shaken for 10 minutes to ensure complete dissolution. The PL spectra of 1ml of the NanoDot™ (MC610) solution was recorded for comparison with the PL spectra of the NanoDots ™ (MC610) after addition of the reagent. Solutions of THF (10ml) containing 0.00025 moles of each reagent were prepared according to **Table 12**. 0.5ml of the reagent solution was added to 0.5ml of the NanoDot™ solution, the mixture was shaken and the PL spectra run immediately.

Reagent	Amount (g)	Amount (ml)
Trifluroacetic acid (TFA)	0.0285	0.019
Aluminium trichloride (AlCl3)	0.0325	-
1,8-Diazabicyclo[5.4.0]undec-7-ene (DBU)	0.0380	0.037
Potassium hydroxide (KOH)	0.0140	
Iodobenzoic acid (IBX)	0.0700	
Potassium permanganate (KMnO4)	0.0390	
Lithium aluminium hydride (LiAlH4)*	-	0.250
n-Butyl lithium (nBuLi)*	-	0.250
Vinyl magnesium bromide (Vinyl MgBr)*	-	0.025
Hydrogen Bromide (HBr)	-	0.040

* 1M in THF

Table 12: Amounts of each reagent used to prepare stock solutions in THF for the investigation into stability

Table 15 provides the PL maximum emissions of the solutions of NanoDots™ after exposure to the reagents listed above. The actual spectra can be viewed in (appendix D, **Figure 69**)

Reagent	PL maximum emission after addition of reagent (nm)
No Reagent	875.50
Trifluroacetic acid (TFA)	74.75
Aluminium trichloride (AlCl3)	33.25
1,8-Diazabicyclo[5.4.0]undec-7-ene (DBU)	1007.75
Potassium hydroxide (KOH)	1211.5
Iodobenzoic acid (IBX)	298.00
Potassium permanganate (KMnO4)	369.00
Lithium aluminium hydride (LiAlH4)*	20.50
n-Butyl lithium (nBuLi)*	16.50
Vinyl magnesium bromide (Vinyl MgBr)*	44.50
Hydrogen Bromide (HBr)	409.25

Table 15: PL maximum emission remaining after exposure to each reagent

4.4.6 Stability of NanoDots™-MC556 upon exposure to a range of reagents

The stability of HDA coated NanoDots ™ (MC556) to a variety of different reagents was evaluated by comparing the PL spectra of a solution of NanoDots ™ (MC556) before the addition of any reagent with the PL spectra recorded after exposure to the reagent. A stock solution of NanoDots™ (MC556) (10mg) in THF (8.0ml) was prepared and the mixture shaken for 10 minutes to ensure complete dissolution. The PL spectra of 1ml of the NanoDot™ (MC556) solution was recorded for comparison with the PL spectra of the NanoDots ™ after addition of the reagent. Solutions of THF (10ml) containing 0.00025 moles of each reagent were prepared according to the **Table 12**. 0.5ml of the reagent solution was added to 0.5ml of the NanoDot™ (MC556) solution, the mixture was shaken and the PL spectra run immediately.

Table 16 provides the PL maximum emission of the solutions of NanoDots™ after exposure to the reagents listed above. The actual spectra can be viewed in (Appendix D, **Figure 70**)

Reagent	PL maximum emission after addition of reagent (nm)
No Reagent	875.50
Trifluroacetic acid (TFA)	74.75
Aluminium trichloride (AlCl3)	33.25
1,8-Diazabicyclo[5.4.0]undec-7-ene (DBU)	1007.75
Potassium hydroxide (KOH)	1211.5
Iodobenzoic acid (IBX)	298.00
Potassium permanganate (KMnO4)	369.00
Lithium aluminium hydride (LiAlH4)*	20.50
n-Butyl lithium (nBuLi)*	16.50
Vinyl magnesium bromide (Vinyl MgBr)*	44.50
Hydrogen Bromide (HBr)	409.25

Table 16: PL maximum emission remaining after exposure to each reagent

4.5 – Ligand Displacement

4.5.1 Displacement of HDA coated NanoDot™ with DMSPA 20

NanoDots™ – OMN44 (0.0100g, 1eqv w/w) were dissolved in DCM (2ml) and stirred under nitrogen. DMSPA **20** (0.2000g, 0.71mmols, 20eqv w/w) was added and the mixture stirred for 72 hours. The clear bright orange solution was then was then transferred to a centrifuge tube containing acetone (10ml) and shaken vigorously to begin the precipitation of the NanoDots™ from solution. The resulting cloudy solution was then centrifuged at 13000rpm for 15 minutes to provide an orange pellet at the bottom of a clear solution. The supernatant was decanted off the pellet and the excess ligand recovered. The pellet was then dissolved in DCM (2ml) and transferred to a RBF, the solvent was removed under reduced pressure and the product dried to a constant mass (12 hours under vacuum). The exchanged NanoDots™ appeared as an orange solid (0.0109g, 109%). IR (KBr disk): ν_{max}/cm^{-1} 3422w/b ($-NH_2$), 3220w/b ($-NH_2$), 2919s, 2848s, 1575m, 1509w, 1461m, 1408w, 1373w, 1116m (P=O), 1080m, 1022m, 898w, 849w, 736m, 690m. ^1H NMR (250 MHz, $CDCl_3$): ∂ 0.83 (bs, $3H_{3H\ HDA}$), 1.23 (m, $30H_{30H\ HDA}$), 3.16 (dd, $4H_{4H\ DMSPA}$), 5.25 (d, $2H_{2H\ DMSPA}$), 5.73 (d, $2H_{2H\ DMSPA}$), 6.68 (dd, $2H_{2H\ DMSPA}$), 6.94 (d, $1H_{1H\ DMSPA}$), 7.15 (d, $4H_{4H\ DMSPA}$), 7.37 (d, $4H_{4H\ DMSPA}$). Displacement ratio 86% DMSPA **20** : 14% HDA **3**.

4.5.2 Displacement of HDA coated NanoDot™ with DUPA 24

NanoDots™ –MNO43 (0.0500g, 1eqv w/w) were dissolved in DCM (5ml) and stirred under nitrogen. DUPA **24** (0.5000g, 1.4mmols, 10eqv w/w) was added and the mixture stirred for 24 hours. The clear bright orange solution was then was then transferred to a

centrifuge tube containing methanol (5ml) and shaken vigorously to begin the precipitation of the NanoDots™ from solution. The resulting cloudy solution was then centrifuged at 13000rpm for 5 minutes to provide an orange pellet at the bottom of a clear solution. The supernatant was decanted off the pellet and the excess ligand recovered. The pellet was then dissolved in DCM (2ml) and transferred to a RBF, the solvent was removed under reduced pressure and the product dried to a constant mass (12 hours under vacuum). The exchanged NanoDots™ appeared as an orange solid (0.0441g, 88%). IR (KBr disk): ν_{max}/cm^{-1} 3400w/b, 3244w/b, 3060w, 2922s, 2851s, 1638w, 1617w, 1577m, 1508w, 1466m, 1435w, 1364w, 111m/s, 1080w/s, 1058m/s, 1024m/s, 908m, 801w, 737w, 689w. ^{1}H NMR (250 MHz, $CDCl_3$): ∂ 0.86 (t, $3H_{3H\ HDA}$), 1.10-2.10 (m, $66H_{30H\ HDA\ \&\ 36H\ DUPA}$), 4.93 (dd, $4H_{4H\ DUPA}$), 5.79 (ddt, $2H_{2H\ DUPA}$). Displacement ratio 33% DUPA **24** : 67% HDA **3**.

4.5.3 Displacement of HDA coated NanoDot™ with DMSDPO 22

NanoDots™ – SD395 (0.0200g, 1eqv w/w) were dissolved in DCM (4ml) and stirred under nitrogen. DMSDPO **22** (0.4000g, 0.95mmols, 20eqv w/w) was added and the mixture shaken for 72 hours. The clear bright yellow solution was then was then transferred to a centrifuge tube containing a mixture of methanol and ethanol (4ml, 50:50) and shaken vigorously to begin the precipitation of the NanoDots™ from solution. The resulting cloudy solution was then centrifuged at 13000rpm for 5 minutes to provide a yellow pellet at the bottom of a clear solution. The supernatant was decanted off the pellet and the excess ligand recovered. The pellet was then dissolved in DCM (2ml) and transferred to a RBF, the solvent was removed under reduced pressure and the product dried to a constant mass (12 hours under vacuum). The exchanged

NanoDots™ appeared as an yellow solid (0.0273g, 136%). ^{1}H NMR (250 MHz, $CDCl_3$): ∂_H 0.86 (t, $6H_{3H\ HDA\ \&\ 3H\ DMSDPO}$), 1.00-1.80 (m, $48H_{30H\ HDA\ \&\ 18H\ DMSDPO}$), 3.04 (dd, $4H_{4H\ DMSDPO}$), 5.22 (d, $2H_{2H\ DMSDPO}$), 5.72 (d, $2H_{2H\ DMSDPO}$), 6.67 (dd, $2H_{2H\ DMSDPO}$), 7.18 (dd, $4H_{4H\ DMSDPO}$), 7.35 (d, $4H_{4H\ DMSDPO}$). Displacement ratio 56% DMSDPO **22** : 48% HDA **3**

4.5.4 Displacement of HDA coated NanoDot™ with DODPO 16

NanoDots™ – OMN29 (0.200g, 1eqv w/w) were dissolved in DCM (6ml) and stirred under nitrogen. DODPO **16** (1.3000g, 3.02mmols, 6.5eqv w/w) was added and the mixture stirred for 16 hours. The clear bright orange solution was then was then transferred to a centrifuge tube containing methanol (10ml) and shaken vigorously to begin the precipitation of the NanoDots™ from solution. The resulting cloudy solution was then centrifuged at 13000rpm for 5 minutes to provide an orange pellet at the bottom of a clear solution. The supernatant was decanted off the pellet and the excess ligand recovered. The pellet was then dissolved in DCM (2ml) and transferred to a sample vial, the solvent was removed under reduced pressure and the product dried to a constant mass (12 hours under vacuum). The exchanged NanoDots™ appeared as an orange solid (0.1796g, 90%). IR (thin film): ν_{max}/cm^{-1} 3250w/b, 2922s, 2852s, 1576w, 1466w, 1435w, 1080m, 1024m. ^{1}H NMR (250 MHz, $CDCl_3$): ∂_H 0.83 (m/b, $9H_{3H\ HDA\ \&\ 6H\ DODPO}$), 1.00-1.70 (m, $62H_{30H\ HDA\ \&\ 32H\ DODPO}$), 3.60 (bs, $2H_{2H\ DODPO}$). Displacement ratio 60% DODPO **16** : 40% HDA **3**

4.5.5 Displacement of HDA coated NanoDot™ with DOOPO 6

NanoDots™ – OMN29 (0.0200g, 1eqv w/w) were dissolved in DCM (2ml) and stirred under nitrogen. DOOPO **6** (0.2000g, 0.52mmols, 10eqv w/w) was added and the

mixture shaken for 16 hours. The clear bright orange solution was then was then transferred to a centrifuge tube containing methanol (4ml) and shaken vigorously to begin the precipitation of the NanoDots™ from solution. The resulting cloudy solution was then centrifuged at 13000rpm for 5 minutes to provide an orange pellet at the bottom of a clear solution. The supernatant was decanted off the pellet and the excess ligand recovered. The pellet was then dissolved in DCM (2ml) and transferred to a sample vial, the solvent was removed under reduced pressure and the product dried to a constant mass (12 hours under vacuum). The exchanged NanoDots™ appeared as an orange solid (0.1796g, 90%). IR (KBr disk): ν_{max}/cm^{-1} 3424w/b (-NH_2), 3246w/b (-NH_2), 2424w/b, 3246w/b, 2951m, 2918s, 2849s, 1575m, 1558w, 1469m, 1456w, 1434w, 1125w (P=O), 1083w, 1022w, 736w, 720w, 687w. ^{1}H NMR (250 MHz, $CDCl_3$): ∂_H 0.86 (t, $9H_{3H\ HDA\ \&\ 6H\ DOOPO}$), 1.00-2.10 (m, $70H_{30H\ HDA\ \&\ 40H\ DOOPO}$), 4.94 (dd, $2H_{2H\ DOOPO}$), 5.76 (m, $1H_{1H\ DOOPO}$). Displacement ratio 11% DOOPO **6** : 89% HDA **3**

4.5.6 Displacement of HDA coated NanoDot™ with DUDSPO 26

NanoDots™ – OMN44 (0.0200g, 1eqv w/w) were dissolved in DCM (2ml) and stirred under nitrogen. DUDSPO **26** (0.2000g, 0.32mmols, 10eqv w/w) was added and the mixture stirred for 24 hours. The clear bright orange solution was then was then transferred to a centrifuge tube containing methanol (2ml) and shaken vigorously to begin the precipitation of the NanoDots™ from solution. The resulting cloudy solution was then centrifuged at 13000rpm for 5 minutes to provide an orange pellet at the bottom of a clear solution. The supernatant was decanted off the pellet and the excess ligand recovered. The pellet was then dissolved in DCM (2ml) and transferred to a RBF, the solvent was removed under reduced pressure and the product dried to a constant

mass (12 hours under vacuum). The exchanged NanoDots™ appeared as an orange solid (0.0195g, 98%). ^{1}H NMR (250 MHz, $CDCl_3$): ∂ 0.02 (s, $6H_{6H\ DUDSPO}$), 0.86 (t, $12H_{9H\ DUDSPO\ \&\ 3H\ HDA}$), 1.10-2.10 (m, $84H_{30H\ HDA\ \&\ 54H\ DUDSPO}$), 3.57 (t, $2H_{2H\ DUDSPO}$), 4.93 (dd, $4H_{4H\ DUDSPO}$), 5.79 (ddt, $2H_{2H\ DUDSPO}$). Displacement ratio 26% DUDSPO **26** : 74% HDA **3**.

4.5.7 Displacement of HDA 3 coated NanoDot™ with DOMSPO 7 (No wash)

NanoDots™ – NLP121 (0.0100g, 1eqv w/w) were dissolved in diethyl ether (1ml) and stirred under nitrogen. DOMSPO **7** (0.1000g, 0.26mmols, 10eqv w/w) was added and the mixture shaken for 12 hours. The clear poppy red solution was then was then transferred to a centrifuge tube containing methanol (1ml) and centrifuged at 13000rpm for 5 minutes to produce a red pellet at the bottom of a clear solution. The supernatant was decanted off the pellet and the excess ligand recovered. The pellet was then dissolved in diethyl ether (2ml) and transferred to a RBF, the solvent was removed under reduced pressure and the product dried to a constant mass (12 hours under vacuum). The exchanged NanoDots™ appeared as a poppy red solid (0.0224g, 112%). ^{1}H NMR (250 MHz, $CDCl_3$): ∂_H 0.86 (t, $9H_{3H\ HDA\ \&\ 6H\ DOMSPO}$), 1.00-1.80 (m, $58H_{30H\ HDA\ \&\ 28H\ DOMSPO}$), 3.09 (d, $4H_{4H\ DOMSPO}$), 5.22 (d, $2H_{2H\ DOMSPO}$), 5.72 (d, $2H_{2H\ DOMSPO}$), 6.67 (dd, $2H_{2H\ DOMSPO}$), 7.18 (d, $4H_{4H\ DOMSPO}$), 7.35 (d, $4H_{4H\ DOMSPO}$). Displacement ratio 50% DOMSPO **7**: 50% HDA **3**

4.5.8 Displacement of HDA coated NanoDot™ with DOMSPO 7 (washed)

NanoDots™ – NLP121 (0.0100g, 1eqv w/w) were dissolved in diethyl ether (1ml) and stirred under nitrogen. DOMSPO 7 (0.1000g, 0.26mmols, 10eqv w/w) was added and the mixture shaken for 12 hours. The clear poppy red solution was then was then transferred to a centrifuge tube containing methanol (1ml) and centrifuged at 13000rpm for 5 minutes to produce a red pellet at the bottom of a clear solution. The supernatant was decanted off the pellet washed further with methanol (1ml). The pellet was then dispersed in diethyl ether (2ml) and transferred to a RBF, the solvent was removed under reduced pressure and the product dried to a constant mass (12 hours under vacuum). The product appeared as an insoluble poppy red solid, no analysis was undertaken.

4.5.9 Displacement of HDA coated NanoDot™ with TUPO 25 (No Wash)

NanoDots™ – NLP121 (0.1000g, 1eqv w/w) were dissolved in DCM (10ml) and stirred under nitrogen. TUPO **25** (0.1000g, 1.98mmols, 10eqv w/w) was added and the mixture shaken for 72 hours. The clear poppy red solution was then was then transferred to a centrifuge tube containing ethanol (10ml) and shaken vigorously to begin the precipitation of the NanoDots™ from solution. The resulting cloudy solution was then centrifuged at 13000rpm for 5 minutes to produce a poppy red pellet at the bottom of a clear solution. The supernatant was decanted off the pellet and the excess ligand recovered. The pellet was then dissolved in DCM (8ml) and transferred to a RBF, the solvent was removed under reduced pressure and the product dried to a constant mass (12 hours under vacuum). The exchanged NanoDots™ appeared as a poppy red solid (0.1929g, 193%). ^{1}H NMR (400 MHz, $CDCl_3$): ∂_H 0.00 (s, grease, D=0.4-0.6 x $10^{-10}m^2s^{-1}$) 0.86 (m, $3H_{3H\ HDA}$, D=1.0-2.2 x $10^{-10}m^2s^{-1}$), 1.00-1.80 (m, $84H_{30H\ HDA\ \&\ 48H\ TUPO}$,

D=1.2-3.5 x $10^{-10}m^2s^{-1}$), 2.00 (bm, $6H_{6H\ TUPO}$ D=0.6-0.8 x $10^{-10}m^2s^{-1}$) 4.93 (dd, $6H_{6H\ TUPO}$, D=0.0-0.3 x $10^{-10}m^2s^{-1}$), 5.79 (ddt, $3H_{3H\ TUPO}$, D=0.3-0.6 x $10^{-10}m^2s^{-1}$). Displacement ratio 37% TUPO **25** : 63% HDA **3**. PL max = 572 nm.

4.5.10 Displacement of HDA coated NanoDot™ with TUPO 25 (washed)

NanoDots™ – NLP121 (0.1000g, 1eqv w/w) were dissolved in DCM (10ml) and stirred under nitrogen. TUPO **25** (0.1000g, 1.98mmols, 10eqv w/w) was added and the mixture shaken for 72 hours. The clear poppy red solution was then was then transferred to a centrifuge tube containing ethanol (10ml) and shaken vigorously to begin the precipitation of the NanoDots™ from solution. The resulting cloudy solution was then centrifuged at 13000rpm for 5 minutes to provide a poppy red pellet at the bottom of a clear solution. The supernatant was decanted off the pellet and the excess ligand recovered. The pellet was then washed by the addition of methanol (10ml) and agitation, followed by a further 5 minutes of centrifugation. The pellet was then dissolved in DCM (8ml) and transferred to a RBF, the solvent was removed under reduced pressure and the product dried to a constant mass (12 hours under vacuum). The exchanged NanoDots™ appeared as a poppy red solid (0.1192g, 119%). ^{1}H NMR (400 MHz, $CDCl_3$): ∂_H 0.00 (s, grease, D=0.4-0.8 x $10^{-10}m^2s^{-1}$), 0.86 (m, $3H_{3H\ HDA}$, D=1.4-2.3 x $10^{-10}m^2s^{-1}$), 0.80-2.40 (m, $30H_{30H\ HDA}$, D=1.4-3.0 x $10^{-10}m^2s^{-1}$). Displacement ratio 0% TUPO **25** : 100% HDA **3**. Combustion analysis (washed with MeOH x 2): 18.89% C, 3.29% H, 1.23% N, 0.33% P and 40.12% Cd.

To quantify the amount of TUPO **25** that can be removed by washing and precipitation with methanol the molar ratio of P to Cd for a sample of TUPO coated NanoDots™ was calculated.

40.12% of the total sample was Cd, therefore in 100g there would be 40.12g of Cd.

The number of moles in 40.12g of Cd

= 40.12/112.4 = 0.34 moles of Cd

0.33% of the total sample was P, therefore in 100g there would be 0.33g of P.

The number of moles in 0.33g of P

= 0.33/31.0 = 0.01 moles of P

Therefore the molar ratio of P to Cd is 0.01 to 0.34

For every one mole of Cd there is 0.03 moles of P in the sample of washed TUPO **25**-coated NanoDots™

4.5.11 Displacement of HDA coated NanoDot™-MC556 with TUPO 25

NanoDots™ – MC556 (0.0500g, 1eqv w/w) were dissolved in DCM (10ml) and stirred under nitrogen. TUPO **25** (1.000g, 1.98mmols, 20eqv w/w) was added and the mixture shaken for 72 hours. The clear red solution was then was then transferred to a centrifuge tube containing ethanol (10ml) and shaken vigorously to begin the precipitation of the NanoDots™ from solution. The resulting cloudy solution was then centrifuged at 13000rpm for 5 minutes to produce a red pellet at the bottom of a clear solution. The supernatant was decanted off the pellet and the excess ligand recovered. The pellet was then dissolved in DCM (8ml) and transferred to a RBF, the solvent was removed under reduced pressure and the product dried to a constant mass (12 hours under vacuum). The exchanged NanoDots™ appeared as a red solid (0.0629g, 126%). IR (KBr disk): v

$_{max}$/cm^{-1} 3400wb, 3078w, 2925s, 2853m, 1459wm, 1262m, 1095bs, 909w, 803m. ^{1}H NMR (400 MHz, $CDCl_3$): ∂_H 0.00 (s, grease) 0.86 (bs, $3H_{3H\ HDA}$), 1.00-1.80 (m, $84H_{30H\ HDA\ \&\ 48H\ TUPO}$), 2.00 (dd, $6H_{6H\ TUPO}$) 4.93 (dd, $6H_{6H\ TUPO}$), 5.79 (ddt, $3H_{3H\ TUPO,}$). Displacement ratio 57% TUPO **25** : 43% HDA **3**. PL max = 617 nm.

4.5.12 Displacement of HDA coated NanoDot™-MC610 with TUPO 25

NanoDots™ – MC610 (0.0500g, 1eqv w/w) were dissolved in DCM (10ml) and stirred under nitrogen. TUPO **25** (1.000g, 1.98mmols, 20eqv w/w) was added and the mixture shaken for 72 hours. The clear orange solution was then was then transferred to a centrifuge tube containing ethanol (10ml) and shaken vigorously to begin the precipitation of the NanoDots™ from solution. The resulting cloudy solution was then centrifuged at 13000rpm for 5 minutes to produce a red pellet at the bottom of a clear solution. The supernatant was decanted off the pellet and the excess ligand recovered. The pellet was then dissolved in DCM (8ml) and transferred to a RBF, the solvent was removed under reduced pressure and the product dried to a constant mass (12 hours under vacuum). The exchanged NanoDots™ appeared as a orange solid (0.0613g, 123%). IR (KBr disk): ν_{max}/cm^{-1} 3400wb, 3068w, 2923s, 2852m, 1459w, 1098bm, 1023bm, 908w, 802m, 725w. ^{1}H NMR (400 MHz, $CDCl_3$): ∂ 0.00 (s, D=2.4-2.6 x 10^{-10}m^{2}s^{-1}, grease) 0.86 (bm, D=2.2-3.4 x 10^{-10}m^{2}s^{-1}, $3H_{HDA}$), 1.10-1.80 (m, D=2.2-5.0 x 10^{-10}m^{2}s^{-1}, $84H_{30H\ HDA\ \&\ 48H\ TUPO}$), 2.00 (dd, D=2.2-5.0 x 10^{-10}m^{2}s^{-1}, $6H_{6H\ TUPO}$) 4.93 (dd, D=4.6-5.0 x 10^{-10}m^{2}s^{-1}, $6H_{6H\ TUPO}$), 5.79 (ddt, D=4.4-5.6 x 10^{-10}m^{2}s^{-1}, $3H_{3H\ TUPO}$). Displacement ratio 66% TUPO **25** : 34% HDA **3**. PL max = 570 nm.

4.5.13 Stability of TUPO coated NanoDots™-MC556 upon exposure to a range of reagents

The stability of TUPO **25** coated NanoDots™ (MC610) to a variety of different reagents was evaluated by comparing the PL spectra of a solution of NanoDots™ before the addition of any reagent with the PL spectra recorded after exposure to the reagent. A stock solution of TUPO **25** (10mg) coated of NanoDots™ (MC610), in THF (8.0ml) was prepared and the mixture shaken for 10 minutes to ensure complete dissolution. The PL spectra of 1ml of the NanoDot™ solution was recorded for comparison with the PL spectra of the NanoDots ™ after addition of the reagent. Solutions of THF (10ml) containing 0.00025 moles of each reagent were prepared according to **Table 12**. 0.5ml of the reagent solution was added to 0.5ml of the NanoDot™ solution, the mixture was shaken and the PL spectra run immediately.

Table 17 provides the PL max of the solutions of NanoDots™ after exposure to the reagents listed above. The actual spectra can be viewed in (Appendix D, **Figure 97**)

Reagent	PL maximum emission after addition of reagent (nm)
No Reagent	1850.75
Trifluroacetic acid (TFA)	350.75
Aluminium trichloride (AlCl3)	186.25
1,8-Diazabicyclo[5.4.0]undec-7-ene (DBU)	1760.5
Potassium hydroxide (KOH)	1677.75
Iodobenzoic acid (IBX)	394.5
Potassium permanganate (KMnO4)	674.75
Lithium aluminium hydride (LiAlH4)	562.45
n-Butyl lithium (nBuLi)	469.75
Vinyl magnesium bromide (Vinyl MgBr)	151.25
Hydrogen Bromide (HBr)	153.50

Table 17: PL maximum emission remaining after exposure to each reagent

4.5.14 Displacement of HDA coated NanoDot™ with styrene

NanoDots™ – NLP121 (0.0100g, 1eqv w/w) were dissolved in DCM (2ml) and stirred under nitrogen. Styrene (0.4000g, 3.85mmols, 40eqv w/w) was added and the mixture shaken for 72 hours. The clear poppy red solution was then was then transferred to a centrifuge tube containing methanol (2ml) and shaken vigorously to begin the precipitation of the NanoDots™ from solution. The resulting cloudy solution was then centrifuged at 13000rpm for 5 minutes to provide a poppy red pellet at the bottom of a clear solution. The supernatant was decanted off the pellet and the excess ligand recovered.. The pellet was then dissolved in DCM (~1ml) and transferred to a RBF, the solvent was removed under reduced pressure and the product dried to a constant mass (12 hours under vacuum). The exchanged NanoDots™ appeared as a poppy red solid (0.0132g, 132%). NMR (250 MHz, $CDCl_3$): ∂ 0.86 (m, $3H_{3H\ HDA}$), 0.80-2.40 (m, $30H_{30H\ HDA}$).

4.6 – Investigation into the Optimisation of HDA Displacement

4.6.1 Displacement of different batches of HDA coated NanoDot™ with DMSPA 20

Five different batches of NanoDots™ **OMN44** (0.0100g, 1eqv w/w), **NLP121** (0.0100g, 1eqv w/w), **OMN43** (0.0100g, 1eqv w/w), **NLP125** (0.0100g, 1eqv w/w) and **OMN29** (0.0100g, 1eqv w/w) were weighed separately into centrifuge tubes. The NanoDots™ were then dissolved in DCM (2ml) and put under nitrogen. DMSPA 20 (0.1000g, 0.35mmols, 10eqv w/w) was then added to each tube and the mixture shaken for 24 hours. Methanol (1.5ml) was then added to the clear solutions and the tubes shaken to begin precipitation of the NanoDots™ from solution. The resulting cloudy solutions were then centrifuged at 13000rpm for 15 minutes to produce a pellet at the bottom of a clear solution in each tube. The supernatant was decanted off the pellets and the excess ligand recovered. Each sample of NanoDots™ were then dried to a constant mass under reduced pressure. The solids were then dissolved in $CDCl_3$ and analysed immediately by ^1H NMR spectroscopy. ^1H NMR (250 MHz, $CDCl_3$): **OMN44** ∂ 0.86 (t, $3H_{3H\ HDA}$), 1.10-1.70 (m, $30H_{30H\ HDA}$), 3.14 (dd, $4H_{4H\ DMSPA}$), 5.25 (d, $2H_{2H\ DMSPA}$), 5.73 (d, $2H_{2H\ DMSPA}$), 6.68 (dd, $2H_{2H\ DMSPA}$), 7.15 (d, $4H_{4H\ DMSPA}$), 7.37 (d, $4H_{4H\ DMSPA}$). Displacement ratio 9% DMSPA **20** : 91% HDA **3**. **NLP121** ∂ 0.86 (m, $3H_{3H\ HDA}$), 1.10-1.70 (m, $30H_{30H\ HDA}$), 3.16 (dd, $4H_{4H\ DMSPA}$), 5.26 (d, $2H_{2H\ DMSPA}$), 5.77 (d, $2H_{2H\ DMSPA}$), 6.68 (dd, $2H_{2H\ DMSPA}$), 7.15 (d, $4H_{4H\ DMSPA}$), 7.37 (d, $4H_{4H\ DMSPA}$). Displacement ratio 33% DMSPA **20**: 67% HDA **3**. **OMN43** ∂ 0.86 (m, $3H_{3H\ HDA}$), 1.10-1.70 (m, $30H_{30H\ HDA}$), 3.14 (dd, $4H_{4H\ DMSPA}$), 5.24 (d, $2H_{2H\ DMSPA}$), 5.78 (d, $2H_{2H\ DMSPA}$), 6.68 (dd, $2H_{2H\ DMSPA}$), 7.15 (d, $4H_{4H\ DMSPA}$), 7.37 (d, $4H_{4H\ DMSPA}$). Displacement ratio 33% DMSPA **20** : 67% HDA **3**. **NLP125** ∂ 0.83 (m, $3H_{3H\ HDA}$), 1.10-1.70 (m, $30H_{30H\ HDA}$), 3.16 (dd,

$4H_{4H\ DMSPA}$), 5.25 (d, $2H_{2H\ DMSPA}$), 5.77 (d, $2H_{2H\ DMSPA}$), 6.68 (dd, $2H_{2H\ DMSPA}$), 7.15 (d, $4H_{4H\ DMSPA}$), 7.37 (d, $4H_{4H\ DMSPA}$). Displacement ratio 14% DMSPA **20** : 86% HDA **3**. **OMN29** ∂ 0.83 (m, $3H_{3H\ HDA}$), 1.10-1.70 (m, $30H_{30H\ HDA}$), 3.15 (dd, $4H_{4H\ DMSPA}$), 5.24 (d, $2H_{2H\ DMSPA}$), 5.78 (d, $2H_{2H\ DMSPA}$), 6.67 (dd, $2H_{2H\ DMSPA}$), 7.15 (d, $4H_{4H\ DMSPA}$), 7.37 (d, $4H_{4H\ DMSPA}$). Displacement ratio 50% DMSPA **20** : 50% HDA **3**. (Appendix A. **Table 5**)

4.6.2 Displacement of HDA coated NanoDot™ with different excesses of DMSPA 20

NanoDots™ NLP121 (0.0100g, 1eqv w/w) were weighed into five separate centrifuge tubes, the NanoDots™ were dissolved in DCM (1ml) and the tubes labelled B-F. DMSPA **20** was then added to each tube, **B** (0.0500g, 0.18mmols, 5eqv w/w), **C** (0.1000g, 0.35mmols, 10eqv w/w), **D** (0.2000g, 0.71mmols, 20eqv w/w), **E** (0.3000g, 1.06mmols, 30eqv w/w), **F** (0.4000g, 1.42mmols, 40eqv w/w). Finally as a control DMSPA **20** (0.4000g, 1.42mmols, 40eqv w/w) was dissolved in DCM (1ml) and the tube labelled **A**. The six tubes were then placed under an atmosphere of nitrogen and shaken for 16 hours. Methanol (1.0ml) was then added to the clear solutions and the tubes shaken to begin precipitation of the NanoDots™ from solution. The resulting cloudy solutions were then centrifuged at 13000rpm for 5 minutes to produce a pellet at the bottom of a clear solution in each tube. The supernatant was decanted off the pellets and the excess ligand recovered. Each sample of NanoDots™ were then dried to a constant mass under reduced pressure. The solids were then dissolved in $CDCl_3$ and analysed immediately by ^1H NMR spectroscopy. ^1H NMR (250 MHz, $CDCl_3$): **A** ∂ 1.50 (H_2O). **B** ∂ 0.86 (m, $3H_{3H\ HDA}$), 1.10-1.70 (m, $30H_{30H\ HDA}$). Displacement ratio 0%

DMSPA **20** : 100% HDA **3**. **C** ∂ 0.86 (m, $3H_{3H\ HDA}$), 1.10-1.70 (m, $30H_{30H\ HDA}$), 3.16 (dd, $4H_{4H\ DMSPA}$), 5.24 (d, $2H_{2H\ DMSPA}$), 5.78 (d, $2H_{2H\ DMSPA}$), 6.68 (m, $2H_{2H\ DMSPA}$), 7.15 (d, $4H_{4H\ DMSPA}$), 7.36 (d, $4H_{4H\ DMSPA}$). Displacement ratio 33% DMSPA **20** : 67% HDA **3**. **D** ∂ 0.86 (m, $3H_{3H\ HDA}$), 1.10-1.70 (m, $30H_{30H\ HDA}$), 3.15 (dd, $4H_{4H\ DMSPA}$), 5.27 (d, $2H_{2H\ DMSPA}$), 5.73 (d, $2H_{2H\ DMSPA}$), 6.68 (dd, $2H_{2H\ DMSPA}$), 7.15 (d, $4H_{4H\ DMSPA}$), 7.37 (d, $4H_{4H\ DMSPA}$). Displacement ratio 63% DMSPA **20** : 37% HDA **3**. **E** ∂ 0.86 (m, $3H_{3H\ HDA}$), 1.10-1.70 (m, $30H_{30H\ HDA}$), 3.15 (dd, $4H_{4H\ DMSPA}$), 5.24 (d, $2H_{2H\ DMSPA}$), 5.77 (d, $2H_{2H\ DMSPA}$), 6.67 (dd, $2H_{2H\ DMSPA}$), 7.15 (d, $4H_{4H\ DMSPA}$), 7.37 (d, $4H_{4H\ DMSPA}$). Displacement ratio 63% DMSPA **20** : 37% HDA **3**. **F** ∂ 0.86 (m, $3H_{3H\ HDA}$), 1.10-1.70 (m, $30H_{30H\ HDA}$), 3.15 (dd, $4H_{4H\ DMSPA}$), 5.24 (d, $2H_{2H\ DMSPA}$), 5.77 (d, $2H_{2H\ DMSPA}$), 6.67 (dd, $2H_{2H\ DMSPA}$), 7.14 (d, $4H_{4H\ DMSPA}$), 7.37 (d, $4H_{4H\ DMSPA}$). Displacement ratio 67% DMSPA **20**: 33% HDA **3**. (Appendix A, **Table 6**)

4.6.3 Displacement of HDA coated NanoDot™ with different excesses of TPhPO 38

NanoDots™ NLP121 (0.0100g, 1eqv w/w) were weighed into five separate centrifuge tubes, the NanoDots™ were dissolved in DCM (1ml) and the tubes labelled **B-F**. **A** different amount of TPhPO **38** was then added to each tube, **B** (0.0500g, 0.18mmols, 5eqv w/w), **C** (0.1000g, 0.36mmols, 10eqv w/w), **D** (0.2000g, 0.72mmols, 20eqv w/w), **E** (0.3000g, 1.08mmols, 30eqv w/w), **F** (0.4000g, 1.44mmols, 40eqv w/w). Finally as a control TPhPO **38** (0.4000g, 1.44mmols, 40eqv w/w) was dissolved in DCM (1ml) and the tube labelled **A**. The six tubes were then placed under an atmosphere of nitrogen and shaken for 16 hours. Methanol (1.0ml) was then added to the clear coloured solutions and the tubes shaken to begin precipitation of the NanoDots™ from solution. The

resulting cloudy solutions were then centrifuged at 13000rpm for 5 minutes to produce a pellet at the bottom of a clear solution in each tube. The supernatant was decanted off the pellets and the excess ligand recovered. Each sample of NanoDots™ were then dried to a constant mass under reduced pressure. The solids were then dissolved in $CDCl_3$ and analysed immediately by ^1H NMR spectroscopy. ^1H NMR (250 MHz, $CDCl_3$): **A** ∂ 1.62 (H_2O). **B** ∂ 0.86 (m, $3H_{3H\ HDA}$), 1.10-1.70 (m, $30H_{30H\ HDA}$) 7.30-7.90 (m, $15H_{15H\ TPPhO}$). Displacement ratio 66% TPhPO **38** : 34% HDA **3**. **C** ∂ 0.86 (m, $3H_{3H\ HDA}$), 1.10-1.70 (m, $30H_{30H\ HDA}$) 7.30-7.90 (m, $15H_{15H\ TPPhO}$). Displacement ratio 67% TPhPO **38** : 33% HDA **3**. **D** ∂ 0.86 (m, $3H_{3H\ HDA}$), 1.10-1.70 (m, $30H_{30H\ HDA}$) 7.30-7.90 (m, $15H_{15H\ TPPhO}$). Displacement ratio 78% TPhPO **38** : 22% HDA **3**. **E** ∂ 0.86 (m, $3H_{3H\ HDA}$), 1.10-1.70 (m, $30H_{30H\ HDA}$) 7.30-7.90 (m, $15H_{15H\ TPPhO}$). Displacement ratio 84% TPhPO **38** : 16% HDA **3**. **F** ∂ 0.86 (m, $3H_{3H\ HDA}$), 1.10-1.70 (m, $30H_{30H\ HDA}$) 7.30-7.90 (m, $15H_{15H\ TPPhO}$). Displacement ratio 84% TPhPO **38**: 16% HDA **3**. (Appendix A, **Table 7**)

4.6.4 Displacement of HDA 3 coated NanoDot™ with DMSPA 20-effect of displacement time

NanoDots™ NLP121 (0.0100g, 1eqv w/w) were weighed into four separate centrifuge tubes, the NanoDots™ were dissolved in DCM (1ml) and the tubes labelled **A-D**. DMSPA **20** (0.2000g, 0.71mmols, 20eqv w/w) was added to each of the tubes and the content placed under an atmosphere of nitrogen. Sample **A** was shaken for 4 days, sample **B** for 6 days, sample **C** for 8 days and sample **D** for 12 days. At the end of the respective displacement times each sample was treated with methanol (1.0ml) and shaken to begin precipitation of the NanoDots™ from solution. The resulting cloudy solutions were then centrifuged at 13000rpm for 5 minutes to produce a pellet at the

bottom of a clear solution in each tube. The supernatant was decanted off the pellets and the excess ligand recovered. Each sample of NanoDots™ were then dried to a constant mass under reduced pressure (12 hours under vacuum). The solids were then dissolved in $CDCl_3$ and analysed immediately by ^1H NMR spectroscopy. ^1H NMR (250 MHz, $CDCl_3$): **A** ∂ 0.86 (m, $3H_{3H\ HDA}$), 1.10-1.70 (m, $30H_{30H\ HDA}$), 3.14 (d, $4H_{4H\ DMSPA}$), 5.23 (d, $2H_{2H\ DMSPA}$), 5.77 (d, $2H_{2H\ DMSPA}$), 6.68 (dd, $2H_{2H\ DMSPA}$), 7.14 (d, $4H_{4H\ DMSPA}$), 7.37 (d, $4H_{4H\ DMSPA}$). Displacement ratio 78% DMSPA **20** : 22% HDA **3**. **B** ∂ 0.86 (m, $3H_{3H\ HDA}$), 1.10-1.70 (m, $30H_{30H\ HDA}$), 3.14 (d, $4H_{4H\ DMSPA}$), 5.23 (d, $2H_{2H\ DMSPA}$), 5.77 (d, $2H_{2H\ DMSPA}$), 6.68 (dd, $2H_{2H\ DMSPA}$), 6.93 (dm, $1H_{1H\ DMSPA}$), 7.14 (d, $4H_{4H\ DMSPA}$), 7.37 (d, $4H_{4H\ DMSPA}$). Displacement ratio 89% DMSPA **20** : 11% HDA **3**. **C** ∂ 0.86 (m, $3H_{3H\ HDA}$), 1.10-1.70 (m, $30H_{30H\ HDA}$), 3.14 (d, $4H_{4H\ DMSPA}$), 5.23 (d, $2H_{2H\ DMSPA}$), 5.77 (d, $2H_{2H\ DMSPA}$), 6.68 (dd, $2H_{2H\ DMSPA}$), 6.93 (dm, $1H_{1H\ DMSPA}$), 7.14 (d, $4H_{4H\ DMSPA}$), 7.37 (d, $4H_{4H\ DMSPA}$). Displacement ratio 98% DMSPA **20** : 2% HDA **3**. **D** ∂ 0.86 (m, $3H_{3H\ HDA}$), 1.10-1.70 (m, $30H_{30H\ HDA}$), 3.14 (d, $4H_{4H\ DMSPA}$), 5.23 (d, $2H_{2H\ DMSPA}$), 5.77 (d, $2H_{2H\ DMSPA}$), 6.68 (dd, $2H_{2H\ DMSPA}$), 6.93 (dm, $1H_{1H\ DMSPA}$), 7.14 (d, $4H_{4H\ DMSPA}$), 7.37 (d, $4H_{4H\ DMSPA}$). Displacement ratio 95% DMSPA **20** : 5% HDA **3**. (Appendix A, **Table 8**)

4.6.5 None competitive comparison of the displacement of HDA coated NanoDot™ with DUPA 24, DUPSA 33, DMSPA 20 and DMSPS 34

NanoDots™ NLP121 (0.0100g, 1eqv w/w) were weighed into four separate centrifuge tubes, the NanoDots™ were dissolved in DCM (1ml) and the tubes labelled **A-D**. DUPA **24** (0.2000g, 0.56mmols, 20eqv w/w) was added to tube **A**, DUPSA **33** (0.2000g, 0.54mmols, 20eqv w/w) to tube **B**, DMSPA **20** (0.2000g, 0.71mmols, 20eqv w/w) to tube **C** and finally DMSPSA **34** (0.2000g, 0.67mmols, 20eqv w/w) to tube **D**.

The four tubes were then placed under an atmosphere of nitrogen and shaken for 16 hours. A mixture of methanol and acetone (2.0ml 50:50 v/v) was then added to the clear coloured solutions and the tubes shaken to begin precipitation of the NanoDots™ from solution. The resulting cloudy solutions were then centrifuged at 13000rpm for 10 minutes to produce a pellet at the bottom of a clear solution in each tube. The supernatant was decanted off the pellets and the excess ligand recovered. Each sample of NanoDots™ were then dried to a constant mass under reduced pressure. The solids were then dissolved in $CDCl_3$ and analysed immediately by ^1H NMR spectroscopy. ^1H NMR (250 MHz, $CDCl_3$): **A** ∂ 0.86 (t, $3H_{3H\ HDA}$), 1.10-2.10 (m, $66H_{30H\ HDA\ \&\ 36H\ DUPA}$), 4.92 (dd, $4H_{4H\ DUPA}$), 5.79 (m, $2H_{2H\ DUPA}$). Displacement ratio 63% DUPA **24** : 37% HDA **3**. **B** ∂ 0.86 (t, $3H_{3H\ HDA}$), 1.10-2.10 (m, $66H_{30H\ HDA\ \&\ 36H\ DUPSA}$), 4.93 (dd, $4H_{4H\ DUPSA}$), 5.74 (ddt, $2H_{2H\ DUPSA}$). Displacement ratio 71% DUPSA **33** : 29% HDA **3**. **C** ∂ 0.86 (m, $3H_{3H\ HDA}$), 1.10-1.70 (m, $30H_{30H\ HDA}$), 3.14 (d, $4H_{4H\ DMSPA}$), 5.24 (d, $2H_{2H\ DMSPA}$), 5.77 (d, $2H_{2H\ DMSPA}$), 6.68 (dd, $2H_{2H\ DMSPA}$), 7.14 (d, $4H_{4H\ DMSPA}$), 7.37 (d, $4H_{4H\ DMSPA}$). Displacement ratio 67% DMSPA **20** : 33% HDA **3**. **D** ∂_H 0.83 (m, $3H_{3H\ HDA}$), 1.10-1.70 (m, $30H_{30H\ HDA}$), 3.23 (d, $4H_{4H\ DMSPSA}$), 5.24 (d, $2H_{2H\ DMSPSA}$), 5.77 (d, $2H_{2H\ DMSPA}$), 6.68 (dd, $2H_{2H\ DMSPS}$), 7.14 (d, $4H_{4H\ DMSPSA}$), 7.37 (d, $4H_{4H\ DMSPSA}$). Displacement ratio 44% DMSPSA **34**: 56% HDA **3**. (Appendix A, **Table 9**)

4.6.6 Competitive comparison of the displacement of HDA coated NanoDot™ TPhPO 38 V/S TOPS 28 and TPhPS 39V/S TOPO 1

NanoDots™ NLP121 (0.0500g, 1eqv w/w) were weighed into two centrifuge tubes, the NanoDots™ were dissolved in DCM (5ml) and the tubes labelled **A** and **B**. TPhPO **38** (0.5000g, 1.8mmols, 10eqv w/w) and TOPS **28** (0.5000g, 1.2mmols, 10eqv w/w) were

added to tube **A**. TPhPS **39** (0.5000g, 1.7mmols, 10eqv w/w) and TOPO **1** (0.5000g, 1.3mmols, 10eqv w/w) were added to tube **B**. The two tubes were then placed under an atmosphere of nitrogen and shaken for 16 hours. Methanol and acetone (5ml 50:50 v/v) was then added to the clear coloured solutions and the tubes shaken to begin precipitation of the NanoDots^{TM} from solution. The resulting cloudy solutions were then centrifuged at 13000rpm for 20 minutes to produce a pellet at the bottom of a clear solution in each tube. The supernatant was decanted off the pellets and the excess ligand recovered. Each sample of NanoDots^{TM} were then dried to a constant mass under reduced pressure. The solids were then dissolved in $CDCl_3$ and analysed immediately by ^{1}H NMR spectroscopy. ^{1}H NMR (250 MHz, $CDCl_3$): **A** ∂ 0.86 (m, $9H_{9H\ TOPS}$), 1.00-1.70 (m, $42H_{42H\ TOPS}$) 7.30-7.90 (m, $15H_{15H\ TPPhO}$). Displacement ratio 39% TPhPO **38** : 61% TOPS **28**. **B** ∂ 0.86 (m, $9H_{9H\ TOPO}$), 1.00-1.70 (m, $42H_{42H\ TOPO}$), 7.30-7.90 (m, $15H_{15H\ TPPhS}$). Displacement ratio 42. % TPhPS **39**: 58% TOPO **1**.

4.7 – Polymerisation *via* ADMET in the absence of NanoDots™

4.7.1 Polymerisation of TUPO 25 using 5 mole percent Grubbs 2nd generation catalyst 42

TUPO **25** (0.100g, 0.2mmols, 1eqv) was dissolved in DCM (2ml) and placed under an atmosphere of nitrogen. A solution of Grubbs second generation catalyst **42** ($8.5x10^{-3}$g, 0.01mmols, 5 mole percent eqv) in DCM (0.5ml) was added and the mixture stirred for 5 minutes. The temperature was then raised to 40°C and the mixture stirred under nitrogen for 3 days. The solvent was then removed under reduced pressure and the crude product dried to a constant mass to product a brown flaky solid (0.1087g). IR (KBr disk): ν_{max}/cm^{-1} 3415w/b, 3069w, 2936s, 2847s, 1634w, 1665w, 1346w, 1256m, 1162m/s (P=O), 1089m, 1014m, 965m, 903w, 804m, 717w. ^{1}H NMR (250 MHz, $CDCl_3$): ∂ 1.10-2.00 (m, aliphatic), 4.90 (dd, $^3J_{HCCH}$=17.6$_{trans}$ Hz and 10.9$_{cis}$ Hz, olefinic, starting material), 5.33 (bm, olefinic, product), 5.76 (ddt, $^3J_{HCCH}$=16.8$_{trans}$, 10.2$_{cis}$, 6.2 Hz, olefinic, starting material).

4.7.2 Polymerisation of TUPO 25 using 10 mole percent Grubbs 2nd generation catalyst 42

TUPO **25** (0.100g, 0.2mmols, 1eqv) was dissolved in DCM (2ml) and placed under an atmosphere of nitrogen. A solution of Grubbs second generation catalyst **42** (0.017g, 0.02mmols, 10 mole percent eqv) in DCM (0.5ml) was added and the mixture stirred for 5 minutes. The temperature was then raised to 40°C and the mixture stirred under nitrogen for 3 days. The solvent was then removed under reduced pressure and the crude product dried to a constant mass to product a brown flaky solid (0.1072g). IR

(KBr disk): ν_{max}/cm^{-1} 3422w/b, 2925s, 2852s, 2368w, 2345w, 1718w, 1686w, 1654w, 1637w, 1560w, 1542w, 1508w, 1466m, 1405w, 1262w, 1166m, 1099w, 1009w, 966m, 806w, 717w. ^{1}H NMR (250 MHz, $CDCl_3$): ∂ 1.10-2.00 (m, aliphatic), 5.35 (bm, olefinic, product). ^{31}P NMR (121.5 MHz, $CDCl_3$, Referenced to 85% phosphoric acid): ∂ 58.3, 50.9, 50.1, 50.2, 49.3, 40.2, 36.3, 34.3.

4.7.3 Polymerisation of TUPO 25using 15 mole percent Grubbs 2nd generation catalyst 42

TUPO **25** (0.100g, 0.2mmols, 1eqv) was dissolved in DCM (2ml) and placed under an atmosphere of nitrogen. A solution of Grubbs second generation catalyst **42** (0.017g, 0.03mmols, 15 mole percent eqv) in DCM (0.5ml) was added and the mixture stirred for 5 minutes. The temperature was then raised to 40°C and the mixture stirred under nitrogen for 3 days. The solvent was then removed under reduced pressure and the crude product dried to a constant mass to product a brown flaky solid (0.1122g). IR (KBr disk): ν_{max}/cm^{-1} 3422w/b, 2925s, 2852s, 2369w, 2944w, 2345w, 1773w, 1718w, 1700w, 1685w, 1676w, 1654w, 1647w, 1636w, 1618w, 1560w, 1542w, 1522w, 1502w, 1438w, 1458m, 1384w, 1262w, 1166m, 1099w, 1018w, 966m, 800w, 724w. ^{1}H NMR (250 MHz, $CDCl_3$): ∂ 0.80-2.60 (m, aliphatic), 5.34 (bm, olefinic, product).

4.7.4 Polymerisation of TUPO 25 using 5 mole percent Hoveyda-Grubbs 2nd generation catalyst 43

TUPO **25** (0.100g, 0.2mmols, 1eqv) was dissolved in DCM (2ml) and placed under an atmosphere of nitrogen. A solution of Grubbs-Hoveyda second generation catalyst **43** (0.0063g, 0.01mmols, 5 mole percent eqv) in DCM (0.5ml) was added and the mixture stirred for 5 minutes. The temperature was then raised to 40°C and the mixture stirred under nitrogen for 3 days. The solvent was then removed under reduced pressure and the crude product dried to a constant mass to product a brown flaky solid (0.1047g). IR (KBr disk): ν_{max}/cm^{-1} 3424w/b, 3070w, 2927s, 2854m, 2365s, 2324s, 1655w, 1665w, 1384w, 1260m, 1161w (P=O), 1112w, 969w, 798w, 720w, 673w. ^{1}H NMR (250 MHz, $CDCl_3$): ∂ 0.80-2.40 (m, aliphatic), 5.34 (bm, olefinic, product).

4.7.5 Polymerisation of TUPO 25 using 10 mole percent Hoveyda-Grubbs 2nd generation catalyst 43

TUPO **25** (0.100g, 0.2mmols, 1eqv) was dissolved in DCM (2ml) and placed under an atmosphere of nitrogen. A solution of Grubbs-Hoveyda catalyst second generation catalyst **43** (0.013g, 0.02mmols, 10 mole percent eqv) in DCM (0.5ml) was added and the mixture stirred for 5 minutes. The temperature was then raised to 40°C and the mixture stirred under nitrogen for 3 days. The solvent was then removed under reduced pressure and the crude product dried to a constant mass to product a brown flaky solid (0.1052g). IR (KBr disk): ν_{max}/cm^{-1} 3423w/b, 2926s, 2852s, 2367w, 2344w, 1735w, 1719w, 1702w, 1686w, 1655w, 1637w, 1560w, 1542w, 1508w, 1458m, 1168m, 967w, 805w, 722w. ^{1}H NMR (250 MHz, $CDCl_3$): ∂ 1.10-2.00 (m, aliphatic), 5.35 (bm, olefinic product). ^{31}P NMR (121.5 MHz, $CDCl_3$, Referenced to 85% phosphoric acid): ∂ 49.4, 49.6, 51.0, 58.3.

4.7.6 Polymerisation of TUPO 25 using 15 mole percent Hoveyda-Grubbs 2nd generation catalyst 43

TUPO **25** (0.100g, 0.2mmols, 1eqv) was dissolved in DCM (2ml) and placed under an atmosphere of nitrogen. A solution of Hoveyda-Grubbs second generation catalyst **43** (0.019g, 0.03mmols, 15 mole percent eqv) in DCM (0.5ml) was added and the mixture stirred for 5 minutes. The temperature was then raised to 40°C and the mixture stirred under nitrogen for 3 days. The solvent was then removed under reduced pressure and the crude product dried to a constant mass to product a brown flaky solid (0.1043g). IR (KBr disk): ν_{max}/cm^{-1} 3448w/b, 2925s, 2852s, 2373w, 2345w, 1773w, 1734w, 1718w, 1636w, 1617w, 1560w, 1542w, 1522w, 1508w, 1498w, 1458w, 1383w, 1166m, 967m, 800w. ^{1}H NMR (250 MHz, $CDCl_3$): ∂ 0.80-2.60 (m, aliphatic), 5.30 (bm, olefinic, product).

4.7.7 Polymerisation of DMSDPO 22 using 5 mole percent Grubbs 2nd generation catalyst 42

DMSDPO **22** (0.100g, 0.2mmols, 1eqv) was dissolved in DCM (2ml) and placed under an atmosphere of nitrogen. A solution of Grubbs second generation catalyst **42** (0.010g, 0.01mmols, 5 mole percent eqv) in DCM (0.5ml) was added and the mixture stirred under nitrogen for 3 days. The solvent was then removed under reduced pressure and the crude product dried to a constant mass to product a brown solid (0.1003g). IR (KBr disk): ν_{max}/cm^{-1} 3384m/b, 3072w, 3030w 3024w, 3020w, 2229s, 2914s, 2345w, 1918w, 1654w, 1628m, 1607m, 1560w, 1510s, 1466m, 1407m, 1234s, 1174s, 1126s, 1018m, 989m, 965m, 902m, 861s, 692m. ^{1}H NMR (250 MHz, $CDCl_3$): ∂ 0.84 (sb, 3H), 0.90-

1.80 (m, 18H), 3.07 (d, $^{3}J_{PCH}$=13.9 Hz, 4H), 7.04 (s, 2H), 7.22 (d, $^{3}J_{HCCH}$=7.6 Hz, 4H), 7.44 (d, $^{3}J_{HCCH}$=7.5 Hz, 4H).

4.7.8 Polymerisation of DMSDPO 22 using 10 mole percent Grubbs 2nd generation catalyst 42

DMSDPO **22** (0.100g, 0.2mmols, 1eqv) was dissolved in DCM (2ml) and placed under an atmosphere of nitrogen. A solution of Grubbs second generation catalyst **42** (0.020g, 0.02mmols, 10 mole percent) in DCM (0.5ml) was added and the mixture stirred under nitrogen for 3 days. The solvent was then removed under reduced pressure and the crude product dried to a constant mass to product a brown solid (0.1078g). IR (KBr disk): ν_{max}/cm^{-1} 3385w/b, 3070w, 3030w 3024w, 3020w, 2923s, 2851s, 2370w, 2345w, 1934w, 1774w, 1734w, 1718w, 1685w, 1675w, 1654m, 1628m, 1607w, 1560w, 1542w, 1511m, 1458m, 1407m, 1233m, 1174m, 1126m, 1018w, 963w, 903w, 856m, 692w. ^{1}H NMR (250 MHz, $CDCl_3$): ∂ 0.84 (sb, 3H), 0.90-1.80 (m, 18H), 3.07 (d, $^{3}J_{PCH}$=13.8 Hz, 4H), 7.03 (s, 2H), 7.22 (d, $^{3}J_{HCCH}$=7.9 Hz, 4H), 7.44 (d, $^{3}J_{HCCH}$=7.7 Hz, 4H).

4.7.9 Polymerisation of DMSDPO 22 using 10 mole percent Hoveyda-Grubbs 2nd generation catalyst 43

DMSDPO **22** (0.100g, 0.2mmols, 1eqv) was dissolved in DCM (2ml) and placed under an atmosphere of nitrogen. A solution of Grubbs-Hoveyda second generation catalyst **43** (0.008g, 0.01mmols, 5 mole percent) in DCM (0.5ml) was added and the mixture stirred for ten minutes. The temperature was then raised to 40°C and the mixture stirred under nitrogen for 3 days. The solvent was then removed under reduced pressure and the

crude product dried to a constant mass. The crude product was furnished as a brown flaky solid (0.1007g). IR (KBr disk): ν_{max}/cm^{-1} 3421m/b, 3024w, 2924s, 2852s, 2371w, 2345w, 1734w, 1718w, 1701w, 1685w, 1654w, 1629w, 1607w, 1542w, 1515m/s, 1458m, 1421m, 1239m, 1168m, 1129m, 1019w, 963m, 939w, 855m, 802w, 714w. ^1H NMR (250 MHz, $CDCl_3$): ∂ 0.74 (t, poor resolution, 3H), 0.90-1.50 (m, 18H), 2.99 (d, $^3J_{PCH}$=13.2 Hz, 4H), 6.96 (s, 2H), 7.13 (d, $^3J_{HCCH}$=6.6 Hz, 4H), 7.35 (d, $^3J_{HCCH}$=8.1 Hz, 4H).

4.8 – Polymerisation *via* ADMET on the surface of NanoDots™

4.8.1 Analysis by ^{1}H NMR Spectroscopy

TUPO **25** coated NanoDots™-NLP121 (0.0050g, 9.9 x 10^{-6}, 1eqv) were dissolved in $CDCl_3$ (74ml) and stirred for 15 minutes under nitrogen. Grubbs 2nd generation catalyst **42** (0.0004g, 4.9 x 10^{-4} mmol, 5 mole percent) was dissolved in $CDCl_3$ (1ml) and injected into the reaction mixture. The reaction temperature was then increased to 40°C and the mixture stirred for 10 days. The progress of the reaction was monitored by ^{1}H NMR spectroscopy. Aliquots of the reaction mixture were removed and analysed on days 2, 3, 6 and 7. A further 5 mole percent of Grubbs 2nd generation catalyst was added to the reaction mixture on day 7. The reaction was allowed to continue as prior to the addition with analysis as before on days 8, 9 and 10. DMSO (0.07ml) was added to deactivate the catalyst and the mixture stirred for 48 hours. The reaction mixture was then split in two portions. One half of the reaction mixture was filtered through a pad of silica. The NanoDots ™ adsorbed irreversibly to the silica, an attempt to wash them off with a range of solvents failed. The second half of the reaction mixture was precipitated with and equal volume of ethanol, subsequent centrifugation afforded a coloured pellet that was dried to a constant mass under vacuum (0.0021g). An attempt to resuspend the powder with the aid of sonication in a range of deuterated solvents ($CDCl_3$, d-toluene, d-benzene, d-DMF, d-methanol and d-DMSO) failed. ^{1}H NMR (250 MHz, $CDCl_3$): **Day 2:** ∂ 0.00 (s, grease), 1.1-1.2 (m, aliphatic), 1.53 (s, H_20), 1.83 (t), 3.73 (t), 4.90 (dd, olefinic, starting material, ***x***), 5.28 (s, olefinic, product, ***y***), 5.76 (m, olefinic, starting material, ***z***). **Day 3:** ∂ 0.00 (s, grease), 1.1-1.2 (m, aliphatic), 1.53 (s, H_20), 1.83 (t), 3.73 (t), 4.90 (dd, olefinic, starting material, ***x***), 5.28 (s, olefinic, product, ***y***), 5.76 (m, olefinic, starting material, ***z***). **Day 6:** ∂ 0.00 (s, grease), 1.1-1.2 (m, aliphatic), 1.53 (s,

H_20), 1.83 (t), 3.73 (t), 4.90 (dd, olefinic, starting material, ***x***), 5.28 (s, olefinic, product, ***y***), 5.76 (m, olefinic, starting material, ***z***). **Day 7:** ∂ 0.00 (s, grease), 1.1-1.2 (m, aliphatic), 1.53 (s, H_20), 1.83 (t), 3.73 (t), 4.90 (dd, olefinic, starting material, ***x***), 5.28 (s, olefinic, product, ***y***), 5.76 (m, olefinic, starting material, ***z***). **Day 8:** ∂ 0.00 (s, grease), 1.1-1.2 (m, aliphatic), 1.53 (s, H_20), 1.83 (t), 3.73 (t), 4.90 (dd, olefinic, starting material, ***x***), 5.28 (s, olefinic, product, ***y***), 5.76 (m, olefinic, starting material, ***z***). **Day 9:** ∂ 0.00 (s, grease), 1.1-1.2 (m, aliphatic), 1.53 (s, H_20), 1.83 (t), 3.73 (t), 4.90 (dd, olefinic, starting material, ***x***), 5.28 (s, olefinic, product, ***y***), 5.76 (m, olefinic, starting material, ***z***). **Day 10:** ∂ 0.00 (s, grease), 1.1-1.2 (m, aliphatic), 1.53 (s, H_20), 1.83 (t), 3.73 (t), 4.90 (dd, olefinic, starting material, ***x***), 5.28 (s, olefinic, product, ***y***), 5.76 (m, olefinic, starting material, ***z***).

Day	**Ratio of starting material olefinic peaks to product olefinic peak. $(x+z) : y$**	**Percentage polymerisation**
2	2.0 : 1.0	$67_{(x+y)} : 33_z$
3	1.1 : 1.0	$53_{(x+y)} : 47_z$
6	1.0 : 1.5	$39_{(x+y)} : 61_z$
7 (+5 mol% catalyst)	1.0 : 1.7	$37_{(x+y)} : 63_z$
8	1.0 : 3.0	$25_{(x+y)} : 75_z$
9	1.0 : 4.7	$17_{(x+y)} : 83_z$
10	1.0 : 3.9	$20_{(x+y)} : 80_z$

Table 18: Percentage composition for the integration of the monomer and polymeric olefinic signals

4.8.2 Effect of Serial dilution on solubility the surface polymerised ADMET product

Five different amounts of TUPO **25** coated NanoDots™ -NLP121 were dissolved in $CDCl_3$ (27ml) and stirred for 15 minutes under nitrogen (Refer to table below). A stock solution of Grubbs 2nd generation catalyst **42** (10 mole percent) was made up in $CDCl_3$ and injected into the reaction mixture. The reaction temperature was then increased to 40°C and the reactions stirred for 8 days. DMSO (0.07ml) was added to each dilution to deactivate the catalyst and the mixture stirred for 48 hours. The volume of the reaction mixtures was then reduced to ~2ml under reduced pressure. The NanoDots™ were then precipitated with an equal volume of methanol and centrifugation. The appearance and solubility (with sonication) in $CDCl_3$ of the pellets produced from the different reaction dilutions evaluated.

Amount of NanoDot™	Amount of Catalyst used	Appearance	Solubility in $CDCl_3$
2.000mg	0.55mg	Red powder	Insoluble
1.000mg	0.27mg	Red powder	Insoluble
0.500mg	0.14mg	Yellow/brown powder	Insoluble
0.2500mg*	0.07mg	Yellow/orange powder	Insoluble
0.1250mg**	0.03mg	Yellow/brown powder	Insoluble

* Two 0.2500mg reactions were set up providing 0.5mg total material for evaluation
** Four 0.1250mg reactions were set up providing 0.5mg total material for evaluation

Table 19: Solubility of polymer coated NanoDots™ prepared in increasing reaction volumes

4.8.3 Analysis by ^{31}P NMR spectroscopy

4.8.3i Grubbs 2nd generation Catalyst 42

TUPO **25** coated NanoDots™-NLP121 (0.0050g, 9.9 x 10^{-6} mol, 1eqv) were dissolved in $CDCl_3$ (14ml) and stirred for 15 minutes under nitrogen (Bulk scale reaction mixture). A sample of the mixture (~1.0ml) was removed to a sample vial and placed in the freezer for later analysis of the reaction mixture at T=0. Grubbs 2nd generation catalyst **42** (0.0008g, 9.9 x 10^{-7} mol, 5 mole percent eqv) was dissolved in $CDCl_3$ (1ml) and injected into the reaction mixture and the temperature increased to 40°C. The reaction mixture was then stirred at 40°C for 15 minutes, a second sample of the mixture was then removed and transferred to an NMR tube (NMR scale reaction mixture). The NMR sample was then immediately placed into the NMR spectrometer at 40°C where the reaction was monitored by ^{31}P NMR for 168 hours. Severn ^{31}P experiment were run for 12 hours each time. The bulk reaction was stirred at 40°C under nitrogen for 17 days. The reaction volume was then reduced to ~1.0 ml under reduced pressure and analysed by ^{1}H and ^{31}P NMR spectroscopy. NMR scale reaction: ^{31}P NMR (121.5 MHz, $CDCl_3$, Referenced to 85% phosphoric acid) **T=0** ∂ 49.2., **T=1** ∂ 48.6, 49.1, 50.4., **T=2** ∂ 49.0, 50.1, 50.4., **T=3** ∂ 48.8, 50.3., **T=4** ∂ 48.9, 50.2., **T=5** ∂ 48.9, 50.3., **T=6** ∂ 48.9, 50.0., **T=7** ∂ 49.1, 50.4., **T=8** ∂ 48.9, 50.3. Bulk scale reaction: ^{1}H NMR (250 MHz, $CDCl_3$) ∂ 0.00 (s, grease), 0.70-2.50 (m, aliphatic), 4.20 (m, impurity), 4.90 (dd, olefin, starting material), 5.30 (bs, olefinic, product), 5.70-5.90 (m, olefinic, starting material), 6.80-7.70 (m, impurity). ^{31}P NMR (121.5 MHz, $CDCl_3$, Referenced to 85% phosphoric acid) ∂ 34.5, 40.7, 50.2, 51.4, 53.9, 59.6, 60.0-67.6 (overlapping broad signals).

4.8.3ii Hoveyda-Grubbs 2nd generation Catalyst 43

TUPO **25** coated NanoDots™-NLP121 (0.0050g, 9.9 x 10^{-6} mol, 1eqv) were dissolved in $CDCl_3$ (14ml) and stirred for 15 minutes under nitrogen (Bulk scale reaction mixture). A sample of the mixture (~1.0ml) was removed to a sample vial and placed in the freezer for later analysis of the reaction mixture at T=0. Hoveyda-Grubbs 2nd generation catalyst **43** (0.0006g, 9.9 x 10^{-7} mol, 5 mole percent eqv) was dissolved in $CDCl_3$ (1ml) and injected into the reaction mixture and the temperature increased to 40°C. The reaction mixture was then stirred at 40°C for 15 minutes, a second sample of the mixture was then removed and transferred to an NMR tube (NMR scale reaction mixture). The NMR sample was then immediately placed into the NMR spectrometer at 40°C where the reaction was monitored by ^{31}P NMR for 36 hours after which the NMR scale reaction was abandoned due to poor resolution. Three ^{31}P experiment were run for 12 hours each time. The bulk reaction was stirred at 40°C under nitrogen for 10 days. The reaction volume was then reduced to ~1.0 ml under reduced pressure and analysed by ^{1}H and ^{31}P NMR spectroscopy. NMR scale reaction: ^{31}P NMR (121.5 MHz, $CDCl_3$, Referenced to 85% phosphoric acid) **T=0** ∂ 49.0., **T=1** ∂ 49.0, **T=2** ∂ 49.0, **T=3** ∂ 49.0. Bulk scale reaction: ^{1}H NMR (200 MHz, $CDCl_3$) ∂ 0.00 (s, grease), 0.70-2.50 (m, aliphatic), 4.20 (m, impurity), 4.90 (m very small, olefin, starting material), 5.30 (bs very small, olefinic, product), 5.70-5.90 (m very small, olefinic, starting material), 7.40-7.70 (m, impurity). ^{31}P NMR (121.5 MHz, $CDCl_3$, Referenced to 85% phosphoric acid) ∂ 49.5, 63.0-66.0 (overlapping broad signals).

4.8.4 Analysis by DOSY ^{1}H NMR Spectroscopy

4.8.4i-NLP121

TUPO **25** coated NanoDots™-NLP121 (0.0300g, 5.9 x 10^{-5} mol, 1eqv) were dissolved in $CDCl_3$ (85ml) and stirred for 15 minutes under nitrogen. Grubbs 2nd generation catalyst **42** (0.0050g, 5.9 x 10^{-6} mol, 10 mole percent eqv) was dissolved in $CDCl_3$ (5ml) and injected into the reaction mixture and the temperature increased to 40°C. The reaction mixture was then stirred at 40°C for 3 weeks. The reaction volume was then reduced to ~1.0 ml under reduced pressure and passed through a 20nm filter. IR (KBr disk):ν_{max}/cm^{-1} 3069w, 2924s, 2853s, 1458w/m, 1262w/m, 1163m, 1094m, 1023w, 909w, 802w. ^{1}H NMR (400 MHz, $CDCl_3$, DOSY): ∂_H 0.00 (s, grease, D=0.6 x $10^{-10}m^2s^{-1}$) 0.80-1.8 (m, D=1.2-4.0 x $10^{-10}m^2s^{-1}$), 1.90 (bs, D=6.5-8.2 x $10^{-10}m^2s^{-1}$), 2.00 (bm, D=0.8 x $10^{-10}m^2s^{-1}$), 2.15 (m, D=3.8-4.2 x $10^{-10}m^2s^{-1}$), 3.80 (s, D=14.4-15.6 x $10^{-10}m^2s^{-1}$), 3.99 (bm, D=3.8-4.3 x $10^{-10}m^2s^{-1}$), 4.90 (dd, olefinic, starting material, D=0.3-0.8 x $10^{-10}m^2s^{-1}$), 5.32 (bm, olefinic, product, D=1.0-1.2 x $10^{-10}m^2s^{-1}$) 5.97 (ddt, olefinic, starting material, D=0.4-0.9 x $10^{-10}m^2s^{-1}$), 6.80-7.10 (m, D=3.6-4.5 x $10^{-10}m^2s^{-1}$), 7.20-7.50 (D=5.5-6.1 & 7.8-10.6 x $10^{-10}m^2s^{-1}$). ^{31}P NMR (121.5 MHz, $CDCl_3$, Referenced to 85% phosphoric acid) ∂ 39.7, 40.3, 49.3, 49.6, 50.1, 58.6, 60.1. Combustion analysis: 14.29% C, 2.66% H, 0.12% N, 0.54% P and 33.99% Cd. PL max = 570nm

To quantify the amount of TUPO **25** polymer that can be removed by washing and precipitation with methanol the molar ratio of P to Cd for a sample of washed NanoDots™ was calculated.

33.99% of the total sample was Cd, therefore in 100g there would be 33.99g of Cd.

The number of moles in 33.99g of Cd

= 33.99/112.4 = 0.30 moles of Cd

0.54% of the total sample was P, therefore in 100g there would be 0.54g of P.

The number of moles in 0.54g of P

= 0.54/31.0 = 0.02 moles of P

Therefore the molar ratio of P to Cd is 0.02 to 0.30

For every one mole of Cd there is 0.07 moles of P in the sample of washed TUPO-polymer coated NanoDots™

4.8.4ii SD396

Three lots of TUPO **25** coated NanoDots™-SD396 (0.0100g, 2.0 x 10^{-5} mol, 1eqv) were dissolved in $CDCl_3$ (19ml) and placed into three carousel tubes. The solutions were stirred for 15 minutes under nitrogen. Grubbs 2nd generation catalyst **42** (0.0016g, 1.7 x 10^{-3} mol, 10 mole percent eqv) was dissolved in $CDCl_3$ (1ml) and injected into the reaction mixture and the temperature increased to 40°C. The reaction mixture was then stirred at 40°C for 3 weeks. The reaction volume was then reduced to ~1.0 ml under reduced pressure and the resulting solution dialysed. The solution was placed into a D-tube dialyser that was then suspended into 250ml of $CDCl_3$ for 1 hour, before being suspended in 250ml of fresh $CDCl_3$. IR (KBr disk):ν_{max}/cm^{-1} 3074w, 2963m, 2926s, 2855m, 1734m, 1459w/m, 1262s, 1097s, 1023s, 802s. ^{1}H NMR (400 MHz, $CDCl_3$, DOSY): ∂_H 0.00 (s, grease, D=0.4-1.0 x $10^{-10}m^2s^{-1}$) 0.80-1.9 (m, D=1.4-6.2 x $10^{-10}m^2s^{-1}$), 2.00 (dd, D=2.4-3.6 x $10^{-10}m^2s^{-1}$), 2.35-2.5 (m, D=3.0-4.8 x $10^{-10}m^2s^{-1}$), 3.9-4.1 (m,

D=3.0-4.8 x $10^{-10}m^2s^{-1}$), 4.80 (dd, olefinic, starting material, D=3.1-3.8 x $10^{-10}m^2s^{-1}$), 5.27 (s, D=13.2-19.5 x $10^{-10}m^2s^{-1}$), 5.35 (bs, D=3.4-4.2 x $10^{-10}m^2s^{-1}$), 5.79 (bm, olefinic, product, D=3.0-4.2 x $10^{-10}m^2s^{-1}$), 5.97 (ddt, olefinic, starting material, D=0.4-0.9 x $10^{-10}m^2s^{-1}$), 6.80-7.10 (m, D=1.8-4.1 x $10^{-10}m^2s^{-1}$), 6.90-7.20 (m, D=5.2-13.8 x $10^{-10}m^2s^{-1}$). PL max = 495nm

4.8.4iii MC556

Two lots of TUPO **25** coated NanoDots™-MC556 (0.0100g, 2.0 x 10^{-5} mol, 1eqv) were dissolved in $CDCl_3$ (19ml) and placed into three carousel tubes. The solutions were stirred for 15 minutes under nitrogen. Grubbs 2nd generation catalyst 42 (0.0016g, 1.7 x 10^{-3} mol, 10 mole percent eqv) was dissolved in $CDCl_3$ (1ml) and injected into the reaction mixture and the temperature increased to 40°C. The reaction mixture was then stirred at 40°C for 3 weeks. The reaction volume was then reduced to ~1.0 ml under reduced pressure and the resulting solution dialysed. The solution was placed into a D-tube dialyser that was then suspended into 250ml of $CDCl_3$ for 1 hour, before being suspended in 250ml of fresh $CDCl_3$. IR (KBr disk):ν_{max}/cm^{-1} 3400wb, 3067w, 2926s, 2855m, 1460w/m, 1262m, 1099m, 1027m, 802m, 694w. ^{1}H NMR (400 MHz, $CDCl_3$, DOSY): ∂ 0.00 (s, grease, D=0.1-1.0 x $10^{-10}m^2s^{-1}$) 0.90 (bm, D=4.2-6.8 x $10^{-10}m^2s^{-1}$), 1.00-1.90 (m, D=4.6-7.3 & 7.8-12.0 x $10^{-10}m^2s^{-1}$), 2.00 (m, D=3.0-7.4 x $10^{-10}m^2s^{-1}$), 2.20-2.50 (m, D=3.0-5.6, 6.6-13.0 & 13.4-15.0 x $10^{-10}m^2s^{-1}$), 3.50 (s, D=24.3-25.6 x $10^{-10}m^2s^{-1}$), 3.65 (s, D=17.2-18.4 & 20.0-21.2 x $10^{-10}m^2s^{-1}$), 3.70 (m, D=20.0-21.2 x $10^{-10}m^2s^{-1}$), 4.10 (m, D=14.6-16.2 x $10^{-10}m^2s^{-1}$) 4.80 (dd, olefinic, starting material, D=4.4-5.3 x $10^{-10}m^2s^{-1}$), 5.2- (bm, olefinic, product, D=4.4-5.4 x $10^{-10}m^2s^{-1}$), 5.79 (ddt, olefinic, starting material, D=4.6-5.8 x $10^{-10}m^2s^{-1}$), 6.90-7.20 (m, D=4.0-5.4 x $10^{-10}m^2s^{-1}$), 5.70 (m, D=5.8-8.0 x $10^{-10}m^2s^{-1}$). PL max = 609nm

4.8.4iv MC610

Two lots of TUPO **25** coated NanoDots™-MC610 (0.0100g, 2.0 x 10^{-5} mol, 1eqv) were dissolved in $CDCl_3$ (19ml) and placed into three carousel tubes. The solutions were stirred for 15 minutes under nitrogen. Grubbs 2nd generation catalyst **42** (0.0016g, 1.7 x 10^{-3} mol, 10 mole percent eqv) was dissolved in $CDCl_3$ (1ml) and injected into the reaction mixture and the temperature increased to 40°C. The reaction mixture was then stirred at 40°C for 3 weeks. The reaction volume was then reduced to ~1.0 ml under reduced pressure and the resulting solution dialysed. The solution was placed into a D-tube dialyser that was then suspended into 250ml of $CDCl_3$ for 1 hour, before being suspended in 250ml of fresh $CDCl_3$. IR (KBr disk):ν_{max}/cm^{-1} 3400wb, 3067w, 2961m, 2925s 2854m, 1460w, 1262s, 1098s, 1021s, 800s. ^{1}H NMR (400 MHz, $CDCl_3$, DOSY): ∂ 0.00 (s, grease, D=0.4-1.0 x $10^{-10}m^2s^{-1}$), 0.80 (bm, D=3.0-5.4 x $10^{-10}m^2s^{-1}$), 1.00-2.00 (m, D=3.7-6.6, 6.8-8.8 & 10.4-13.0 x $10^{-10}m^2s^{-1}$), 2.10-2.70 (m, D=2.6-5.2 x $10^{-10}m^2s^{-1}$), 3.50 (s, D=23.4-25.2 x $10^{-10}m^2s^{-1}$), 3.65 (s, D=5.2-10.4 x $10^{-10}m^2s^{-1}$), 3.70 (m, D=18.6-21.0 x $10^{-10}m^2s^{-1}$), 3.90-4.20 (m, D=14.6-16.2 & 13.4-15.0 x $10^{-10}m^2s^{-1}$) 4.90 (dd, olefinic, starting material, D=4.4-5.0 x $10^{-10}m^2s^{-1}$), 5.2- (bm, olefinic, product, D=3.0-5.2 x $10^{-10}m^2s^{-1}$), 5.79 (ddt, olefinic, starting material, D=3.9-5.0 x $10^{-10}m^2s^{-1}$), 6.80-7.10 (m, D=2.4-5.4 x $10^{-10}m^2s^{-1}$), 5.40-8.7 (m, D=4.2-6.7 x $10^{-10}m^2s^{-1}$). PL max = 551nm

4.8.5 Stability of polymer-coated NanoDots™-MC610 upon exposure to a range of reagents

The stability of polymer-coated NanoDots™ -MC610 to a variety of different reagents was evaluated by comparing the PL spectra of a solution of polymer-coated

NanoDots™ before the addition of any reagent with the PL spectra recorded after exposure to the reagent. A stock solution of polymer-coated MC610 NanoDots™ (10mg) in THF (8.0ml) was prepared and the mixture shaken for 10 minutes to ensure complete dissolution. The PL spectra of 1ml of the NanoDot™ solution was recorded for comparison with the PL spectra of the NanoDots ™ after addition of the reagent. Solutions of THF (10ml) containing 0.00025 moles of each reagent were prepared according to **Table 12**. 0.5ml of the reagent solution was added to 0.5ml of the NanoDot™ solution, the mixture was shaken and the PL spectra run immediately.

Table 20 provides the PL max of the solutions of NanoDots™ after exposure to the reagents listed above. The actual spectra can be viewed in (Appendix D, **Figure 98**).

Reagent	PL max after addition (nm)
No Reagent	1138.50
Trifluroacetic acid (TFA)	373.25
Aluminium trichloride (AlCl3)	168.25
1,8-Diazabicyclo[5.4.0]undec-7-ene (DBU)	1737.00
Potassium hydroxide (KOH)	1253.75
Iodobenzoic acid (IBX)	911.00
Potassium permanganate (KMnO4)	537.00
Lithium aluminium hydride (LiAlH4)	211.50
n-Butyl lithium (nBuLi)	288.75
Vinyl magnesium bromide (Vinyl MgBr)	172.50
Hydrogen Bromide (HBr)	492.50

Table 20: PL maximum emission recorded after exposure to each reagent for polymer-coated NanoDots™

4.9 – NanoDot™ Encoded Resin

4.9.1 Preparation of 2% cross-linked resin

Styrene (1.0g, 1.1ml, 9.6mmols, 1 eqv), and divinylbenzene (0.025g, 0.027ml, 0.192mmols, 0.02 eqv) were placed in a carrousel tube and stirred at room temperature for 15 minutes. AIBN (0.012g, 0.0729mmols, $7.6x10^{-3}$eqv) was then added to the monomer and the mixture stirred for a further 10mins. A 1% solution of polyvinylalcohol (10ml) was added and stirring continued for 4 hours. The temperature of the reaction was then raised to 72°C and the suspension stirred under nitrogen for 4 hours. The suspension was then allowed to stand for 24 hours before washing. The suspension was placed into a sieve and the resin washed with tap water until the washings ran clear. The beads were then transferred to a sintered glass filter and washed with 100ml of distilled water and methanol (1:1), 100ml of methanol 100ml of methanol and THF (1:1), 100ml of THF and 100ml of methanol. The resin was then transferred to the vac oven and dried o a constant weight.

4.9.2 Preparation of 20% cross-linked resin

Styrene (1.0g, 1.1ml, 9.6mmols, 1 eqv), and divinylbenzene (0.25g, 0.27ml, 192mmols, 0.2 eqv) were placed in a carrousel tube and stirred at room temperature for 15 minutes. AIBN (0.012g, 0.0729mmols, $7.6x10^{-3}$eqv) was then added to the monomer and the mixture stirred for a further 10mins. A 1% solution of polyvinylalcohol (10ml) was added and stirring continued for 4 hours. The temperature of the reaction was then raised to 72°C and the suspension stirred under nitrogen for 4 hours. The suspension was then allowed to stand for 24 hours before washing. The suspension was placed into

a sieve and the resin washed with tap water until the washings ran clear. The beads were then transferred to a sintered glass filter and washed with 100ml of distilled water and methanol (1:1), 100ml of methanol 100ml of methanol and THF (1:1), 100ml of THF and 100ml of methanol. The resin was then transferred to the vac oven and dried o a constant weight.

4.9.3 Preparation of CMS functionalised resin

Styrene (27ml, 0.2mols, 1 eqv), divinylbenzene (14ml, 0.08mols, 0.2 eqv), CMS (31ml, 0.2mols), toluene (77ml) and AIBN (0.694g, $7.6x10^{-3}$eqv) were stirred and degassed for 30 minutes. A 1% solution of polyvinylalcohol (500ml) was degassed for 15minutes. The monomer mixture was then added to the PVA solution and the two stirred under nitrogen for 30 minutes. The temperature of the reaction was then raised to 72°C and the suspension stirred under nitrogen overnight. The suspension was then allowed to cool, then washed with tap water until the washings ran clear. The resin was transferred to a sintered glass filter and washed with 500ml of distilled water, distilled water and MeOH (250ml:250ml), MeOH (500ml), MeOH and THF (250ml:250ml), THF (500ml), THF and DCM (250ml:250ml), THF (500ml) and finally MeOH (500ml). The resin was then dried over suction then under vacuum to a constant weight (40.6g).

4.9.4 Preparation of 20% cross-linked resin containing DOMSPO coated NanoDots™

Styrene (46ml, 0.4mols, 1 eqv), divinylbenzene (18ml, 0.1mols, 0.2 eqv), DOMSPO coated SD396 NanoDots ™ (0.2400g) and AIBN (1.6420g, 0.01mols, $7.6x10^{-3}$eqv)

stirred and degassed for 30 minutes. A 1% solution of polyvinylalcohol (500ml) was degassed for 15minutes. The monomer mixture was then added to the PVA solution and the two stirred under nitrogen for 30 minutes. The temperature of the reaction was then raised to 72°C and the suspension stirred under nitrogen overnight. The suspension was then allowed to cool, then washed with tap water until the washings ran clear. The yellow resin was transferred to a sintered glass filter and washed with 500ml of distilled water, distilled water and MeOH (250ml:250ml), MeOH (500ml), MeOH and THF (250ml:250ml), THF (500ml), THF and DCM (250ml:250ml), THF (500ml) and finally MeOH (500ml). The resin was then dried over suction then under vacuum to a constant weight (42.5g)and the PL of the resin recorded. The resin was then Soxhlet extracted in hot DCM for 8 hours dried and the PL recorded again. PL max (before soxhelt)=524nm. PL max (after soxhelt)=520nm

4.9.5 Preparation of CMS functionalised 20% cross-linked resin containing DOMSPO coated NanoDots™

Styrene (0.80ml, 8mmols, 1 eqv), divinylbenzene (0.36ml, 2mmols, 0.2 eqv), CMS (0.14ml, 1mmol, 0.1 eqv), DOMSPO coated SD396 NanoDots ™ (5.000mg) and AIBN (0.0340g, 0.2mmols, $7.6x10^{-3}$eqv) stirred and degassed for 30 minutes. A 1% solution of polyvinylalcohol (10ml) was degassed for 15minutes. The monomer mixture was then added to the PVA solution and the two stirred under nitrogen for 30 minutes. The temperature of the reaction was then raised to 72°C and the suspension stirred under nitrogen overnight. The suspension was then allowed to cool and washed with tap water until the washings ran clear. The yellow resin was transferred to a sintered glass filter and washed with 50ml of distilled water, distilled water and MeOH (25ml:25ml),

MeOH (50ml), MeOH and THF (25ml:25ml), THF (50ml), THF and DCM (25ml:25ml), THF (50ml) and finally MeOH (50ml). The resin was then dried over suction then under vacuum to a constant weight (0.93g) and the PL of the resin recorded. The resin was then soxhlet extracted in hot DCM for 8 hours dried and the PL recorded again. PL max (before soxhlet)=505nm. PL max (after soxhlet)=505nm (Appendix D, **Figure 101**)

CHAPTER 5

REFERENCES

[1] M. Green and P. O'Brien, *J. Chem. Soc., Chem. Commun.*, 1999, 2235.
[2] News feature, *Nature*, 2001, **413**, 450.
[3] www.qdots.com.
[4] A. Sutherland, *Curr.Opin. Solid State Mater. Sci.*, 2002, **6**, 365.
[5] C. B. Murray and C. R. Kagan and M.G Bawendi, *Annu. Rev. Mater. Sci.*, 2000, **30**, 545.
[6] H. Weller, *Angew. Chem., Int. Ed. Engl.*, 1993, **32**, 41.
[7] M. L. Steigerwald and L. E. Brus, *Acc. Chem. Res.*, 1990, **23**, 183
[8] Johnathan Cox, *Chemistry in Britain.*, 2003, 21.
[9] N. Chestnoy, T. D. Harris, R. Hull and L. E. Brus., *J. Phys. Chem.* 1986, **90**, 3393.
[10] B. O. Dabbousi, J. Rodriguez-Viejo, F. V. Milulec, J. R. Heine, H. Mattoussi, R. Ober, K. F Jensen and M. G. Bawendi., *J Phys. Chem. B.*, 1997, **101**, 9463.
[11] M. G. Bawendi, A.R. Kortan, M. L. Steigerwald, L. E. Brus., *J Phys. Chem.*, 1989, **91**, 7282.
[12] Nanoparticles: From theory to application. Edited by Gunter Schmid., Wiley and Son., 2004.
[13] L. E. Brus, *J. Phys. Chem.*, 1986, **90**, 2555
[14] P. Dobson, *Commercial and Industrial Applications for Microeng. and Nanotech.*, 1999, **1**
[15] www.nanoco.biz
[16] W. C. W Chan, D. J. Maxwell, X. Gao, R. E. Bailey, M. Han, S. Nie., *Curr. Op. Biotech.*, 2002, **13**, 40.
[17] www.evidenttech.com
[18] N. Herron, Y. Wang and H. Eckert,. *J. Am. Chem. Soc.* 1990, **112**, 1322.
[19] M. Lazell and P. O'Brien., *Chem. Commun.*, 1999, 2041.
[20] P. S. Nair, N. Revaprasadu, T. Radhakrishnan and G. A. Kolawole., *J. Mater. Chem.*, 2001, **11**, 1555.
[21] M. Lazell and P. O'Brien., *J. Mater. Chem.*, 1999, **9**, 1381.
[22] B. Ludolph, M. A. Malik, P. O'Brien and N Revaprasadu., *Chem. Commun.*, 1998, 1849.
[23] D. J. Crouch, P. O'Brien, M. A. Malik, P. J. Skabara and S. P. Wright., *Chem. Commun.*, 2003, 1454.
[24] J. Hambrock, A. Birkner and R. A. Fischer., *J. Mater. Chem.*, 2001, **11**, 3197.
[25] N. Revaprasadu, M. Malik, P. O'Brien, M. Zulu and G. Wakefield., *J. Mater. Chem.*, 1998, **8**, 1885
[26] N. Revaprasadu, M. Malik, J. Carsten and P. O'Brien., *J. Mater. Chem.*, 1999, **9**, 2885.
[27] X. Peng, M. Schlamp, A. Kadavanich and A. Alivisatos., *J. Am. Chem. Soc.*, 1997, **119**, 7019.
[28] M. A. Hines and P. Guyot-Sionnest., *J. Phys. Chem.*, 1995, **100**, 468.
[29] N. Revaprasadu, M. Malik, P. O'Brien and G. Wakefield., *Chem. Commun.*, 1999, 1573.
[30] P. Reiss, J. Bleuse and A. Pron., *Nano Lett.*, 2002, **2**, 781.
[31] Y.Tian, T. Newton, A. Kotov, M. Guldi, J. Fendler,. *J. Chem. Phys.*, 1996, **100**, 8927.
[32] A. Mews, A. Eychmuller, M. Giersig, D. Schoos, H. Weller., *J. Phys. Chem.* 1994, **98**, 934.
[33] A. Eychmuller, A. Mews and H. Weller., *Chem. Phys. Lett.*, 1993, **208**, 59.
[34] J. Aldana, Y. Wang and X. Peng., *J. Am. Chem. Soc.*, 2001, **123**, 8844.
[35] J. Bowen Katari, V. Colvin and A. Alivisatos., *J Phys.Chem.*, 1994, **98**, 4109.
[36] G. Rafeletos, S. Norager and P. O'Brien., *J. Mater. Chem.*, 2001, **11**, 2524
[37] P. O'Brien, S. Cummins, D. Darcy, A. Dearden, O. Masala, N. Pickett, S. Ryley and A. Sutherland., *Chem. Commun.*, 2003, 2532.
[38] H. Skaff, M. Iiker, E. Coughlin, T. Emrick., *J. Am. Chem. Soc.*, 2002, **124**, 5729.
[39] W. Guo and X. Peng., *Chimie.*, 2003, **6**, 989.
[40] X. Peng, J. Wickham, A. Alivisatos., *J Am. Chem. Soc.*,1998, **120**, 5343.
[41] S. Pathak, S. Choi, N. Arnheim and M. Thompson., *J. Am. Chem. Soc.*, 2001, **123**, 4103.
[42] N. Charvet, P. Reiss, A. Roget, A. Dupuis, D. Grunwald, S. Carayon, F. Chandezon and T. Livache., *J. Mater. Chem.*, 2004, **14**, 2638.
[43] R. Hong, T. Emrick, V. Rotello., *J. Am. Chem. Soc.*, 2004, **126**, 13572.
[44] X. Peng, T. Wilson, A. Alivisatos and P. Schultz., *Angew. Chem. Int. Ed. Engl.*, 1997, **36**, 145.
[45] S. Wuister, I. Swart, F. Van Driel, S. Hickey and C. De Mello Donega., *Nano Lett.*, 2003, **3**, 503.
[46] W. Guo, J. Li, A. Wang and X. Peng., *J. Am. Chem. Soc.*, 2003, **125**, 3901
[47] H. Skaff and T. Emrick., *Chem Commun.*, 2003, 52.
[48] N. Myung, Y. Bae and A. Bard., *Nano Lett.*, 2003, **3**, 1053.
[49] S. Coe, W. Woo, M. Bawendi and V. Bulovle., *Nature*, 2002, **420**, 800
[50] M. Green., *Current Opinion in Solid state and Materials Science.*, 2002, **6**, 355.
[51] D. Crouch, S. Norager, P. O'Brien, J. Park, N. Pickett., *Phil. Trans. R. Soc. Lond. A.*, 2003, **361**, 297.
[52] V. LaMer and R. Dinegar., *J Am. Chem. Soc.*, 1950, **72**, 4847.
[53] I. Johnson and V. LaMer., *J Am. Chem. Soc.*, 1947, **69**, 1184.

[54] Y. Wada, Hiromitsu, J.Anand, T. Kitamura, T. Sakata, H. Mori and S. Yanagida., *J. Mater. Chem.*, 2001, **11**, 1936.
[55] Y. Wang and N. Herron., *J. Phys. Chem.*, 1987, **91**, 257.
[56] J. Mac Dougall, H. Eckert, G. Stucky, N. Herron, Y. Wang, K. Moller, T. Bein and D. Cox., *J Am. Chem. Soc.*, 1989, **111**, 8007.
[57] A. Seidel, J. Loos and B. Boddenberg., *J. Mater. Chem.*, 1999, **9**, 2495.
[58] E. Brigham, C. Weisbecker, W. Rudzinski and T. Mallouk., *Chem. Mater.*, 1996, **8**, 2121.
[59] T. Abe, Y. Tachibana, T. Uematsu and M. Iwamoto., *Chem. Commun.*, 1995, 1617.
[60] A. Kortan, R. Hull, R. Opila, M. Bawendi, M. Steigerwald, P. Carroll and L. Brus., *J. Am. Chem. Soc.*, 1990, **112**, 1327.
[61] J. Cha, H. Birkedal, L. Euliss, M. Bartl, M. Wong, T. Deming and G. Stucky., *J. Am. Chem. Soc.*, 2003, **125**, 8285.
[62] T. Hirai, H. Okubo and I. Komasawa., *J. Mater. Chem.*, 2000, **10**, 2592.
[63] S. Haggata, D. Cole-Hamilton and J. Fryer., *J. Mater. Chem.*, 1997, **7**, 1969.
[64] X. Li, C. Lindall, D. Foster and D. Cole-Hamilton., *J. Mater. Chem.*, 1994, **4**, 657.
[65] M. Meyer, C. Wallberg, C. Kurihara, J. Fendler., *Chem. Commun.*, 1984, 90.
[66] C. Murray, D. Norris and M. Bawendi., *J. Am. Chem. Soc.*, 1993, **115**, 8706.
[67] T. Trindade and P. O'Brien, *Adv. Mater.*, 1996, **8**, 161.
[68] T. Trindade and P. O'Brien, *Chem. Mater.*, 1997, **9**, 523.
[69] L. Pavesi, L. Negro, C. Mazzoleni, G. Franzo and F.Priolo., *Nature.*, 2000, **408**, 440.
[70] B. Dubertret, P. Skourides, D. Norris, V. Noireaux, A. Brivanlou and A. Libchaber., *Science.*, 2002, **298**, 1759.
[71] M. Han, X. Gao, J. Su and S. Nie., *Nature biotectnology.*, 2001, **19**, 631.
[72] D. Maclean, J. Balwdwin, V. Ivanov, Y. Kato, A. Shaw, P. Schnider and E. Gordon., *J Comb. Chem.*, 2000, **2**, 562.
[73] F. Balkenhohl, C. von dem Bussche-Hunnefeld, A. Lansky and C. Zechel., *Angew. Chem. Int. Engl.*, 1996, **35**, 2288.
[74] R. Merrifield., *Angew. Chem. Int. Engl.*, 1985, **24**, 799.
[75] S. Kaldor and M. Siegel., *Current Opinion in Chemical Biology.*, 1997, **1**, 101.
[76] G. Bhalay., *Chemistry in Britain.*, 1999, 25.
[77] D. Sherrington., *Chem. Commun.*, 1998, 2275.
[78] D. Sherrington, A. Lanver, H. Schmalz, B. Wilson, X. Ni and S. Yuan., *Angew. Chem. Int. Ed.*, 2002, **41**, 2656.
[79] M. McCairn., *Solid Phase Combinatorial Chemistry and Scintillation Proximity Assay.*, Ph.D Thesis, 2003, Aston University.
[80] S. Rana, P. White and M. Bradley., *J. Combi. Chem.*, 2001, **3**, 9.
[81] S. Wang., *J. Am Chem. Soc.*, 1973, **95**, 1328.
[82] H. Rink., *Tetrahedron lett.*, 1987, **28**, 3787.
[83] A.Czarik., *Curr. Opin. Chem. Biol.*, 1997, **1**, 60
[84] H. M. Greysen, R. Meloen, S. Barleling., *Proc. Natl. Acad. Sci. USA.*, 1984, **81**, 3998.
[85] X. Xiao, Z. Parandoosh and M. Nova., *J. Org. Chem.*, 1997, **62**, 6029.
[86] TranSort™,.www.irori.com
[87] J. Kerr, S. Banville and R. Zuckermann., *J. Am. Chem. Soc.*, 1993, **115**, 2529.
[88] W. Still., *Acc. Chem. Res.*, 1996, **29**, 155.
[89] M. Ohlmeyer, R. Swanson, L. Dillard, J. Reader, G. Asouline, R. Kobayashi, M. Wigler and W. Still., *Proc. Natl. Acad. Sci. USA.*, 1993, **90**, 10922.
[90] B. Egner, S. Rana, H. Smith, N. Bouloc, J. Frey, W. Brocklesby and M. Bradley., *Chem Commun.*, 1997, 735.
[91] B. Battersby, G. Lawrie, A. Johnston and M. Trau., *Chem Commun.*, 2002, 1435.
[92] Y. Li, E. Liu, N.Pickett, P. Skabara, S. Cummins, S. Ryley, A. Sutherland and P. O' Brien., *J. Mater. Chem.*, 2005, **15**, 2.
[93] Z. Qiao, G. Xie, J. Huang, S. Zhao and X. Chen., *J. Mater. Chem.*, 2002, **12**, 611.
[94] P. Mulvaney, L. Liz-Marzan, M. Giersig and T. Ung., *J. Mater. Chem.*, 2000, **10**, 1259.
[95] T. Nann and P. Mulvaney., *Angew. Chem. Int. Ed.*, 2004, **43**, 5393.
[96] T. von Wern and T. Patten., *J. Am. Chem. Soc.*, 2001, **123**, 7497.
[97] S. Nuss, H. Bottcher, H. Wurm and M. Hallensleben., Angew. Chem. Int. Ed., 2001, 40, 4016.
[98] T. Mandal, M. Fleming and D. Walt., *Nano. Lett.*, 2002, **2**, 3.
[99] Y. Wang, J. Li, H. Chen and X. Peng., *J. Am. Chem. Soc.*, 2002, **124**, 2293.

[100] M. Wu, S. O' Neill, L. Brousseau, W. Mc Connell, D. Shultz, R. Linderman and D. Feldheim., *Chem Commun.*, 2000, 775.
[101] T. Trnka and R. Grubbs., *Acc. Chem. Res.*, 2001, **34**, 18.
[102] K. Ivin and C. Mol., *Olefin Metathesis & Metathesis Polymerization.*, Academic Press., London, 1997
[103] M. Rouhi., *Chem. & Eng. News.*, 2002, Dec 23, **34**.
[104] N. Calderon., *Acc. Chem. Res.*, 1972, **5**, 127.
[105] N. Calderon, Y. Chen and W. Scott., *Tetrahedron Lett.*, 1967, **34**, 3327.
[106] N. Calderon, E. Ofstead, J. Ward, W. Judy, K. Scott,. *J. Am. Chem. Soc.*, 1968, **90**, 4133.
[107] R. Grubbs, T. Brunck., *J. Am. Chem. Soc.*, 1972, **94**, 2538.
[108] R. Grubbs., *Tetrahedron.*, 2004, **60**, 7117.
[109] G. Lewandos, R. Pettit., *J. Am. Chem. Soc.*, 1971, **93**, 7087.
[110] Y. Chauvin and J. Herrisson., *Makromol. Chem.*, 1971, **141**, 161.
[111] J. McGinnis and T. Katz., *J. Am. Chem. Soc.*, 1975, **97**, 1592.
[112] J. Love, M. Sanford, M. Day and R. Grubbs., *J. Am. Chem. Soc.*, 2003, **125**, 10103.
[113] M. Sanford, J. Love and R. Grubbs., *J. Am. Chem. Soc.*, 2001, **123**, 6543.
[114] M. Sanford, M. Ulman and R. Grubbs., *J. Am. Chem. Soc.*, **123**, 749.
[115] Encyclopedia of Nucleur Magnetic Resonance., Edited by D. Grant and R.Harris., Vol. 9., Wiley and Son Ltd., 2002., (Chapter by G. Morris., Diffusion ordered Spectroscopy)
[116] R. Huo, R. Wehrens, J. van Duynhoven and L. Buydens., *Analytica Chimica Acta.*, 2003, **490**, 231.
[117] H. Barjat, G. Morris, S. Smart, A. Swanson and S. Williams., *J. Magn. Reson. B.*, 1995, **108**, 170.
[118] Y. Cohen, L. Avram and L. Frish., *Angew. Chem. Int. Ed.*, 2005, **44**, 520.
[119] Bruker, User guide for XWinNMR 3.1 / 3.5, Version 1.03., 2004
[120] B. Antalek. Concepts in *Magnetic Resonance.*, 2002, **14**, 225.
[121] R. Miller, C. Miller, W. Rogers and L. Hamilton., *J. Am. Chem. Soc.*, 1956, **79**, 424.
[122] W. Williams and L.Hamilton., *J. Am.Chem. Soc.*, 1955, 77, 3411.
[123] H.Hays., *J.Org. Chem.*, 1968, **33**, 3690.
[124] N. Platzer, F. Dardoise, W. Bergeret, J. Gautier and S. Raynal., *phosphorus & Sulfur*, 1986, **27**, 275.
[125] R. Williams and L. Hamilton., *J. Am. Chem. Soc.*, 1952, **74**, 5418.
[126] J. Hendrickson, M. Maddox, J. Sims and H Kaesz., *Tetrahedron.*, 1964, **20**, 449.
[127] The Chemistry of Organophosphorus Compounds., Edited by F. Hartley., Vol 2., Wiley and Son Ltd., 1992 (Chapter by D. Davidson. Spectroscopy of phosphine chalcogenides.)
[128] S.Grim and L. Satek., *J. Inorg. Nucl.Chem.*, 1977, **39**, 499.
[129] T. Albright , W.Freeman and E. Schwizer., *J. Org.Chem.*, 1975, **40**, 3437.
[130] G. Gray, S. Cremer and K.Marsi., *J. Am. Chem. Soc.*, 1976, **98**, 2109.
[131] G. Gray and S. Cremer., *J. Org. Chem.*, 1972, **37**, 3458.
[132] March,s Advanced Organic Chemistry: Reactions, Mechanisms and Structure., M. Smith and J. March., Fifth edition, Wiley Interscience., 2001.
[133] Synthesis of Carbon-Phosphorus Bonds., R.Engel and J.Cohen., Second edition., CRC press., 2004.
[134] E. Corey and A. Venkateswarlu., *J. Am Chem. Soc., 1972*, **94**, 6190.
[135] T. Nelson and R. Crouch., *Synthesis.*, 1996, 1031.
[136] Spectroscopic methods in organic chemistry., Revised by D. Williams and I. Fleming., Fourth edition., McGraw-Hill., 1989.
[137] C. Griffin and T. Mitchell., *J. Am. Chem. Soc.*, 1965, **30**, 1935.
[138] P. Clark, J. Curtis, P. Garrou and G. Hartwell., *Can. J. Chem.*, 1974, **52**, 1714.
[139] J. Davies, J. Mierzwiak and R. Syed., *J. Coord. Chem.*, 1988, **17**, 25.
[140] The Chemistry of Organophosphorus Compounds., Edited by F. Hartley.,Vol 2., Wiley and Son Ltd., 1992., (Chapter by D. Davidson. Spectroscopy of phosphine chalcogenides).
[141] S.Grim and L. Satek., *J. Inorg. Nucl..Chem.*, 1977, **39**, 499.
[142] P. Haake, R. Cooke and G.Hurst., *J. Am. Chem. Soc.*, 1967, **89**, 2650.
[143] C. Santelli-Rovier., Synthesis., 1987, 64.
[144] The Chemistry of Organophosphorus Compounds., Edited by F. Hartley., Vol 2., Wiley and Son Ltd., 1992., (Chapter by T. Lobana., Coordination chemistry of phosphine chalcogenides).
[145] T.Lobana, *Prog. Inorg. Chem.*, 1989, **37**, 495.
[146] B.Yde, N. Yousif, U.Pedersen, I. Thomsen and S. Lawesson., *Tetrahedron,* 1984, **40**, 2047.
[147] S. Ley, A. Leach and R. Storer., *J. Chem. Soc., Perkin. Trans. 1.*, 2001, 358.
[148] Z. Tashma., *J. Org. Chem.*, 1983, **48**, 3966.
[149] M. Cava and M. Levinson., *Tetrahedron.*, 1985, **41**, 5061.
[150] H. Skaff and T. Emrick., *Angew. Chem. Int. Ed.*, 2004, **43**, 5583.
[151] Personal Communication N. Pickett. (NanoCo)

[152] E.Dias, S. Nguyen and R. Grubbs., *J. Am. Chem. Soc.*, 1997, **119**, 3887.
[153] Personal Communication Mr. P. Ashton, Birmingham University.
[154] Personal Communication Dr. M. Perry, Aston University.
[155] Personal Communication Pr. G. Morris, Manchester University.
[156] Physical Chemistry of Macromolecules., C. Tanford., Wiley and Son., Second edition., 1963.
[157] J.Homer and M.C.Perry, *J. Chem. Soc., Chem Commun.* 1994, 373.

CHAPTER 6

APPENDICES

Appendix A

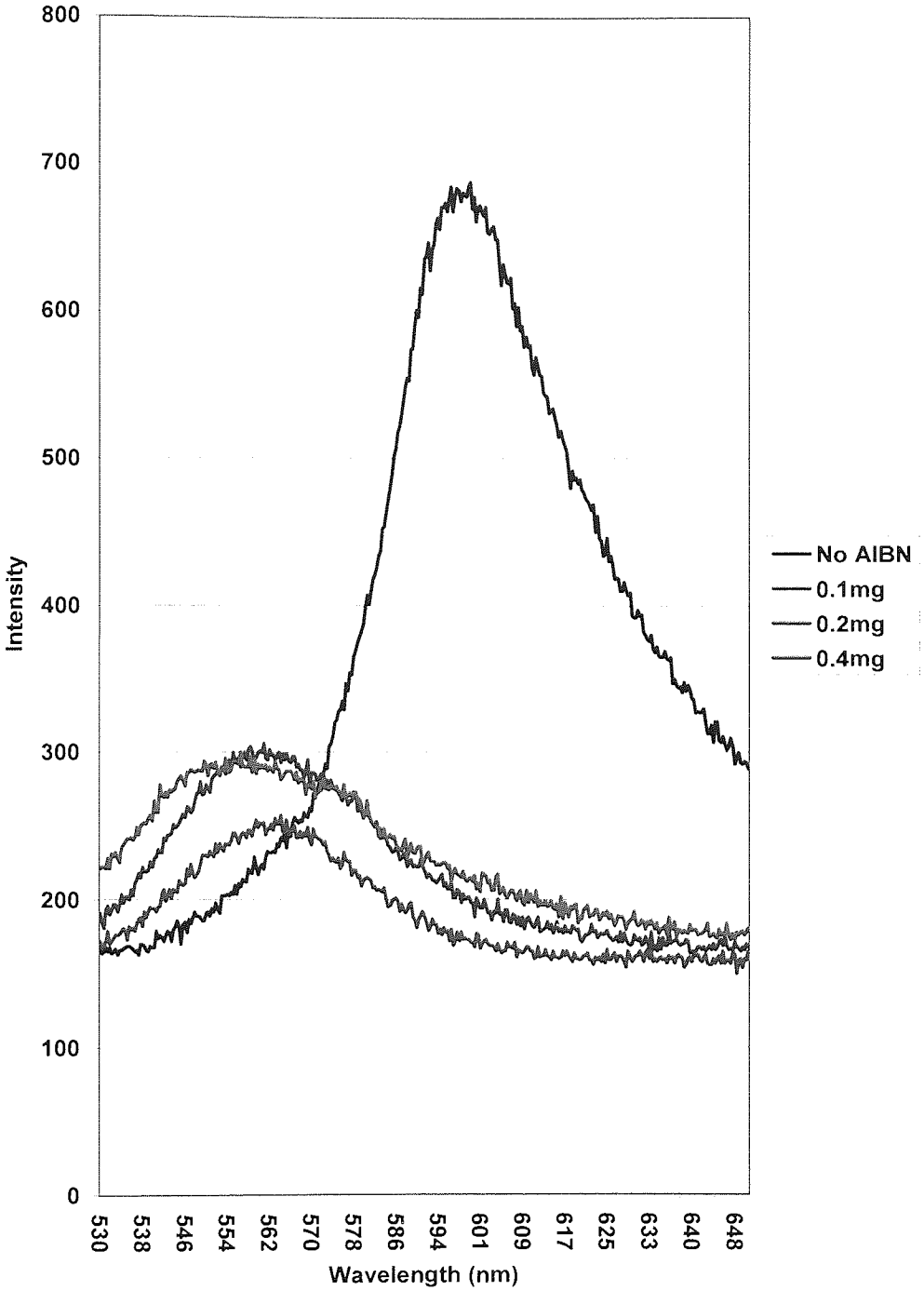

Figure 68: PL spectra of HDA 3 coated NanoDots™ upon exposure to increasing amounts of AIBN at 72°C

NanoDot™	Percentage HDA 3	Percentage DMSPA 20
OMN44	91	9
NLP121	67	33
OMN43	67	33
NLP125	86	14
OMN29	50	50

Table 5: **Table comparing the percentage ligand composition of five different batches of NanoDots™ following displacement with DMSPA 20**

Equivalents DMSPA **20**	% DMSPA **20**	% HDA **3**
5	0	100
10	33	67
20	63	37
30	63	37
40	67	33

Table 6: **Table showing the percentages of NanoDot™ binding ligands DMSPA 20 and HDA 3 following displacement procedures with increasing excesses of DMSPA 20**

Equivalents TPhPO **38**	% TPhPO **38**	% HDA **3**
5	67	33
10	67	33
20	78	22
30	84	16
40	84	16

Table 7: **Table showing the percentages of NanoDot™ binding ligands TPhPO 38 and HDA 3 following displacement procedures with increasing excesses of TPhPO 38**

Displacement Time	% DMSPA **20**	% HDA **3**
4	78	22
6	89	11
8	98	2
12	95	5

Table 8: **Table showing the percentage of NanoDot™ binding ligand DMSPO 20 over time**

LIGAND	% New Ligand	% HDA
DUPA	62.5	37.5
DUPSA	71.4	28.6
DMSPA	62.5	32.8
DMSPSA	43.6	56.4

Table 9: **Table demonstrating the effect of anchoring group on percentage displacement of HDA 3 ligand**

Appendix B

	Carbon	Hydrogen	Cadmium
Before soxhlet	87.60	7.50	0.19
After soxhlet	90.31	8.22	0.17

Table 10: **Combustion analysis before and after Soxhlet extraction on resin containing covalently incorporated NanoDot™**

Appendix C

MC-610 HDA 3 coated NanoDots™

$r_h = k T / 6 \pi \eta D$ **Eqn1i**

Where

$D = 4.4 \times 10^{-10}$ m^2 s^{-1} (from DOSY spectrum)

$k = 1.38 \times 10^{-23}$ J K^{-1}

$T = 298$ K

$\eta = 0.569 \times 10^{-3}$ N s m^{-2} (viscosity of $CDCl_3$)

$r_h = (1.38 \times 10^{-23}) \times (298) / 6\pi (0.569 \times 10^{-3}) \times (4.4 \times 10^{-10})$

$r_h = 8.6 \times 10^{-10}$ m or 0.86 nm

The diameter of MC-610 calculated from the diffusion coefficient obtained from DOSY ^{1}H NMR investigation id 1.72 nm.

TUPO-polymer-coated MC-610 NanoDots™

$r_h = k T / 6 \pi \eta D$ **Eqn1i**

Where

$D = 4.2 \times 10^{-10}$ m^2 s^{-1} (from DOSY spectrum)

$k = 1.38 \times 10^{-23}$ J K^{-1}

$T = 298$ K

$\eta = 0.569 \times 10^{-3}$ N s m^{-2} (viscosity of $CDCl_3$)

$r_h = (1.38 \times 10^{-23}) \times (298) / 6\pi (0.569 \times 10^{-3}) \times (4.2 \times 10^{-10})$

$r_h = 9.0 \times 10^{-10}$ m or 0.90 nm

The diameter of TUPO-polymer-coated MC-610 calculated from the diffusion coefficient obtained from DOSY ^{1}H NMR investigation id 1.8 nm.

MC556 HDA 3 coated NanoDots™

$r_h = k T / 6 \pi \eta D$ **Eqn1i**

Where

$D = 2.47 \times 10^{-10}$ m^2 s^{-1} (from DOSY spectrum)

$k = 1.38 \times 10^{-23}$ J K^{-1}

$T = 298$ K

$\eta = 0.569 \times 10^{-3}$ N s m^{-2} (viscosity of $CDCl_3$)

$r_h = (1.38 \times 10^{-23}) \times (298) / 6\pi (0.569 \times 10^{-3}) \times (2.47. \times 10^{-10})$

$r_h = 1.52 \times 10^{-9}$ m or 1.52 nm

The diameter of MC-556 calculated from the diffusion coefficient obtained from DOSY ^{1}H NMR investigation id 3.0 nm.

TUPO-polymer-coated MC-556 HDA 3 coated NanoDots™

$r_h = k T / 6 \pi \eta D$ **Eqn1i**

Where

$D = 4.9 \times 10^{-10}$ m^2 s^{-1} (from DOSY spectrum)

$k = 1.38 \times 10^{-23}$ J K^{-1}

$T = 298$ K

$\eta = 0.569 \times 10^{-3}$ N s m^{-2} (viscosity of $CDCl_3$)

$r_h = (1.38 \times 10^{-23}) \times (298) / 6\pi (0.569 \times 10^{-3}) \times (4.9 \times 10^{-10})$

$r_h = 7.7 \times 10^{-9}$ m or 0.77 nm

The diameter of TUPO-polymer-coated MC-556 calculated from the diffusion coefficient obtained from DOSY ^{1}H NMR investigation id 1.5 nm.

TUPO-polymer-coated SD-396 NanoDots™

$r_h = k T / 6 \pi \eta D$ **Eqn1i**

Where

$D = 3.60 \times 10^{-10}$ m^2 s^{-1} (from DOSY spectrum)

$k = 1.38 \times 10^{-23}$ J K^{-1}

$T = 298$ K

$\eta = 0.569 \times 10^{-3}$ N s m^{-2} (viscosity of $CDCl_3$)

$r_h = (1.38 \times 10^{-23}) \times (298) / 6\pi (0.569 \times 10^{-3}) \times (3.60. \times 10^{-10})$

$r_h = 1.05 \times 10^{-9}$ m or 1.05 nm

The diameter of SD-396 calculated from the diffusion coefficient obtained from DOSY ^{1}H NMR investigation id 2.1 nm.

Appendix D

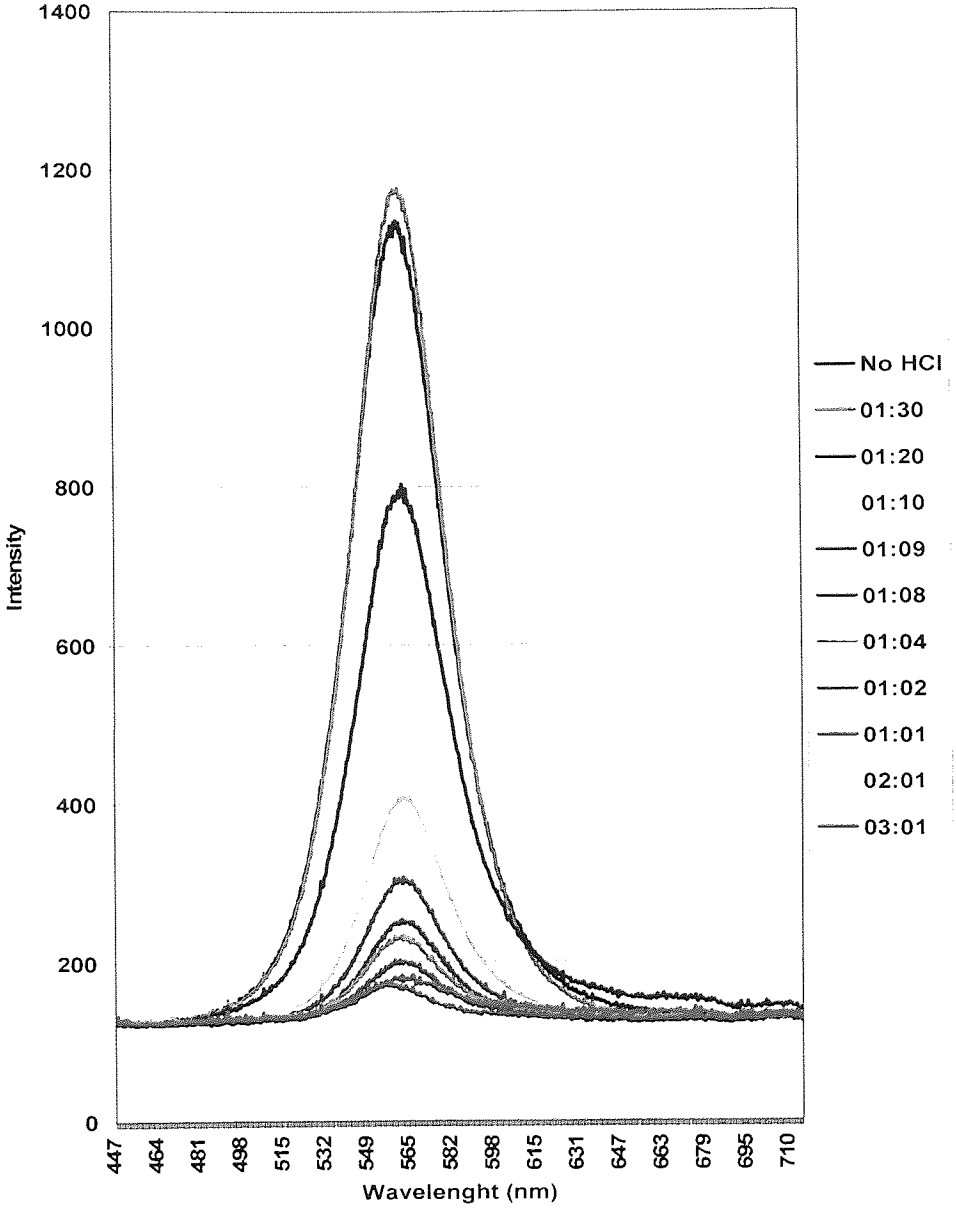

NB – The serial dilutions in **Figure 66** correspond to the volumetric ratio of pH 1.5 HCl acid solution to NanoDot™ stock solution respectively.

Figure 66: PL Spectra of HDA 3 coated NanoDots™ upon exposure to increasing volumes of concentrated acid

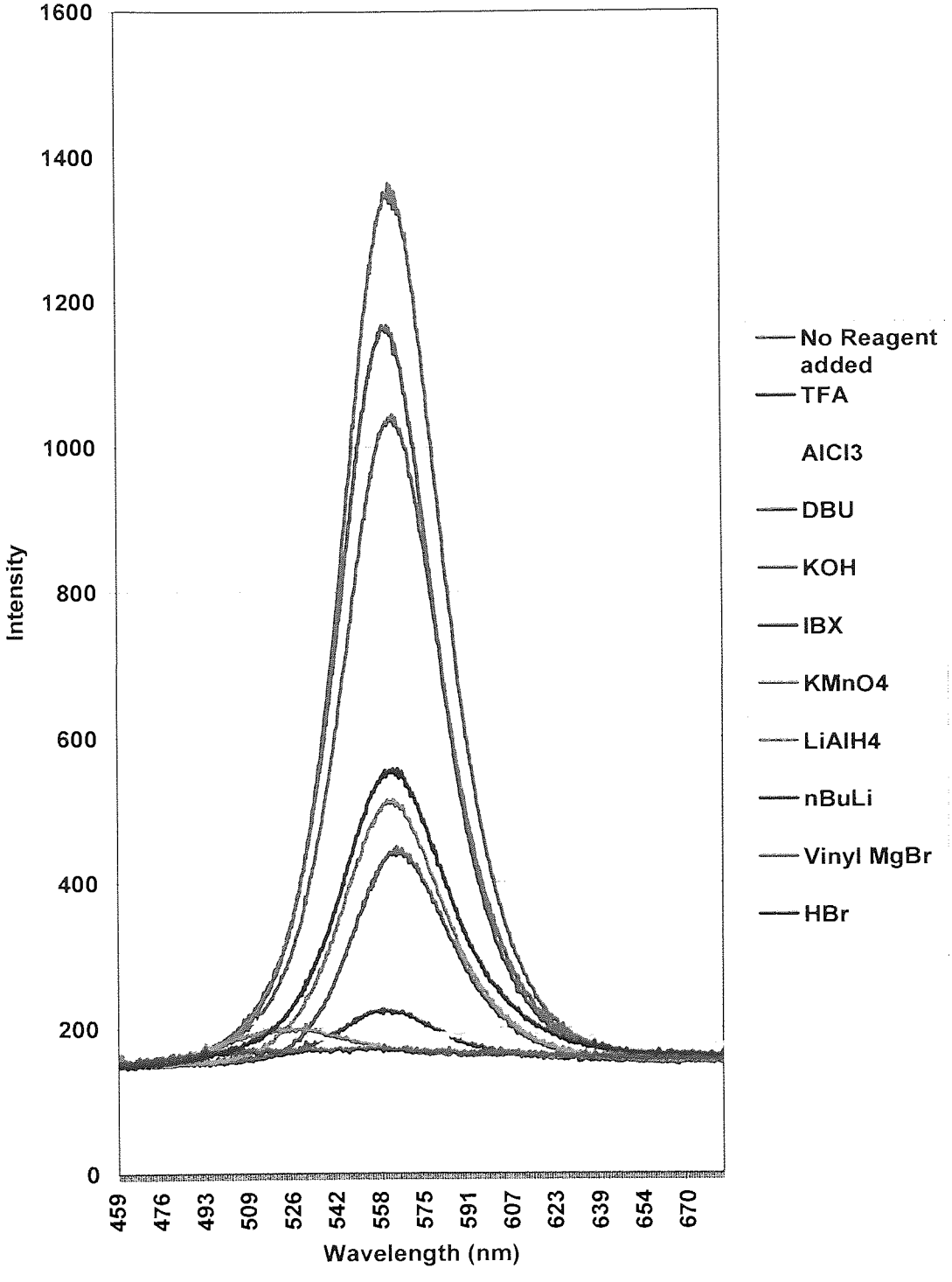

Figure 69: PL spectra of HDA coated NanoDot ™ batch MC610 upon exposure to a variety of reagents

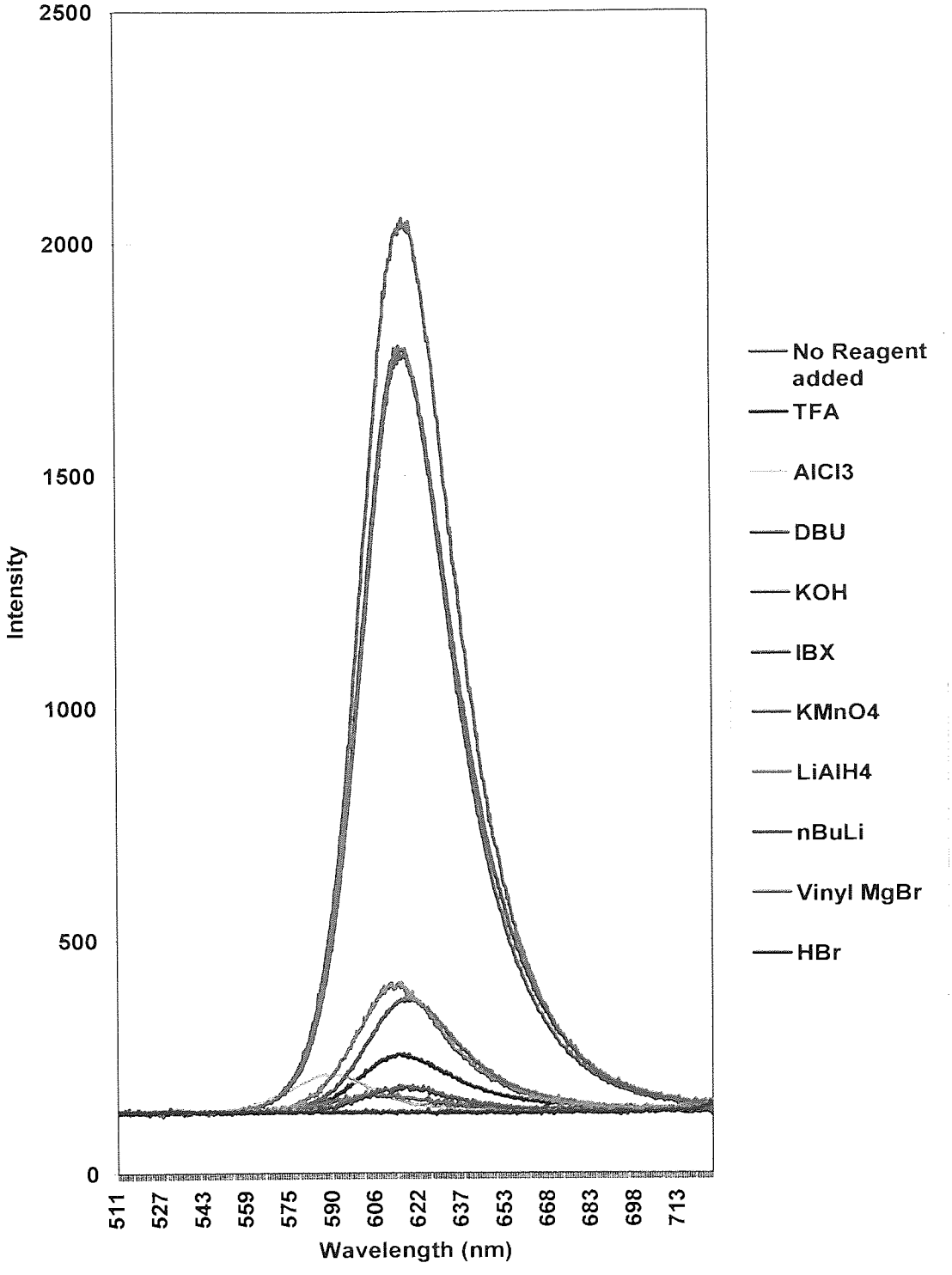

Figure 70: PL spectra of HDA coated NanoDot ™ batch MC556 upon exposure to a variety of reagents

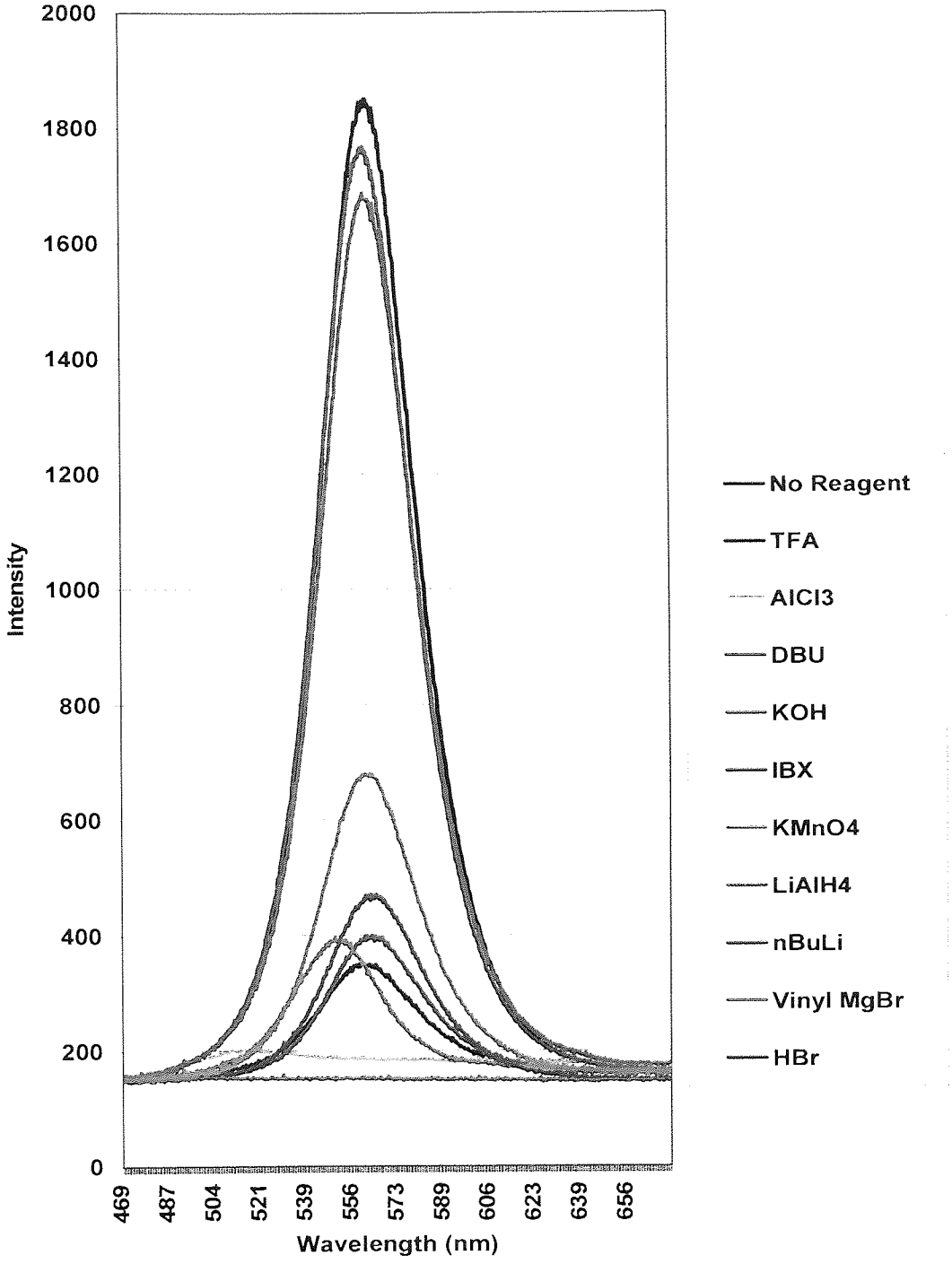

Figure 97: PL spectra of TUPO-coated NanoDot ™ batch MC556 upon exposure to a variety of reagents

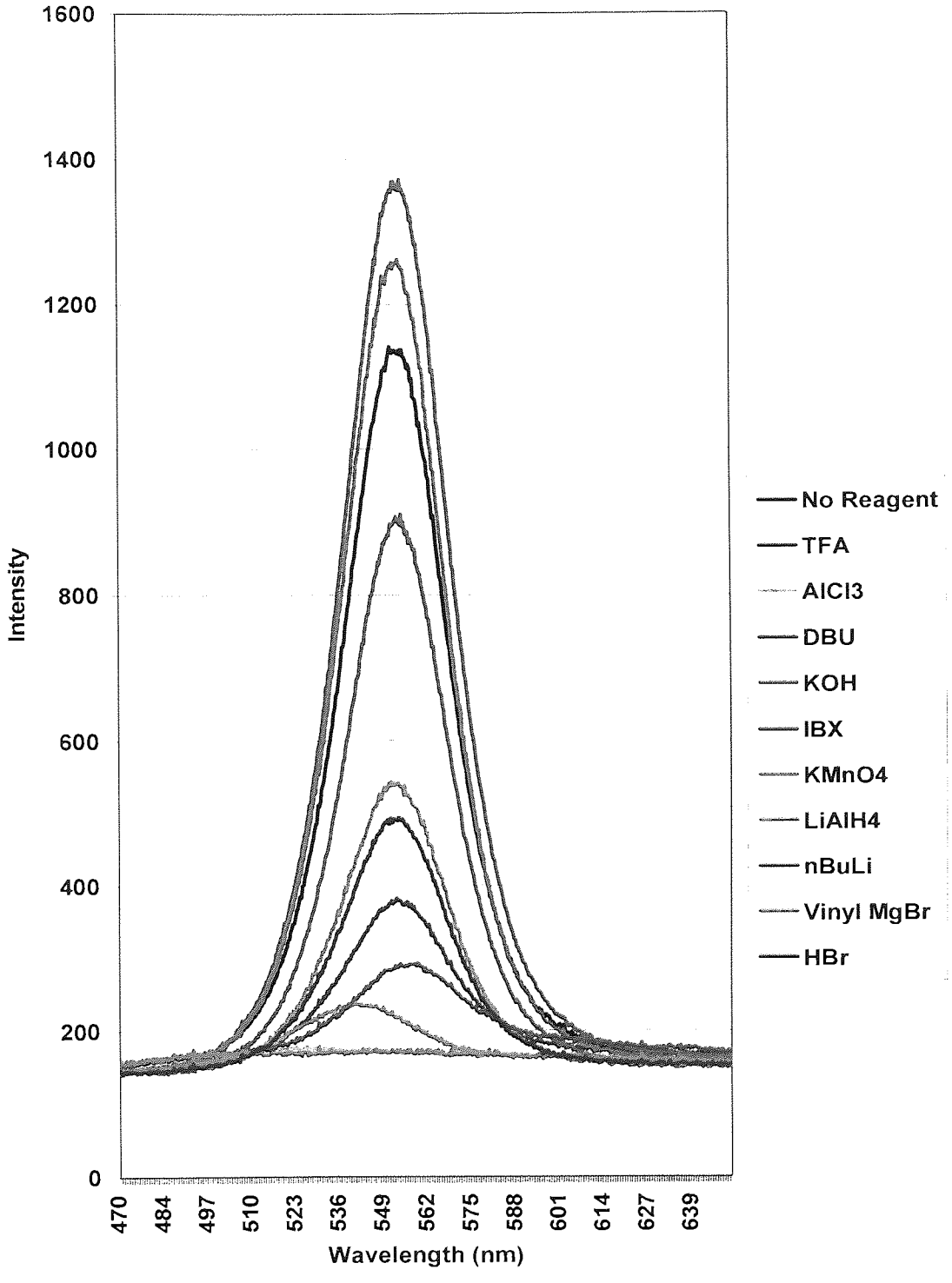

Figure 98: PL spectra of TUPO-polymer-coated NanoDot ™ batch MC556 upon exposure to a variety of reagents

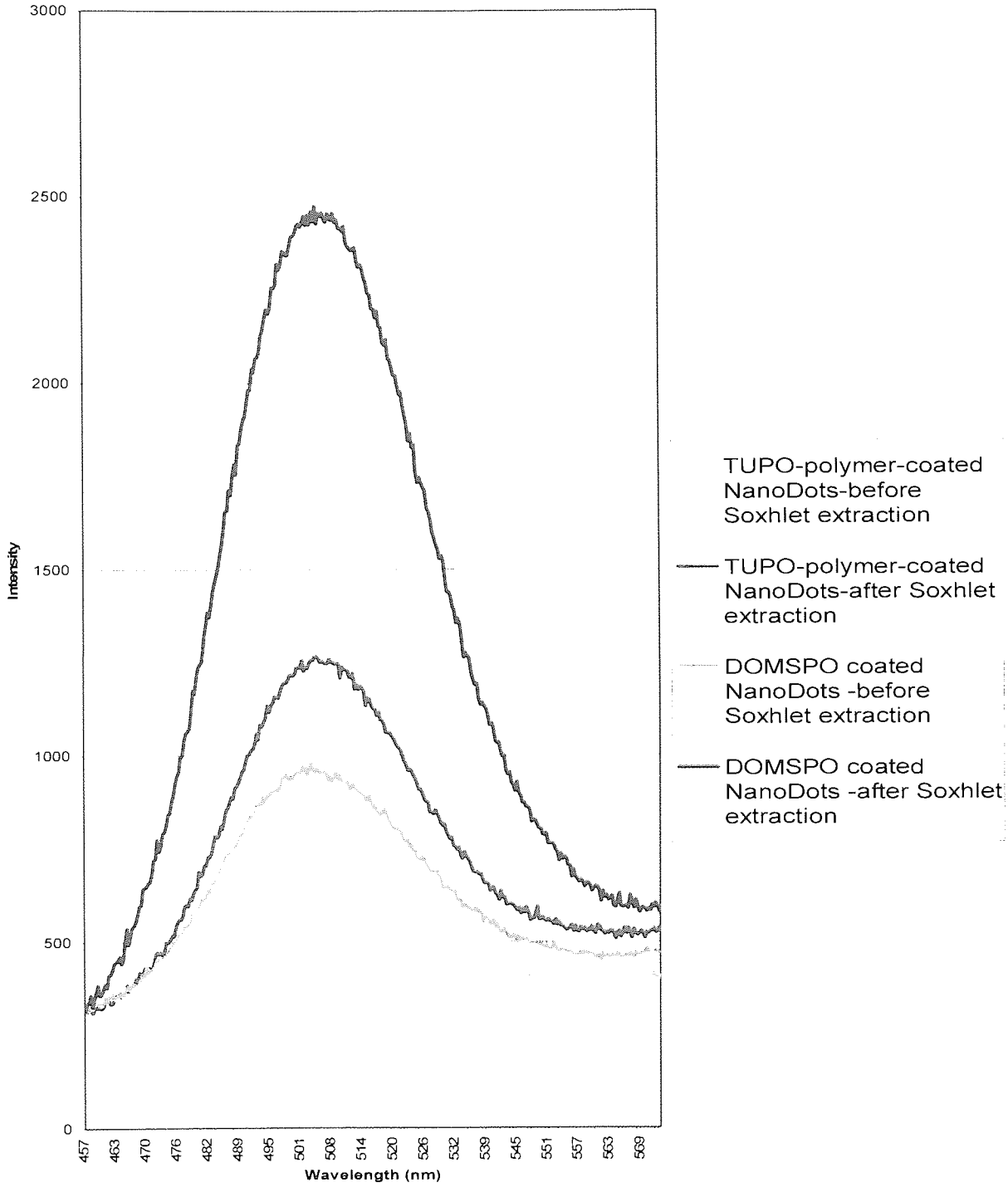

Figure 101: PL spectra before and after Soxhlet extraction of resin containing DOMSPO 7-coated NanoDots™ and TUPO-polymer-coated NanoDots™

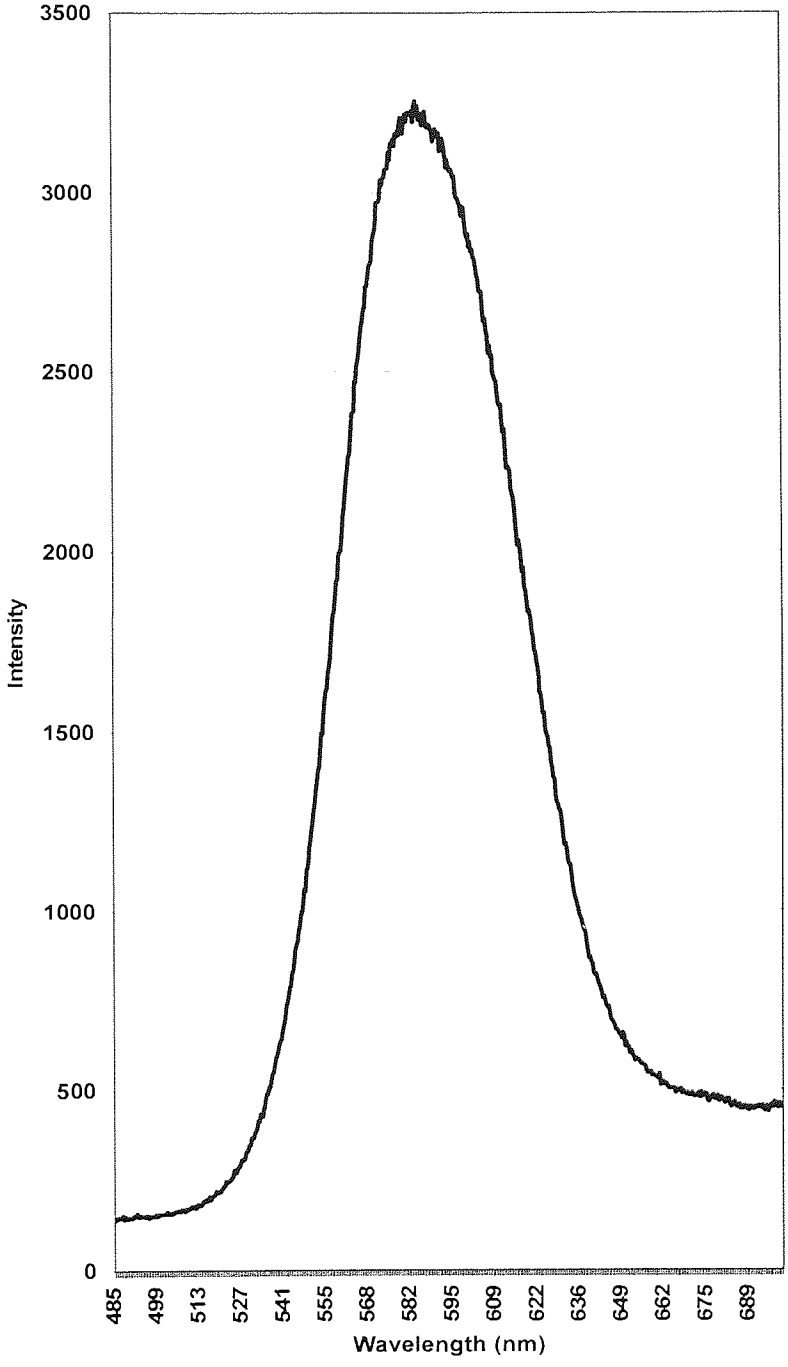

Figure 102: PL spectra NLP121 in DCM

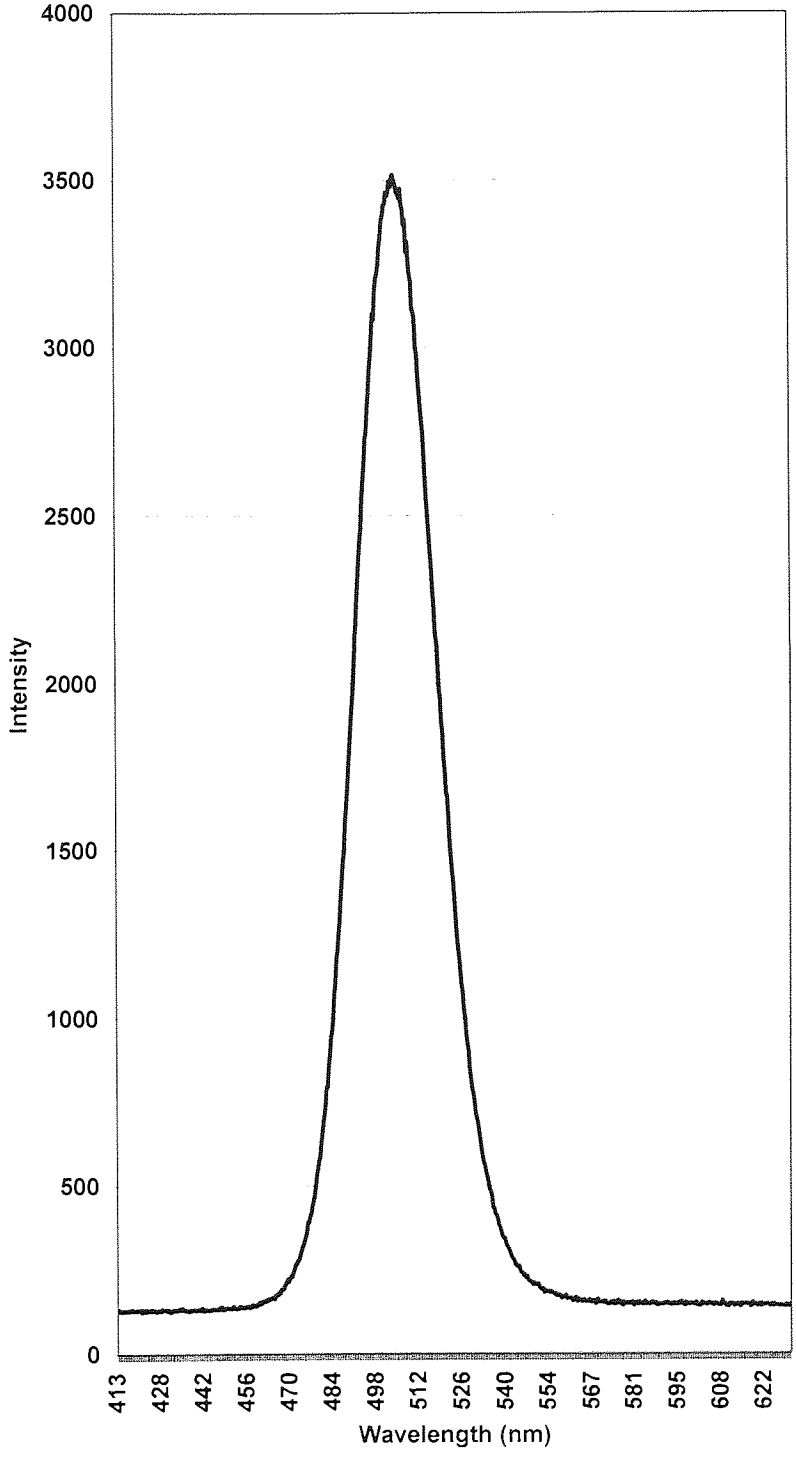

Figure 103: PL spectra SD396 in DCM

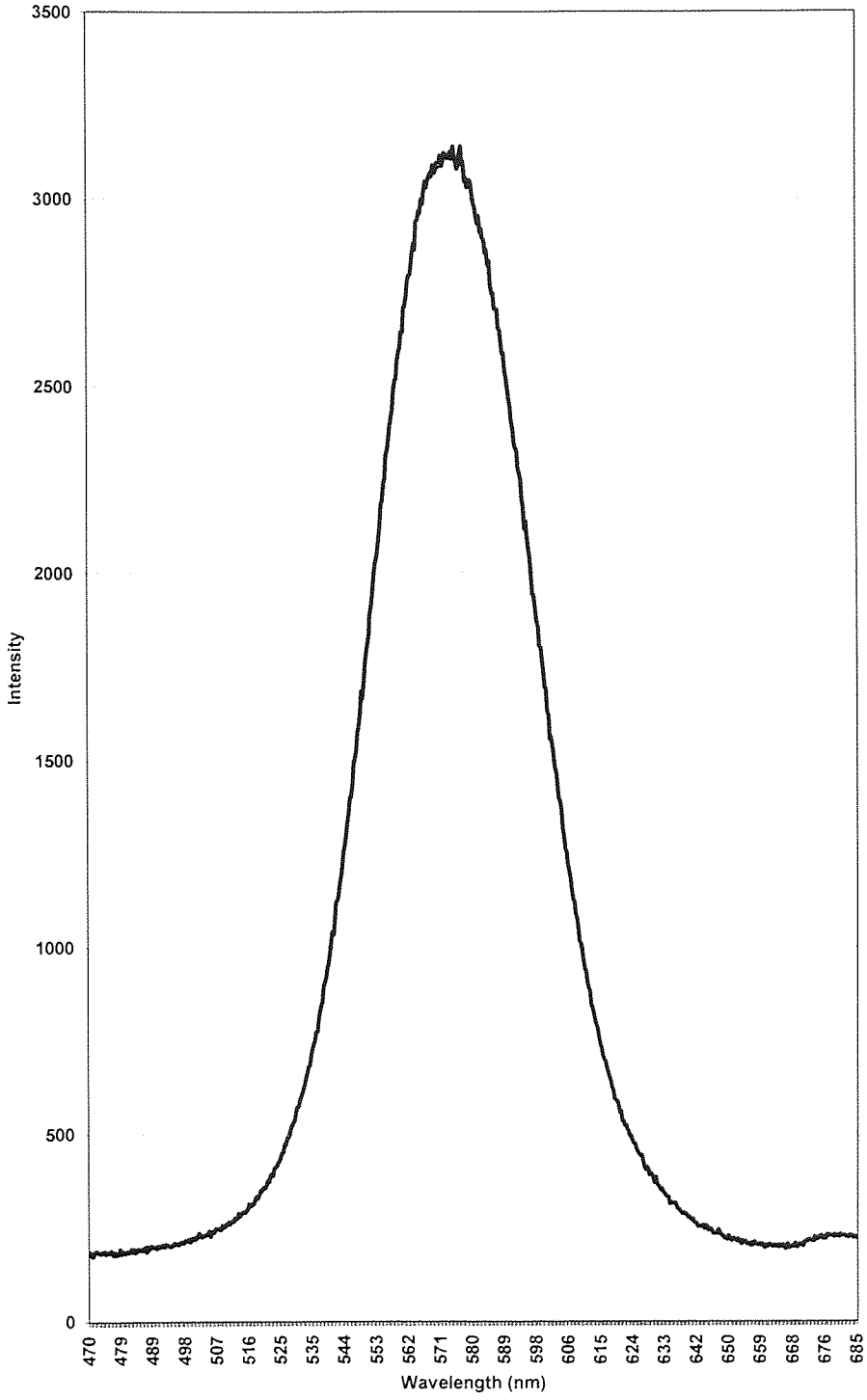

Figure 104: PL spectra MC610 in DCM

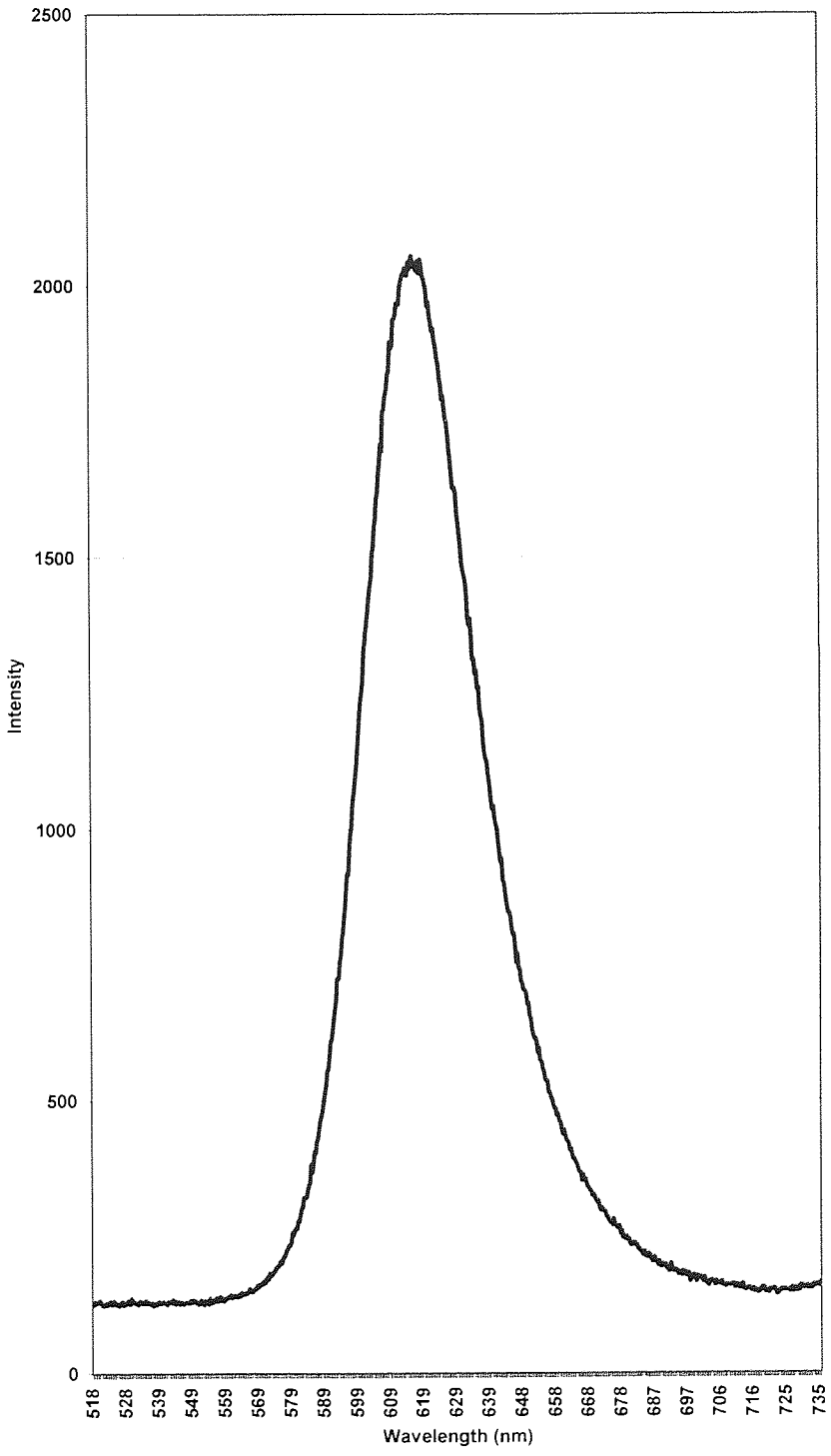

Figure 105: PL spectra MC556 in DCM